STUDY OF BACTERIAL INTERACTIONS USING COMPARATIVE METABOLOMICS FOR ACCELERATED ANTIBIOTIC DISCOVERY

A thesis submitted in the fulfilment of the requirements

for the degree of Doctor of Philosophy

by

LAIA CASTAÑO I ESPRIU

Strathclyde Institute of Pharmacy and Biomedical Sciences, University of Strathclyde Glasgow

October 2021

Declaration of authenticity and author's rights

'This thesis is the result of the author's original research. It has been composed by the author and has not been previously submitted for examination which has led to the award of a degree.'

Signed: 

Date: 22/10/2021

Acknowledgments

I would like to express my most sincere thanks and highest gratitude to everyone that has made this PhD thesis possible. Also, to the Strathclyde Institute of Pharmacy and Biomedical Sciences where most of this thesis was carried out. To CMAC and NPL for their collaboration and for allowing me to use their facilities and equipment.

A special thank you to my PhD supervisor Dr. Katherine R. Duncan for giving me the opportunity to carry out this thesis research under her supervision, for welcoming me into the Duncan Lab and for always encouraging and supporting me throughout the entire PhD. I truly enjoyed being part of your team. Also, thanks to all the Duncan group members! It has been absolutely amazing getting to know you all and working with you!

I would like to thanks all the microbiology group as a whole that in some measure have helped or collaborated in the development of this PhD thesis. Also, to all the other members of staff such as all the technicians for their hard work. To all the administration staff members. Furthermore, to Microbiology Society for their awarded grants to attend several conferences.

I am extremely thankful to Jonathan Parra for the place that he occupies in the success of completing this PhD. Thank you for your most sincere advice and for always willing to help with everything. Thanks for being not only an amazing person colleague and scientist but even a more incredible friend. For many more good times to come!

Thank you to my family and friends. For your support and encouragement. For all the life values that you have given me, for believing in me. To my nephews Kai, Elias and Matthäus for bringing so much happiness into my life.

Finally, and most importantly, to my partner Sam. No words can describe how much I appreciate your patience, kindness and absolutely everything that you have done for me during these three years. I am extremely proud of you. Thanks for motivating me every time that things were not working, for listening to me. For listening to all my talks again and again, for not letting me fall. For celebrating my achievements but also being there for my failures! Thank you for always supporting me in the decisions I have made and for constantly encouraging me to keep going. You are the best!

Dedicated to all of you.

Table of contents

List of Figures

List of Tables

Abbreviations

ACN: Acetonitrile

AMR: Antimicrobial Resistance

AntiSMASH: Antibiotics and Secondary Metabolite Analysis Shell

AT: Acyltransferase

BGC: Biosynthetic gene cluster

BiG-SCAPE: biosynthetic gene similarity clustering and prospecting engine

bld: Bald

Da: Dalton

DNP: Dictionary of Natural Products

ESKAPE: *Enterococcus faecalis, Staphylococcus aureus, Klebsiella pneumoniae, Acinetobacter baumannii, Pseudomonas aeruginosa, Enterobacter* sp.

EtOAc: Ethyl Acetate

FA: Formic acid

Glk: Glucokinase

GNPS: Global Natural Product Social Molecular Networking

H2O: Water

ISP2: International *Streptomyces* Project-2 Medium

IMS: Imaging Mass Spectrometry

keV: Kilo-electronvolt

KS: Ketosynthase

LC-MS: Liquid Chromatography-Mass Spectrometry

LC-MS/MS: Liquid Chromatography-Tandem Mass Spectrometry

LESA: liquid extraction surface analysis.

MALDI-ToF: Matrix-Assisted Laser Desorption/Ionisation-Time-of-Flight

Mbp: Mega base pairs

MC: Maximal counts

mg: Milligramm

mL: Milliliter

mm: Millimeter

MS: Mass Spectrometry

m/z: Mass-to-charge ratio

NA: Nutrient Agar

NMR: Nuclear Magnetic Resonance

NaPDos: Natural Product Domain Seeker

NP: Natural Product

NPatlas: The Natural Products Atlas

NRP: Non-ribosomal peptide

NRPS: Non-ribosomal Peptide-Synthetase

OD: Optical Density

OSMAC: One Strain - Many Compounds

pA: picoamp

PCA: Principal Component Analysis

PC: Principal Component

PKS: Polyketide Synthases

PLS-DA: Partial Least Squares-Discriminant Analysis

ppm: Parts per million

RiPPs: Ribosomally synthesized and post-translationally modified peptides

rpm: Revolutions per minute

rRNA: Ribosomal RNA

TC: Total counts

TE: Thioesterase

ToF-SIMS: Time-of-Flight Secondary Ionisation Mass Spectrometry

V: Volt

VIP: Variable Importance in Projection

whi: White

µg: Microgram

µL: Microliter

µm: Micrometer

µs: Microsecond

Abstract

Bacteria produce approximately 70% of microbial natural products with the bacterial class *Actinobacteria* being the major producer. They can contain over 30 Biosynthetic Gene Clusters (BGCs) encoding specialised metabolites. However, only a portion (up to 10%) of these BGCs are transcribed under normal laboratory conditions. Interspecies interactions play a role in the elicitation of specialised metabolites. Metabolites are often produced as a defence mechanism to kill or communicate with other strains. Therefore, co-culture techniques represent a potential method to elicit specialised metabolites that are not produced under mono-culture. In order to understand the chemical exchange between strains, the impact of bacterial interactions was assessed on the strains' ability to produce specialised metabolites resulting in altered phenotypes. The study comprised a total of 51 strains (48 *Actinobacteria*, two *Pseudomonas* and one *Bacillus*) across 72 tri-cultures (three strains) and 63 one-to-one cultures (two strains). Four co-culture techniques were used; tri-cultures, one-to-one cultures, pre-conditioned media and mixed fermentations. A total of 21 tri-cultures and 40 one-to-one cultures resulted in altered phenotypes as a result of bacterial interactions. Pre-conditioned media revealed that specialised metabolites were responsible for these alterations. The antibacterial screening showed that seven bioactive strains displayed larger inhibition zones under co-culture. The LC/MS-based metabolomics of five strains' mono-culture, six one-to-one cultures and two tri-cultures extracts revealed the production of interaction-specific metabolites. One interaction was subjected to Imaging Mass Spectrometry (IMS) in collaboration with CMAC and the National Physical Laboratory (NPL). The results demonstrated that bacterial interactions increase chemical diversity and that mass spectrometry-based comparative metabolomics represent an exciting strategy to prioritise novel chemistry.

Keywords: Bacterial interactions, natural products, marine environment, rare *Actinobacteria*, co-culture, bacterial competition, specialised metabolites, Imaging Mass Spectrometry, comparative metabolomics.

CHAPTER 1: INTRODUCTION

1.1 Natural products

Natural products (NPs) are molecules of low molecular weight (<1500 Da) that are produced by organisms including plants, animals, protozoa, fungi and bacteria (Sorokina and Steinbeck, 2020). While primary metabolites are essential for the growth, development, reproduction and survival of the organism, secondary metabolites are not involved in primary metabolism (Petersen *et al.*, 2020). However, they play a role in the survival of the organism and the adaptation to environmental stimuli (Katz and Baltz, 2016; Pye *et al.*, 2017; Chen *et al.*, 2019). Specialised metabolites are involved in ecological functions that include defence mechanisms, signalling molecules and protection from environmental stress (Evans *et al.*, 2018; Petersen *et al.,* 2020). Fungi and bacteria alone are producers of 45% of bioactive microbial NPs to date (Newman and Cragg, 2020). The first microbially produced NP was discovered in 1928 by Alexander Fleming from a *Penicillium* fungus that contaminated a *Staphylococcus* culture (Fleming, 1929). This suggested that penicillin protected the fungal strain from the *Staphylococcus*. The discovery of penicillin was the start of a NP period known as “the golden age of natural product discovery” and it later revealed the co-culture approach as a technique to elicit metabolites (Fleming, 1929). During this period (late 1920s to 1970s) NPs were isolated using low-throughput methods with over 70% of the discovered antibiotics being either NPs, or derived (semi-synthetic) from natural products (Newman and Cragg, 2020). For instance, streptomycin was discovered in 1942 from the bacterial strain *Streptomyces griseus* after screening approximately 10,000 microbial cultures (Schatz, Bugle and Waksman, 1944; Comroe, 1978).

NPs are classified according to their biological activity which include antibacterial, antifungal, antiviral, antidiabetic, anthelmintic and anticancer (Newman and Cragg, 2020). Furthermore, secondary metabolites are classified according to their biosynthesis. The main classes are polyketides, peptides, terpenoids and alkaloids. Polyketides is one of the largest class of secondary metabolites comprising 30% of known NPs (Yu *et al.*, 2012). This class includes pharmacologically relevant metabolites such as macrolides, tetracyclines and ansamycins (Yu *et al.*, 2012). The antibiotic pikromycin (macrolide) isolated from *Streptomyces venezuelae* in 1950 was the first known polyketide (Brockmann and Henkel, 1951). Another outstanding polyketide to treat bacterial infections is erythromycin A (**Figure 1.1**) isolated from

Saccharopolyspora erythraea in 1952 (Mcguire *et al.*, 1952). Polyketides are biosynthesised through decarboxylative condensation of carboxylic acids by the modular enzymes polyketide synthases (PKSs) (Yu *et al.*, 2012). PKSs consist of three core domains, the acyltransferase domain which activates and binds the acyl starter substrate and transfers it onto an acyl carrier protein (ACP domain). The ACP domain, holds the growing polyketide chain and finally, the ketosynthase domain catalyses the elongation step of polyketide chain (Wang *et al.*, 2020). The chain elongation is usually terminated by the thioesterase domain (Wang *et al.*, 2020). In addition, PKSs can have optional domains which include the ketoreductase domain, the dehydratase domain and the enoyl reductase domain. The ketoreductase domain reduces the keto group to a hydroxyl group, the dehydratase domain removes the hydroxy group to form a double bond, and the enoyl reductase domain generates a completely saturated bond (Bayly and Yadav, 2017). According to the basis of their domain structures and subunit organisations, PKSs are classified into type I, II, and III (Shimizu, Ogata and Goto, 2017). The type I PKSs are a large assembly of multifunctional peptides that contain a series of linearly arranged multiple domains (Wang *et al.*, 2020). Type II PKSs are a large multi-enzyme complex composed of monofunctional enzymes that are involved in the production of diverse aromatic polyketides (Hertweck *et al.*, 2007). Unlike type I and II, type III PKSs lack the acyl carrier protein domain to produce polyketides but contain enzymes that construct homodimers and catalyse many reactions (Risdian *et al.,* 2019).

Peptides are secondary metabolites that consist of short chains of amino acids connected by amide bonds. According to their biosynthetic mechanism, peptides are classified into ribosomally synthesized and post-translationally modified peptides (RiPPs) and non-ribosomal peptides (NRPs) (Dang and Süssmuth, 2017). RiPPs are a group of NPs of ribosomal origin that are characterised by precursor peptides which undergo post-translational processing (Dang and Süssmuth, 2017). The precursor peptides consist of a leader, a core and a follower amino acid sequence (Vignolle *et al.*, 2020). The leader and follower sequences specify the post-translational modifications of the core peptide which are mediated by modifying enzymes (Vignolle *et al.*, 2020). After removal of the leader and the follower sequences, the RiPP is released (Vignolle *et al.*, 2020). To date, RiPPs are classified into more than 20 families including amatoxins, lanthipeptides, lasso peptides, cyanobactins and thiopeptides (Dang and Süssmuth, 2017; Montalbán-López *et al.*, 2020). Thiopeptides are one of the most well-studied subclasses of RiPPs and are predominantly

produced by *Actinobacteria* (Travin *et al.,* 2020). A good representative of this subclass is the first discovered member of the family, micrococcin (**Figure 1.1**) which was isolated in 1948 from a strain belonging to the actinobacterial genus *Micrococcus* (Su, 1948). Micrococcin reported antibacterial activity against Gram-positive and Gram-negative bacteria (Su, 1948).

The NRPs are secondary metabolites that are biosynthesised by multi-modular enzymes called non-ribosomal peptide synthetases (NRPSs) and the main producers are bacteria and fungi (Süssmuth and Mainz, 2017; Le Govic *et al.*, 2019). Each module consists of the adenylation domain, the thiolation domain and the condensation domain which carry out the biosynthesis of NRPs (Le Govic *et al.*, 2019). The adenylation domain activates and loads the thiolation domain. The thiolation domain substrates may be modified by the optional epimerization, formylation, methylation, heterocyclisation, reduction and oxidation domains which are incorporated into the respective module. It can also be modified by tailoring enzymes that add additional modifications (Süssmuth and Mainz, 2017). Then, the thiolation domain binds the activated amino acid to their cofactor 4′-phosphopantetheine arm and transfers the activated peptide to the condensation domain. The condensation domain catalyses the peptide bond formation (Martínez-Núñez and López, 2016; Miller and Gulick, 2016). After the condensation step, the peptide is released from the final carrier protein domain by the thioesterase domain which catalyses either hydrolysis or cyclization of the peptide (Martínez-Núñez and López, 2016; Miller and Gulick, 2016). NRPSs include pharmacologically relevant metabolites such as the beta-lactam antibiotics. Beta-lactam antibiotics contain a 3-carbon and 1-nitrogen ring (Pandey *et al.,* 2021), commonly called beta-lactam ring. They are amongst the most important antibiotics in clinical use (Hamed *et al.,* 2016). Generally, the biosynthesis of many beta-lactams (penicillin, cephalosporins, clavams, carbapenems and tabtoxin) involves non-heme iron-dependent oxygenase or oxidases in several catalytic steps (Tahlan and Jensen, 2013). An example of beta-lactam is penicillin (Fleming, 1929) (**Figure 1.1**).

Terpenoids are the largest (approximately, 60% of known NPs) and structurally most diverse class of NPs. They comprise more than 70,000 metabolites that are classified under more than 400 structural families (Firn, 2010; Helfrich *et al.*, 2019). All terpenoids are formed from five-carbon repeating units called isoprenes. The terpenoid biosynthesis pathway uses a single enzyme to form a cyclised hydrocarbon

backbone with subsequent modifications using tailoring enzymes (Helfrich *et al.*, 2019). Terpenoids are classified based on whether their scaffolds are derived from isoprenyl units (mono-, sesqui-, di-, or triterpenoids, carotenoids and sesterterpenoids) or are of mixed biosynthetic origin (meroterpenoids, indole diterpenoids and prenylated aromatic NPs) (Schmidt-Dannert, 2015). The majority of these metabolites are isolated from plants (Reddy *et al.*, 2020). However, fungi and bacteria also produce terpenoids such as the sesquiterpenoid pentalenolactone (**Figure 1.1**) isolated from over 30 different *Streptomyces* species (Koe *et al.,* 1956; Ogawa and Yonehara, 1969; Reddy *et al.*, 2020).

Alkaloids are a group of nitrogen-containing NPs that include more than 20,000 metabolites and are traditionally isolated from medicinal plants, but also from animals and microorganisms (Lichman, 2020). Alkaloids include more than 20 subclasses such as pyrrolidines, purines, indole alkaloids, tropanes and pyrrolizidines (Dey *et al.*, 2020). A relevant alkaloid is vinblastine (**Figure 1.1**) which was isolated from the plant *Catharanthus roseus* in 1958 and is used to treat different types of cancer (Noble *et al.*, 1959). They are characterised for their structural diversity and for containing one or more nitrogen atoms in their molecule, often forming part of a heterocyclic ring (Eguchi *et al.*, 2019). The biosynthesis of alkaloids often initiates with the condensation of two amino acids derivatives that form a precursor scaffold as the first step of a complex biosynthetic pathway (Desgagné-Penix, 2020). This is followed by a series of reactions such as bond formations, functional group additions and modifications, which lead to the production of a diverse range of alkaloids (Desgagné-Penix, 2020). Alkaloids are grouped according to their plant sources or based on the structure of the ring system containing the nitrogen atom (Dey *et al.*, 2020).

Actinobacterial strains are also producers of other natural or semisynthetic natural products such as aminoglycosides, nucleosides and glycopeptides. Aminoglycosides are broad-spectrum antibiotics that are active against various Gram-positive and Gram-negative bacteria (Krause *et al.,* 2016). They are used since the discovery of the first aminoglycoside streptomycin, in 1944 (Schatz, Bugle and Waksman, 1944). Aminoglycosides include an aminocyclitol core (streptamine, streptidine, or 2-deoxystreptamine), that can be decorated with various amino-sugars to make pseudo-oligosaccharides (Kudo and Eguchi, 2016). Other important aminoglycosides are neomycin, discovered in 1949 from *Streptomyces fradiae* (Waksman and Lecehevalier, 1949), kanamycin in 1957 from *Streptomyces kanamyceticus*

(Umezawa *et al.,* 1958) and gentamicin in 1963 from *Micromonospora purpurea* (Weinstein *et al.,* 1963). Nucleosides are structural subunits of nucleic acid-derived macromolecules that are well-known for their diverse biological activities (Serpi *et al.,* 2016). While their biosynthesis is still poorly understood, nucleoside antibiotics are classified into N-nucleosides and C-nucleosides where a sugar and a nucleobase are linked via a C–N or a C–C bond (Shiraishi and Kuzuyama, 2019). An example of nucleosides is muraymycin isolated in 2002 from a *Streptomyces* strain (McDonald *et al.,* 2002). Glycopeptides are a class of NPs that are produced by the interplay of two biosynthetic pathways, the NRPS and the oxidative cyclisation cascade (Greule *et al.,* 2019). Vancomycin, isolated from the actinobacterial strain *Amycolatopsis orientalis* is a representative of a glycopeptide antibiotic that is effective against Gram-positive bacteria such as *Staphylococcus aureus* (Griffith, 1981).

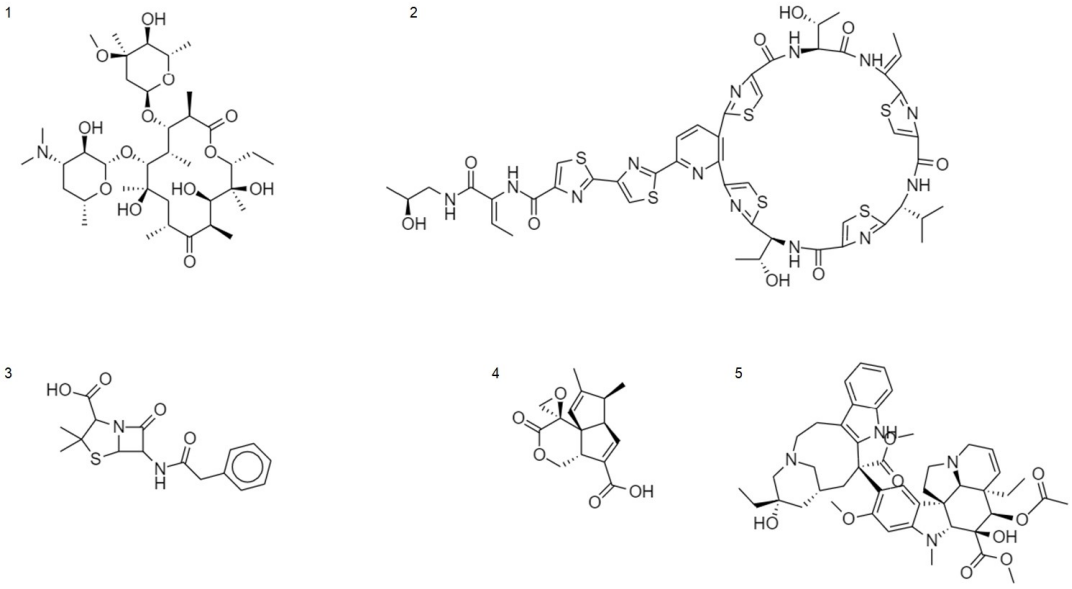

Figure 1.1. Chemical structures of representative NPs of main classes. From one to six: erythromycin A (Mcguire *et al.*, 1952), micrococcin (Su, 1948), penicillin (Fleming, 1929), pentalenolactone (Koe *et al.,* 1956) and vinblastine (Noble *et al.*, 1959).

1.1.1 Ecological function of microbial NPs in nature

To exploit the potential that microorganisms harbour for producing NPs, is necessary to understand the ecological roles of specialised metabolites. However, these ecological roles are not yet fully understood. According to the chemical co-evolution model (Firn, 2010), natural products can function as chemical weapons to reduce competitors as a result of their toxic nature (Patin *et al.*, 2016, 2018; Adnani *et al.*,

2017; Tyc, Song, *et al.*, 2017; Cabral *et al.*, 2018). In these lines, specialised metabolites can also function as agents of symbiosis which is the relationship or interaction between two organisms (Engl *et al.*, 2018). For instance, *Actinobacteria* associated with fungus-growing leaf-cutter ants produce specialised metabolites to protect the ants against other bacteria and fungi (Chang *et al.*, 2020). Additionally, symbiosis mediated by specialised metabolites can serve as niche defence. The natural ecological niches of female beewolf digger wasps are protected by the symbiosis with *Streptomyces philanthi*, which is found in their antennal glands (Goettler *et al.*, 2007; Engl *et al.*, 2018). When these wasps lay eggs, they deposit *S. philanthi* onto the inner walls of the burrows which protect the larval cocoons by secreting nine specialised metabolites (Kroiss *et al.*, 2010). These metabolites are detected at a higher concentration in the outer surface of the cocoon to protect it from pathogens and at lower concentrations in the inner surface to prevent disruption of larval development (Kroiss *et al.*, 2010). This suggests that specialised metabolite production occurs as a defence mechanism to outcompete neighbouring organisms (Patin *et al.*, 2016, 2018; Adnani *et al.*, 2017; Behie *et al.*, 2017; Tyc, Song, *et al.*, 2017; Cabral *et al.*, 2018). Similarly, bacteria produce specialised metabolites as a defence against viruses that can infect them (bacteriophages). Specialised metabolites can act as inhibitors of bacteriophage replication representing an anti-bacteriophage defence system (Kronheim *et al.* 2018). A previous study observed that the metabolites daunorubicin and doxorubicin protect *Streptomyces coelicolor* and *Streptomyces peucetius* from lysis by bacteriophages (Kronheim, *et al.* 2018). While in the absence of daunorubicin and doxorubicin, bacteriophages were able to propagate, in the presence of these two metabolites phage replication was inhibited (Kronheim, *et al.* 2018). These data indicate that specialised metabolites are also produced as anti-bacteriophage defence. Despite these observations, the defence theory is limited by the fact that specialised metabolites are produced at subinhibitory concentrations.

Specialised metabolites can also be produced as signalling molecules and to protect against environmental stress (Evans *et al.*, 2018). Iron-scavenging metabolites (siderophores) are used for iron uptake when it is limited in the environment (Chen et al., 2019) and the production of pigments can provide protection against ultraviolet radiation (Reis-Mansur et al., 2019). The microbiologist Julian Davies proposed that microbially produced specialised metabolites are products that were previously used by the producers to regulate their own biosynthetic activities (Davies, 1990; Firn,

2010). However, this explanation accounts for only a small fraction of NPs since it does not justify the production of other metabolites without bioactive properties (Firn, 2010). Specialised metabolites are also involved in the morphological differentiation of sporulating *Actinobacteria* by developing aerial growth and inhibiting or stimulating spore germination under stressful conditions (Demain and Fang, 2000).

1.1.2 Antibacterial resistance and decline in the discovery of novel NPs

Many natural products contributed to the prevention and control of infectious diseases in humans and animals. Antibiotics greatly improved the practice of medicine (Li and Webster, 2018), the safety of surgical procedures, organ transplants and chemotherapy. However, the decline of antibiotic discovery and the overuse of these resulted in the rapid emergence of antibacterial resistance (AMR) to multiple antibiotics (**Figure 1.2**) by the clinically relevant ESKAPE (*E. faecalis*, *S. aureus*, *Klebsiella pneumoniae, Acinetobacter baumannii, P. aeruginosa* and *Enterobacter*) pathogens (De Socio *et al.*, 2019). AMR occurs naturally as part of the evolutionary process of bacteria. Bacteria that produce antibiotics are resistant to their own specialised metabolites which may form the basis of AMR mechanisms (Peterson and Kaur, 2018). Furthermore, antibiotic resistance genes of ancient bacteria are 99–100% identical to those of clinical bacteria suggesting that these mechanisms are of ancient origin (Mindlin and Petrova, 2017). AMR can also occur from gene mutations such as the increased resistance to fosfomycin by methicillin-resistant *S. aureus* due to mutations in the *glpT* and *uhpT* genes (Lee *et al.*, 2020). Bacteria can acquire antimicrobial resistance genes from another bacterium via horizontal gene transfer from mobile plasmids, phages or transposons (Bello-López *et al.*, 2019). In addition, some antibiotics are unable to penetrate the outer membrane of Gram-negative bacterial strains since it provides a permeability barrier or are removed by efflux pumps (Li and Webster, 2018). Nonetheless, a major factor that accelerates the AMR process is the overuse and misuse of antibiotics in humans, animals and agriculture (Baker *et al.*, 2018). For instance, antibiotics are used in agriculture to promote the growth of animals. The genes that encode the mechanisms of resistance in bacteria of animal origin can then spread to other bacteria by horizontal gene transfer in the environment through the food chain or animal waste (Manyi-Loh *et al.*, 2018).

Another problem facing AMR is the decline in the discovery of NPs, with two new classes of antibiotics discovered in the last 30 years (**Figure 1.2**) compared to more than 10 classes that were discovered between 1930 and 1960 (Högberg *et al.,* 2010).

These two classes are lipopeptides (Arbeit *et al.*, 2004) and oxazolidinones (Brickner *et al.*, 1996). One factor that impacts the decline of drug discovery is the high expense (cost efficiency) of developing antibacterial drugs and the reduction in new leads for the drug development pipeline (Li and Webster, 2018). The drug development process takes an average of ten years for a new drug to be in the market since its discovery, with clinical trials taking an average of six years and an estimated cost of $2.6 billion (DiMasi *et al.,* 2016). This includes the cost of failures (thousands of metabolites that are in the early stage of the development process, that will not make it to the market), with an estimated 10% of clinical success (Hay *et al.*, 2014). Therefore, if AMR continues increasing at this rate, it is estimated that the number of deaths as a result of bacterial infections will rise to 10 million people annually by 2050 from approximately 700,000 cases reported in 2014 (O'Neill, 2014).

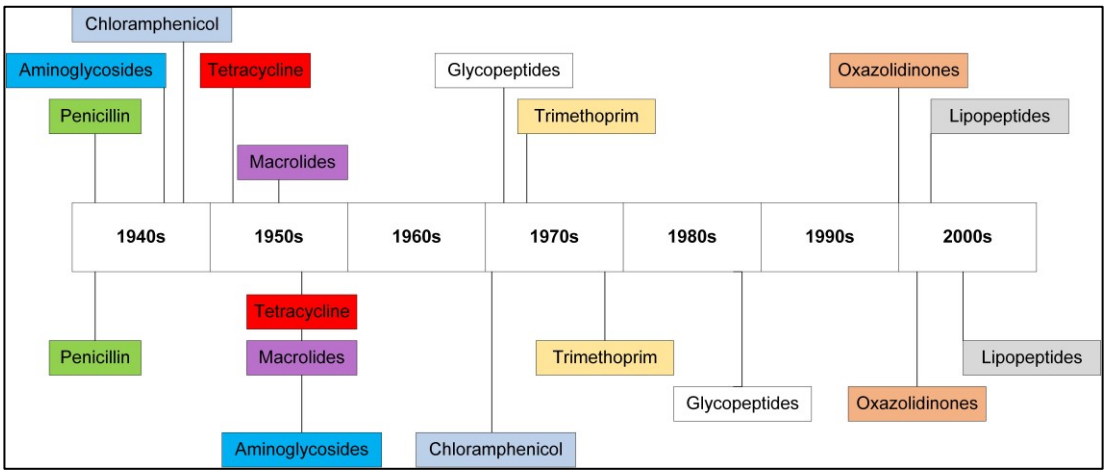

Figure 1.2 NPs discovery by class and development of AMR against these antibiotics between the 1930s and 2000s adapted from Högberg *et al.* The upper boxes show the antibiotic classes that were discovered and the lower boxes show developed AMR against these antibiotics. Most NPs to date were isolated between 1930 and 1960 with a decline in drug discovery after the 1970s (Högberg *et al.,* 2010).

1.2 The *Actinobacteria* phylum

The bacterial phylum *Actinobacteria* includes six classes (*Actinobacteria, Acidimicrobiia, Nitriliruptoria, Coriobacteriia, Thermoleophilia* and *Rubrobacteria*) that comprise 22 orders, 54 families, 250 genera and approximately, 3000 species (Ludwig *et al.*, 2012; Nudrat-Hazarika and Thakur, 2020). The largest class, *Actinobacteria*, includes 15 orders and 43 families (Bergey *et al.,* 2012). *Actinobacteria* are Gram-positive aerobic bacteria that represent one of the most

ecologically diverse microbial taxa in nature with approximately 10^{6-9} cells per one gram of soil (Goodfellow and Williams, 2003). They are distributed across soil and marine environments and as such, have important roles in the degradation and use of organic compounds (Goodfellow and Williams, 2003). Additionally, they are characterised by containing genomes with an average of 5Mbp and high guanine and cytosine content that ranges from 51% in some members of the genus *Corynebacterium* to more than 70% in *Streptomyces* and *Frankia* (Goodfellow and Williams, 2003; Ventura *et al.*, 2007). This phylum displays a great diversity in morphology including coccoid, short-rod and branched filaments, in physiology, and in metabolism. Many actinobacterial strains such as *Streptomyces* and *Micromonospora* have a complex life cycle that includes the development of vegetative mycelia and aerial hyphae and sporulation (Barka *et al.*, 2016). Furthermore, this phylum is considered as the most prolific source of bioactive specialised metabolites (van Bergeijk *et al.*, 2020). This is evidenced by the fact that they produce approximately two-thirds of all antibiotics in clinical use today from which 70–80% of these are isolated from the genus *Streptomyces* (van Bergeijk *et al.*, 2020; López-Agudelo *et al.,* 2021). For instance, since the discovery of streptomycin (Schatz *et al.,* 1944), *Actinobacteria* continue to be the main source of microbially produced specialised metabolites due to their unsurpassed ability for yielding novel NPs (Baltz, 2017).

The phylum *Actinobacteria* represents one of the earliest lineages within the prokaryotes and the phylogenetic backbone for its classification is based on the 16S ribosomal RNA (16S rRNA) genes (Barka *et al.*, 2016). However, 16S rRNA sequences present limitations when resolving species that are closely related or that recently diverged (Maroniche *et al.*, 2017; Earl *et al.*, 2018). For this reason, this method constrains the taxonomic relationships to the family or genus level and relationships between species are still unclear (Maroniche *et al.*, 2017; Earl *et al.*, 2018). For instance, the taxonomic status of the genus *Kitasatospora* within the family *Streptomycetaceae* was under debate for many years. Wellington *et al.,* reduced this genus to synonymy with *Streptomyces* in 1992 but was re-established as a separate genus by Zhang *et al.*, in 1997 (Wellington *et al.*, 1992; Zhang, Wang and Ruan, 1997). According to the phylogenetic analysis of the 16S rRNA genes based on the maximum-likelihood and maximum-parsimony analyses by the Bergey's Manual of Systematic Bacteriology, the *Actinobacteria* class is divided into two large clades (Ludwig *et al.*, 2012). The first clade comprises the orders *Actinopolysporales*,

Corynebacteriales, Glycomycetales, Jiangellales, Micromonosporales, Propionibacteriales, and the *Pseudonocardiales*; while the second clade comprises the *Actinomycetales, Bifidobacteriales, Kineosporiales*, and the *Micrococcales* (Ludwig *et al.*, 2012). The *Catenulisporales, Streptomycetales*, and *Streptosporangiales* form lineages emerging from the base of the class and the order *Frankiales* form independent lineages at the base of the tree. These clades were identified in our 16S rRNA phylogenetic tree. However, as previously stated, 16S rRNA analysis lacks the resolution to distinguish between closely related genera (Nouioui *et al.,* 2018). Within the first cluster, the order *Corynebacteriales* which comprises more than 10 genera including *Corynebacterium*, *Rhodococcus* and *Nocardia* is related to the order *Pseudonocardiales* which includes the genus *Pseudonocardia* (**Figure 1.3**). Within the *Corynebacteriales*, *Rhodococcus* and *Nocardia* belonging to the *Nocardiaceae* family clustered in one subclade while *Corynebacteria* classified under the *Corynebacteriaceae* family clustered in a second subclade. The presence of opimelate, arabinose and galactose in the cell wall (cell wall chemotype IV) is a common characteristic among members of these orders (Bergey *et al.,* 2012). In addition, the enzyme UDP-galactopyranose mutase is present in a conserved region only found in *Corynebacteriales* and *Pseudonocardiales* (Gao and Gupta, 2012). These shared characteristics support the relationship between these two orders and a common ancestor.

The order *Micromonosporales* is also placed on the first clade and contains 20 genera including the *Micromonospora* genus (**Figure 1.3**). Members of this order share three conserved signature indels with the *Corynebacteriales, Pseudonocardiales* and *Glycomycetales* that are not found in the rest of *Actinobacteria*. The first is a 2-aa insert in the delta subunit of DNA polymerase III (Gao and Gupta, 2012). The second conserved signature indel is in a highly conserved region of the ribosomal protein S3 and finally, the enzyme alpha-ketoglutarate decarboxylase. The order *Micrococcales* which clusters on the second clade, is the most diverse in the *Actinobacteria* class and includes genera such as *Micrococcus*, *Agrococcus* and *Microbacterium* (**Figure 1.3**). From these, *Microbacterium* and *Agrococcus* which belong to the *Microbacteriaceae* family clustered on the same subclade while *Micrococcus* which belongs to the *Micrococcaceae* family clustered on a second subclade (**Figure 1.3**). The order *Streptomycetales* which is separated from the other two clades forming its own lineage comprises the genera *Streptomyces*, *Kitasatospora* and *Streptacidiphilus* (**Figure 1.3**). Three conserved signature indels are specific to this order. The four-

amino-acid insertion found in the enzyme porphobilinogen deaminase, the one-amino-acid insertion in a conserved region of adenylate kinase and 11 conserved signature indel proteins are only present in members of the *Streptomycetales* (Gao and Gupta, 2012). This supports that *Streptomycetales* come from an ancestor exclusive from the other *Actinobacteria*.

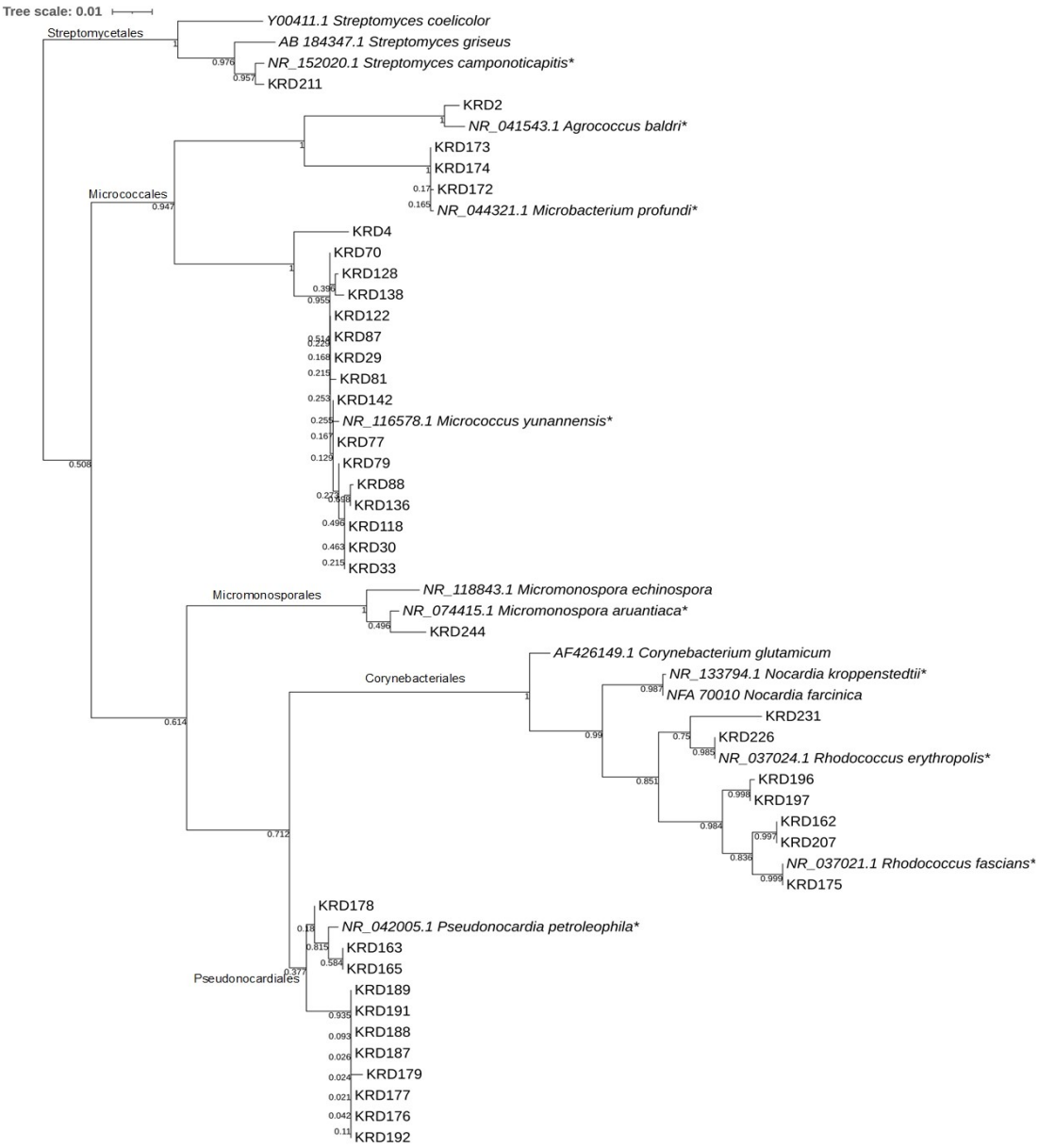

Figure 1.3. Maximum Likelihood phylogenetic tree of actinobacterial strains used in this project based on the 16s rRNA gene sequences. Bootstrap values (0-1) based on 1000 replications are shown. The scale bar indicates one per 1000 substitutions of nucleotides sequence of 16S rRNA gene. All positions with less than 50% site

coverage were eliminated. Asterisk: closely-related reference strains with accession numbers.

1.2.1 Actinobacterial life cycle, morphological and metabolic differentiation

The complex life cycle of sporulating *Actinobacteria* begins with the germination of a dormant spore when environmental conditions are favourable (Barka *et al.*, 2016). Spores become long filamentous hyphae to obtain nutrients from the substrate through hydrolytic enzymes. This network of hyphal branching and tips, forms a mycelium, called vegetative or substrate mycelium (Van Der Heul *et al.*, 2018). When nutrients are scarce or as a result of physical and chemical stresses, sporulating *Actinobacteria* enter into a morphological differentiation (Tenconi *et al.*, 2020). This differentiation starts with the degradation of the vegetative mycelium serving as nutrients for the development of the aerial hyphae which may be accompanied by the production of specialised metabolites (Tenconi *et al.*, 2018). These metabolites can be produced to protect nutrients, to slow down spore germination until encountering the favourable growth conditions and to inhibit the growth of competing microorganisms during germination (Demain and Fang, 2000; Čihák *et al.*, 2017). Then, the aerial hyphae curl up to form septa, resulting in the production of spores. Spores mature and are released into the environment. When they find favourable environmental conditions, they germinate and the cycle starts again (Barka *et al.*, 2016). Therefore, this morphological differentiation is related to secondary metabolism (Manteca and Yagüe, 2018; Tenconi *et al.*, 2020).

In the case of *Streptomyces*, the genes required for the formation of the aerial hyphae are the bald (*bld*) genes (Barka *et al.*, 2016). Mutants lacking the *bld* genes do not develop aerial hyphae and, therefore, have a “bald” phenotype (Merrick, 1976). More than twenty *bld* genes are known such as *bldA*, *bldB*, *bldC* and *bldD*. The *bldA* encodes the transfer ribonucleic acid which translates the UUA codon into the amino acid leucine (Lawlor *et al.,* 1987). Consequently, *bldA* mutants are not capable of developing aerial hyphae and spores, and are defective in the production of specialised metabolites (Lawlor *et al.,* 1987). The *bldB* gene encodes a small acidic protein required for antibiotic production and formation of aerial hyphae (Doroghazi and Buckley, 2014). Additionally, the *bldC* gene encodes a small 68 amino acid protein that is necessary for actinorhodin and undecylprodigiosin biosynthesis in *S. coelicolor* (Hunt *et al.*, 2005). Furthermore, the *bldD* which is considered the master regulator of development, is a transcriptional regulator that belongs to the xenobiotic

response element transcription factors (Tschowri *et al.*, 2014). *BldD* is found in almost all sporulating *Actinobacteria* and is regulated by the second messenger 3´,5´-cyclic diguanylic acid (Tschowri *et al.*, 2014). C-di-GMP signals through *bldD* to repress expression of the *bldD* regulon (containing approximately 170 sporulation genes such as *bldA*) during vegetative mycelium growth which blocks the developmental progress (Schumacher *et al.*, 2017). Furthermore, the SapB peptide, the chaplins and the rodlins are involved in the formation of the aerial hyphae. SapB is formed by the post-translational modification of the RamS protein and functions as a biosurfactant facilitating the erection of the aerial hyphae (Tillotson *et al.*, 1998). The chaplins are small proteins that make up the surface layer surrounding the spores while the rodlins intervene in the organisation of chaplins (Claessen *et al.*, 2003, 2004). The maturation of spores in *Streptomyces* is controlled by the white (*whi*) genes from which seven (*whiA*, *whiB*, *whiD*, *whiE*, *whiG*, *whiH* and *whiI*) encode transcriptional factors required for spore formation (Chater and Chandra, 2006). Mutants that lack the *whi* genes form aerial hyphae but do not produce spores since their development is blocked before sporulation (McCormick and Flärdh, 2012). Therefore, they are unable to complete their life cycle (Barka *et al.*, 2016). The *whiG* gene encodes a sigma factor that is required in the early stages of spore formation (Chater *et al.*, 1989). *WhiG* controls *whiH* and *whiI*, which encode transcriptional regulators that are related to septation while the *whiA* and *whiB* genes encode transcriptional factors that are required to block the growth of aerial hyphae *(Flärdh et al.,* 1999). While the *whi* mutants are not affected in the production of specialised metabolites the *bld* mutants are defective in this production, establishing a direct relationship between morphological and metabolic differentiation.

1.2.2 *Actinobacteria* specialised metabolite BGCs

The production of specialised metabolites by the *Actinobacteria* phylum represents a wide range of chemical diversity that includes the previously described polyketides, peptides, terpenoids and alkaloids. These specialised metabolites are encoded as biosynthetic gene clusters (BGCs) (Sekurova *et al.,* 2019) with sizes that range from one Kb to sometimes, over 100 Kb (Nah *et al.*, 2017). Additionally, BGCs contain all the necessary enzymes required for the biosynthesis of specialised metabolites (Nah *et al.*, 2017). The majority of these BGCs include the PKS and NRPS enzymes which encode the biosynthesis of polyketides and non-ribosomal peptides respectively (Zotchev, 2014; Dhakal *et al.,* 2019). Interestingly, the advancement in next

generation sequencing technologies and genome mining approaches revealed that *Actinobacteria* are capable of producing more specialised metabolites than previously detected under laboratory conditions (Bentley *et al.*, 2002; Belknap *et al.*, 2020). This results from the fact that some strains dedicate up to 10% of their genomes to secondary metabolism and can contain up to approximately 70 BGCs (Bentley *et al.*, 2002; Nett *et al.*, 2009; Sekurova *et al.*, 2019; Belknap *et al.*, 2020). For instance, one of the first whole genome analysis of *Streptomyces* was *S. coelicolor* which revealed 23 BGCs encoding for the production of more than 20 specialised metabolites (Bentley *et al.*, 2002). However, only three were previously expressed and linked to their products (calcium-dependent antibiotic, actinorhodin and undecylprodigiosin) (Bentley *et al.*, 2002). The genome sequencing of *Salinispora tropica* CNB-440 revealed that this strain dedicates 9.9% of its 5.18 MB genome to NPs assembly and 19 BGCs from which only five were linked to specialised metabolites (Udwary *et al.*, 2007; Nett *et al.,* 2009; Kersten *et al.*, 2013). This suggested that approximately 90% BGCs are cryptic or poorly expressed under standard laboratory conditions. This provides a great opportunity for the discovery of novel NPs.

Emerging tools that are used to detect cryptic or poorly expressed BGCs under standard laboratory conditions include the antibiotics and secondary metabolite analysis shell (antiSMASH) and the Natural Product Domain Seeker (NaPDos) (Ziemert *et al.*, 2012; Blin *et al.*, 2019). In addition, the biosynthetic gene similarity clustering and prospecting engine (BiG-SCAPE) and nplinker are used to link the BGCs with their products (Eldjárn *et al.*, 2020; Navarro-Muñoz *et al.*, 2020). For example, detoxin-rimosamide analogs were linked to their producing BGCs by using BiG-SCAPE (Navarro-Muñoz *et al.*, 2020). Therefore, these are excellent tools to look for BGCs of a known biosynthetic class or to unravel all detectable BGCs in bacterial genomes (Chen *et al.,* 2019). Despite these advances, one challenge remains in how to effectively prioritise the strains with the greatest NPs potential (Chen *et al.,* 2019).

1.2.3 Rare *Actinobacteria*

To date, the main challenge with screening actinobacterial strains for novel NPs remains in the re-discovery of known strains and metabolites (Genilloud, 2017, 2018). This problem comes from the fact that in a soil sample approximately 90% of strains are *Streptomyces* (Baltz, 2006; Takahashi and Nakashima, 2018). This, often leads to the isolation of known metabolites. For instance, streptomycin is produced by approximately 1% of soil *Actinobacteria* (Baltz, 2006). However, the advances in

isolation and cultivation techniques from unexploited ecological niches such as supplementing the media with salts (Betancur *et al.*, 2017), offer the possibility to discover strains that are less frequently isolated and more difficult to cultivate than *Streptomyces* (Qin *et al.*, 2009; Genilloud, 2018). This group of strains are known as rare *Actinobacteria* and consists of more than 200 genera such as *Nocardia, Salinispora* and *Micromonospora*, from which at least nine were discovered between 2013 and 2017 (Subramani and Sipkema, 2019). From these, a total of 97 were new species (Subramani and Sipkema, 2019). Rare *Actinobacteria* are a potential source of novel specialised metabolites since previously uncultivated strains reduce the chance of re-discovery (Schorn *et al.*, 2016; Subramani and Sipkema, 2019; Amin *et al.*, 2020). In fact, they are producers of approximately 25% of the total discovered NPs (Subramani and Sipkema, 2019). By 2010, 3,300 bioactive specialised metabolites were isolated from rare *Actinobacteria* from a total of approximately 13,700 metabolites produced by *Actinobacteria* (Subramani and Sipkema, 2019). An outstanding example includes the anticancer agent salinosporamide A which is produced by the rare *Actinobacteria S. tropica* and *Salinispora arenicola* (Feling *et al.*, 2003). Therefore, due to the further discoveries of metabolites from *Streptomyces*, screening and interest for rare *Actinobacteria* is increasing.

1.3 Bacterial interactions

1.3.1 Negative interactions: bacterial competition

Bacteria produce diffusible specialised metabolites which in some cases act as antagonistic metabolites. For instance, antibiotics can induce competitive interactions (Hibbing *et al.*, 2010; Stubbendieck and Straight, 2016; Westhoff *et al.*, 2017; Zhang *et al.*, 2018). Bacteria evolved to respond to biotic factors such as competitors occupying the same ecological niches that affect their survival (Schäberle *et al.*, 2014; Traxler and Kolter, 2015; Patin *et al.*, 2018). Saprophytic *Actinobacteria* lack motility which results in the production of NPs that act synergistically or contingently against competitors (Challis and Hopwood, 2003). Two factors that can lead multiple species to compete are phylogenetic distance and metabolic niche similarity (Darwin, 1860; Zelezniak *et al.*, 2015; Ghoul and Mitri, 2017; Russel *et al.*, 2017). This suggests that closely-related species occupying the same ecological niches may share a higher metabolic similarity, resulting in stronger competition for limited resources (Ghoul and Mitri, 2017). Contrary to this, it is proposed that bacterial interactions are not

correlated with phylogeny but with coexisting communities and the probability that two random strains interact with each other or not is balanced (Vetsigian *et al.,* 2011).

Independently of these theories, defence mechanisms give a selective advantage to the producers for the acquisition of nutrients and space (Traxler *et al.*, 2012; Behie *et al.*, 2017; Petersen *et al.,* 2020). In this context, specialised metabolites-mediated competition plays a role in determining which strains survive (Stubbendieck *et al.*, 2019). A previous study revealed that *Corynebacterium propinquum* strains inhibited *Staphylococcus* strains by the production of dehydroxynocardamine (Stubbendieck *et al.*, 2019). This indicated that inhibition was a result of iron competition and that the production of dehydroxynocardamine increased the competitive fitness and survival of *Corynebacterium propinquum* (Stubbendieck *et al.*, 2019). Similarly, to enhance production of red, *S. coelicolor* was co-cultured with *Corallococcus coralloides* (Schäberle *et al.,* 2014). Some co-culture-elicited NPs are represented in **Figure 1.4** (Oh *et al.*, 2005; Hoshino *et al.*, 2017; Abdel-Razek *et al.*, 2018; Anjum *et al.*, 2018). For example, the janthinopolyenemycins were discovered from the ecologically relevant co-culture between the bacterial strains *Janthinobacterium* ZZ145 and ZZ148 which were isolated from the same soil sample (Anjum *et al.*, 2018).

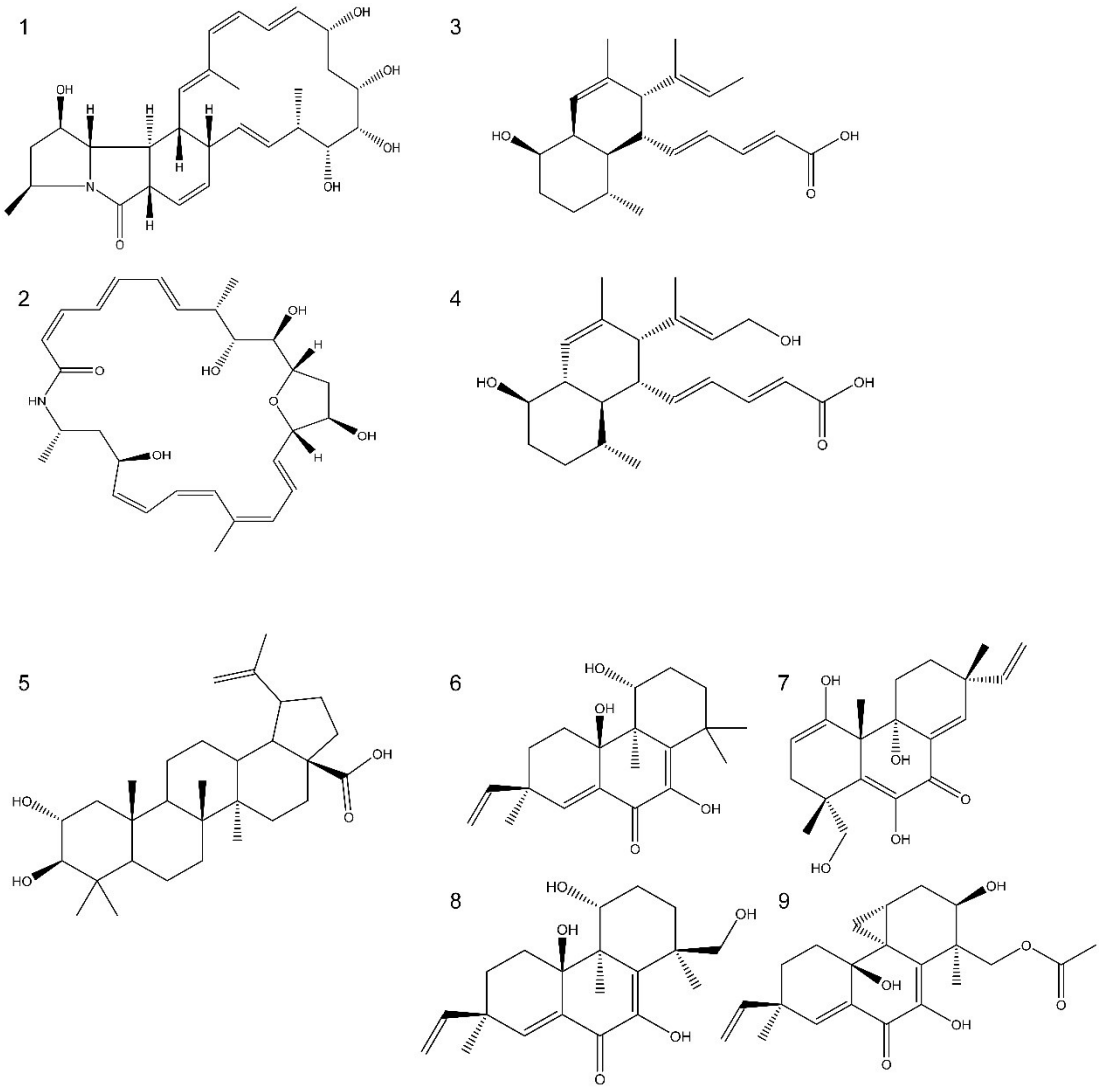

Figure 1.4. Chemical structures of NPs elicited by co-culture approaches. From one to nine: dracolactam A and B (Hoshino *et al.*, 2017), janthinopolyenemycin A and B (Anjum *et al.*, 2018), penicisteroid C (Abdel-Razek *et al.*, 2018) and libertellenones A, B, C and D (Oh *et al.*, 2005).

1.3.1.1 Interference and exploitative competition

According to Ghoul and Mitri (2017), the two main types of bacterial competition are interference and exploitative competition as represented in **Figure 1.5** (Ghoul and Mitri, 2017). In interference competition, also known as direct competition, one strain directly kills or harm competitors by producing specialised metabolites (Ghoul and Mitri, 2017). Interference competition is mediated through the production of specialised metabolites including broad-spectrum antibiotics and bacteriocins to reduce competitor strains (Paquette and Reuter, 2020; Westhoff, Otto, *et al.*, 2020).

On the other hand, in exploitative competition, also known as indirect competition, one strain consumes a limiting resource (nutrients) depleting it to the neighbouring competitor strains (Stubbendieck and Straight, 2016). Exploitative competition can arise in two ways; through increased nutrient consumption or through the secretion of specialised metabolites that harvest nutrients as a response to stressful conditions (Stubbendieck and Straight, 2016).

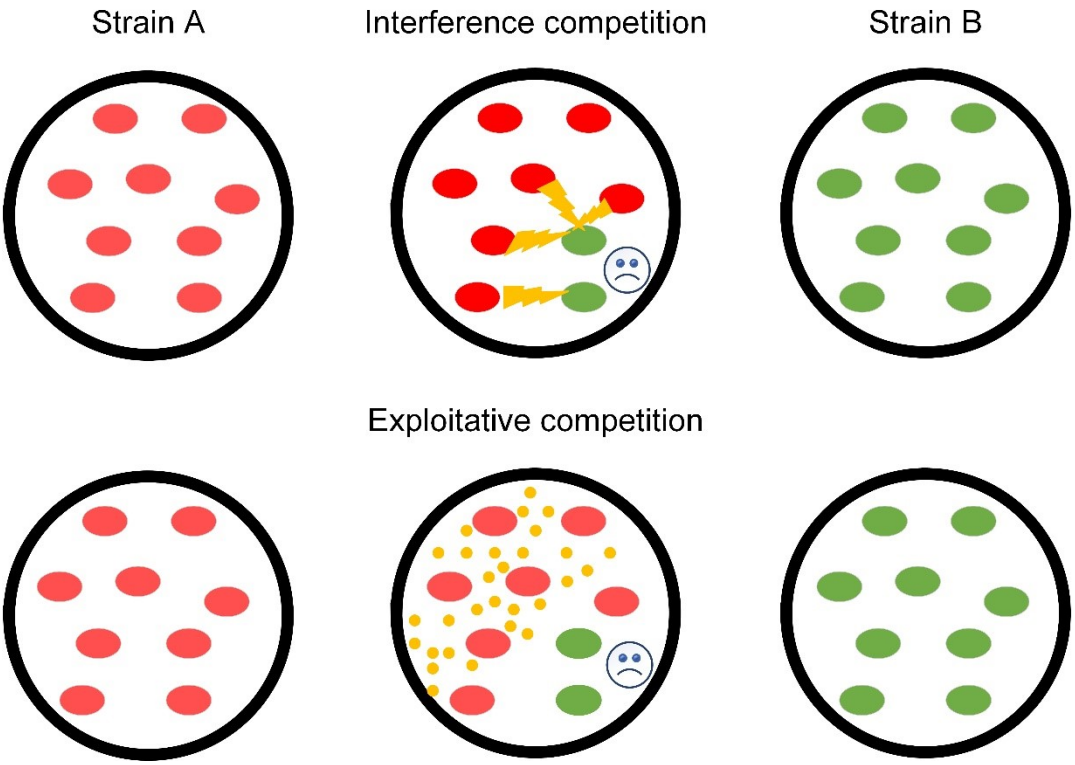

Figure 1.5. Types of bacterial competition. The upper row represents interference competition where strain A (red) directly inhibits growth of strain B (green). The lower row represents exploitative competition where strain A (red) uptakes the nutrient resources depleting them to strain B (green) resulting in growth reduction.

A recent study demonstrated interference competition through the production of bacteriocins by *Escherichia coli* strain (O103F) which outcompeted other 31 strains (Paquette and Reuter, 2020). Another example is the ability of *S. griseus* to produce streptomycin (Westhoff *et al.*, 2020). Streptomycin production enables *S. griseus* to inhibit and invade a population of drug-susceptible *S. coelicolor* strains (Westhoff *et al.*, 2020). Interference competition can also be mediated by cell-to-cell contact through growth inhibition and type VI secretion systems (Bayer-Santos *et al.*, 2019). Type VI secretion system was observed by the bacterial antagonism of

Stenotrophomonas maltophilia X-T4SS against other strains. The competition advantage observed by the *Stenotrophomonas* strain was a result of the type VI secretion system since a mutant strain lacking this system was not capable of inhibiting the growth of competitors (Bayer-Santos *et al.*, 2019).

Bioactive metabolites produced during exploitative competition include siderophores (Stubbendieck and Straight, 2016). Siderophores are iron-scavenging metabolites produced to obtain iron from the environment, preventing it from being available to other microorganisms. The interaction between the *Actinobacteria Amycolatopsis* sp. AA4 and *S. coelicolor* M145 showed that amychelin, a siderophore produced by the *Amycolatopsis* strain is used to sequester iron from the environment and as a result inhibits the development of *S. coelicolor* M145 aerial hyphae (Traxler *et al.*, 2012). Furthermore, another example is the utilisation of the metabolite deferrioxamine E (produced by *S. coelicolor*) by *Amycolatopsis* strain as iron source (Traxler *et al.*, 2012). Hence, these results demonstrated the selective advantage of this strain over *S. coelicolor* under a competitive environment. A well-known example of exploitative competition through the increased nutrient consumption is the interaction between *S. coelicolor* and *Myxococcus xanthus* (Pérez *et al.,* 2011). Pérez and colleagues carried out a study where they co-cultivated *M. xanthus* with *S. coelicolor* and found that *M. xanthus* depleted the nutrients to *S. coelicolor* which stimulated aerial hyphae development and actinorhodin production of *S. coelicolor* (Pérez *et al.*, 2011). This study demonstrated the chemical response of one strain under competition and nutrient limitation.

1.3.1.2 Influence of competition on phenotype

Bacterial competition results in physiological changes of competitor strains which enhances the competitive fitness of the producers (Stubbendieck and Straight, 2016; Geesink *et al.*, 2018). These phenotypic alterations include inhibition (Guo *et al.*, 2017), development alterations such as inhibition of sporulation (Traxler *et al.*, 2012) and changes in the strain's secondary metabolism (Tyc *et al.*, 2014; N. Lee *et al.*, 2020). For example, the ecologically relevant interaction assay between the termite-associated bacterial strain *Actinomadura* sp. 5-2 and the fungal pathogen *Trichoderma* led to the growth inhibition of *Trichoderma* by the production of specialised metabolites (Guo *et al.*, 2017). Additionally, co-culturing led to the isolation of the novel rubterolones A–F (Guo *et al.*, 2017). Another study revealed that *Bacillus subtilis* CMCC(B) 63501 was capable of inhibiting *Cladosporium* sp. WUH1

by producing surfactins (Shi *et al.*, 2017). Unusual diphenyl ethers with polyhydroxy sidechains were isolated from the co-culture. This suggested that these metabolites are a defensive response of *Cladosporium* sp. WUH1 against the surfactins produced by *B. subtilis* (Shi *et al.*, 2017).

1.3.1.3 Competition in the marine environment

The marine environment covers 71% of the Earth's surface (Costello *et al.,* 2010) and contains 50-80% of all organisms inhabiting the earth with more than 200,000 described species (Costello *et al.,* 2010). However, it is estimated that the total number of species to be discovered is approximately 1,000,000 (Costello *et al.,* 2010). This makes it a potential rich source of novel biodiversity and chemical diversity. Competition in such complex habitats is believed to be prevalent as a result of limited resources and complex microbial communities. It is estimated that the number of prokaryotic cells in these communities per millilitre (mL) of water is 10^4–10^7 (Whitman *et al.,* 1998; Marmann *et al.*, 2014). Defence mechanisms such as the production of metabolites enable a selective advantage under these environments (Marmann *et al.*, 2014). This was observed in the marine *S. arenicola* strain which produces rifamycins that are believed to play a role in defence mechanism (Patin *et al.*, 2016). Two strains of this species, each isolated from one location, inhibited the growth of competitors in ecologically relevant mesocosm assays (Patin *et al.*, 2017). Chemical analysis revealed that the two *Salinispora* strains produced distinct bioactive specialised metabolites. This indicates that their secondary metabolism evolved independently to provide a selective competitive advantage within their ecological niches (Patin *et al.*, 2017). Another example was the growth inhibition of rare Actinobacterial strains such as *Vibrio* sp., *Rhodococcus* sp. and *Micrococcus* sp. as well as *Streptomyces* strains in interaction assays by *Salinispora* (Patin *et al.*, 2018). Comparative metabolomics revealed that the chemical response of *S. tropica* under competition with other ecologically relevant bacterial strains varied depending the competitor (Patin *et al.*, 2018). This demonstrated that bacterial interactions are dynamic.

1.3.2 Neutral and positive interactions

For a long time, it was believed that microbial interactions are inhibitory in the natural environment (Foster and Bell, 2012; Tshikantwa *et al.*, 2018). This resulted from the difficulty to predict which species are able to coexist or metabolically cooperate, which remains a current challenge. However, interactive patterns are classified as either

positive (win), negative (loss) as previously described, or neutral (D'Souza *et al.*, 2018; Tshikantwa *et al.*, 2018). Positive interactions include mutualism, cooperation and commensalism (Kong *et al.*, 2018; Zhao *et al.*, 2019; Camus *et al.*, 2020). Mutualism refers to the beneficial effects of all the interacting species as a result of coexistence (D'Souza *et al.*, 2018; Zhao *et al.*, 2019). During mutualistic interactions, bacterial species synthesise metabolites which are later released to the exterior of the cell (D'Souza *et al.*, 2018). Therefore, the interacting strains metabolically benefit from each other. These interactions are obligatory for the interacting strains as they can only grow when the required metabolites are provided (Mee *et al.*, 2014). In cooperation, the interacting strains benefit from each other but in contrast to mutualism, the interaction between strains is not obligatory and they can survive on their own (Camus *et al.*, 2020). In bacterial cooperation the metabolites produced by one strain such as siderophores are consumed by the other (Cavaliere *et al.*, 2017). In commensalism, one interacting strain benefits from the other while the other remains unaffected (D'Souza *et al.*, 2018).

A positive interaction was demonstrated between *S. aureus* and *P. aeruginosa* (Camus *et al.*, 2020). Acetoin produced by *S. aureus* strains was catabolized by *P. aeruginosa* which improved the survival of both pathogens. Acetoin served as carbon source for *P. aeruginosa* which decreased the toxic accumulation of acetoin for *S. aureus* (Camus et al., 2020). Therefore, promoting the persistence of both strains in the cystic fibrosis lung environment. A microcosm study showed that the production of siderophores by *Pseudomonas fluorescens* benefited non-producer *P. fluorescens* strains and led to coexistence (Luján *et al.,* 2015). While non-producer *P. fluorescens* grew poorly under mono-culture, they were able to exploit siderophores from producing strains (Luján *et al.,* 2015). Non-producers invaded producer strains but were not able to outcompete them (Luján *et al.,* 2015). Despite that these studies gained insights in microbial ecology, they do not capture how these interactions affect a bacterial community.

1.4 Co-culture techniques for specialised metabolites elucidation

Mimicking the possible stressors to which bacteria are exposed in the natural environment enables the elicitation of metabolites that may be cryptic or not expressed under normal conditions (Benndorf *et al.*, 2018). One technique used to replicate the natural conditions of microorganisms and to elicit metabolites is the co-culture approach (van Der Meij *et al.*, 2017). The co-culture method is defined as "the

cultivation of two or more organisms together" and also known as "mixed/combined fermentations", "mixed/combined cultures". This technique is one of the strategies used to elicit novel metabolites encoded by cryptic or poorly expressed BGCs (Traxler *et al.*, 2012; Patin *et al.*, 2016). The ecological explanation to this is that normal laboratory conditions do not mimic the natural environment (Liang *et al.*, 2019). One reason is that *Actinobacteria* are part of diverse microbial communities (Duncan *et al.*, 2014), and therefore, they engage in chemical exchange (Traxler *et al.*, 2012; Patin *et al.*, 2016; Adnani *et al.*, 2017; van Der Meij *et al.*, 2017). These co-culture techniques include mixed fermentations (El-Hawary *et al.*, 2018), pre-conditioned media (Cabral *et al.*, 2018), solid media co-culture and membrane co-culture (Moutinho *et al.*, 2017). A mixed fermentation involves growing two or more strains together under liquid culture. The ecologically relevant mixed fermentation between S*accharomonospora* sp. UR22 and *Dietzia* sp. UR66 resulted in the production of the novel saccharomonosporine A and convolutamydine F (El-Hawary *et al.*, 2018). However, mixed fermentations are limited by the fact that is not possible to measure the growth of multiple strains by optical density readings (Moutinho *et al.*, 2017). Therefore, despite the success observed by this technique, is not an appropriate approach to understand the interactions between bacterial strains.

Pre-conditioned media co-cultures consist of sterilising the culture of a producer strain by autoclaving or filtering the media to remove bacterial growth followed by the inoculation of a challenged strain into the pre-conditioned media (Cabral *et al.*, 2018). Pre-conditioned media co-cultures between *E. coli* and *Candida albicans* revealed that a toxic soluble factor produced by *E. coli* was responsible for inhibiting *C. albicans* (Cabral *et al.*, 2018). However, the main limitation of this method is that the strains are not under physical (Moutinho *et al.*, 2017), therefore it does not capture the chemical response to growing with a competitor. The membrane co-culture technique consists of separating the bacterial strains by a membrane but enabling the diffusion of specialised metabolites (Moutinho *et al.*, 2017; Maglangit *et al.*, 2020). A common technique involves growing two strains in a chamber separated by a membrane not enabling direct contact between them but allowing the diffusion of metabolites and nutrients (Maglangit *et al.*, 2020). For instance, this technique elicited the production of a pyrroloindolocarbazole alkaloid named BE-13793C 1 from a *Streptomyces* and *Pseudomonas* that exhibited strong antiproliferative activity against HT29 cells (Maglangit *et al.*, 2020). As with pre-conditioned media, the main limitation of the membrane co-culture is that it does not capture the chemical response to multiple

strains growing physically together (Moutinho *et al.*, 2017). Finally, the solid media co-culture involves growing two strains or more together in solid medium. This method is also commonly applied to understand the interactions between bacterial strains since enables the phenotypic screening of the strains. Recently, the solid media co-culture between *Shiraia* sp. and *Pseudomonas fulva* SB1 resulted in the production of perylenequinonoid pigments by the *Shiraia* sp. as a chemical response to *P. fulva* SB1 (Ma *et al.,* 2019). This interaction was prioritised since the phenotypic screening led to the observation of red pigmentation under co-culture. The main challenges faced by solid media co-cultures is the distance between the strains, the inoculum used and mixing strains that require different times to grow since this complicates the replication of interactions.

1.5 Comparative metabolomics for the analysis of chemical exchange

Metabolomics is the study of primary and secondary metabolites produced by an organism (Fiehn, 2001). Metabolomics is based on the use of analytical techniques such as mass spectrometry (MS) for the detection and quantification of small secondary metabolites (Grim *et al.,* 2019). Comparative metabolomics is the study and comparison of metabolites produced in biological samples between and within experimental conditions and control conditions (Covington *et al.,* 2017). Bacterial extracts are analysed by MS-based comparative metabolomics in order to compare conditions such as axenic cultures and co-cultures. This approach is used in the study of microbial interactions in order to identify interaction-elicited metabolites (Caraballo-Rodríguez, Dorrestein and Pupo, 2017; Shi *et al.*, 2017; Benndorf *et al.*, 2018; Covington *et al.*, 2018). A previous study isolated a new dechlorinated diketopiperazine derivative and two new tetracyclic lanthipeptides (rubrominins A and B) from two actinobacterial strains by following the co-culture comparative metabolomics approach (Benndorf *et al.*, 2018). Similarly, comparative metabolomics was applied to reveal chemical responses to bacterial co-culture (Covington *et al.*, 2018). For example, *Streptosporangium* sp. KDCAGE35 showed a chemical response to co-cultivation with a *B. subtilis* strain. Multivariate data analysis compared mono-cultures and co-cultures and identified a specialised metabolite that was elicited under co-cultures but not under mono-culture (Covington *et al.*, 2018). This metabolite was prioritised for further chemical analyses and it was identified as funisamine, a previously unreported polyketide (Covington *et al.*, 2018). This demonstrates that MS-based comparative metabolomics facilitates the identification of interaction-elicited

metabolites and the prioritisation of bacterial strains and metabolites to accelerate the discovery of novel NPs.

1.5.1 Multivariate data analysis

Comparative metabolomics data analysis is performed with platforms such as MetaboAnalyst (Chong *et al.,* 2019). MetaboAnalyst software was designed for metabolomic analysis of liquid chromatography-mass spectrometry (LC-MS) data (Chong *et al.,* 2019). MetaboAnalyst enables the visualisation and statistical interpretation of biological extracts allowing the identification of potential parent ions (*m/z*) of interest (Chong *et al.,* 2019). In particular, the Principal Component Analysis (PCA) and the Partial Least Squares-Discriminant Analysis (PLS-DA) are powerful variable reduction techniques for the analysis of large datasets such as metabolomics data (Mogollón *et al.*, 2018). PCA and PLS-DA enable the identification of chemically similar bacterial extracts (Mogollón *et al.*, 2018) and the identification of parent ions that discriminate experimental groups (Yao *et al.*, 2016). PCA and PLS-DA summarise the data into fewer variables (scores) from the weighted average of the original variables (parent ions). Each score represents one biological extract based on the weighted average of its parent ions. The first principal component (PC1) accounts for the largest variance in the dataset and each subsequent principal component explains the next highest variance. According to Hair *et al*., the acceptable variance explained for PCA and PLS-DA to be valid is 60% (Hair *et al.*, 2017).

The objective of PCA is to arrive at a linear transformation where the output data contains as much variance from the original variables as possible (Worley and Powers, 2013). This unsupervised method achieves unbiased dimensionality reduction used to formulate initial biological questions. However, PCA reveals separations between experimental groups only when within-group variation is less than between-group variation (Worley and Powers, 2013). For this reason, supervised methods such as the PLS-DA are performed to verify and test in more detail the PCA observations. The advantage of PLS-DA is that it uses multivariate regression techniques to extract via linear combination of original variables (X) the information that can predict the class membership (Y). Therefore, PLS-DA represents a variable reduction and a classifier method for a large number of variables (Rashid *et al.*, 2019). In addition, cross-validation is used to evaluate the quality of the resulting statistical model considering the diagnostic measures R2 (predicted variation of the model) and Q2 (calculation of quality of the fit). The theoretical maximum of these values is 1 and

a value of ≥ 0.4 is considered an acceptable model (Worley and Powers, 2013). For this reason, PLS-DA classification guided by PCA produces relevant results. After calculating PLS-DA, variables are selected using the variable importance in projection (VIP). VIP is a weighted sum of squares of the PLS-DA loadings considering the amount of explained Y-variation in each dimension (Galindo-Prieto *et al.,* 2014). In VIP, if all variables (X) contribute equally to the PLS-DA model, their VIP value is equal to 1 (Galindo-Prieto *et al.,* 2014). Therefore, variables with values larger than 1 are considered the most relevant while variables with values below 0.5 are considered irrelevant. Metaboanalyst also includes a scatter plot called volcano plot which is used to identify significant chemical changes between two experimental groups in large data sets (de Sousa *et al.*, 2020). The volcano plot combines the magnitude of change (log2 fold change of means) of the two groups of samples on the x-axis and the -log10 of the t-test p-values on y-axis (de Sousa *et al.*, 2020). The resulting plot forms a V shape where the interesting metabolites are placed at the upper corners. Finally, hierarchical clustering is an algorithm that groups data points based on their similarity creating clusters (Gardinassi *et al.*, 2017). In Metaboanalyst, hierarchical clustering is presented as a heatmap which enables the visualisation of detected metabolites across samples and experimental groups and the clusters to which they belong (Xia *et al.*, 2015).

All these methods provided by Metaboanalyst are used in the detection of interaction elicited specialised metabolites in chemical exchange studies (Yao *et al.*, 2016) and for strain prioritisation. For example, the multivariate data analysis (PCA and hierarchical cluster analysis) of the co-culture extracts from *Trametes versicolour* and *Ganoderma applanatum* revealed sixty-two parent ions that were either elicited (such as *m/z* 298.0930, 300.1075 and 230.1155) or up-regulated (such as *m/z* 165.0555) by the co-culture compared to mono-cultures (Yao *et al.*, 2016). MetaboAnalyst allowed the rapid prioritisation of these specialised metabolites for further chemical analyses, reducing the number of metabolites of interest (Yao *et al.*, 2016). The main limitation of MetaboAnalyst is that it does not consider ion fragmentation, adducts, isotopes, in-source fragments, LC-MS contaminants and background signals are detected by MetaboAnalyst complicating the prioritisation of parent ions for dereplication (Demarque *et al.*, 2020). Despite this, since MetaboAnalyst considers the retention time, it facilitates the identification of these features (background noise, adducts, isotopes, etc) as well as interesting metabolites in the extract chromatograms (Demarque *et al.*, 2020). Furthermore, comparative metabolomics

faces several limitations such that many uncharacterised metabolites are not isolated by conventional isolation methods or detected by MS (Wolfender *et al.*, 2019). Additionally, most specialised metabolites that are detected in untargeted metabolomics remain unknown (Blaženović *et al.*, 2018). Nonetheless, comparative metabolomics analyses accelerate microbial NPs discovery pipelines by aiming microorganism prioritisation, identifying specialised metabolites that result from environmental stimuli, and by dereplicating prioritised metabolites. Therefore, it is important to recognise the potential of metabolomics to rapidly identify interesting metabolites in complex mixtures.

1.5.2 Imaging Mass Spectrometry for the analysis of bacterial interactions

Imaging mass spectrometry (IMS) is a technique that complements chemical analysis and the imaging of chemical data from colonies growing in agar plates with minimal preparation and disruption of bacterial cultures (Dunham *et al.*, 2017). IMS enables the visualisation of the spatial distribution of metabolites within the bacterial cultures. This technique was first introduced in clinical microbiology in 2002 and, since then more than 100 studies in molecular analysis (e.g., genomics and metabolomics) combined with IMS were carried out (Dunham *et al.*, 2017). IMS techniques include matrix-assisted laser desorption–ionisation (MALDI), coupled to a ToF (time of flight) analyser (MALDI-ToF) and time of flight secondary ion mass spectrometry (ToF-SIMS). MALDI-ToF is an ionisation technique used in IMS that allows the analysis of metabolites from bacterial colonies growing on solid media (Yang *et al.*, 2009). MALDI-ToF it is also used in other research areas such the identification of proteins. In MALDI-ToF, a matrix (designed mixture of acids) is applied to the sample and irradiated with ultraviolet light from a laser (Robinson, 2016). The laser produces heat which leads to the vaporization of the matrix and sample surface, resulting in ionisation (Robinson, 2016; Spraker, Luu *et al.,* 2020). The ions move through a flight tube (time of flight), then are separated by mass to charge ratio (*m/z*) and detected by a detector (Robinson, 2016). The outcome is a spectrum of the ionized fragments of the sample (Robinson, 2016). For more than two decades, MALDI-ToF is applied in molecular pathology studies (Yang *et al.*, 2012). However, in the last few years it was applied in the study of bacterial interactions (Spraker *et al.*, 2018).

Yang *et al.* developed an IMS method to visualise the chemical exchange between an interaction of a *B. subtilis* and a *S. coelicolor* colony using MALDI (Yang *et al.*, 2009). This approach is shown in **Figure 1.6** (Yang *et al.*, 2012). Spatial visualisation

of this interaction revealed that surfactin inhibited aerial hyphae and SapB of *S. coelicolor* (Yang *et al.*, 2009). Similarly, a previous report demonstrated that the cellular differentiation and the specialised metabolites biosynthesis of *Fusarium fujikuroi* were elicited by the lipopeptide ralsolamycin produced by *Ralstonia solanacearum* (Spraker *et al.*, 2018). The imaging of these interactions suggested the role of specialised metabolites in these interactions. For example, the induction of bikaverin (fungal metabolite) when co-cultured with *R. solanacearum* enhanced the survival of *F. fujikuroi* (Spraker *et al.*, 2018). Michelsen *et al.* (Michelsen *et al.*, 2016) characterised the metabolic exchange during the interaction of *S. aureus* and *P. aeruginosa* DK2-P2M24-2003 and *S. aureus* and *P. aeruginosa* PAO1 by MALDI-ToF IMS and molecular networking. The results showed a variance of the phenotypic colony characteristics and interaction patterns in both interactions. Furthermore, it was found that 4-hydroxy-2-heptylquinoline, the precursor of the signalling metabolite of *Pseudomonas* was responsible for the thickened colony at the *P. aeruginosa* DK2-P2M24-2003-*S. aureus* interface. These studies demonstrated the potential application of MALDI-ToF for the analysis of chemical exchange between strains (Yang *et al.*, 2009; Michelsen *et al.*, 2016; Spraker *et al.*, 2018) to reveal the possible roles of secondary metabolites under specific interactions.

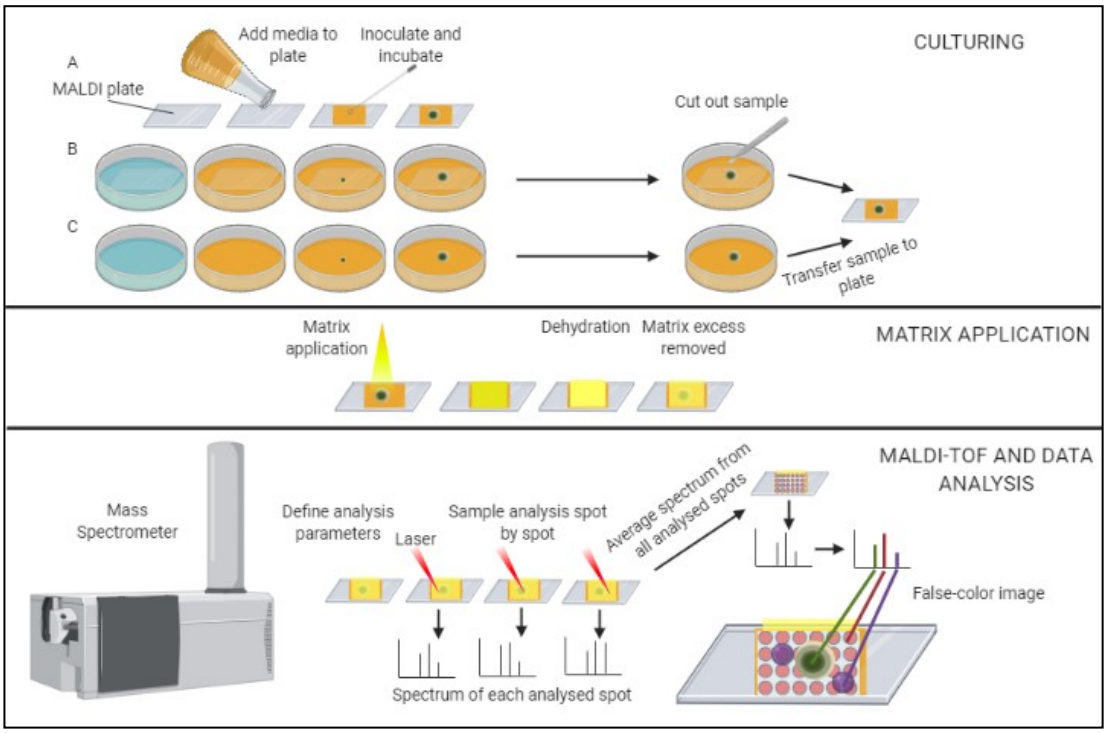

Figure 1.6. MALDI-ToF approach for the analysis of bacterial colonies directly from solid media adapted from Yang *et al*. The first step is culturing the strains: a) on the MALDI plate, (b) placing the MALDI plate in the Petri dish prior inoculation and incubation and (c) normal petri dish culture, excising the bacterial culture area of interest and placing it on top of the MALDI plate. This first step is followed by the matrix application using a 20- or 53-µm test sieve. The third step is bacterial culture dehydration at an elevated temperature (37°C) and the removal of matrix excess. The bacterial culture is inserted into the instrument and analysed. The last step is data analysis where colours are assigned to each ion in the average mass spectrum of the whole culture and displayed as a false colour map image. The same workflow is used for ToF-SIMS except that matrix application is not required (Yang *et al.*, 2012).

In ToF-SIMS, bacterial samples are analysed without chemical disruption (matrix is not required). The analysis is performed with a high-energy ion beam (primary ions) that bombards the uppermost layers causing intact metabolites to be ejected from the surface (Sjövall and Lausmaa, 2011). This results in the ionisation of some of these particles producing secondary ions. As in MALDI-ToF, the secondary ions are then directed into a time-of-flight tube and separated by the mass analyser into their mass to charge ratio. The outcome is the mass spectrum from the bacterial surface at the point of impact of the primary ion beam (Sjövall and Lausmaa, 2011). To obtain the spatial distribution of metabolites found in the bacterial surface it is necessary to

record separate mass spectra from a large number of points (pixels) from several areas of the sample (Sjövall and Lausmaa, 2011). A previous report demonstrated the application of ToF-SIMS in bacteria with minimal surface disruption (Vaidyanathan *et al.*, 2008). *S. coelicolor* was prepared in liquid and solid cultures and the spatial distribution of metabolites was recorded by ToF-SIMS (Vaidyanathan *et al.*, 2008). The ion peaks for the two antibiotics produced by *S. coelicolor*, actinorhodin and undecylprodigiosin in liquid medium were detected while in solid cultures only undecylprodigiosin was detected (Vaidyanathan *et al.*, 2008). This suggested that actinorhodin was produced at low concentrations (Vaidyanathan *et al.*, 2008). These results demonstrated that ToF-SIMS allows the identification of spatially distributed metabolites in bacterial cultures and the analysis of bacterial chemistry without disrupting the bacterial surface. Nevertheless, despite the increasing advances of these methods, the elucidation of metabolite distribution in biological samples is still challenging due to technical limitations. Chemical signals are affected by the matrix effect (in MALDI-ToF), the extraction efficiency and the suppression of ions induced by co-eluting molecules (Ho *et al.*, 2017). In addition, IMS techniques are limited in the collection of MS/MS data which difficulty data interpretation and the identification of specialised metabolites (Ho *et al.,* 2017). Data normalisation can also lead to false interpretation of IMS data by creating artifacts. In particular in heterogeneous biological samples when peaks are detected with very high intensities in specific regions of the sample (Rzagalinski and Volmer, 2017).

1.5.3 Dereplication for novel NPs discovery

Techniques such as IMS can aid prioritisation for the detection of novel specialised metabolites. Yet, the discovery of previously reported NPs represents a major challenge since the golden age of natural product discovery. Early dereplication approaches were performed by searching for metabolites based on their extracted chemical formula in databases such as the Dictionary of Natural Products (DNP) (Mohimani *et al.*, 2018). However, this method often fails at identifying previously reported NPs since this approach is manual and these databases contain many metabolites with identical formulas (Mohimani *et al.*, 2018). The advances in next-generation sequencing technologies and the combination of genome mining, LC-MS data analysis and antimicrobial activity screenings accelerated the prioritisation of strains with a high probability of containing novel metabolites (Soldatou *et al.*, 2021). Combining these approaches with recently developed dereplication tools such as the

Global Natural Product Social Molecular Networking (GNPS) in the early pipeline discovery enables the rapid identification of previously known secondary metabolites further minimising re-discovery (Henke and Kelleher, 2016; Kim *et al.*, 2019). Dereplication tools identify these metabolites by comparing MS data of metabolite extracts with MS data in databases (Kildgaard *et al.*, 2017). GNPS is an open-access database that analyses, organises and compares MS/MS data to all available public data, allowing dereplication of known metabolites as well as their analogues (Wang *et al.*, 2016). Furthermore, it allows the visualisation of MS/MS data (Wang *et al.*, 2016; Fox Ramos *et al.*, 2019). GNPS detects metabolites that are related and visualises them as spectral networks even if they are not known metabolites. A recent study cultured six *Streptomyces* strains belonging to the same clade and identified a cluster of novel metabolites by comparing extracts from the six strains with GNPS (Bauermeister *et al.*, 2019). This tool is also used to map metabolites with the place of isolation of bacterial strains (Purves *et al.*, 2016). GNPS was used to characterise the production of specialised metabolites from 85 bacterial strains isolated from Antarctica and Scotland, revealing that over 80% of the metabolites were location-specific (Purves *et al.*, 2016). Results demonstrated the efficacy and rapidity of this method to prioritise strains and specialised metabolites and suggested that advances of such dereplication tools will facilitate the discovery of novel metabolites. While the combination of metabolomic and genomic techniques is a potential approach for NPs discovery pipeline, it faces several challenges that need to be addressed. The fact that up to 90% of BGCs are cryptic or silent hinders the understanding of specialised metabolites (Baltz, 2017). Another challenge is metabolite detection as a result of the extraction method and solvents used or the analytical technique limitations such as ionisation (Crüsemann *et al.*, 2017). Additionally, this is aggravated by the chosen experimental conditions such as growth stage and media composition which impact the number of produced metabolites.

1.6 Aims and objective

The aim of this project was to understand the chemical exchange occurring during Actinobacterial interactions combining LC-MS, IMS, and comparative metabolomics. The work described in this thesis aimed to understand microbial interactions and the elicitation of specialised metabolites under co-culture. In addition, to understand the correlation between phenotypic changes in actinobacterial strains and chemical exchange. Finally, this work aimed to gain insights in the impact of bacterial

interactions in antibacterial activity against the indicator strains *E. faecalis*, *S. aureus*, *K. pneumoniae, A. baumannii, P. aeruginosa* and *E. coli*.

Objective 1: to evaluate the impact of bacterial interactions on the strains ability to produce specialised metabolites with a main focus on actinobacterial species. This was evaluated by a phenotypic screening of bacterial co-cultures using three co-cultivation methods (one-to-one cultures, tri-cultures and pre-conditioned media), a bioactivity screening and MS-based comparative metabolomics.

Objective 2: to determine the chemical response of co-cultures as a result of bacterial interactions compared to monocultures and detect co-culture-elicited parent ions.

Objective 3: to explore the secondary metabolite potential of a bioactive co-culture previously prioritised (*Rhodococcus* KRD226 and *Micromonospora* KRD244) by changing growth parameters (incubation time and growth phase) to understand how this impact the secondary metabolism and chemical exchange.

Objective 4: to develop a ToF-SIMS method to visualise the spatial distribution of specialised metabolites elicited by bacterial interactions.

CHAPTER 2: MATERIALS AND METHODS

2.1 Bacterial strain selection, growth conditions and maintenance

All strains were obtained from the microbiology collection at the University of Strathclyde (**Table 2.1**). Actinobacterial strains (except *S. rimosus*) were grown on ISP2 medium (Shirling and Gottlieb, 1966). *S. rimosus* ATCC10970 was grown on Emerson agar (Whiffen *et al.,* 1946) and non-*Actinobacteria* and indicator strains (*E. faecalis*, *S. aureus*, *K. pneumoniae, A. baumannii, P. aeruginosa* and *E. coli*) on nutrient agar (NA). Plates were incubated at 30°C until growth was observed. *B. subtilis* and indicator strains were incubated at 37°C for 24 hours. All strains were maintained in 20% glycerol stocks at -80ºC.

Table 2.1. Bacterial strains used in this project.

Strain	Sediment isolation location	Reference
KRD2	Antarctica	This study
KRD4	Antarctica	This study
KRD29	Antarctica	This study
KRD30	Antarctica	This study
KRD33	Antarctica	This study
KRD70	Arctic	SAMN14679894
KRD77	Arctic	SAMN14679895
KRD79	Arctic	This study
KRD81	Arctic	This study
KRD87	Arctic	This study
KRD88	Arctic	This study
KRD118	Arctic	This study
KRD122	Arctic	This study
KRD128	Artic	SAMN14679897
KRD136	Antarctica	This study
KRD138	Antarctica	This study
KRD142	Antarctica	This study
KRD162	Antarctica	SAMN14679900
KRD163	Antarctica	MH725317
KRD165	Antarctica	MH725315
KRD172	Arctic	SAMN14679902
KRD173	Arctic	This study
KRD174	Arctic	SAMN14679903
KRD175	Arctic	SAMN14679904
KRD176	Antarctica	MH725304
KRD177	Antarctica	MH725303
KRD178	Antarctica	MH725302
KRD179	Antarctica	MH725301

KRD187	Antarctica	MH725293
KRD188	Antarctica	MH725292
KRD189	Antarctica	MH725291
KRD191	Antarctica	MH725289
KRD192	Antarctica	MH725288
KRD196	Antarctica	MH725284
KRD197	Antarctica	SAMN14679906
KRD207	Antarctica	This study
KRD211	Scotland Falls of Lora	This study
KRD226	Scotland subsurface of Trallee Bay	This study
KRD231	Scotland Falls of Lora	This study
KRD240	Scotland Falls of Lora	This study
KRD244	Scotland subsurface of Trallee Bay	This study
KRD247	Scotland Falls of Lora	This study
KRD257	Scotland subsurface of Trallee Bay	This study
Bacillus subtilis		ATCC 23857
Streptomyces griseus		NBRC 13350
Streptomyces coelicolor		ATCC BAA-471
Streptomyces rimosus		ATCC 10970
Corynebacterium glutamicum		ATCC 13032
Pseudomonas aeruginosa		UCBPP-PA14
Pseudomonas baetica a390		DSMZ 26532
Micromonospora echinospora		ATCC 15837
Nocardia farcinica		IFM 10152
Staphylococcus aureus		ATCC 43300
Escherichia coli		ATCC 25922
Enterococcus faecalis		ATCC 51299
Klebsiella pneumoniae		ATCC 700603
Acinetobacter baumannii		ATCC 19606

2.2 Phylogenetic analysis

The 16S rRNA gene (V1-V9) was amplified by PCR with the primers 27F (5′-AGAGTTTGATCMTGGCTCAG-3′) and 1492R (5′-TACGGY TACCTTGTTACGACTT-3′) (Lane, 1991) from Sigma-Aldrich UK. The 16S rRNA gene sequences of 51 strains used in this study and 14 reference strains were compared with GenBank sequences using the Basic Local Alignment Search Tool (https://blast.ncbi.nlm.nih.gov/Blast.cgi, Altschul *et al.*, 1990).

2.3 Tri-cultures and one-to-one cultures on solid media

Tri-cultures with three strains were performed on ISP2 media (30°C, seven days). Tri-cultures with *Pseudonocardia* strains were incubated for 15 days, until growth of

Pseudonocardia strains was observed. The phenotypic screening (changes in strain morphology, pigmentation, sporulation and inhibition) was performed at day seven of incubation. Interactions observed in tri-cultures were tested a second time in a one-to-one culture (two strains). Plates were incubated (30°C, seven days) and screened for interactions.

2.4 Pre-conditioned solid media culture metabolite elicitation

A sterilised cellulose filter paper (Fisherbrand™ Grade 111 Cellulose Fast Qualitative Filter Paper) was added to a Petri dish containing 15mL of ISP2 medium and covered with 5mL of ISP2. The tri-culture was performed by streaking two producer strains on the cellulose paper and incubated (30°C, seven days). After the incubation time, the cellulose paper was removed and the challenged strain was streaked on the conditioned medium and incubated (30°C, seven days). One-to-one cultures were performed by streaking a producer strain on the cellulose paper and incubating (30°C, seven days). After the incubation time, the cellulose paper was removed and the challenged strain was streaked on the conditioned medium and incubated (30°C, seven days) as represented in **Figure 2.1.** A positive control of each culture was performed without growing strains on the conditioned media. ISP2 media with no bacterial culture and cellulose paper was used as a negative control.

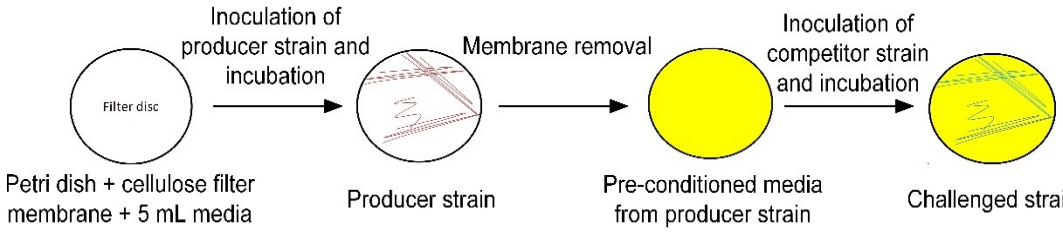

Figure 2.1. Pre-conditioned media method. A sterilised cellulose filter paper was added to a Petri dish and covered with ISP2. The producer strains were streaked on the cellulose paper and incubated. Then the cellulose paper was removed and the challenged strain was streaked on the conditioned medium.

2.5 Antibacterial activity plug assays

Indicator strains (*P. aeruginosa* PAO1, *S. aureus* ATCC43300, *E. faecalis* ATCC51299, *K. pneumoniae* ATCC700603, *A. baumannii* ATCC19606 and *E. coli* ATCC25922) were grown overnight in 5mL of nutrient broth (37°C, 200rpm). Bacterial cultures were then mixed with 5mL of soft nutrient agar to a final OD_{600} of 0.1 and

poured onto a Petri dish containing 10mL of nutrient agar. Once solidified, agar plugs (8.8mm in diameter) of the interactions and mono-cultures were deposited on the agar surface of the plates previously inoculated by the pathogens. An ISP2 media plug was used as control. Plates were incubated (24 hours, 37ºC) and the inhibition zones were measured (mm).

2.6 Metabolite extraction of bacterial cultures on solid media

Solid ISP2 media cultures were cut in 10 x 10mm pieces and freeze-dried (Labconco FreeZone 2.5L Freeze Dry System). Dried cultures were transferred to a clean Erlenmeyer flask (50mL). Metabolites were twice extracted (over two days) with 20mL of ethyl acetate (EtOAc). The EtOAc was removed each time into a pre-weighted 20mL glass scintillation vial, evaporated under nitrogen and the extract weight recorded (mg).

2.7 Antibacterial assays of bacterial extracts

Extracts were screened for antibacterial activity against indicator strains as per section 2.5. Instead of plugs sterile paper discs (6 mm diameter) with 20µL of each EtOAc bacterial extract (1mg / 1mL) were placed onto the agar plates previously inoculated with each pathogen. ISP2 media was used as a negative control and the antibiotics chloramphenicol (*S. aureus* and *E. coli*) and imipenem (*K. pneumoniae*, *Actinobacter baumannii*, *P. aeruginosa* and *E. faecalis*) (Sigma-Aldrich UK) were used as a positive control.

2.8 Time-course experiment in liquid media (ISP2 broth)

Time-course experiments were performed on ISP2. Sterile glass beads (one mm) were added to the the *Micromonospora* KRD244 cultures before strain inoculation. Optical density $(OD)_{600}$ readings were taken every two hours for *Rhodococcus* KRD226 and every 24 hours for *Micromonospora* KRD244. Prior to the OD measurements, cultures were vortexed for 30 seconds.

For the co-cultures, the liquid mono-culture of each strain (20mL) was mixed in a 250mL Erlenmeyer flask at the same time when both strains were in transitional phase (transitional phase co-culture). Co-cultures were incubated in a shaker (seven days, 30°C, 200rpm). For the second co-culture, both strains were incubated until they reached transitional phase. Then, a single colony of the competitor strain was inoculated on the mono-culture growing in transitional phase. Co-cultures were

incubated in a shaker (seven days, 30°C, 200rpm). For the third co-culture, the liquid mono-culture of each strain (20mL) was mixed in a 250mL Erlenmeyer flask at the same time when both strains were in transitional phase (transitional phase co-culture) and incubated in a shaker (30°C, 200rpm). Co-cultures were extracted at four time points (seven days, 14 days, 21 days and 28 days). Co-cultures of both strains inoculated together from time point zero (lag-phase co-culture) and mono-cultures of each strain were used as controls.

Viability tests were performed by streaking 20µL aliquots of each liquid co-culture on an ISP2 plate. Plates were incubated (seven days, 30°C).

2.8.1 Pre-conditioned liquid media culture

The *Rhodococcus* KRD226 and *Micromonospora* KRD244 strains were cultured on ISP2 broth with sterile beads for the *Micromonospora* cultures and incubated (30°C, 200 rpm) until they reached transitional phase. The liquid transitional-phase mono-culture of each strain was filtered with a 0.22µm syringe filter. *Rhodococcus* KRD226 transitional-phase mono-culture (not-filtered) was inoculated into the *Micromonospora* KRD244 pre-conditioned medium. *Micromonospora* KRD244 transitional-phase mono-culture (not-filtered) was inoculated into the *Rhodococcus* KRD226 pre-conditioned medium. For time-course experiments the pre-conditioned media co-cultures were extracted at each time point (seven, 14, 21 and 28 days). Transitional-phase mono-cultures and pre-conditioned media cultures of each strain were used as controls.

2.9 Metabolite extraction from liquid cultures

Autoclaved Diaion® HP20 (Alfa aesar) was added to each culture (5% w/v) and shaken overnight. Cultures were centrifuged (2000rpm, 10min, 4°C) and the supernatant was discarded. The cell/HP-20 resin pellet for each strain was frozen (-80°C) and lyophilised (Labconco FreeZone 2.5L Freeze Dry System). Once dry, each cell/HP-20 resin pellet was transferred to a clean Erlenmeyer flask (250mL) and twice extracted over two days with 20mL of EtOAc. The EtOAc was removed each time into a pre-weighted 20mL glass scintillation vial. The EtoAc was evaporated under nitrogen and the extract weight was recorded (mg).

2.10 LC-MS

2.10.1 Sample preparation

EtOAc extracts were resuspended in acetonitrile (ACN) to a concentration of 1mg / 1mL and one mL was transferred to a 1.5mL LC-MS vial. ISP2 medium and solvent blanks were used as controls.

2.10.2 LC-MS analysis of solid cultures

The LC-MS was performed with a Thermo Scientific Exactive mass spectrometer with Dionex UltiMate 3000 U-HPLC. ACE UltraCore 2.5 Super C18, 50 x 2.1mm, 5µm column (Advanced Chromatography Technologies Limited, Aberdeen, Scotland). The LC-MS system was run in binary gradient mode with an injection volume of 10µL at a flow rate of 400µL/min and 25°C. The gradient profiles consisted of (A) H2O + 0.1% FA and (B) ACN + 0.1% FA. Initially, the gradient conditions were 70% A to 10% A from 0min to 35min, followed by 10% A from 35min to 40min, and finally, from 90% to 70% A from 40min to 41min and maintained for 4 minutes at 70% A until the end of the chromatographic step. Collision energy was 35V. The analysis was done in both positive and negative ionisation modes.

2.10.3 LC-MS analysis of liquid cultures

The LC-MS system was run in binary gradient mode with an injection volume of 10 µL at a flow rate of 400 µL/min and 25 °C. The gradient profiles consisted of (A) H2O + 0.1% FA and (B) ACN + 0.1% FA. Initially, the gradient conditions were 70% A to 50% A from 0min to 5min, followed by 50% A from 5min to 30min, 5% A from 30min to 36min and from 5%A to 70% A from 36min until the end of the chromatographic step. Collision energy was 35 V. The analysis was done in both positive and negative ionisation modes.

2.10.4 Metabolomics data pre-processing

LC-MS data was split into positive mode and negative mode using MassConvert tool from Proteowizard (Chambers *et al.*, 2012). Data (mzML format) was processed with MZmine 2.38 (Pluskal *et al.*, 2010) for peak detection, chromatogram deconvolution and peak alignment. Peak detection analysis was carried out by using the centroid mode in each spectrum and noise level of 1×10^3. Chromatograms were built for each of the mass values with the minimum time span of 0.2 min and *m/z* tolerance of 5

ppm. The minimum intensity of the highest data point in the chromatogram was set at 1×10^4. Chromatogram deconvolution was carried out with the local minimum search algorithm. Peaks were then deisotoped and aligned. The resulting aligned peak list was gap-filled and all peaks found in solvent and media blanks above $1x10^5$ intensity level were subtracted. Adducts and complexes were identified and the molecular formula for all other ion peaks was predicted. The final peak lists for positive and negative mode were imported as CSV files which included one sample per column and one variable (peak) per row.

2.10.5 Multivariate data analysis of LC-MS data

The resulting CSV files were uploaded into MetaboAnalystR 2.0 (Chong *et al.,* 2019) software for data normalisation by Pareto scaling (mean-centred and divided by the square root of the standard deviation of each variable) and further multivariate analysis. Pareto scaling reduced the effect of larger intensity ions. PCA and PLS-DA were built using the weighted average of the original variables, summarising the dataset into much fewer variables (scores) and using the first five principal components (PCs). The PCA analysis was performed using the prcomp package, the PLS regression using the plsr function provided by R pls package and cross validation with the caret package. PLS-DA cross-validation was performed using the R2 and Q2 coefficients. VIP scores were determined using the weighted sum of squares of the PLS-DA loadings. The hierarchical clustering was generated by organising the variables and experimental groups according to their similarity. Hierarchical clustering was performed with the hclust function from the package stat. Euclidean distance was used as similarity measure. Each sample began as a separate cluster and the Ward's linkage algorithm (clustering to minimize the sum of squares of any two clusters) proceeded to combine them until all samples belonged to one cluster. Hierarchical clustering was visualised with a heatmap representation. Volcano test combined fold change analysis and t-tests. The volcano plot was constructed by comparing absolute value changes between two group means. This was performed by plotting the fold change against the negative log (-10) of the p value.

2.11 ToF-SIMS

2.11.1 Bacterial culture dehydration by oven-drying

ISP2 plates (10mL) were prepared (all in triplicate); 1- agar alone 2- *S. griseus* and 3- *Rhodococcus* KRD231. Plates were incubated (7 days, 30°C). After incubation,

cultures were cut into small sections (10mm x 2mm), and placed on the side (transversal sections). These were transferred to a microscope and dried (2 hours, 45°C).

2.11.2 Bacterial culture dehydration by freeze-drying

Bacterial cultures were prepared following the oven-dried method (transversal sections of 10mm x 2mm). Cultures were transferred to a microscope slide, frozen overnight (-80°C) and lyophilised (Thermo Electron micro modulyo-230 freeze-drier) during four hours.

2.11.3 Metabolite imprinting on cellulose membranes

Cellulose membranes (Fisherbrand™ Grade 111 Cellulose Fast Qualitative Filter Paper) were placed on top of the bacteria and a slight pressure was applied for 30s. Bacterial imprinting was oven-dried for ten minutes. A cellulose membrane and agar imprinting were used as controls.

2.11.4 Bacterial culture dehydration by nitrogen-drying

Nitrogen-dried cultures were prepared following a protocol from Dunham *et al.* (Dunham *et al.,* 2018). ISP2 plates were prepared (7.5mL). Bacterial cultures were incubated (7 days, 30°C). After incubation, a slice containing bacterial lawn was cut (10mm x 5mm) and transferred to a microscope slide, where double sided sticky tape was previously placed. Cultures were dried under nitrogen during one hour.

2.11.5 ToF-SIMS instrument, mode and data analysis

Bacterial samples were analysed with a TOF.SIMS^5 (IONTOF GmbH, Münster, Germany). An electron flood gun was used for charge compensation, and the surface potential of the sample holder was adjusted as necessary. Data was collected over a 500 x 500µm area of the culture in delayed extraction mode and standard spectrometry mode with a Bismuth Ion Cluster Bi_3^+ primary ion source at 30 keV over an *m/z* range of 0 to 2062. The primary ion beam current was 0.53 – 0.56 pA at a cycle time of 150µs. Cultures were analysed in both positive and negative ion mode across the surface with a 128x128µm pixel raster size and a primary ion dose density of $5x10^{11}$ ions/cm^2. To reassure reproducibility, the analysis was performed three times for each of the three conditions in each ionisation mode. This was a total of six repeats per each experimental replicate (three repeats per each mode) and 18

repeats for each condition (all experimental replicates, nine repeats per each mode). Data processing and analyses were performed using SurfaceLab 7.0 (IONTOF GmbH, Germany).

2.11.6 Method validation for bacterial culture nitrogen-drying sample preparation

The bacterial interaction between *Microbacterium* KRD174, *Rhodococcus* KRD231 and *S. griseus* and a *S. rimosus* ATCC10970 mono-culture (oxytetracycline producer) were analysed following the nitrogen-drying method as per section 2.11.4. Mono-cultures of each strain, pure tetracycline in a disc and pure tetracycline (Sigma-Aldrich UK) added to Emerson's agar at a concentration of 1mg / mL, 10µg / mL and 1µg / mL were used as controls.

CHAPTER 3: SCREENING OF BACTERIAL INTERACTIONS

The natural environment contains a high microbial diversity. For this reason, it is assumed that specialised metabolites are produced for the acquisition of nutrients and space or to compete against other organisms (Ruhe *et al.,* 2013). Specialised metabolites are also produced as beneficial resources leading to coexistence and survival of strains in a bacterial community (Wright and Vetsigian, 2016). However, there is still a lack of knowledge for how bacterial species interact and the impact of these interactions in secondary metabolism (Zhang *et al.*, 2020). A main challenge remains in understanding the likeliness that two strains interact with each other and the balance between competition and cooperation (Coyte and Rakoff-Nahoum, 2019). Furthermore, the fact that it is not clear if these interactions are correlated with phylogeny and isolation location, complicates the understanding of bacterial interactions (Vetsigian *et al.,* 2011; Garbeva *et al.*, 2014; Kinkel *et al.*, 2014; Zelezniak *et al.*, 2015; Ghoul and Mitri, 2017; Russel *et al.*, 2017). Additionally, competition and cooperation patterns differ depending the number of strains involved in the interaction. For instance, co-culture elicitation approaches of two-strain interactions might not predict all interactions that occur between more than two competitors (Hiscox *et al.*, 2017; Mayfield and Stouffer, 2017; Momeni *et al.,* 2017). Therefore, strains that co-exist in two-strain systems may not co-exist in multi-strain communities and a strain that outcompetes neighbouring species in pairwise assays can go extinct in multi-species interactions (Manhart and Shakhnovich, 2018). Despite this uncertainty, bacterial interactions are a potential approach for the production of bioactive specialised metabolites against clinically relevant human pathogens (Yu *et al.*, 2019).

As previously discussed, bacterial interactions often affect the strain phenotype such as producing inhibitory growth or producing a bald phenotype (sporulating strains), which is correlated with the production of specialised metabolites (Romano *et al.*, 2018; Smith and Velicer, 2019; Sathe and Kümmerli, 2020). For instance, *B. subtilis* inhibited mycelial growth and spore germination of two fungal strains as a result of the production of fengycin and surfactin homologs (Defilippi *et al.*, 2017). In addition, bacterial interactions leading to inhibition of aerial hyphae development in *Actinobacteria* can impact the production of specialised metabolites as a result of the correlation between morphological and metabolic differentiation (Som *et al.*, 2017). Therefore, metabolites that affect the life cycle of sporulating *Actinobacteria*, might restrict the production of specialised metabolites by the sporulating strains, and this

should be considered. A previous study showed that *S. coelicolor* failed to produce aerial hyphae and spores under co-culture with *B. subtilis* (Straight *et al.,* 2006). Close examination of this assay revealed that surfactin produced by *B. subtilis* interfered with *S. coelicolor* aerial hyphal development resulting in a bald phenotype (Straight *et al.,* 2006). For instance, surfactin mutants did not affect *S. coelicolor* growth development. These results suggested that specialised metabolites produced by one strain can affect the development of other strains and, in turn, the production of metabolites that are linked with morphological differentiation. Other bacterial mechanisms that can also lead to morphological alterations are nutrient depletion and inhibitory systems (Ruhe, Low and Hayes, 2013; Patin *et al.*, 2016; Perault and Cottera, 2018). Strains that contain inhibition systems are capable of inhibiting competitors during cell-to-cell contact. *Burkholderia dolosa* strain AU0158 contains three contact-dependent growth inhibition systems that are capable of inhibiting the growth of neighbouring bacterial strains (Perault and Cottera, 2018). Furthermore, nutrient depletion was observed by *S. tropica* CNY-681 when co-cultured with environmental strains (Patin *et al.*, 2018). The co-culture assay revealed that the increased production of lomaiviticin observed in the co-cultures was linked to nutrient depletion (Patin *et al.*, 2018). This indicated that the environmental strain enhanced the growth cycle of *S. tropica* CNY-681 in response to nutrient depletion, increasing lomaiviticin production at earlier incubation times (Patin *et al.*, 2018). These findings suggested that metabolite production is not always responsible for phenotypic effects and this should be considered.

A technique that is successful in the identification of strain phenotypic alterations as a result of metabolite production is pre-conditioned media (Pishchany *et al.*, 2018). The fact that under pre-conditioned media the strains are not in physical contact, observed phenotypic alterations are likely a result of metabolite production. However, it is important to consider that bacterial interactions in a community are complex (Freilich *et al.*, 2011). For that reason, interactions observed in a laboratory setting do not reflect nature but aid the understanding of chemical exchange (Freilich *et al.*, 2011). An important limitation to consider when using co-culture methods in the laboratory is the poor reproducibility of these which can result from the chosen co-culture method, culture media, distance between the strains and incubation time (Martínez-Buitrago *et al.,* 2019). For instance, specialised metabolite production in *Actinobacteria* is linked to nutrient resources and the conditions found in the environment (van Der Meij *et al.*, 2017). This results from the fact that bacteria must

constantly adapt to changes in the environment. Therefore, they have developed mechanisms such as carbon catabolite repression to modulate metabolism and growth (Romero-Rodríguez *et al.,* 2016). Carbon catabolite repression enables bacteria to use a preferred carbon source in a mixture present in the culture medium (Romero-Rodríguez *et al.,* 2016). Generally, the preferred source of carbon for *Streptomyces* is glucose which enables fast growth (Demain, 1989). However, the repression of genes used in the uptake of glucose can lead to the expression of a minimal number of secondary metabolites-associated genes (Romero-Rodríguez *et al.,* 2017). Therefore, limiting the production of metabolites. Diverse mechanisms are described to explain the negative effects of carbon catabolite repression on specialised metabolite production. In *Streptomyces*, glucokinase (Glk) is a key player in carbon catabolite repression (Gubbens *et al.,* 2012). The enzyme Glk catalyses the phosphorylation of glucose to yield glucose 6-phosphate with a phosphoryl donor such as ATP, ADP, or inorganic polyphosphate (Kawai *et al.,* 2005). For instance, mutants of *S. coelicolor* resistant to the non-metabolizable glucose analogue 2-deoxyglucose that use glycerol, arabinose, galactose and fructose in the presence of glucose (Hodgson, 1982) indicated that Glk encoded by *glkA* is the main effector of repression (Kwakman *et al.,* 1994). *S. coelicolor* grown with high glucose concentration led to bald phenotypes and the down-regulation of seven genes involved in actinorhodin production and ten genes involved in undecylprodigiosin production (Romero-Rodríguez *et al.*, 2016). Similarly, 0.1% of glucose repressed the expression of *afsR2* gene necessary for the production of actinorhodin by *Streptomyces lividans* (Kim *et al.* 2001). This prevented actinorhodin production (Kim *et al.* 2001). Other carbon sources such as glycerol, maltose and sucrose can also lead to carbon catabolite repression. For example, cephalosporin production in *Streptomyces clavuligerus* depends on glycerol concentration (Aharonowitz and Demain 1978). High glycerol concentration reduced the production of metabolites (Aharonowitz and Demain 1978). Therefore, since carbon sources are linked to morphological and metabolic differentiation (Demain, 1989), they can also play a role in competition between strains. This results from the fact that microbial growth rate and specialised metabolites production can support successful competition (Gorke and Stülke, 2008). Additionally, because co-cultures generate biotic factors, represent an approach that can activate cryptic or poorly expressed BGCs (Tomm *et al.,* 2019).

In this chapter, bacterial one-to-one cultures (two strains), tri-cultures (three strains) and pre-conditioned media were phenotypically screened in order to identify bacterial

interactions. This consisted of a phenotypic assessment of the bacterial strains at day seven of incubation where co-culture morphological alterations indicated possible bacterial interactions. The phenotypic alterations included in this criterion were; strain morphology such as slower growth, inhibition of aerial hyphae growth or sporulation (bald and *whi* phenotypes), growth inhibition and pigmentation production. Pre-conditioned media tested if the variations observed in the morphology of the strains were a result of metabolite production.

3.1 Aims and objective

The objective of this chapter was to evaluate the impact of bacterial interactions on the strains ability to produce specialised metabolites with a main focus on actinobacterial species. This was evaluated by a phenotypic screening of bacterial co-cultures using three co-cultivation methods (one-to-one cultures, tri-cultures and pre-conditioned media).

Aim 1: to optimise and conduct co-culture solid media experiments and correlate bacterial interactions to strain phenotypic alterations.

Aim 2: to assess phenotypic alterations, strain taxonomy and bioactivity screening results to prioritise co-cultures for metabolite extractions.

Aim 3: to assess bioactivity screening results from metabolite extractions to prioritise co-cultures for MS-based comparative metabolomics.

3.2 Results

In order to prioritise bacterial interactions for MS-based comparative metabolomics, the workflow of this chapter was separated in several steps (**Figure 3.1**). A total of 51 strains were selected from the laboratory collection to include strains isolated from different locations as well as from the same gram of sediment and to include strains belonging to a range of rare *Actinobacteria* genera as well as the *Streptomyces* genus. Additionally, *B. subtilis*, *P. baetica* and *P. aeruginosa* were included in the study to evaluate the likeliness of non-actinobacterial strains to interact with *Actinobacteria*. In order to achieve growth of the strains, ISP2 supplemented with instant ocean was used as enrichment protocol for growth of marine *Actinobacteria*. Instant ocean was used to mimic marine environmental conditions where salt concentration is higher than in freshwater. After strain selection, tri-cultures were performed in order to identify phenotypic alterations as a result of the interactions. Tri-cultures were selected as a co-culture method since they allow the screening of bacterial interactions without losing information of the interacting strains as opposed to competition assays with a larger number of strains. In order to analyse which strains induced phenotypic responses, tri-cultures showing morphological alterations were analysed in one-to-one cultures (two strains). All mono-cultures, tri-cultures and one-to-one cultures were screened for antibacterial activity against indicator strains to prioritise interactions for metabolite extraction. Solid media metabolites of bioactive mono-cultures, tri-cultures and one-to-one cultures were extracted and screened for antibacterial activity in order to prioritise bacterial interactions for LC-MS analysis.

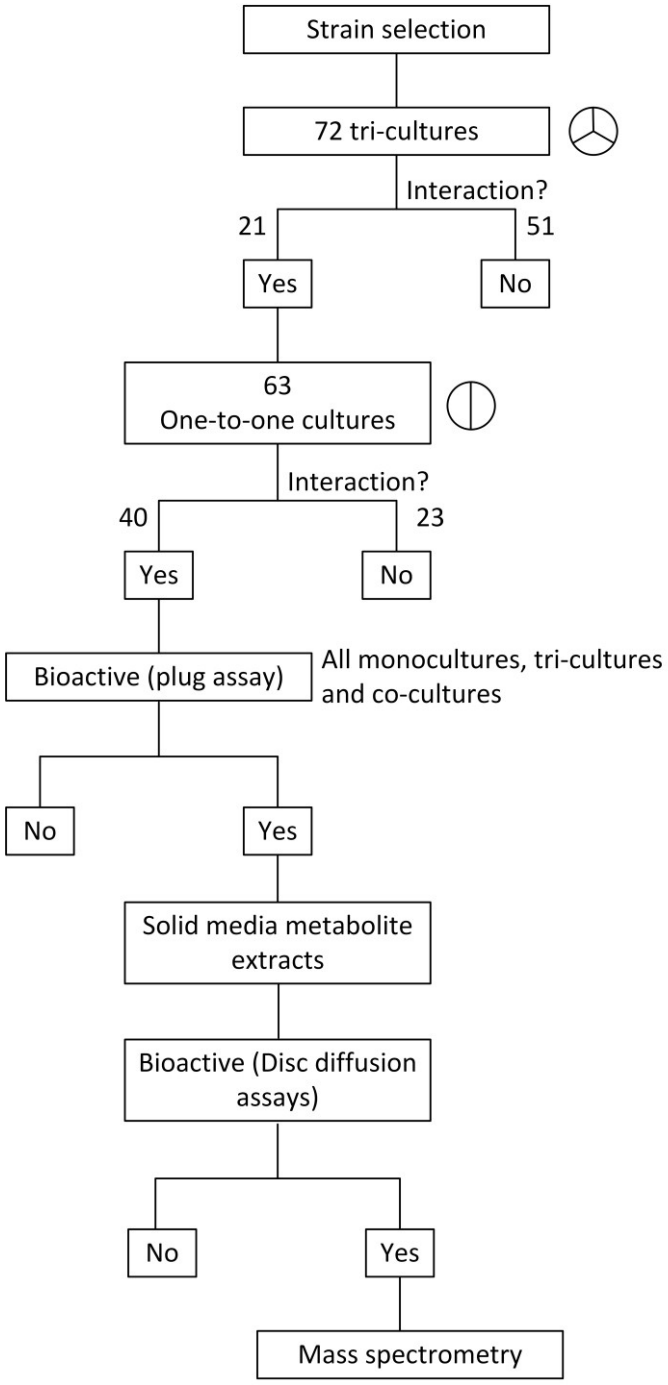

Figure 3.1. Diagram outlining the workflow followed in this chapter. Strains were selected and 72 tri-culture assays were performed and screened for phenotypic alterations. One-to-one cultures (63) were performed and screened with tri-cultures that showed a phenotypic response (21). All bacterial cultures were screened for antibacterial activity against indicator strains. Solid media metabolites of bioactive cultures were extracted and screened for antibacterial activity. One-to-one cultures and tri-cultures were prioritised for LC-MS analysis.

3.2.1 Phylogenetic analysis of bacterial strains

To identify the environmental isolates at genus level, the 43 16S rRNA gene sequences were compared with GenBank sequences. This analysis revealed that all strains isolated from marine sediments belonged to the *Actinobacteria* phylum (**Table 3.1**) and were classified into eight genera (16 *Micrococcus* sp., 11 *Pseudonocardia* sp., seven *Rhodococcus* sp., three *Microbacterium* sp., three *Streptomyces* sp., one *Micromonospora* sp., one *Salinibacterium* and one *Agrococcus* sp.). Strains isolated from other environments (*B. subtilis, S. griseus, S. coelicolor, Corynebacterium glutamicum, P. aeruginosa, P. baetica, Micromonospora echinospora* and *Nocardia farcinica*) represented three phyla (*Actinobacteria*, *Firmicutes* and *Proteobacteria*) and six genera; *Streptomyces, Corynebacterium, Micromonospora* and *Nocardia* for *Actinobacteria*, *Bacillus* for *Firmicutes* and *Pseudomonas* for *Proteobacteria*.

Table 3.1. 16S rRNA blast analysis results of environmental strains. ID (identity) and QC (query cover).

Strain	Closest NCBI Blast strain	Accession n°	%ID	%QC
KRD2	*Agrococcus baldri* IAM 15147	NR_041543.1	99%	99%
KRD4	*Micrococcus terreus* V3M1	NR_116649.1	100%	99%
KRD29	*Micrococcus yunnanensis* YIM 65004	NR_116578.1	100%	99%
KRD30	*Micrococcus yunnanensis* YIM 65004	NR_116578.1	100%	99%
KRD33	*Micrococcus aloeverae* AE-6	NR_134088.1	100%	99%
KRD70	*Micrococcus yunnanensis* YIM 65004	NR_116578.1	99%	99%
KRD77	*Micrococcus yunnanensis* YIM 65004	NR_116578.1	99%	99%
KRD79	*Micrococcus yunnanensis* YIM 65004	NR_116578.1	100%	99%
KRD81	*Micrococcus yunnanensis* YIM 65004	NR_116578.1	100%	99%
KRD87	*Micrococcus yunnanensis* YIM 65004	NR_116578.1	100%	99%
KRD88	*Micrococcus yunnanensis* YIM 65004	NR_116578.1	100%	99%
KRD118	*Micrococcus yunnanensis* YIM 65004	NR_116578.1	100%	99%
KRD122	*Micrococcus yunnanensis* YIM 65004	NR_116578.1	100%	99%
KRD128	*Micrococcus yunnanensis* YIM 65004	NR_116578.1	99%	99%
KRD136	*Micrococcus aloeverae* AE-6	NR_134088.1	99%	99%
KRD138	*Micrococcus yunnanensis* YIM 65004	NR_116578.1	99%	100%
KRD142	*Micrococcus yunnanensis* YIM 65004	NR_116578.1	99%	100%
KRD162	*Rhodococcus fascians* CF17	NR_037021.1	100%	99%
KRD163	*Pseudonocardia petroleophila* IMSNU 22072	NR_042005.1	100%	99%
KRD165	*Pseudonocardia petroleophila* IMSNU 22072	NR_042005.1	100%	99%
KRD172	*Microbacterium profundi* Shh49	NR_044321.1	100%	99%
KRD173	*Microbacterium profundi* Shh49	NR_044321.1	100%	99%
KRD174	*Microbacterium profundi* Shh49	NR_044321.1	100%	99%
KRD175	*Rhodococcus fascians* CF17	NR_037021.1	100%	100%
KRD176	*Pseudonocardia petroleophila* IMSNU 22072	NR_042005.1	100%	98%
KRD177	*Pseudonocardia seranimata* YIM 63233	NR_108393.1	99%	100%
KRD178	*Pseudonocardia petroleophila* IMSNU 22072	NR_042005.1	100%	99%
KRD179	*Pseudonocardia petroleophila* IMSNU 22072	NR_042005.1	100%	98%
KRD187	*Pseudonocardia petroleophila* IMSNU 22072	NR_042005.1	100%	98%
KRD188	*Pseudonocardia petroleophila* IMSNU 22072	NR_042005.1	100%	98%
KRD189	*Pseudonocardia seranimata* YIM 63233	NR_108393.1	100%	99%
KRD191	*Pseudonocardia seranimata* YIM 63233	NR_108393.1	99%	99%
KRD192	*Pseudonocardia seranimata* YIM 63233	NR_108393.1	99%	99%
KRD196	*Rhodococcus yunnanensis* YIM 70056	NR_043009.1	100%	99%
KRD197	*Rhodococcus yunnanensis* YIM 70056	NR_043009.1	100%	99%
KRD207	*Rhodococcus fascians* CF17	NR_037021.1	100%	99%
KRD211	*Streptomyces camponoticapitis* 2H-TWYE14	NR_152020.1	99%	99%
KRD226	*Rhodococcus erythropolis* N11	NR_037024.1	99%	99%
KRD231	*Rhodococcus wratislaviensis* NCIMB 13082	NR_026524.1	99%	99%
KRD240	*Salinibacterium amurskyense* KMM 3673	NR_041932.1	99%	98%
KRD244	*Micromonospora aurantiaca* ATCC 27029	NR_074415.1	99%	99%
KRD247	*Streptomyces* sp. strain MCA2	MT176506.1	99%	98%
KRD257	*Streptomyces fulvissimus* NA06532	CP054926.1	99%	98%

3.2.2 Tri-culture phenotypic screening reveals phenotypic alterations

In order to identify bacterial interactions, a phenotypic assessment of 72 tri-cultures with three cultivated strains was performed. Bacterial interactions were identified based on alterations in strain morphology, pigmentation, sporulation and inhibition in comparison to mono-culture controls. The phenotypic assessment revealed that 21 tri-cultures (29%) resulted in phenotypic alterations of at least one strain (**Figure 3.2**). From these, 17 tri-cultures (81%) showed inhibition of at least one strain, five tri-cultures (24%) induced pigmentation production, four showed bald phenotypes (19%), and one (5%) enhanced sporulation. Finally, one tri-culture (5%) showed increased production of pigmentation (**Figure 3.2**). **Figure 3.3A** shows an example of a tri-culture interaction where *Micrococcus* KRD172 was partly inhibited.Furthermore, pigmentation production of *S. coelicolor* towards the third strain (*Rhodococcus* KRD231) increased when compared to the mono-culture (**Figure 3.3B**). These data suggest that under co-cultivation, some bacterial strains have the ability to produce phenotypic alterations and this is specific to each interaction.

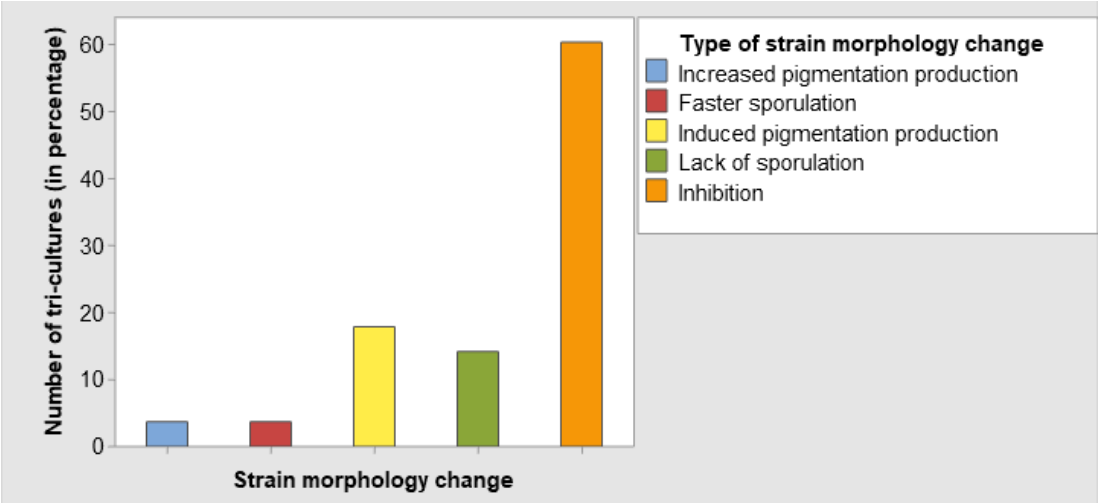

Figure 3.2. Tri-cultures revealed strain morphological alterations. Phenotypic alterations were classified into five classes (x-axis). The number of tri-cultures showing a phenotypic response is represented as percentage (y-axis).

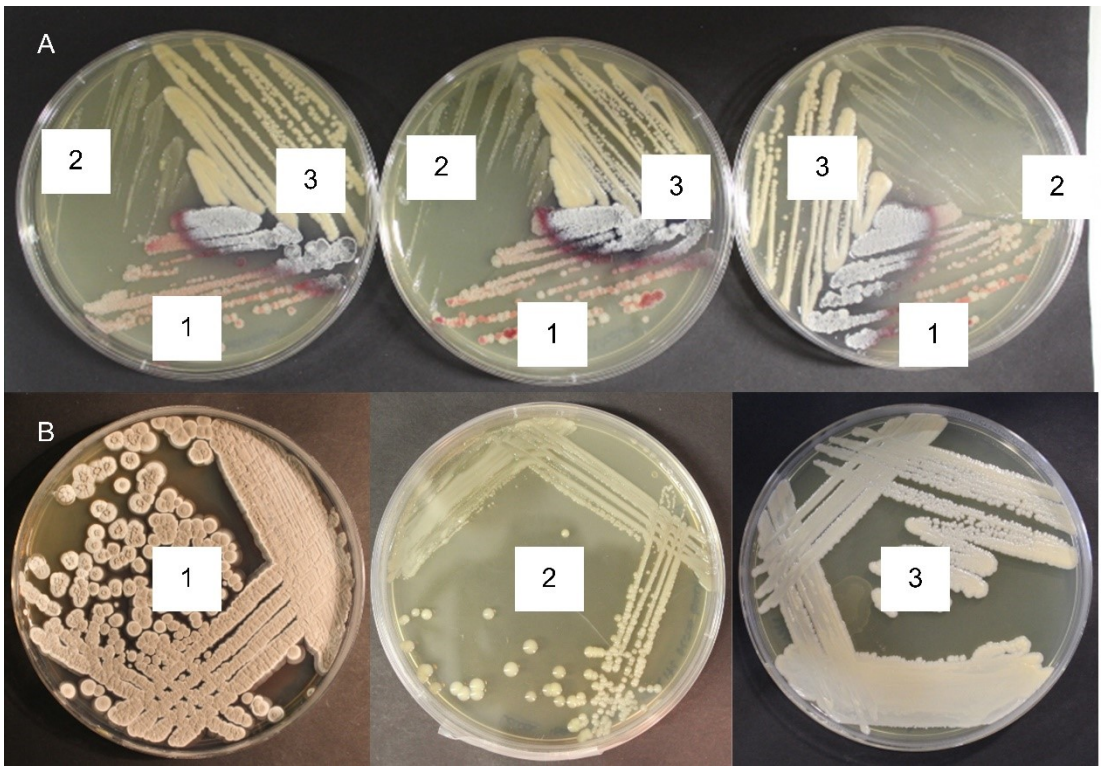

Figure 3.3. Tri-culture (in triplicate) reveals phenotypic alterations between the three strains. The tri-culture (A) shows inhibition of strain 2 (*Micrococcus* KRD172) and increased metabolite production of strain 1 (*S. coelicolor*) towards strain 3 (*Rhodococcus* KRD231). B) mono-culture of each strain (1: *S. coelicolor*, 2: *Micrococcus* KRD172 and 3: *Rhodococcus* KRD231).

Tri-culture results revealed that all cultures with *P. aeruginosa* inhibited at least one strain. Only *B. subtilis* was not affected by *P. aeruginosa*. *Micrococcus*, *Agrococcus* and *Microbacterium* strains were inhibited (**Figure 3.4**). Therefore, no growth of these three bacterial species was observed. For example, the tri-culture of *P. aeruginosa*, KRD29 (*Micrococcus* sp.) and KRD174 (*Microbacterium* sp.), showed inhibition of both KRD29 and KRD174 strains (**Figure 3.4**). Inhibition of *Rhodococcus* and *Streptomyces* was detected at the edge of the strains closer to the *P. aeruginosa* strain. For example, the tri-culture of *P. aeruginosa*, KRD142 (*Micrococcus* sp.) and KRD226 (*Rhodococcus* sp.), showed larger inhibition of KRD142 than of KRD226 (**Figure 3.5**). These data suggests that the capacity of *P. aeruginosa* to produce siderophores and scavenge iron, play an important role in the survival of this strain under co-culture. Furthermore, *Rhodococcus* strains inhibited or reduced sporulation and growth of some *Streptomyces* and *Microbacterium* strains. For example, the tri-

culture of *Micrococcus* KRD88, *Streptomyces* KRD211 and *Rhodococcus* KRD226 revealed that the *Streptomyces* was inhibited (**Figure 3.6**).

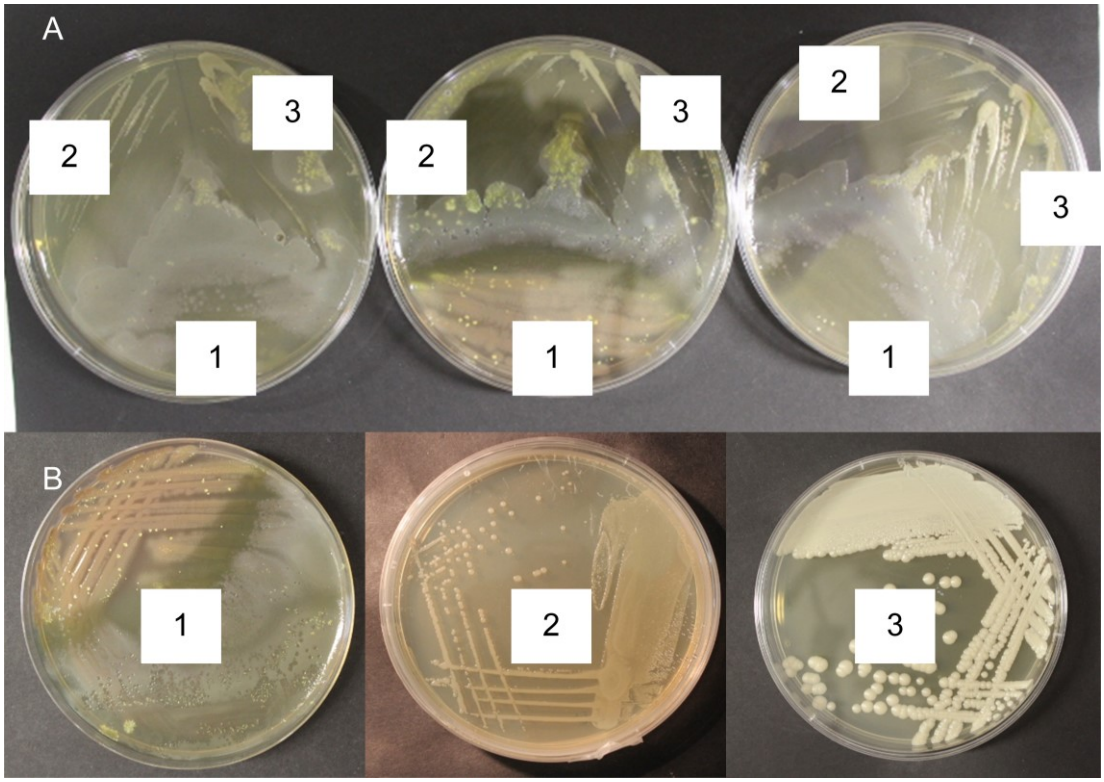

Figure 3.4. Tri-culture (in triplicate) reveals growth inhibition of *Micrococcus* KRD29 and *Microbacterium* KRD174. A-B) Tri-culture in triplicate and mono-cultures of *P. aeruginosa* (1), *Microbacterium* KRD174 (2) and *Micrococcus* KRD29 (3).

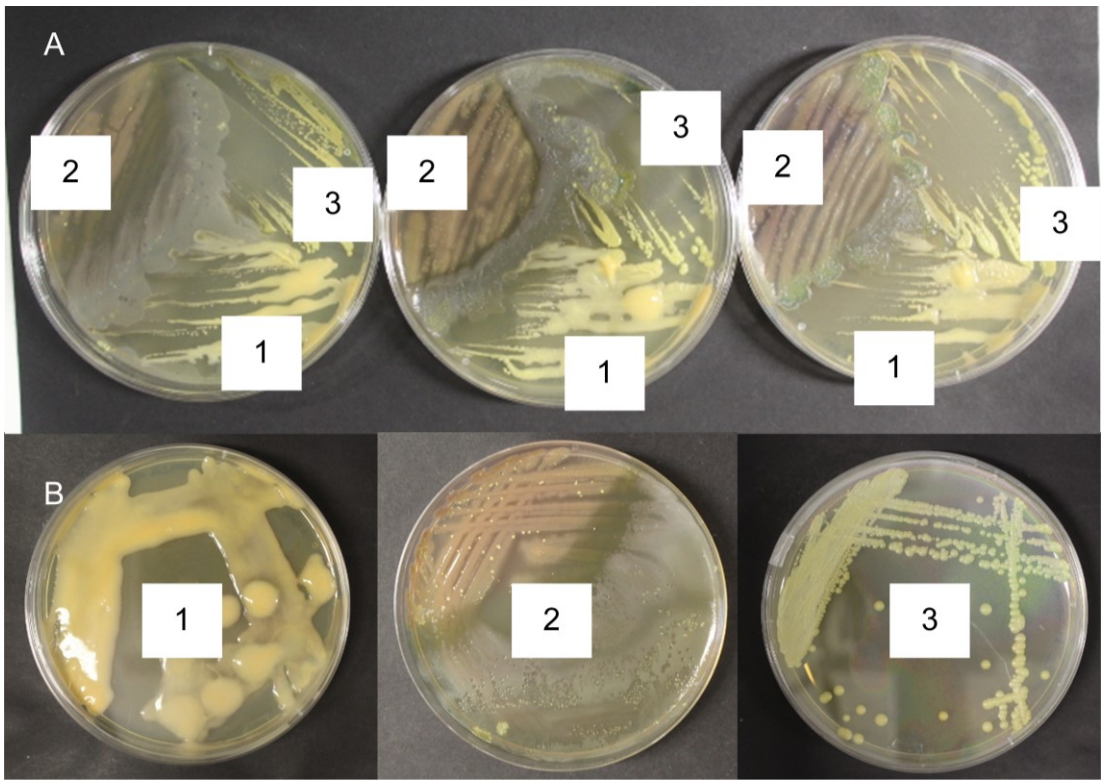

Figure 3.5. Tri-culture reveals growth inhibition of *Micrococcus* KRD142 and *Rhodococcus* KRD226 at the edge interface. A-B) Tri-culture in triplicate and mono-cultures of *Rhodococcus* KRD226 (1), *P. aeruginosa* (2) and *Micrococcus* KRD142 (3).

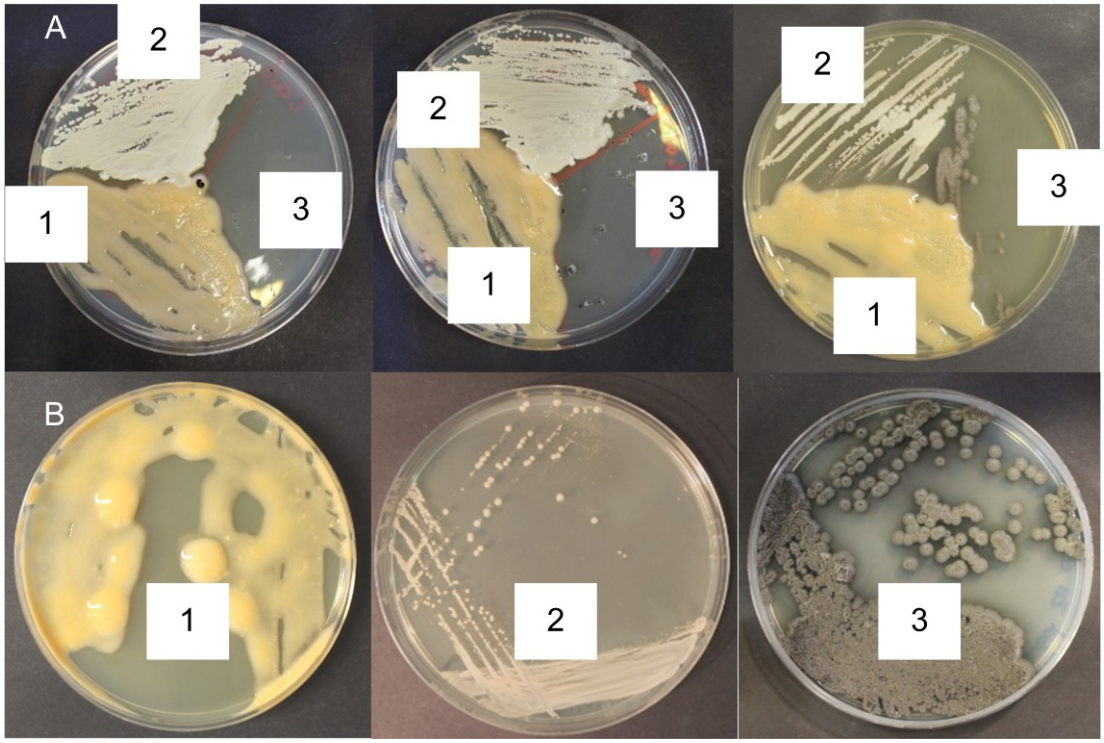

Figure 3.6. Tri-culture reveals growth inhibition of *Streptomyces* KRD211. A-B) Tri-culture in triplicate and mono-cultures of *Rhodococcus* KRD226 (1), *Streptomyces* KRD211 (2) and *Micrococcus* KRD88 (3).

The phenotypic screening of tri-cultures revealed that *Rhodococcus* strains induced pigment production. This pigmentation was not observed under mono-culture. For example, the interaction of *Rhodococcus* strains (KRD197 and KRD207) and *Microbacterium* KRD173, showed elicited pigmentation of KRD197 towards strain KRD207 (**Figure 3.7**). Furthermore, the tri-culture of *Rhodococcus* KRD226, *Micromonospora* KRD244, and *Streptomyces* KRD257 showed that *Streptomyces* KRD257 produced pigmentation turning the media to a greenish colour (**Figure 3.8**). This suggests the production of pigmented specialised metabolites as a result of bacterial interactions. In addition, the *Micromonospora* KRD244 presented reduced growth compared to the mono-culture and life cycle of the *Streptomyces* KRD257 (**Figure 3.8**). *Streptomyces* KRD257 also presented a white phenotype. These results suggest that the *Micromonospora* produced a bioactive metabolite that led to the elicitation of metabolites by the *Streptomyces.*

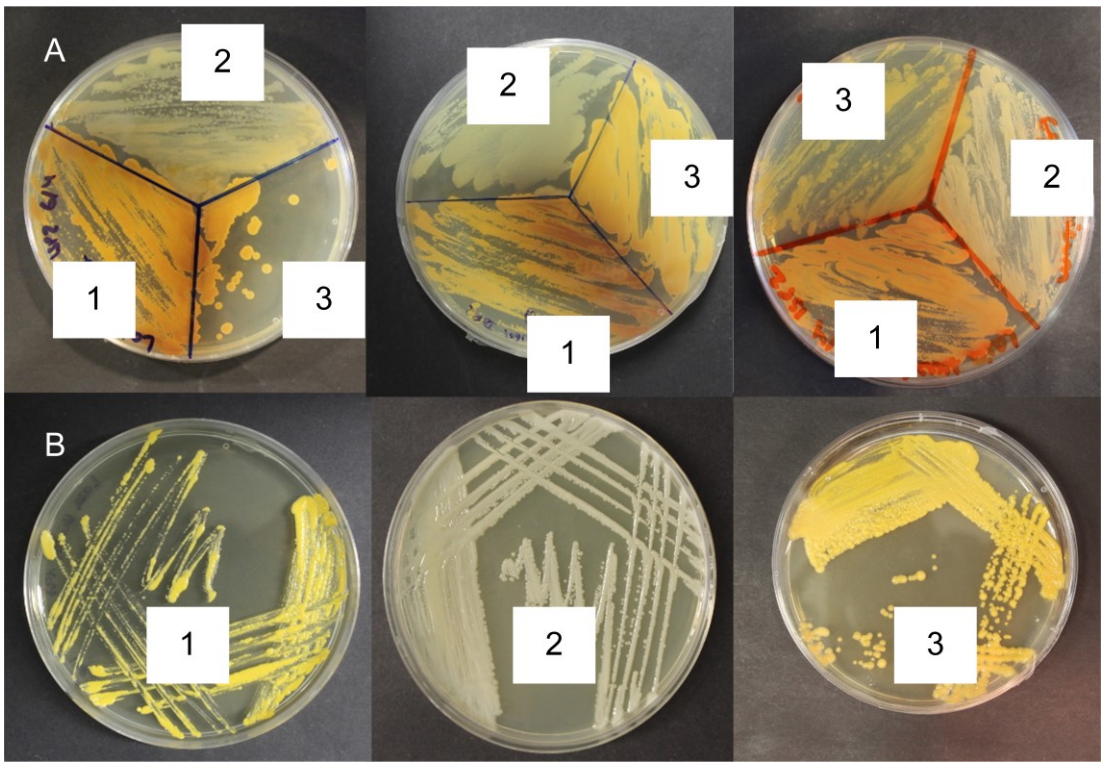

Figure 3.7. Tri-culture reveals elicited pigmentation by the *Rhodococcus* KRD197 against *Rhodococcus* KRD207. A-B) Tri-culture in triplicate and mono-cultures of *Rhodococcus* KRD197 (1), *Microbacterium* KRD173 (2) and *Rhodococcus* KRD207 (3).

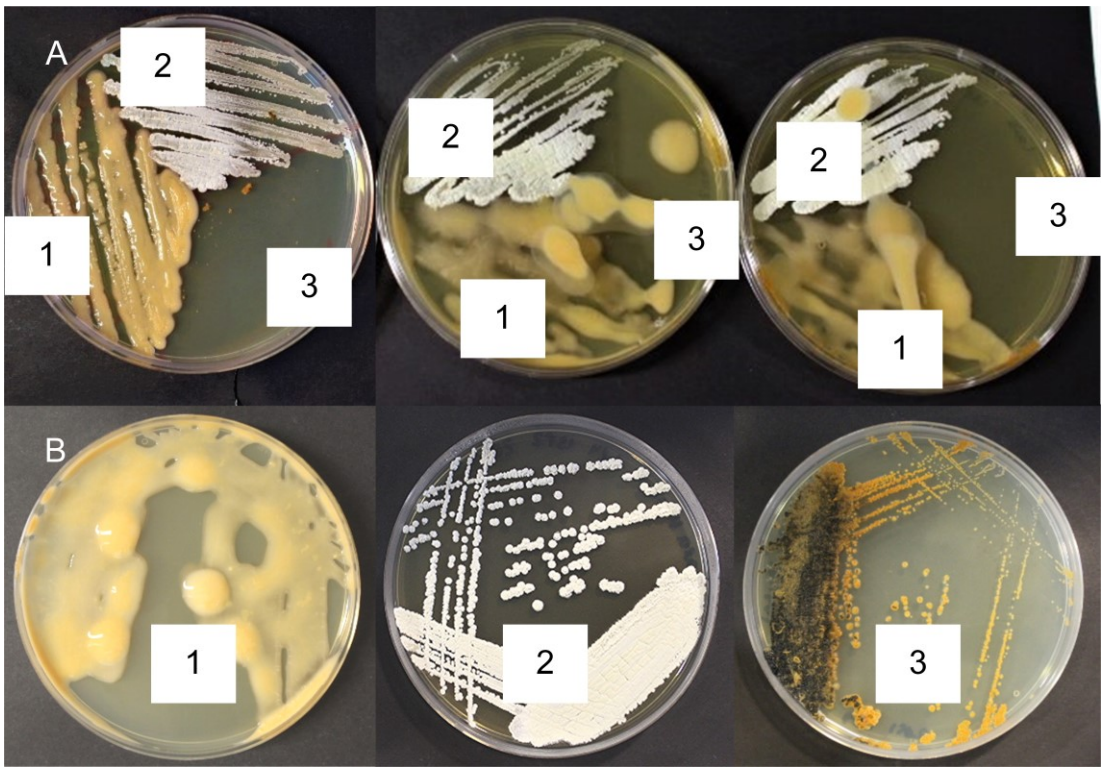

Figure 3.8. Tri-culture reveals a greenish pigmentation and a white phenotype of *Streptomyces* KRD257. A-B) Tri-culture in triplicate and mono-cultures of *Rhodococcus* KRD226 (1), *Streptomyces* KRD257 (2) and *Micromonospora* KRD244 (3).

A total of 43 (60%) tri-cultures did not result in morphological alterations. These were considered neutral interactions where the three strains coexisted. An example of this includes the tri-culture of *Micrococcus* KRD138, *Rhodococcus* KRD231 and *Streptomyces* KRD257 (**Figure 3.9**). Most (34) neutral interactions included *Micrococcus* strains, *Microbacterium* strains, *Pseudonocardia* strains or a combination of these. These data suggests that these three genera showed less reaction to growing with competitors than *Rhodococcus, Streptomyces* and *Pseudomonas* which were involved in more negative interactions. Additionally, these findings suggest that under these conditions, only a few bacterial strains resulted in competitive behaviours. Since tri-cultures showing morphological alterations compared to mono-cultures were prioritised for antibacterial activity screening, cultures that showed coexistence were not further analysed.

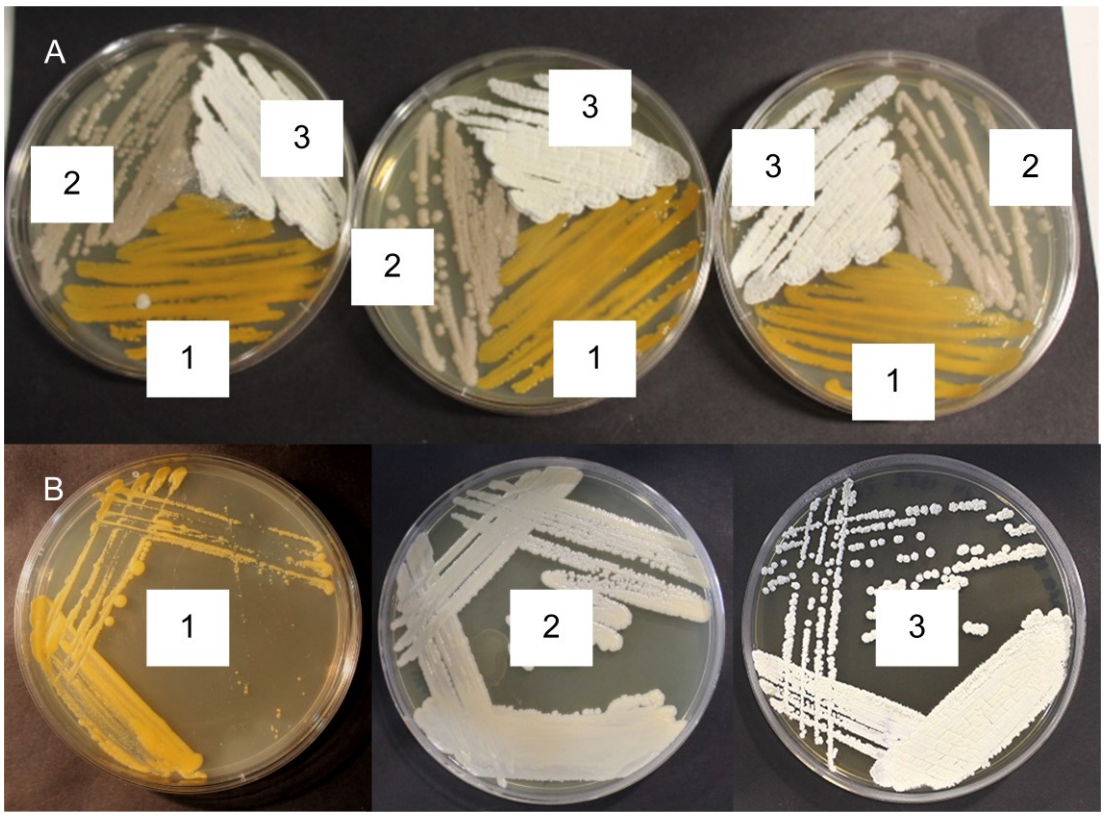

Figure 3.9. Tri-culture reveals coexistence between *Micrococcus* KRD138, *Rhodococcus* KRD231 and *Streptomyces* KRD257. A-B) Tri-culture in triplicate and mono-cultures of *Micrococcus* KRD138 (1), *Rhodococcus* KRD231 (2) and *Streptomyces* KRD257 (3).

3.2.3 One-to-one cultures phenotypic screening reveals strain specific interactions

In order to test if the interaction was a result of the presence of all three strains or if it was strain specific, tri-cultures were tested in a one-to-one culture (two strains). If the phenotypic alterations were tri-culture specific, the three strains were involved in the interaction while if they were strain specific the interaction was correlated to two strains. Therefore, the later would be also observed in the one-to-one cultures. To identify these phenotypic alterations one-to-one cultures were compared to mono-cultures.

The phenotypic screening revealed that a total of 40 (63%) one-to-one cultures resulted in a strain morphological alteration of at least one strain (**Figure 3.10**). Most one-to-one cultures (78%) showed inhibition of at least one strain, 15% of cultures elicited pigmentation, 15% showed lack of aerial hyphae growth or sporulation while

3% showed growth promotion (enhanced sporulation and/or spreading) (**Figure 3.10**). Finally, 5% of one-to-one cultures showed an increased production of pigmentation (**Figure 3.10**).

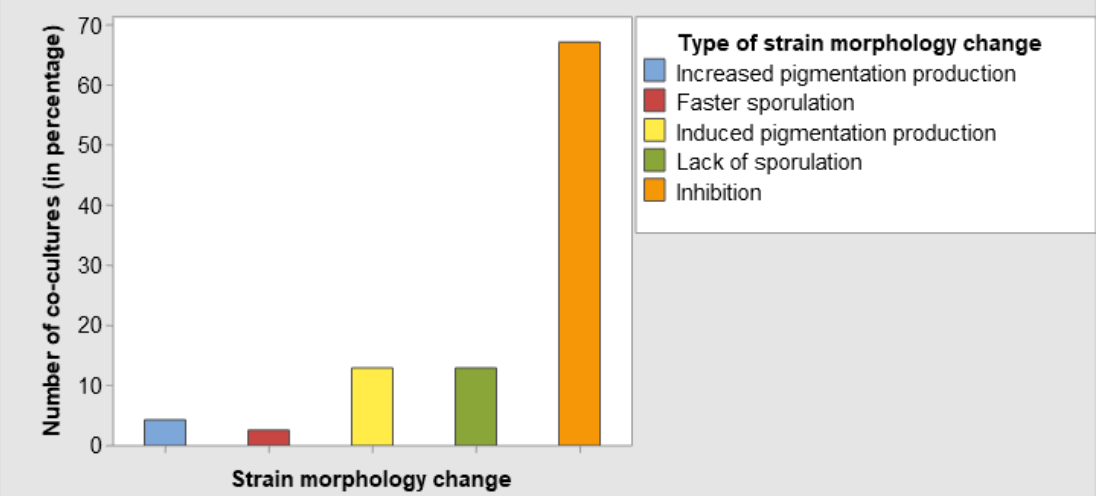

Figure 3.10. One-to-one cultures revealed strain morphological alterations. Phenotypic alterations were classified into five classes (x-axis). The number of tri-cultures showing a phenotypic response is represented as percentage (y-axis).

The phenotypic analysis of one-to-one cultures showed inhibition of all strains challenged against *P. aeruginosa* as previously observed in the tri-cultures. While *P. aeruginosa* inhibited complete growth of *Micrococcus*, *Agrococcus* and *Microbacterium* strains, *Rhodococcus* and *Streptomyces* strains were inhibited at the edge where in contact with *P. aeruginosa*. These patterns were previously observed in the tri-cultures. For example, while the *P. aeruginosa* inhibited complete growth of *Micrococcus* KRD128 (**Figure 3.11**), the growth of *Rhodococcus* KRD226 was inhibited at the edge where in contact with *P. aeruginosa* as previously observed in **Figure 3.5**. These data suggest a strain specific interaction induced by *P. aeruginosa*.

Rhodococcus strains affected the growth of *Streptomyces* strains. *S. griseus* showed delayed sporulation in the one-to-one culture against *Rhodococcus* KRD231 (**Figure 3.12**). Despite that these results suggest that cell-to-cell contact/metabolite production of the *Rhodococcus* affects the normal life cycle of the *Streptomyces* sp., *S. griseus* also grew poorly in mono-culture presenting a *whi* phenotype. In addition, one-to-one cultures revealed inhibition within strains of the genus *Rhodococcus* that was not observed previously in the tri-cultures. For example, strain KRD197 inhibited strain KRD207 in one-to-one cultures (**Figure 3.13**). This suggests that the interactions

observed in the tri-cultures were tri-culture specific while the interactions observed in the one-to-one cultures were strain specific. In addition, this indicates that pairwise interactions do not predict multi-strain interactions.

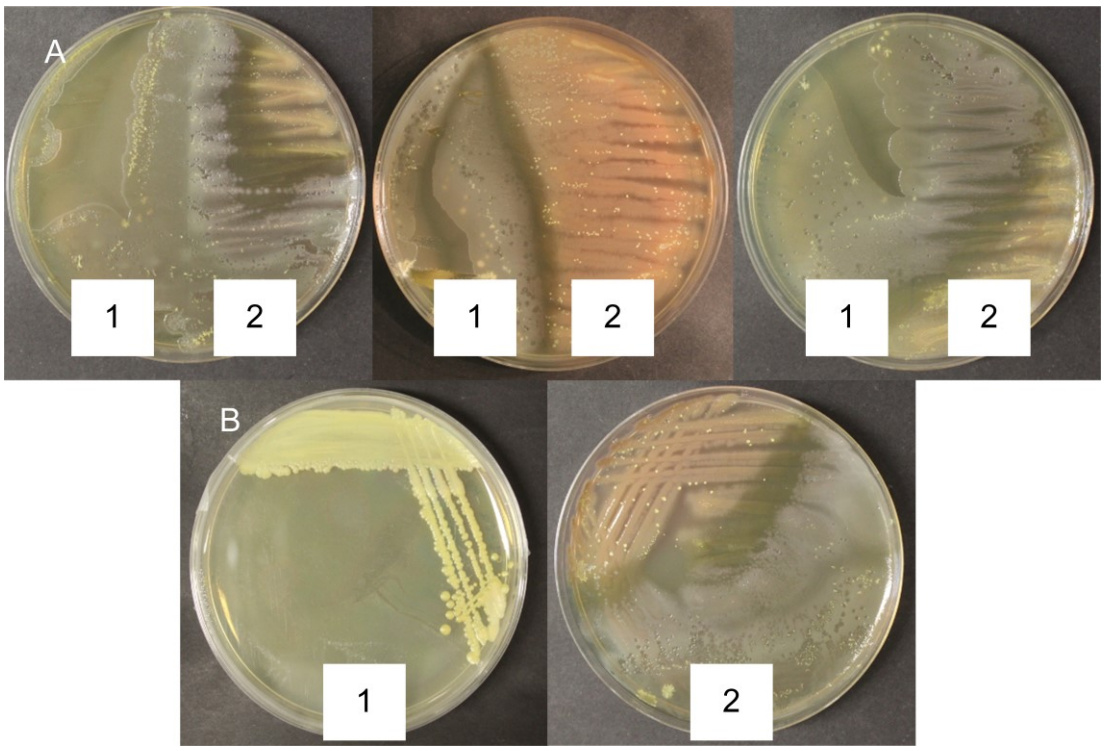

Figure 3.11. One-to-one culture reveals *P. aeruginosa* inhibiting *Micrococcus* KRD128. A-B) One-to-one culture in triplicate and mono-cultures of *Micrococcus* KRD128 (1) and *P. aeruginosa* (2).

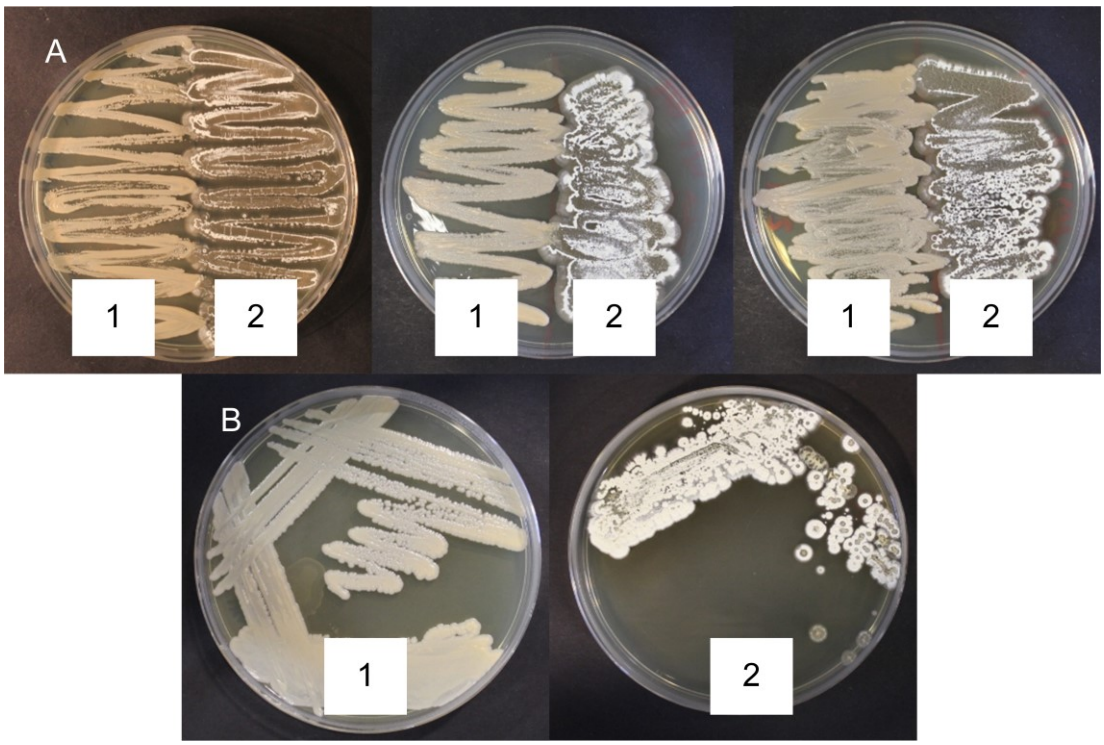

Figure 3.12. One-to-one culture reveals a bald phenotype of *S. griseus*. A-B) One-to-one culture in triplicate and mono-cultures of *Rhodococcus* KRD231 (1) and *S. griseus* (2).

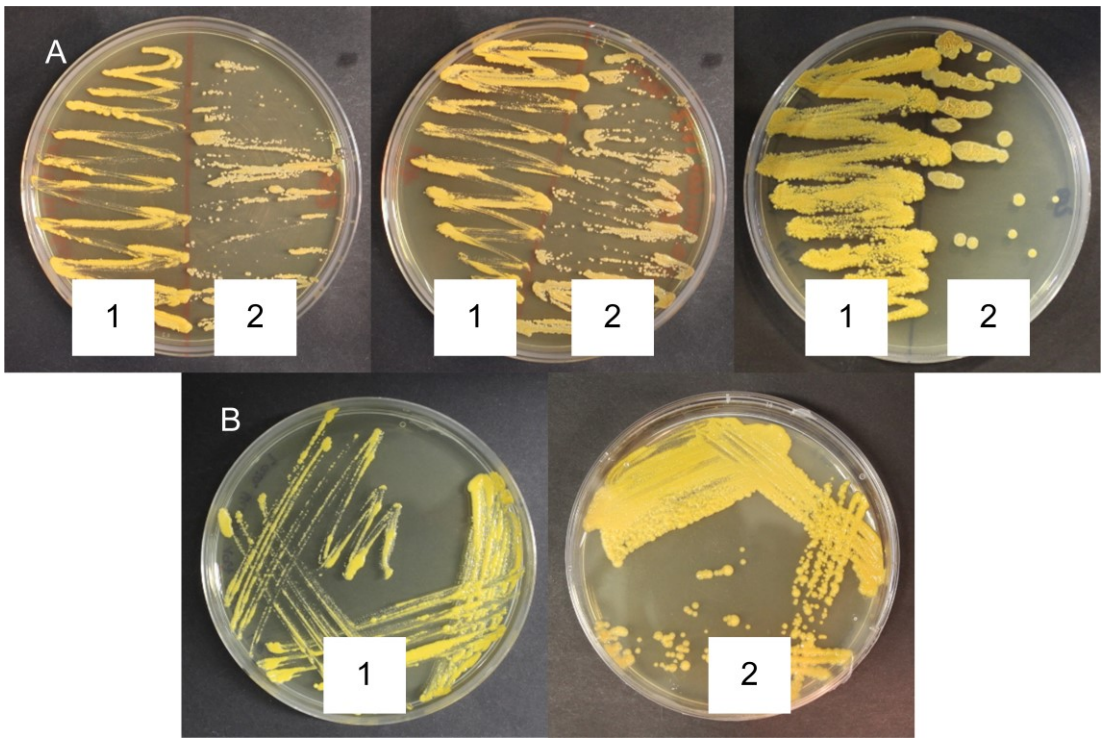

Figure 3.13. One-to-one culture reveals inhibition of *Rhodococcus* KRD207. A-B) One-to-one culture in triplicate and mono-cultures of *Rhodococcus* KRD197 (1) and *Rhodococcus* KRD207 (2).

One-to-one cultures of *Streptomyces* and *Microbacterium* strains revealed growth inhibition of *Microbacterium* strains (**Figure 3.14**). In addition, previous tri-cultures results with three *Micrococcus* strains, three *Microbacterium* strains, or with *Microbacterium* and *Micrococcus* strains growing together, showed coexistence between strains. However, the one-to-one culture of the *Microbacterium* KRD173 and the *Micrococcus* KRD2, resulted in growth inhibition of the two strains. Furthermore, it was previously observed that the tri-culture of *Salinibacterium* KRD240, *Rhodococcus* KRD197 and *C. glutamicum* induced pigmentation production. However, in the one-to-one cultures, this pattern was only observed in the one-to-one culture between *Salinibacterium* KRD240 and *Rhodococcus* KRD197. This suggests that the *Salinibacterium* KRD240 induced pigmentation production of *Rhodococcus* KRD197, and indicated a strain specific interaction.

Finally, as previously observed, the *Micromonospora* KRD244 affected growth and sporulation of the *Streptomyces* KRD257. Furthermore, in concordance with tri-culture findings, the one-to-one culture of the *Micromonospora* KRD244 and the *Rhodococcus* KRD226 showed inhibition of the *Micromonospora* KRD244. The

growth of *Rhodococcus* KRD196 was inhibited in the one-to-one cultures with the *Rhodococcus* KRD197 and the *Streptomyces* KRD247 (**Figure 3.15**). These interactions were not observed in the tri-cultures, which suggests strain specific interactions.

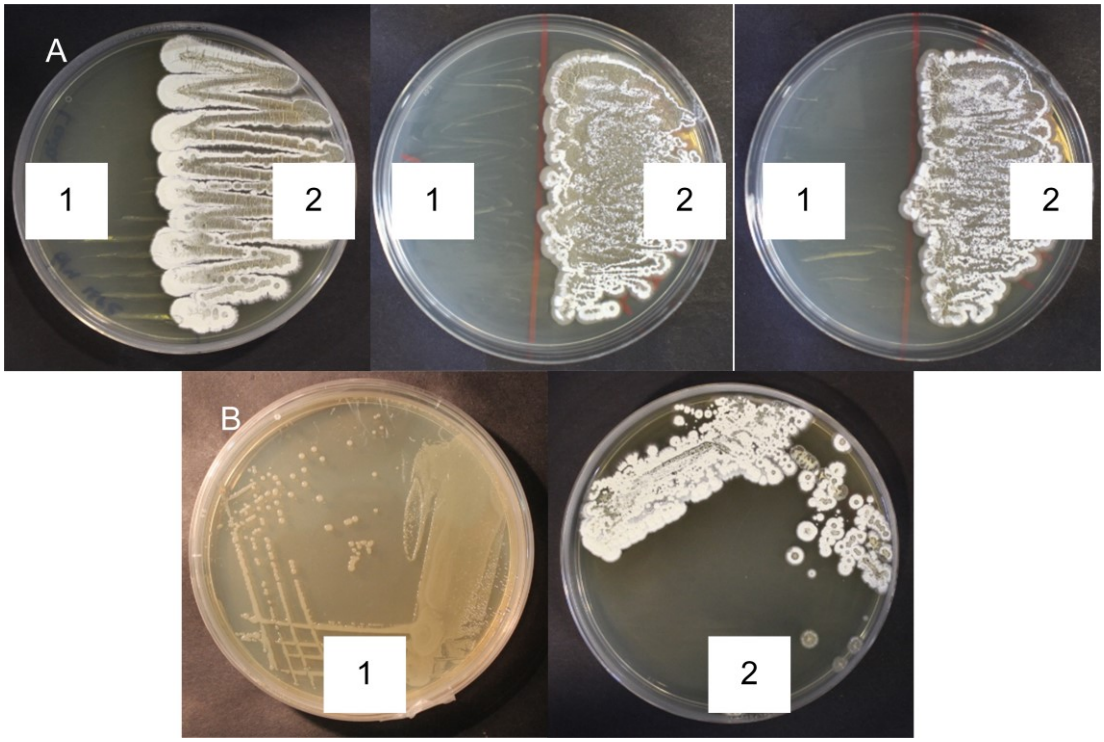

Figure 3.14. One-to-one culture reveals *Microbacterium* KRD174 growth inhibition. A-B) One-to-one culture in triplicate and mono-cultures of *Microbacterium* KRD174 (1) and *S. griseus* (2).

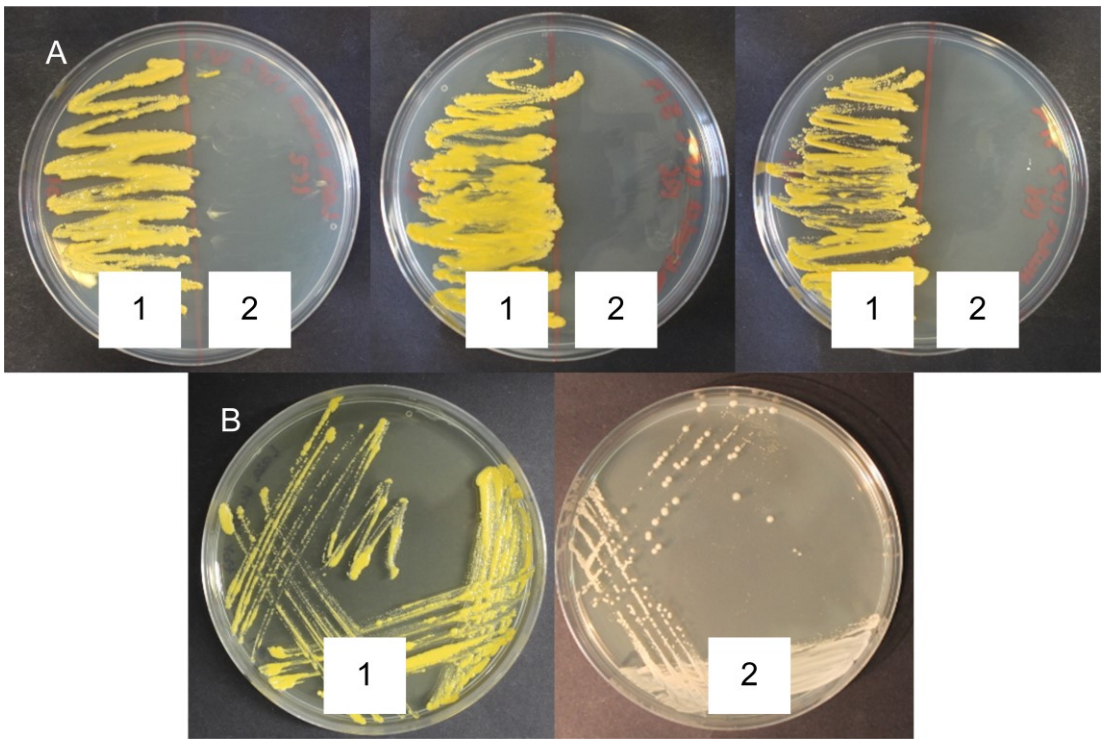

Figure 3.15. One-to-one culture reveals *Rhodococcus* KRD196 inhibition. A-B) One-to-one culture in triplicate and mono-cultures of *Rhodococcus* KRD197 (1) and *Rhodococcus* KRD196 (2).

A total of 23 (37%) one-to-one cultures showed neutral interactions where the strains were able to coexist. In concordance with previous findings, neutral interactions included *Micrococcus* and *Microbacterium* strains. This suggests that when these strains are challenged with a third strain (tri-cultures) phenotypic alterations are produced. Therefore, these bacterial interactions were tri-culture and strain specific.

3.2.4 Pre-conditioned media shows that phenotypic alterations were a result of potential specialised metabolites production

In order to assess if the phenotypic alterations observed in the tri-cultures and one-to-one cultures correlated with specialised metabolite production, bacterial strains were analysed by pre-conditioned media assays. Sterilised cellulose filter papers (membranes) were added to ISP2 plates which served as a membrane to stop the bacteria from growing in the media. It was observed that the cellulose filter paper was effective in stopping bacterial growth in the media since mono-culture controls did not show bacterial growth after membrane removal and further seven days of incubation. Pre-conditioned media revealed that 71% of tri-culture pre-conditioned media and

66% of one-to-one pre-conditioned media cultures showed a phenotypic change in the challenged strain (**Figure 3.16** and **Figure 3.17**). In concordance with the previous findings, the most common trait was inhibition of the challenged strains with 85% of tri-culture pre-conditioned media and 78% of one-to-one pre-conditioned media cultures showing growth inhibition. As previously observed, pre-conditioned media cultures revealed that *Pseudomonas* strains inhibited all challenged strains. In addition*, Pseudomonas* strains growth was also reduced (**Figure 3.18**). Interestingly, *Rhodococcus* strains grown in media containing metabolites produced by *Streptomyces* were inhibited. The same behaviour was observed by *Streptomyces* strains when growing in pre-conditioned media containing metabolites produced by *Rhodococcus* strains. The one-to-one pre-conditioned media culture of the producer *Rhodococcus* KRD226 and the challenged *Streptomyces* KRD211, showed inhibition of KRD211 (**Figure 3.19**). *Rhodococcus* KRD226 was also inhibited when challenged against the producer *Streptomyces* KRD211. However, these findings do not necessarily suggest that these strains were affected by metabolites produced by other strains since the consumption of glucose can lead to carbon catabolite de-repression of repressed genes. Therefore, carbon catabolite de-repression might also explain these phenotypic alterations.

Despite these findings, pre-conditioned media posed limitations that were considered. Secondary metabolites that were produced under bacterial competition as a result of physical contact between the strains might not be produced under pre-conditioned media. As a result, several morphological alterations that were previously observed by the tri-cultures and the one-to-one cultures were not detected by pre-conditioned media. In addition, the strains were cultured in a thinner layer of ISP2 compared to the normal conditions for metabolites to diffuse through the membranes. The addition of the membranes and limiting the nutrients to the producer strains can alter their growth and secondary metabolism. However, no morphological changes of the producer strains were observed which reinforces the pre-conditioned media findings.

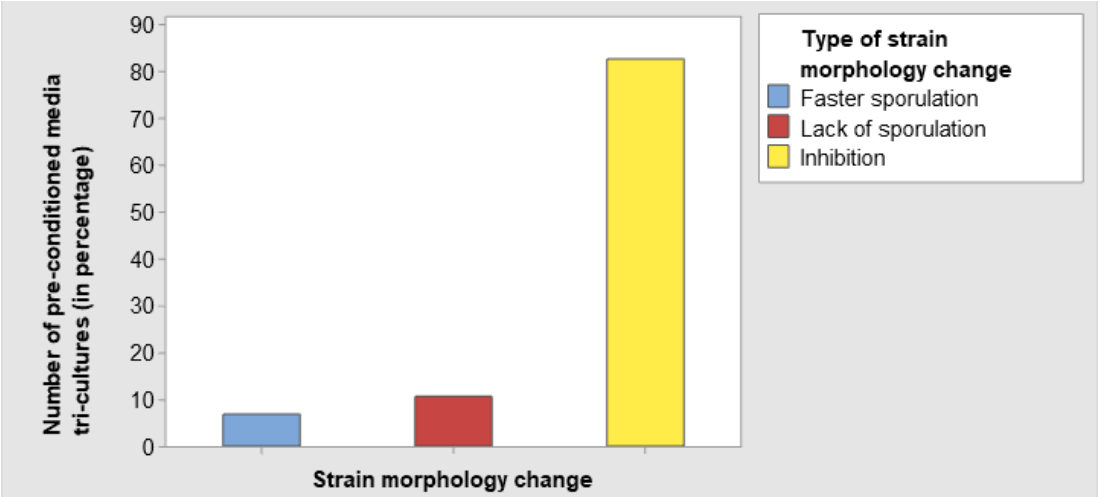

Figure 3.16. Tri pre-conditioned media cultures revealed strain morphological alterations. Phenotypic alterations were classified into five classes (x-axis). The number of tri-cultures showing a phenotypic response is represented as percentage (y-axis).

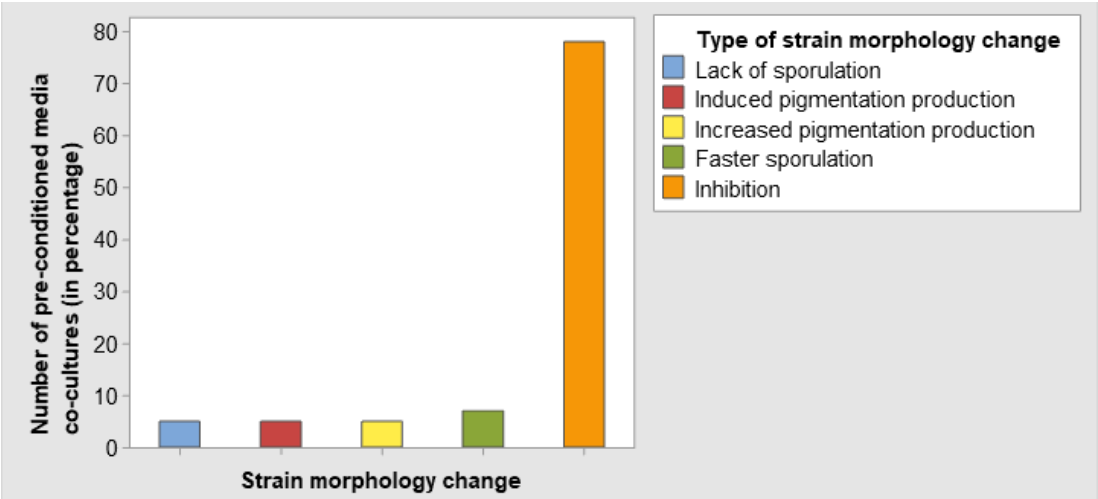

Figure 3.17. One-to-one pre-conditioned media cultures revealed strain morphological alterations. Phenotypic alterations were classified into five classes (x-axis). The number of tri-cultures showing a phenotypic response is represented as percentage (y-axis).

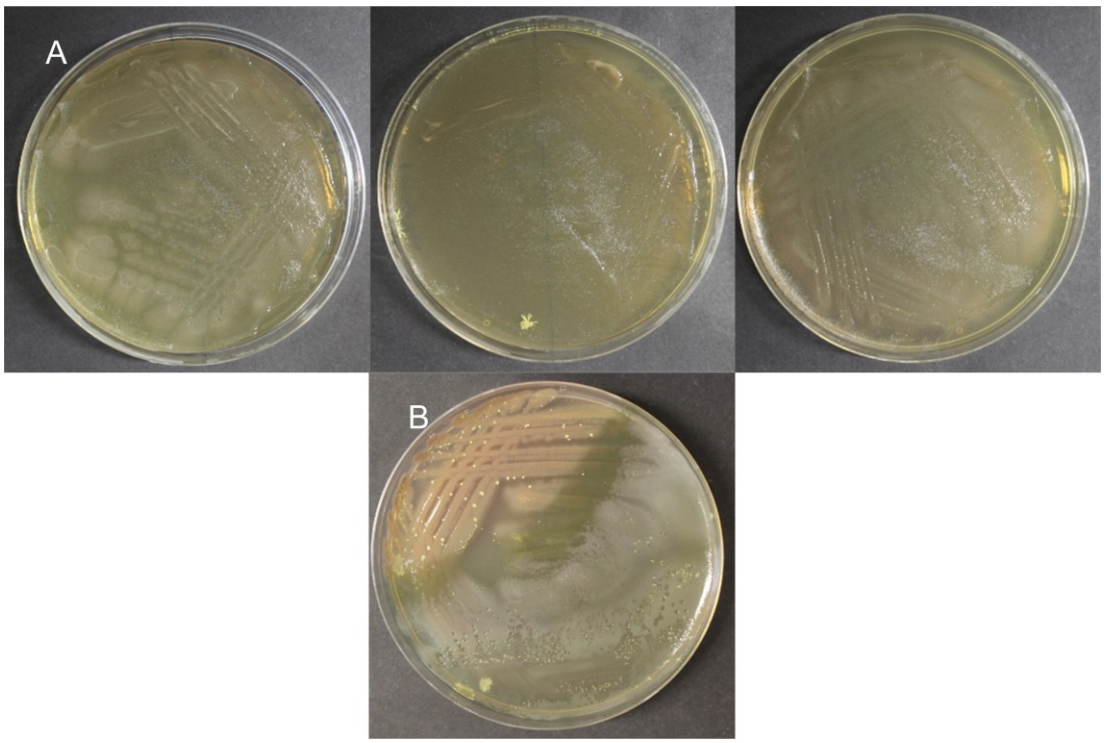

Figure 3.18. *P. aeruginosa* growth is affected (reduced growth) when growing on pre-conditioned media from *Rhodococcus* KRD226. A-B) *P. aeruginosa* growing on *Rhodococcus* KRD226 pre-conditioned media and *P. aeruginosa* control.

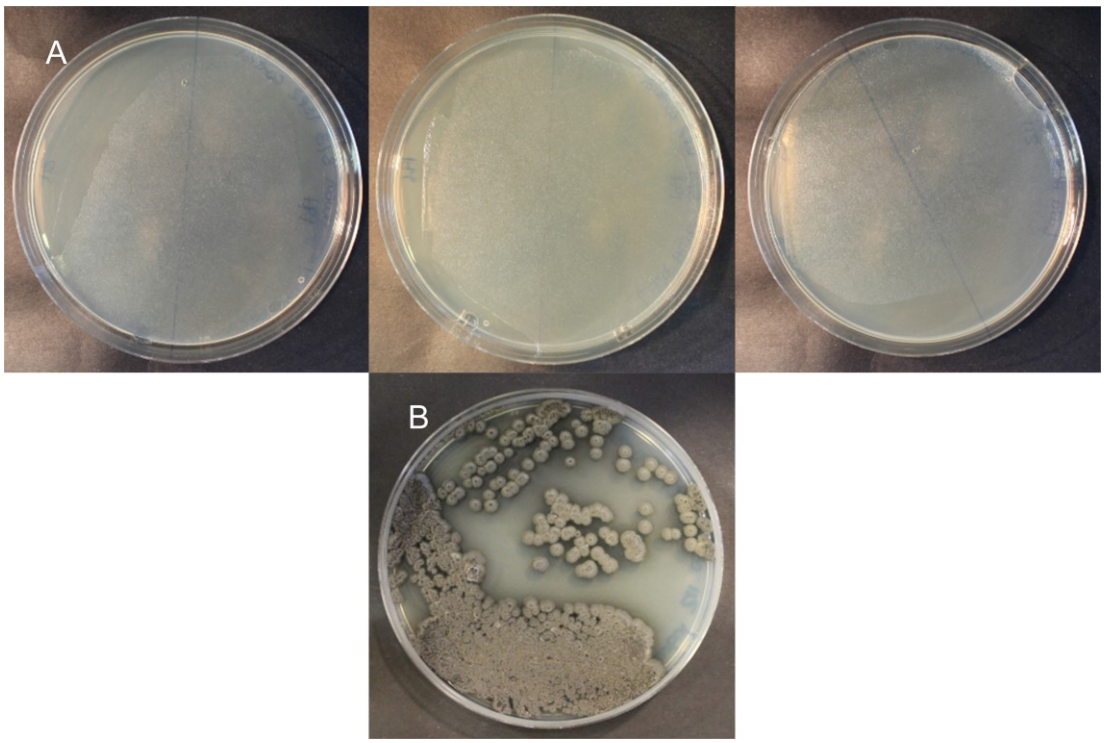

Figure 3.19. *Streptomyces* KRD211 growth is inhibited when growing on pre-conditioned media from *Rhodococcus* KRD226. A-B) *Streptomyces* KRD211 growing on *Rhodococcus* KRD226 pre-conditioned media and *Streptomyces* KRD211 control.

3.2.5 Antibacterial screening reveals antimicrobial activity against indicator strains

In order to evaluate the potential production of interaction specific metabolites all mono-cultures, tri-cultures, one-to-one cultures and pre-conditioned media cultures that showed phenotypic alterations were screened for antibacterial activity against *E. faecalis*, *S. aureus*, *K. pneumoniae, A. baumannii, P. aeruginosa* and *E. coli.*

The antibacterial screening results revealed that eleven strains showed antimicrobial activity against indicator strains. From these, four were non-marine strains while seven were isolates from marine sediments.

3.2.5.1 Antibacterial activity screening of tri-cultures and one-to-one cultures

The antibacterial screening revealed that three marine isolates displayed antibacterial activity against *S. aureus* and *E. faecalis* while two against *E. faecalis* (**Table 3.2**). One tri-culture showed bioactivity against *S. aureus,* while the mono-cultures did not display antibacterial activity (**Table 3.2F**). Furthermore, from the non-marine isolates,

two strains showed bioactivity against *S. aureus* and *E. faecalis. P. aeruginosa* displayed antibacterial activity against *E. faecalis* and *S. aureus* under mono-culture, tri-culture and one-to-one culture (**Table 3.2**). Interestingly, most tri-cultures and one-to-one cultures with *P. aeruginosa* showed larger inhibition zones against *S. aureus* than in mono-culture (**Table 3.2**). However, when *P. aeruginosa* was challenged against *B. subtilis* and *Rhodococcus* KRD226 lower bioactivity than in mono-culture was detected (**Table 3.2D** and **I**). Antimicrobial activity screening showed that all *P. aeruginosa* cultures displayed bioactivity against *E. faecalis*. However, in the tri-culture with *Micrococcus* KRD128 and *Rhodococcus* KRD175 (**Table 3.2B**) and the one-to-one culture of *P. aeruginosa* and *Microbacterium* KRD174 (**Table 3.2A**), antimicrobial activity was suppressed. This suggests that bioactive metabolite production by *P. aeruginosa* was suppressed as a result of bacterial interactions between these strains.

Micromonospora KRD244 showed activity against both *S. aureus* and *E. faecalis* in mono-cultures and mixed cultures. However, inhibition zones were not observed when this strain was in one-to-one culture with *Streptomyces* KRD257 (**Table 3.2C**). This was interesting since strain KRD257 was bioactive under mono-culture. In addition, the one-to-one culture between *Rhodococcus* KRD226 and *Micromonospora* KRD244 increased bioactivity against both *S. aureus* and *E. faecalis*. This suggests that under these specific conditions production of bioactive metabolites was interaction dependant with one interaction suppressing the bioactive metabolites production and the other eliciting these. Inhibition zones were also observed in the tri-culture of *Micrococcus* KRD88, *Streptomyces* KRD211 and *Rhodococcus* KRD226 against *S. aureus*, but not in mono-cultures and one-to-one cultures (**Table 3.2F**). These results suggest that bioactivity was induced by the bacterial interaction.

Table 3.2. Antibacterial activity of mono-cultures, one-to-one cultures and tri-cultures against *E. faecalis* and *S. aureus*. Each box (A-K) indicates each strain mono-culture, the tri-culture and each one-to-one culture. Colours indicate the intensity of bioactivity. Black X: refers to larger inhibition zone produced by the co-culture compared to the mono-culture, and red X: indicates inhibition zones produced by the co-culture or/and tri-culture and not observed in the mono-culture.

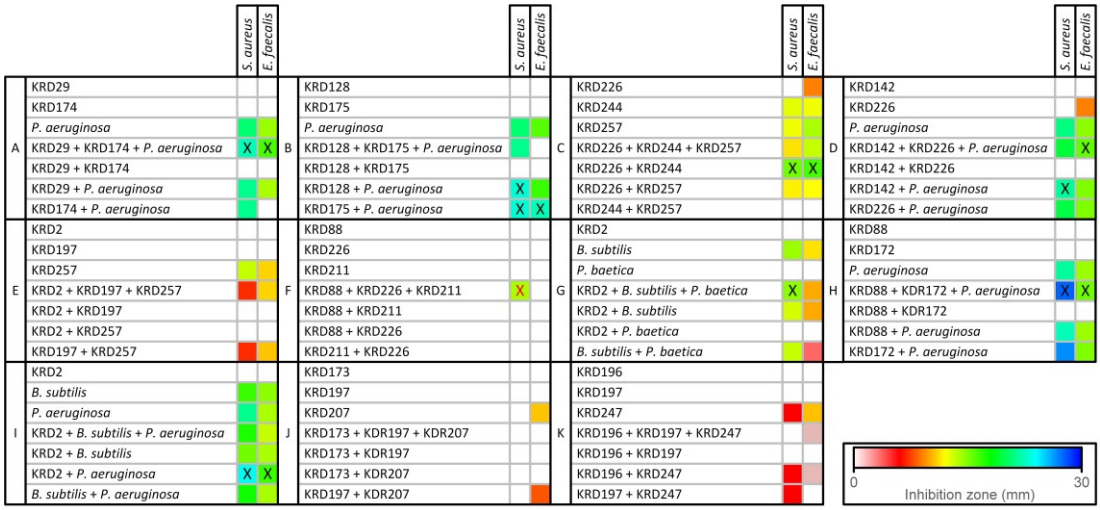

3.2.5.2 Antibacterial activity screening of pre-conditioned media

The antibacterial screening of the tri-culture and one-to-one culture pre-conditioned media (**Table 3.3**) revealed that antimicrobial activity was consistent with the previous findings. Four marine isolates were bioactive, three against *S. aureus* and one against both *S. aureus* and *E. faecalis* (**Table 3.3**). From the other strains, two showed antibacterial activity against *S. aureus* and one against both *S. aureus* and *E. faecalis*. *P. aeruginosa* consistently showed bioactivity against both *S. aureus* and *E. faecalis*. Furthermore, all strains that showed inhibition zones using this method showed bioactivity from the tri-cultures and/or one-to-one cultures method. These data suggest that these strains produce metabolites with inhibitory activity against *S. aureus* and *E. faecalis* across experimental conditions.

Contrary to previous findings, the *Streptomyces* KRD211, *S. coelicolor* and *Rhodococcus* KRD197 tri-culture showed bioactivity against *S. aureus* by using pre-conditioned media (**Table 3.3F, H and J**) but not under tri-culture method. This indicates that the challenged strains that are not inhibited in the pre-conditioned media produce specialised metabolites as a result of the effect of pre-conditioned media.

Table 3.3. Antibacterial activity of mono, one-to-one and tri pre-conditioned media cultures against *E. faecalis* and *S. aureus*. Each box (A-J) indicates each strain mono pre-conditioned media culture, tri pre-conditioned media culture and each one-to-one pre-conditioned media culture. Colours indicate the intensity of bioactivity. Black X: refers to larger inhibition zone produced by the co-culture compared to the mono-culture, and red X: indicates inhibition zones produced by the co-culture or/and tri-culture and not observed in the mono-culture. +: refers to assays where a halo was observed.

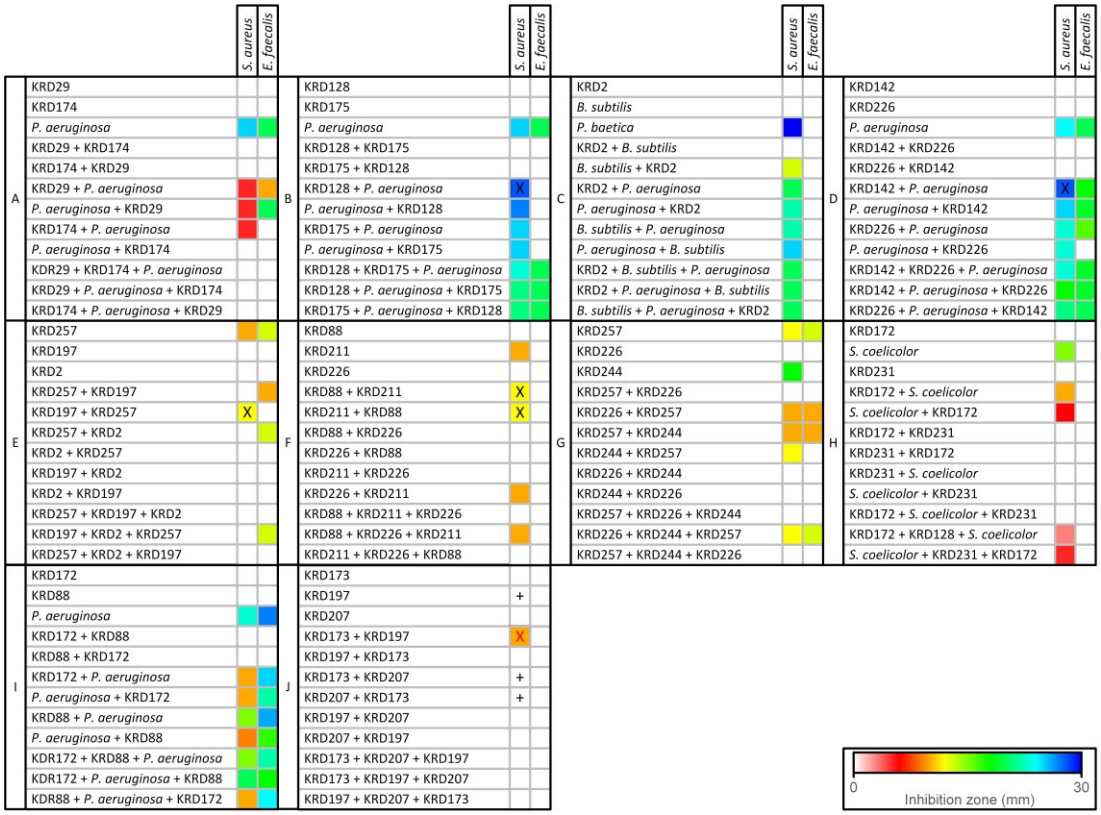

3.2.5.3 Antibacterial activity screening of bacterial extracts

In order to prioritise bacterial interactions for LC-MS analysis, metabolites from bioactive tri-cultures, one-to-one cultures and mono-cultures were extracted and tested against indicator strains. The antibacterial screening revealed that the bacterial extract of one marine isolate (*Streptomyces* KRD257) showed antibacterial activity against both *S. aureus* and *E. faecalis* under mono-culture and mixed cultures (**Table 3.4E and C**). *Micromonospora* KRD244 and *Streptomyces* KRD247 showed antibacterial activity against *S. aureus* (**Table 3.4C and K**). However, inhibition zones were small (less than 1mm).

P. aeruginosa, showed antibacterial activity against *E. faecalis* and *S. aureus* in all mono-cultures, tri-cultures and one-to-one cultures (**Table 3.4**) possibly as a result of siderophore production. It was previously observed that the one-to-one culture of *P. aeruginosa* and *Microbacterium* KRD174 and the tri-culture of *P. aeruginosa*, KRD128 and KRD175, was not bioactive against *E. faecalis*. However, after metabolite extraction from solid media, inhibition zones from these interactions were observed (**Table 3.4A and B**). These results suggest that bioactive metabolites were obtained in higher concentrations by solid media extraction.

In addition, several mono-cultures, one-to-one cultures and tri-cultures that showed antibacterial activity by plug assay, did not show bioactivity from the bacterial extracts. For example, *Micromonospora* KRD244 did not show antibacterial activity against *E. faecalis* by solid media metabolite extraction method contrary to previous results (**Table 3.4C**). These results suggest that these metabolites are not extracted by the extraction process due to the high polarity of the solvent (extracts polar metabolites) or at extracted at lower concentration.

Based on these results, two groups of interactions were prioritised for LC-MS analysis; 1- *Micrococcus* KRD142, *Rhodococcus* KRD226 and *P. aeruginosa*, 2- *Rhodococcus* KRD226, *Micromonospora* KRD244 and *Streptomyces* KRD257. These groups included the mono-cultures, the three one-to-one cultures and the tri-culture. The inclusion criteria included the previously observed biological activity. The genera; a group where the three strains belonged to *Actinobacteria* (group two) and a group where at least one strain belonged to another phyla (bacterial strains group one). Finally, the ecological criteria; a group where the three strains were isolated from the same place (bacterial strains group two) and a group where the three strains were isolated from separate environments (group one).

Table 3.4. Antibacterial activity of mono-culture and tri-culture metabolite extracts against *E. faecalis* and *S. aureus*. Each box (A-K) indicates each strain mono-culture, co-culture and tri-culture. The blue colour indicates the cultures that showed bioactivity by the plug assay. +: indicates the bacterial extracts that were bioactive against *S. aureus* or *E. faecalis* by disc diffusion assay. Groups highlighted in orange were prioritised for LC-MS analysis.

		S. aureus	*E. faecalis*
A	KRD29		
	KRD174		
	P. aeruginosa	+	+
	KRD29 + KRD174 + *P. aeruginosa*	+	+
	KRD29 + KRD174		
	KRD29 + *P. aeruginosa*	+	+
	KRD174 + *P. aeruginosa*	+	+
B	KRD128		
	KRD175		
	P. aeruginosa	+	+
	KRD128 + KRD175 + *P. aeruginosa*	+	+
	KRD128 + KRD175		
	KRD128 + *P. aeruginosa*	+	
	KRD175 + *P. aeruginosa*	+	+
C	KRD226		
	KRD244	+	
	KRD257	+	+
	KRD226 + KRD244 + KRD257	+	+
	KRD226 + KRD244	+	+
	KRD226 + KRD257	+	+
	KRD244 + KRD257	+	+
D	KRD142		
	KRD226		
	P. aeruginosa	+	+
	KRD142 + KRD226 + *P. aeruginosa*	+	+
	KRD142 + KRD226		
	KRD142 + *P. aeruginosa*	+	+
	KRD226 + *P. aeruginosa*		
E	KRD2		
	KRD197		
	KRD257	+	+
	KRD2 + KRD197 + KRD257	+	+
	KRD2 + KRD197		
	KRD2 + KRD257	+	+
	KRD197 + KRD257	+	+
F	KRD88		
	KRD226		
	KRD211		
	KRD88 + KRD226 + KRD211		
	KRD88 + KRD211		
	KRD88 + KRD226		
	KRD211 + KRD226		
G	KRD2		
	B. subtilis		
	P. baetica		
	KRD2 + *B. subtilis* + *P. baetica*		
	KRD2 + *B. subtilis*		
	KRD2 + *P. baetica*		
	B. subtilis + *P. baetica*		
H	KRD88		
	KRD172		
	P. aeruginosa	+	+
	KRD88 + KRD172 + *P. aeruginosa*	+	+
	KRD88 + KRD172		
	KRD88 + *P. aeruginosa*	+	+
	KRD172 + *P. aeruginosa*	+	+
I	KRD2		
	B. subtilis		
	P. aeruginosa	+	+
	KRD2 + *B. subtilis* + *P. aeruginosa*	+	+
	KRD2 + *B. subtilis*		
	KRD2 + *P. aeruginosa*	+	+
	B. subtilis + *P. aeruginosa*	+	+
J	KRD173		
	KRD197		
	KRD207		
	KRD173 + KRD197 + KRD207		
	KRD173 + KRD197		
	KRD173 + KRD207		
	KRD197 + KRD207		
K	KRD196		
	KRD197		
	KRD247	+	
	KRD196 + KRD197 + KRD247	+	
	KRD196 + KRD197		
	KRD196 + KRD247	+	
	KRD197 + KRD247	+	

3.3 Discussion

In order to identify bacterial strains with the ability to produce bioactive specialised metabolites as a result of bacterial interactions co-culture experiments were performed. The methods followed here (tri-culture, one-to-one culture and pre-conditioned media) enabled the correlation of bacterial interactions with strain phenotypic alterations and the further assessment of antibacterial screening. The project focused on actinobacterial strains isolated from marine sediments since these are less studied than their terrestrial counterparts (Jiménez, 2018). The first objective was to identify the 43 environmental isolates based on the 16s rRNA sequences which revealed that all strains belonged to the *Actinobacteria* phylum and were classified in eight genera (*Micrococcus* sp., *Pseudonocardia* sp., *Rhodococcus* sp., *Microbacterium* sp., *Streptomyces* sp., *Micromonospora* sp., *Salinibacterium* and *Agrococcus* sp.). All strains were subjected to tri-cultures and one-to-one cultures in order to achieve closer environmental conditions where interactions are prevalent and this can lead to the production of specialised metabolites (Serrano *et al.*, 2017; Ding *et al.*, 2018; Jomori *et al.*, 2020).

The main findings were strain phenotypic alterations (29% of tri-cultures and 63% of one-to-one cultures) of at least one strain when compared to mono-cultures. Five main types of phenotypic patterns were observed; inhibition, bald*/whi* phenotypes, growth promotion, induced pigmentation and increased production of pigmentation. While enhanced growth was the least observed phenotype (5% of tri-cultures and 3% of one-to-one cultures), inhibition was the most common alteration pattern (81% in tri-cultures and 78% in one-to-one cultures). These phenotypic effects were previously observed in co-culture experiments where inhibition was induced in a larger number of interactions in comparison to growth promotion (Geesink *et al.*, 2018). This suggests that inhibition was a result of competition while growth-promoting effects of cooperative interactions (Patin *et al.*, 2016; Liu *et al.*, 2017). Inhibition of aerial hyphae development was detected in *Streptomyces* strains when growing in co-culture as previously observed (Yang *et al.*, 2009; Seyedsayamdost *et al.*, 2011; Schneider *et al.*, 2012; Traxler *et al.*, 2012). This could be explained by the fact that some specialised metabolites are capable of blocking aerial hyphae development and the production of spores by altering the expression of developmental genes. This arrests the life cycle of *Streptomyces* and the production of metabolites. For instance, previous work determined that the metabolite amychelin, produced by *Amycolatopsis*

sp. AA4 altered the expression of the developmental gene *bldN* in *S. coelicolor* which restricted *S. coelicolor* from erecting aerial hyphae (Traxler *et al.*, 2012). Similarly, *B. subtilis* induced the expression of the *ytnP* gene under co-culture with *S. griseus* which caused *S. griseus* to fail at developing aerial hyphae and at producing streptomycin (Schneider *et al.*, 2012). Furthermore, the fact that these morphological alterations were observed at the interface edges between the strains, suggests that these alterations were linked to specialised metabolite production (Benndorf *et al.*, 2018). This was reinforced by the pre-conditioned media assays which revealed that most challenged strains (85% in tri-cultures and 66% in one-to-one cultures) were inhibited. Similarly, inhibition patterns of marine isolates induced by *S. arenicola* were linked to specialised metabolite production (Patin *et al.*, 2016). Therefore, in line with previous findings, these results concluded that interaction outcomes between bacterial strains are mainly determined by metabolite production (Vetsigian *et al.*, 2011; Patin *et al.*, 2016).

Interestingly, 60% of tri-cultures resulted in neutral interactions. Despite that it was not possible to determine the benefit of these interactions, these results suggest that in the natural environment strains may cooperate for growth benefits (Freilich *et al.*, 2011). Contrary to these findings, recent growing evidence suggests that competition is prevalent over cooperation (Venturelli *et al.*, 2018; Coyte and Rakoff-Nahoum, 2019). For instance, the pairwise interactions between 12 human-associated intestinal strains revealed that competition predominated over neutral or cooperative interactions with 68% of assays resulting in negative interactions (Venturelli *et al.*, 2018). Our findings suggest that the balance between negative and positive interactions is unclear and should be further addressed. In addition, it was not possible to determine if phylogenetic closely-related strains were more likely to compete or remain neutral under co-culture than more distantly-related strains as previously suggested (Kinkel *et al.*, 2014; Patin *et al.*, 2016; Guillonneau *et al.*, 2018; Westhoff *et al.*, 2020). However, actinobacterial strains were able to interact with phylogenetic distant strains (*Pseudomonas* and *B. subtilis*). This suggests that other factors such as survival strategies including the formation of biofilms or quorum-sensing influence bacterial interactions (Lories *et al.*, 2020). For instance, *Salmonella typhimurium* responded to the presence of two competing strains (another strain of *S. typhimurium* and *E. coli*) by the up-regulation of genes involved in the process of biofilm formation, epithelial invasion, and antibiotic tolerance (Lories *et al.*, 2020). In addition, culture conditions (e. g. media components, pH and selective pressure) can also influence

bacterial interactions (Justice *et al.*, 2017; Liu *et al.*, 2017; Ratzke and Gore, 2018; Lories *et al.*, 2020). Media with high concentration of carbon sources, such as ISP2, allow faster bacterial growth but repress morphological differentiation and secondary metabolite production (Romero-Rodríguez *et al.*, 2018). In this study, glucose was used as carbon source which likely led to carbon catabolite repression and reduced the production of specialised metabolites (Romero-Rodríguez *et al.*, 2017). In fact, it was observed that *S. griseus* presented a *whi* phenotype. Previous studies have reported the suppression of specialised metabolites by different carbon sources (Romero-Rodríguez *et al.,* 2016). For example, *rok7B7* which is a member of the repressor open reading frame kinase family regulators was upregulated by the consumption of glucose in *S. coelicolor*. This promoted actinorhodin production but suppressed undecylprodigiosin and calcium-dependent antibiotic (Romero-Rodríguez *et al.,* 2016). Similarly, under rich-nutrient conditions, N-Acetylglucosamine accumulated which promoted growth and blocked developmental processes (Świątek *et al.,* 2012). Therefore, the use of the repressing carbon source in the medium likely blocked development and specialised metabolite production. Despite these limitations, using this medium, *Streptomyces* KRD257 was capable of producing pigments under co-culture which were not detected under mono-culture. This was exciting as it indicated that metabolites were produced as a result of co-cultivation. Furthermore, correlation between place of isolation and bacterial interactions was also not observed. This suggests that strains that co-evolved in the same environment are able to co-exist, explaining the observation of neutral interactions. In line with these results, it is suggested that strains that are isolated from the same environment are less competitive against each other, while strains that do not meet in nature but are closely-related share niche similarities (Zhao *et al.,* 2016) engaging in stronger competition (Ketola *et al.,* 2017).

The findings reported here showed that bacterial interactions are dynamic and complex but laboratory experiments are directly impacted by culture conditions and other factors. Therefore, they do not reflect bacterial interactions in nature. The co-culture techniques used in this chapter presented several limitations that should be addressed in future experiments. First, the strains involved in this study represented a small percentage of the total bacterial species that are found within the same environment. Many more bacterial species (10^9) and other organisms compete for resources in natural communities (Coyte *et al.*, 2017). Therefore, interactions among a higher number of strains can variate the competition outcome as reported elsewhere

(Ren *et al.*, 2015). Another limitation of the laboratory co-culture experiment is that it does not mimic the environmental conditions to which bacteria are exposed to. For example, the co-culture method was optimised with one medium, temperature, and incubation time. In addition, as previously discussed, in these co-cultures nutrient availability was high while in the natural environment is limited (D'Souza *et al.*, 2018). This influences specialised metabolite production and the outcome of bacterial interactions. Despite this, the fact that a total of 10 interactions showed larger inhibition zones against *S. aureus* and/or *E. faecalis* than the mono-cultures, demonstrated that co-culture techniques are a potential strategy to elicit specialised metabolites.

In conclusion, this chapter provides strong evidence that bacterial strains can compete for resources under specific co-cultures by producing specialised metabolites. This production is a response to their environment even if these interactions are not always competitive. Further research using co-culture techniques could lead to the production of pharmaceutically relevant novel metabolites. In future, using other media such as media with low carbon sources and longer incubation times for these co-cultures may enhance chemical diversity. Since the production of secondary metabolites is preceded by environmental changes or nutrient limitation (McCormick and Flärdh, 2012), low nutrient conditions would likely promote the development and production of secondary metabolites. However, the challenge of reproducing co-culture experiments increases as more parameters are added with some of them being complicated to control, such as the inoculum of each culture (Arora *et al.*, 2020). Therefore, improved co-culture methods will gain insights in the roles of bacterial interactions and specialised metabolite production in natural environments. In addition, they will provide better understanding of the factors involved in the induction of cryptic or poorly expressed Biosynthetic Gene Clusters.

CHAPTER 4: LC/MS-BASED COMPARATIVE METABOLOMICS OF BACTERIAL INTERACTIONS

Microbial NPs are recognised as outstanding sources for drug discovery (Wright, 2019). However, the analysis of microbial extracts by conventional methods such as bioassay-guided structure elucidation often leads to the discovery of known metabolites (Trivella and de Felicio, 2018). In addition, conventional approaches present limitations which include time-consuming and laborious experiments. Currently, the advancement of methods to analyse LC-MS data from microbial extracts provides the rapid identification of previously reported metabolites (Kuhlisch and Pohnert, 2015). LC-MS combines a chromatographic separation system and a mass spectrometer (Arpino *et al.,* 1974). The chromatographic separation system separates each metabolite found within a complex mixture and after elution from the LC column, metabolites are directed to the mass spectrometer where are ionised and further separated based on their mass-to-charge ratio (parent ions). However, several caveats need to be considered when analysing bacterial extracts with LC-MS. For instance, not all metabolites present in a bacterial culture are extracted, which is influenced by the polarity of the organic solvent used for the extraction. In addition, not all metabolites are ionised, which is influenced by the ionisation mode and the LC-MS parameters such as the ion source (De Vijlder *et al.*, 2018). Furthermore, metabolites found in the extracts can be suppressed by the ionisation of co-eluting ions (Milne *et al.*, 2013).

Comparative metabolomics is the data analysis of specialised metabolites detected by MS in biological samples across experimental conditions (Covington *et al.,* 2017). One software used for pre-processing untargeted LC-MS data is MZmine (Pluskal *et al.*, 2010). The processing of the data using MZmine includes importing the raw data files, chromatogram building, deconvolution, data filtering, peak picking, peak deisotoping and peak alignment across data from multiple extracts, gap filling and data normalisation (Pluskal *et al.*, 2010). Furthermore, the latest version of MZmine enables data visualisation such as the total ion current chromatogram (summed total ion intensity across the masses detected during the entire analysis), and data interpretation by statistical analysis such as the PCA which indicates distance and relatedness across samples (Pluskal *et al.*, 2010). Data analysis is performed with tools such as MetaboAnalyst as previously described in chapter one, which detects metabolites in the experimental groups leading to the rapid prioritisation of bacterial

strains (Chong *et al.,* 2019; Demarque *et al.*, 2020). Another important advantage of comparative metabolomics is that it enables the identification of metabolic responses of microorganisms to experimental conditions such as environmental stimuli (Senges *et al.*, 2018). For that reason, comparative-metabolomics provides the suitable tools to compare mono-culture and co-culture extracts (Kuhlisch and Pohnert, 2015; Boya *et al.*, 2019). Furthermore, comparative metabolomics enables the detection of specialised metabolites elicited by bacterial interactions (Patin *et al.*, 2018; Reverter *et al.*, 2018).

Despite the fact that comparative metabolomics accelerated the discovery of novel natural products, a major challenge remains in their elicitation. Metabolites are not always produced when microorganisms are cultured under standard laboratory conditions (Baltz, 2017; Nai and Meyer, 2018; Wolfender *et al.*, 2019). Sequencing technologies and genome mining revealed that actinobacterial genomes contain more BGCs encoding the production of metabolites than previously thought (Bentley *et al.*, 2002; Belknap *et al.*, 2020). The production of secondary metabolites is controlled by a diverse range of regulators, including cluster-situated regulators, global regulators and pleiotropic regulators that trigger or repress the expression of genes encoding secondary metabolites (Bibb, 2005; Liu *et al.,* 2013; Lu *et al.,* 2017; Wei, 2018). As previously mentioned, some of these respond to environmental stress such as nutrient depletion which is linked to morphological differentiation (Liu *et al.,* 2019). For example, in several *Streptomyces,* phosphate control is mediated by the global regulator PhoP (Rodríguez-García *et al.,* 2007). Phosphate starvation leads to DNA binding of phosphorylated PhoP which activates the expression of phosphate-responsive genes such as the phosphate transporter system (Rodríguez-García *et al.,* 2007). However, PhoP represses other genes such as *afsS* which regulates actinorhodin and undecylprodigiosin production in *S. coelicolor* (Santos-Beneit *et al.,* 2009). The pleiotropic regulator AfsR binds the *afsS* promoter stimulating the expression of pathway-specific regulatory genes (*actII*-ORF4 and *redD*) that encode actinorhodin and undecylprodigiosin (Fujii *et al.,* 1996). However, in competition with AfsR, PhoP binds the *afsS* promoter interfering with the AfsR binding, negatively affecting metabolite production (Santos-Beneit *et al.,* 2009). AfsR belongs to the *Streptomyces* Antibiotic Regulatory Protein (SARP) regulators which are found in *Actinobacteria* and can express many BGCs by acting as pathway-specific activators (Bibb, 2005). SARPs are found in many types of BGCs including type I and type II-PKSs and NRPSs (Bibb, 2005). Similarly, under low phosphate conditions the gene

otcC which encodes anhydrotetracycline oxygenase and *otcY* which encodes tetracycline polyketide in *S. rimosus* were expressed (McDowall et al. 1999). Expression of BGCs is also regulated by the master regulator of development, BldD, as previously described in chapter one. For example, BldD binds to the promoters of the erythromycin BGC and regulates the production of erythromycin and morphological differentiation in *S. erythraea* (Chng *et al.,* 2008). Deletion of *bldD* decreased erythromycin production and blocked morphological differentiation (Chng *et al.,* 2008). Furthermore, the two-component regulatory system AbsA which consists of the *absA1* (sensor kinase) and *absA2* (response regulator), plays a negative regulatory role in the production of actinorhodin, undecylprodigiosin, calcium-dependant antibiotic and methylenomycin in *S. coelicolor* (Brian *et al.,* 1996). While mutations in *absA1* blocked metabolite biosynthesis, deletion of these mutations enhanced antibiotic production (Brian *et al.,* 1996). Other important regulators include the GlnR (master response regulator for nitrogen metabolism) (Wray and Fisher, 1993), the MtrAB two component system (Som *et al.,* 2017), other two component systems such as AfsQ1/Q2 (Ishizuka *et al*., 1992) and other SARP, LuxR, AraC/XylS and LysR-type regulators. Furthermore, signalling molecules also play a role in metabolite production and morphological differentiation via specific receptor proteins normally belonging to the TetR regulators (Niu *et al.,* 2016). For example, A-factor induces streptomycin production and morphological differentiation in *S. griseus.* A-factor triggers a regulatory cascade that involves the A-factor-specific receptor ArpA, the pleiotropic regulator AdpA and the activator StrR that activates the streptomycin BGC (Horinouchi and Beppu, 2007).

In order to express BGCs several approaches can be followed including genetic manipulation of essential genes (Kealey *et al.,* 2017). For instance, one method is to overexpress positive regulatory genes or to disrupt the negative regulatory genes (Kealey *et al.,* 2017). For example, the pleiotropic regulator Lsr2 of *S. venezulae* represses the transcription of BGCs leading to unexpressed BGCs under normal laboratory conditions such as the chloramphenicol cluster (Gehrke *et al*., 2019). The chloramphenicol biosynthetic cluster comprises *sven0913/cmlR* which encodes a pathway-specific activator (Zhang *et al.,* 2021). Lsr2 binding within the cluster, spanning *sven0926* and upstream the cluster, spanning *sven0904* and *sven0905* limits chloramphenicol production (Zhang *et al.,* 2021). In addition, Lsr2 binds 223 sites distributed throughout the chromosome, including sites within 17 specialised BGCs that affect production of metabolites (Gehrke *et al*., 2019). Deleting the *lsr2*

gene increased the production of specialised metabolites when compared to the wild type strain, including previously unreported metabolites (Gehrke *et al.*, 2019). Furthermore, another approach for the elicitation of specialised metabolites include the improvement of culture conditions (Nai and Meyer, 2018). These include chemical elicitation (Tyurin *et al.,* 2018) and the one strain many compounds (OSMAC) approach (Bode *et al.*, 2002) which are performed under mono-culture. Yet, given that bacterial interactions are prevalent in nature, is preferential to move to co-culture methods (Martínez-Buitrago *et al.,* 2019). These methods combined with comparative metabolomics demonstrated the successful elicitation of bioactive specialised metabolites. For instance, the cultivation of seven actinobacterial strains in the pre-conditioned media of four strains (*B. subtilis, P. aeruginosa, Mycobacterium smegmatis,* and *Aspergillus flavus*) led to the production of 28 metabolites that were not produced under mono-culture (Liang *et al.*, 2019). The comparative metabolomics analysis by MZmine and the R package revealed that the co-culture of *Streptomyces* sp. RKBH-B178 and *M. smegmatis* represented the most chemical diverse co-culture (containing 21 of 28 up-regulated and elicited parent ions in response to pre-conditioned media from the entire dataset). Therefore, comparative metabolomics allowed the prioritisation of this co-culture for further analyses which enabled the isolation of the novel hydrazidomycin D (Liang *et al.*, 2019). In addition, comparative metabolomics provides insights of elicited specialised metabolites during interactions in ecological niches (Kuhlisch and Pohnert, 2015; Boya *et al.*, 2019). The analysis of antagonistic interactions between *Streptomyces* strains isolated from the ant *Acromyrmex echinatior* and the fungal pathogen *Escovopsis* sp. isolated from their nests facilitated the identification of specialised metabolites that were found at the inhibition zones of the pairwise assays between the strains (Boya *et al.*, 2019). Hence, this indicates the need to understand how these metabolites are produced to facilitate the discovery of novel natural products (Patin *et al.*, 2018).

This chapter analysed prioritised bacterial interactions identified in chapter three by LC-MS and multivariate data analysis in order to compare the metabolite profiles between mono-cultures, co-cultures and tri-cultures.

4.1 Aims and objective

The main objective of this chapter was to determine the chemical response of co-cultures as a result of bacterial interactions compared to mono-cultures and detect co-culture-elicited parent ions.

Aim 1: to compare metabolite profiles between mono-cultures, co-cultures and tri-cultures by comparative metabolomics.

Aim 2: to prioritise bacterial one-to-one cultures and tri-cultures showing the highest number of parent ions elicited as a result of bacterial interactions.

4.2 Results

To detect parent ions that were elicited by the two prioritised groups of bacterial interactions, one-to-one cultures (two strains) and tri-cultures (three strains) were subjected to LC-MS and data was analysed with MetaboAnalyst. These two groups were: *P. aeruginosa*, *Micrococcus* KRD142 and *Rhodococcus* KRD226 (bacterial strains group one, **Figure 4.1**) and *Rhodococcus* KRD226, *Micromonospora* KRD244 and *Streptomyces* KRD257 (bacterial strains group two, **Figure 4.2**). These were prioritised based on antibacterial activity; the two groups showed bioactivity by plug diffusion method and by testing culture metabolite extracts. The genera; bacterial strains group one included a non-actinobacterial strain and bacterial strains group two included three actinobacterial strains. Ecological criteria; bacterial strains group one included strains isolated from separate locations and group two included strains isolated from the same sediment.

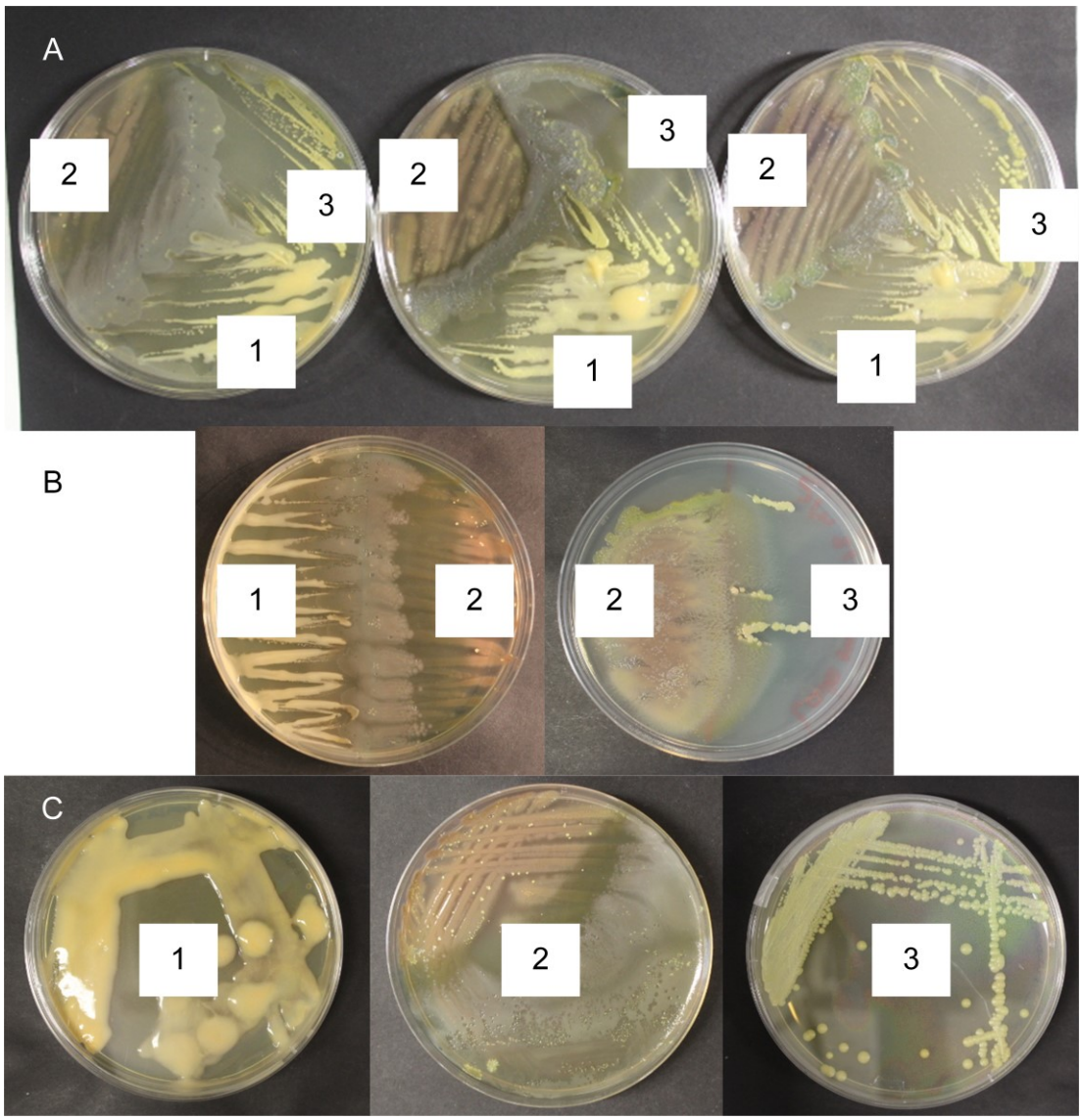

Figure 4.1. Tri-culture and one-to-one cultures from the prioritised bacterial group one (*Micrococcus* KRD142, *Rhodococcus* KRD226 and *P. aeruginosa*) that showed phenotypic alterations. A-C) Tri-culture in triplicate, one-to-one cultures and mono-cultures of *Rhodococcus* KRD226 (1), *P. aeruginosa* (2) and *Micrococcus* KRD142 (3).

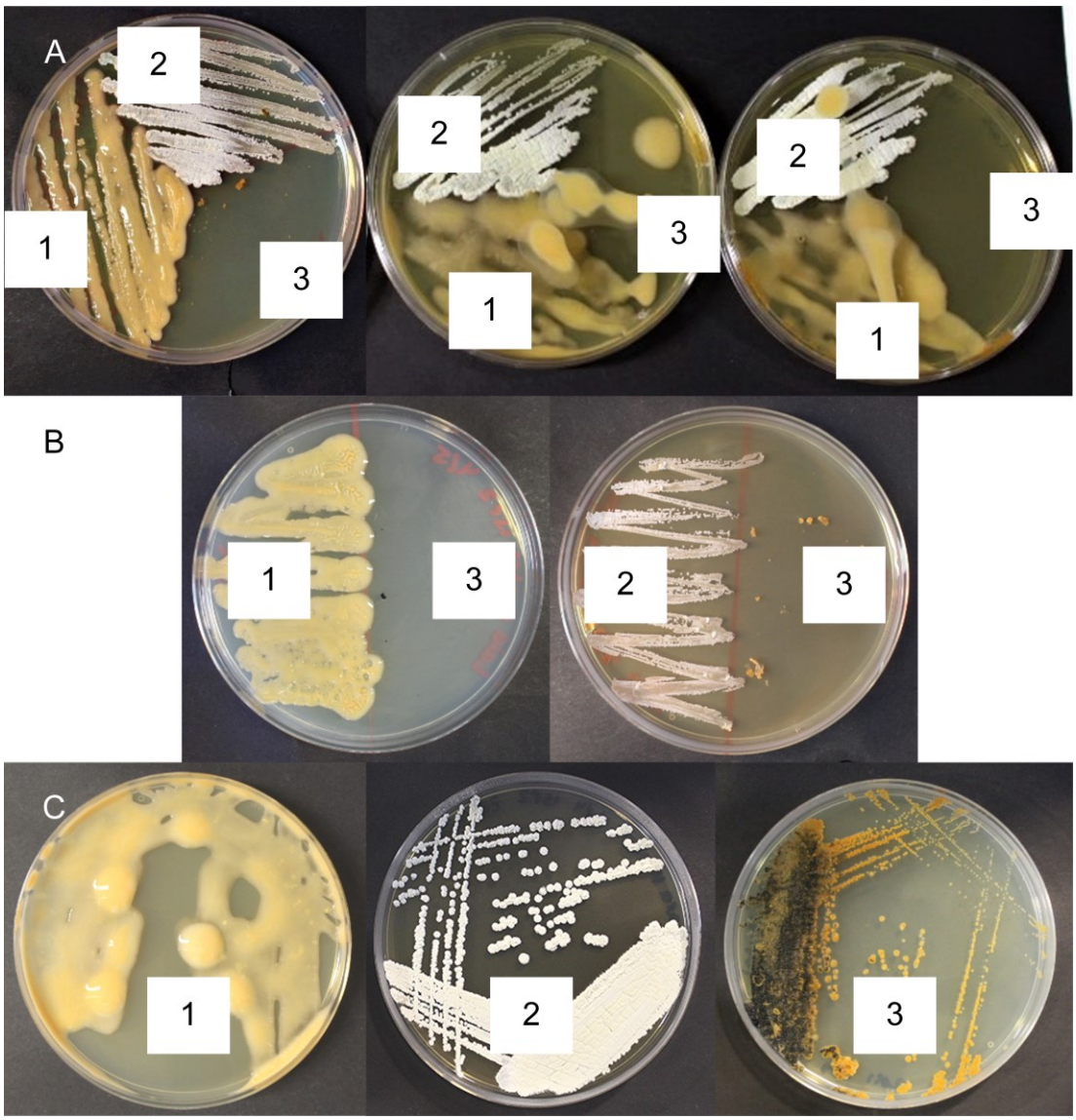

Figure 4.2. Tri-culture and one-to-one cultures from the prioritised bacterial group two (*Rhodococcus* KRD226, *Micromonospora* KRD244 and *Streptomyces* KRD257) that showed phenotypic alterations. A-C) Tri-culture in triplicate, one-to-one cultures and mono-cultures of *Rhodococcus* KRD226 (1), *Streptomyces* KRD257 (2) and *Micromonospora* KRD244 (3).

4.2.1 LC-MS analysis of group one (*P. aeruginosa*, *Micrococcus* KRD142 and *Rhodococcus* KRD226) reveals interaction specific parent ions

To determine the total number of parent ions that were interaction specific, all parent ions detected in each group were identified from all bacterial extracts. The total number of parent ions detected was 31839, from which eight originated from the media control, 1457 were *Micrococcus* KRD142 mono-culture specific, 1696 were

Rhodococcus KRD226 mono-culture specific and 5810 were *P. aeruginosa* mono-culture specific (**Table 4.1**). A total of 5918 were detected in the tri-culture extracts, 663 in the one-to-one cultures of *Micrococcus* KRD142 and *Rhodococcus* KRD226, 2575 were detected in the bacterial extracts of the *P. aeruginosa* and *Micrococcus* KRD142 one-to-one cultures, and 3847 were *P. aeruginosa* and *Rhodococcus* KRD226 one-to-one cultures specific (**Table 4.1**). There were then 9865 parent ions, 6408 of these were detected in more than one interaction and 3457 were shared between mono-cultures and co-cultures. These data revealed that 60% of all parent ions detected in this group (excluding the parent ions detected in the media controls) were elicited by bacterial interactions (**Table 4.1**).

Table 4.1. Number of parent ions detected in positive ionisation mode for the bacterial strains group one (*Micrococcus* KRD142, *Rhodococcus* KRD226 and *P. aeruginosa*). The columns indicate the replicate specific parent ions: ions detected only in one replicate, commonly detected: parent ions detected in two replicates of the same experimental group, and present in the three replicates: parent ions detected in the three replicates of the same experimental group. The last row (shared between two or more experimental groups), indicates the total number of parent ions that were detected in two or more experimental groups.

Bacterial extract	Replicate specific parent ions			Parent ions commonly detected in two experimental replicates			Present in the three replicates	Total
	1	2	3	1 and 2	1 and 3	2 and 3		
Micrococcus KRD142 mono-culture	81	169	204	96	65	271	842	1457
Rhodococcus KRD226 mono-culture	118	66	14	317	198	304	679	1696
P. aeruginosa mono-culture	356	508	369	499	698	264	3125	5810
One-to-one culture of *P. aeruginosa* and *Micrococcus* KRD142	36	55	193	111	76	94	2010	2575
One-to-one culture of *P. aeruginosa* and *Rhodococcus* KRD226	267	26	11	499	79	57	2908	3847
One-to-one culture of *Micrococcus* KRD142 and *Rhodococcus* KRD226	9	3	18	54	152	196	231	663
Tri-culture	34	33	158	221	1098	786	3588	5918
Shared between two or more interactions								6408
Shared between mono-cultures and interactions								3457

In order to assess the chemical similarity between experimental groups prior to multivariate data analysis, a PCA of the unprocessed raw LC-MS data was performed. The PCA was generated by reducing the number of original variables (retention times, *m/z* values and peak ion intensity) to facilitate data interpretation. Furthermore, to reveal outlier bacterial extracts to be prioritised for further analysis. This is important since outlier extracts indicate a variance in the metabolite profile of a specific experimental group. This separation or clustering between the experimental groups represents the covariance between the parent ions detected in the bacterial extracts. If the covariance is small, experimental groups cluster closer to each other based on parent ions that are present in more than one experimental group. The PCA results revealed the discrimination of the *P. aeruginosa* and *Micrococcus* KRD142 one-to-one culture, the *P. aeruginosa* and *Rhodococcus* KRD226 one-to-one culture, the tri-culture and the *P. aeruginosa* mono-culture from the other experimental groups (**Figure 4.3** and **Table S4.1**). Tri-cultures presented the highest number (5918) of specific parent ions and contributed the most to the variance of the PCA plot (eigenvalues PC1: -175.618642, -71.8180446 and 2.42437554, PC2: 24.8277222, 59.5405149, 300.467533) (**Table S4.1**). Furthermore, the *P. aeruginosa* and *Rhodococcus* KRD226 mono-cultures, the *Micrococcus* KRD142 and *Rhodococcus* KRD226 one-to-one culture, the media extracts and solvent blanks clustered together (**Figure 4.3**). These data suggest that while the tri-culture elicited the production of metabolites, the *Micrococcus* KRD142 and *Rhodococcus* KRD226 produced limited metabolites.

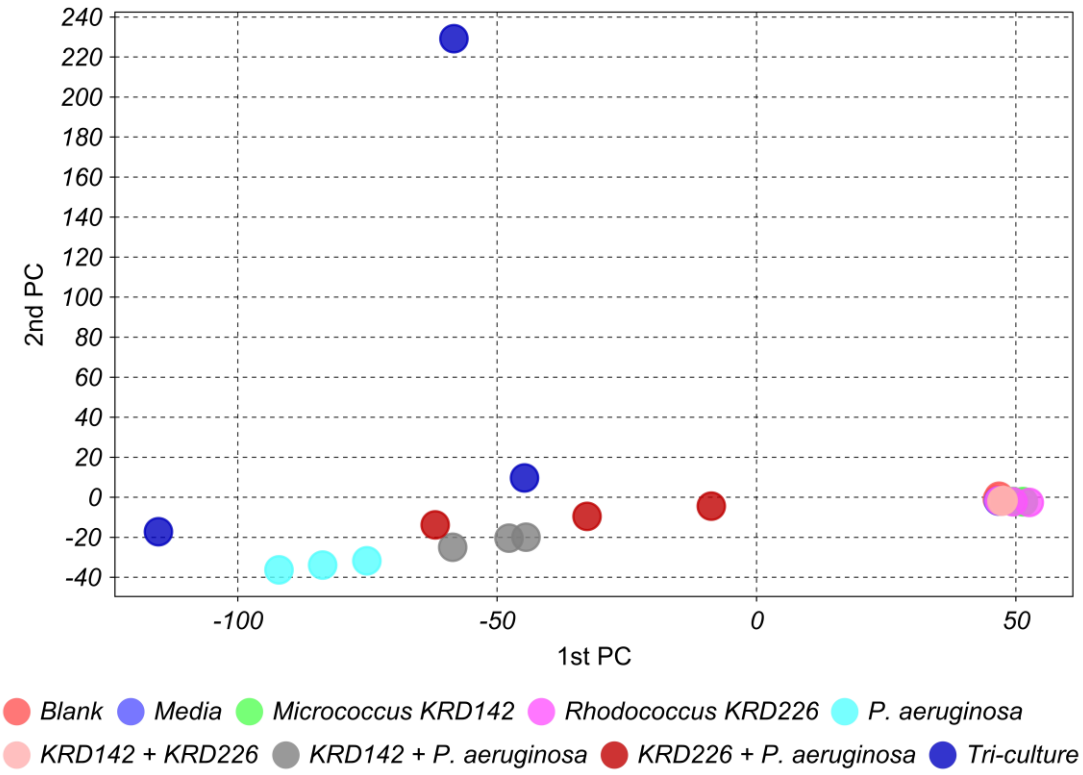

Figure 4.3. PCA scores reveal the separation between mono-cultures, one-to-one cultures and tri-cultures of *Micrococcus* KRD142, *Rhodococcus* KRD226 and *P. aeruginosa* bacterial extracts. PCA scores are based on the first and second PCs (x-axis and y-axis). Each dot of the plot belongs to one bacterial extract. Each experimental group is color-coded.

In order to detect LC-MS peaks that were interaction specific, chromatograms for all experimental groups were overlaid. Despite the discrimination of the one-to-one cultures and tri-cultures, overlaid LC-MS chromatograms did not reveal group specific parent ions (**Figure S4.1**). However, these chromatograms show the most intense mass peaks of the mass spectra. Therefore, those signals with lower intensity that may be of interest are not visible in the base peak chromatograms. For example, *m/z* 930.5801 which was detected in the extracts of the tri-culture had an ion intensity of $1x10^4$ compared to most intense ions of $1x10^9$ (**Figure 4.4**). These data suggest that the groups that were discriminated by the PCA produced interaction specific ions that were not detected under mono-culture.

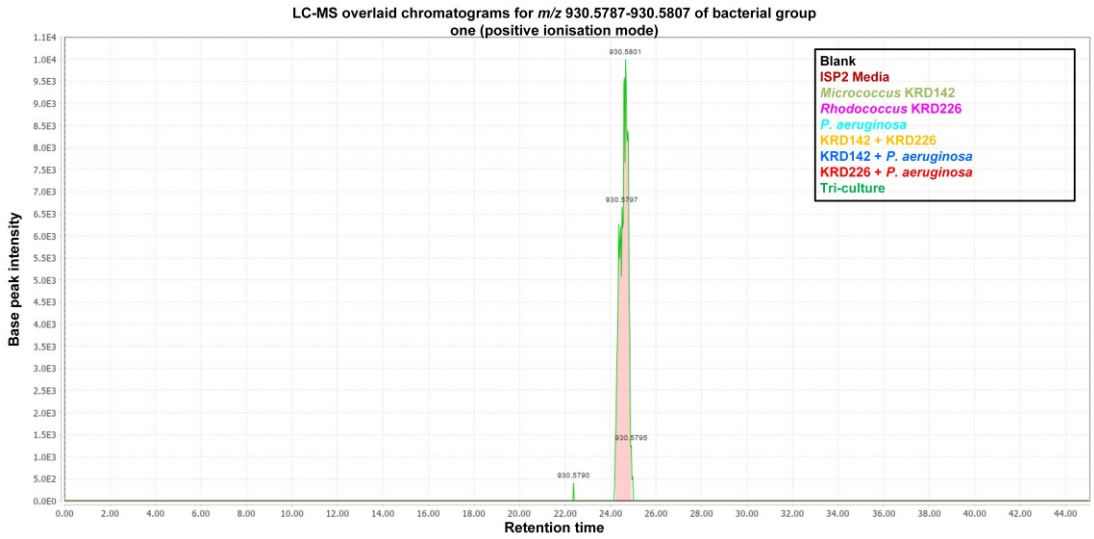

Figure 4.4. Parent ion *m/z* 930.5787 - 930.5807 elicited as a result of the *Micrococcus* KRD142*, Rhodococcus* KRD226 and *P. aeruginosa* tri-culture interaction detected in the LC-MS positive ionisation mode data. The chromatogram indicates the parent ion intensity (y axis) and the retention time (x axis). These peaks (*m/z* 930.5790 and 930.5801) are elicited by the tri-culture (colour-coded in green).

4.2.2 Comparative metabolomics of bacterial group one confirms metabolite production elicited by co-cultures

To detect the parent ions that were responsible for the PCA separation, processed LC-MS data was normalised (intensity values were mean-centred and divided by the square root of the standard deviation of each variable) (**Figure S4.2**). This reduced the effect of larger intensity ions. Then, data was subjected to multivariate data analysis.

PCA was applied to determine the clustering trends between tri-cultures, one-to-one cultures and mono-cultures, and to visualise potential outliers. The PCA plot was generated using Pareto scaling and the first five PCs. The PCA showed that the first two PCs explained 76.9% of the variance in the data set and these were enough to capture most of the information without losing important data (**Figure 4.5**). This was observed by the scree plot which showed the cumulative and individual variance explained by each PC (**Figure 4.6**). The scree plot revealed a large variation in slopes at the first PC and a smaller change at the second PC followed by straight line. This indicates that the two first PCs captured enough variance to project the data in a low-dimensional subspace (**Figure 4.6**). The PCA (**Figure 4.5**) revealed the separation of

all experimental groups in two subgroups. The first subgroup was the media control, *Micrococcus* KRD142 and *Rhodococcus* KRD226 mono-cultures and the *Micrococcus* KRD142 and *Rhodococcus* KRD226 one-to-one culture. The second subgroup was *P. aeruginosa* mono-culture*, Micrococcus* KRD142 and *P. aeruginosa* one-to-one culture, *Rhodococcus* KRD226 and *P. aeruginosa* one-to-one culture and the tri-cultures (**Figure 4.5**). Since PCA clusters the data according to chemical similarity, these results suggest that the bacterial extracts within the subgroups were more related than between subgroups. This was expected since limited production of metabolites was detected in the *Micrococcus* KRD142 and *Rhodococcus* KRD226 mono-cultures and the *Micrococcus* KRD142 and *Rhodococcus* KRD226 one-to-one culture. Therefore, these groups clustered together with the media extracts. Similarly, the ability of *P. aeruginosa* to produce metabolites under mono-culture and co-culture was potentially responsible for the second cluster. Additionally, the replicates for each experimental group clustered together which indicates that the chemical response was consistent and reproducible.

In order to identify the parent ions that were responsible for the separation of these two subgroups, the PCA loadings plot (**Figure 4.5B**) was generated from the scores plot. The loadings plot indicated the parent ions corresponding to each bacterial extract outlier found in the PCA scores. The PCA loadings plot revealed four parent ions (*m/z* 626.4027, 626.4079, 626.4134 and 626.4187) that were elicited by the tri-cultures as they were classified as outliers in the tri-culture quadrants (upper left quadrants in **Figure 4.5B**). In addition, they contributed to the largest variance of PC2. These were not correlated with other parent ions from the dataset. For example, they were situated in a 180°C angle (orthogonal loadings) from the parent ions of subgroup one. To reinforce that these were elicited under tri-culture, the LC-MS overlaid chromatogram for each of these ions was visualised. LC-MS chromatograms confirmed that they were tri-culture specific (**Figure S4.3** and **Figure S4.4**). Additionally, the loadings plot revealed that the parent ions (*m/z* 225, 260 and 286) that were identified as outliers from the subgroup two were only detected in the bacterial interactions involving *P. aeruginosa* (lower right outliers in **Figure 4.5B**). This explains the clustering of these experimental groups by the PCA. These parent ions were classified as outliers since they were not detected in the *Micrococcus* KRD142 and *Rhodococcus* KRD226 mono-cultures or the one-to-one culture between these two strains. Finally, the loadings plot showed that parent ions produced by the *Micrococcus* KRD142 and *Rhodococcus* KRD226 mono-cultures and the one-to-one

culture between these two strains (situated in the lower left quadrants of the loadings plot) were correlated between each other and with those from the media control (**Figure 4.5**). This explains the clustering of these samples in the PCA scores plot. These results suggest that metabolites detected in these bacterial extracts were related to media components or these strains produced a limited number of metabolites.

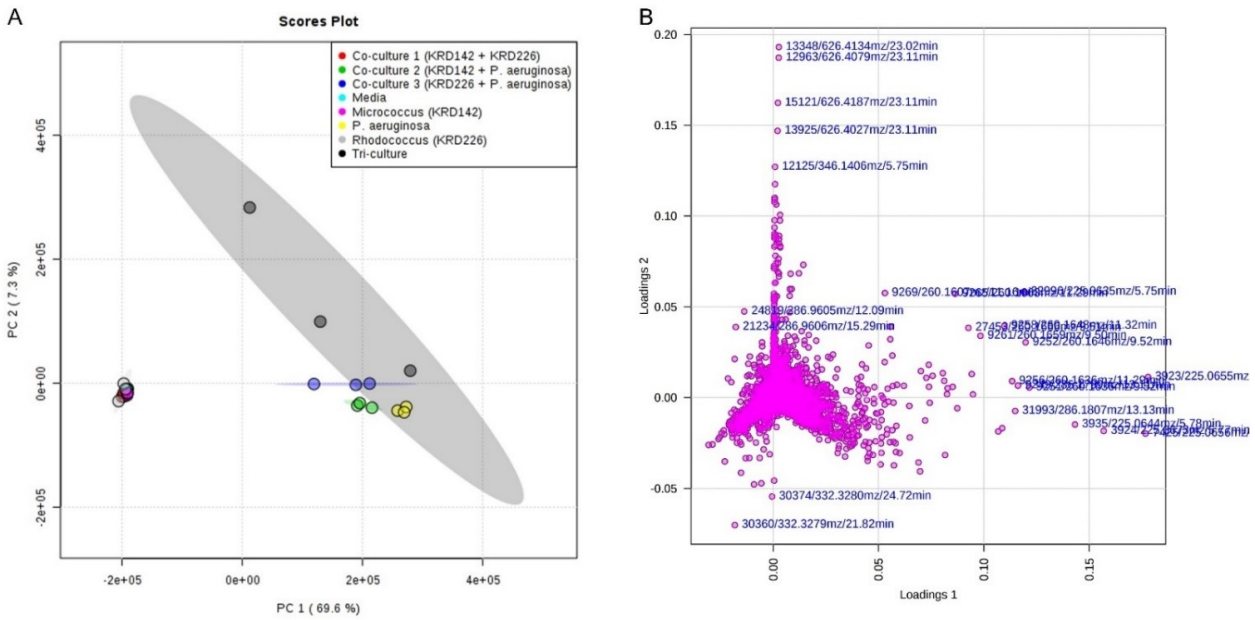

Figure 4.5. PCA scores reveal the separation between mono-cultures, one-to-one cultures and tri-cultures of *Micrococcus* KRD142, *Rhodococcus* KRD226 and *P. aeruginosa* bacterial extracts and the loadings plot indicates the parent ions responsible for this separation. A) PCA scores plot based on the two first PCs (PC1 and PC2). Each experimental group is colour-coded (red: *Micrococcus* KRD142 and *Rhodococcus* KRD226 one-to-one culture, green: *Micrococcus* KRD142 and *P. aeruginosa* one-to-one culture, blue: *Rhodococcus* KRD226 and *P. aeruginosa* one-to-one culture, turquoise: media control, pink: *Micrococcus* KRD142 mono-culture, grey: *Rhodococcus* KRD226 mono-culture, yellow: *P. aeruginosa* mono-culture and black: tri-culture). The ellipses show the 95% confidence limit. B) PCA loadings plot. Each dot represents one parent ion from the dataset. Those parent ions situated with greater distance from the starting point of the loadings plot drive the variance in the PCA plot.

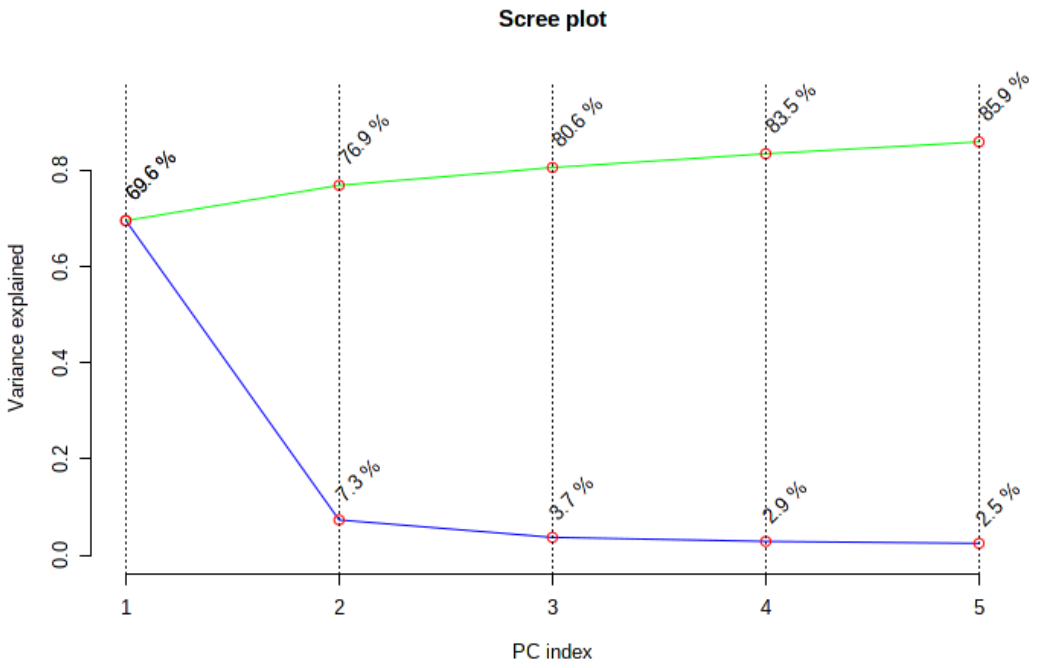

Figure 4.6. Scree plot shows the PCA variance explained by the first five PCs. The green line on top shows the accumulated variance explained; the blue line underneath shows the variance explained by individual PCs.

To improve the separation between experimental groups and to confirm the variables (parent ions) that are responsible for the classification of these, data was further subjected to a supervised PLS-DA. PLS-DA was generated by rotating the PCA components to achieve the maximum separation and discriminate the co-cultures from the mono-cultures. PLS-DA was cross-validated using the coefficients Q2 (quality of the fit) and R2 (predicted variation of the model). In each cross validation the predicted data were compared with original data and the sum of squared errors was calculated. The prediction error was summed over all experimental samples, divided by the initial sum of squares and subtracted from one to resemble the scale of R2. An acceptable model is that Q2 and R2 must be at least > 0.4 and an excellent model is Q2 and R2 = 1 (Worley and Powers, 2013). In addition, if the model is not predictive or is overfitted, the Q2 value is negative. Q2 was used to select an optimal number of principal components.

The PLS-DA cross validation showed that the R2 value was 0.76 and the Q2 value was 0.51, which were high enough to confirm a well-fitted model and a good prediction of variables. Furthermore, 76% of the variance was explained by the first and second

PCs where the *P. aeruginosa* mono-culture and the tri-culture contributed to the largest variance (32% and 49%, respectively) of PC1. The *Rhodococcus* KRD226 mono-culture and the tri-culture contributed to the largest variance of PC2 (36% and 38%, respectively). PLS-DA revealed a more efficient separation between experimental groups than in PCA since the projection of the X-axis data (spectra of each bacterial extract) was guided by the provided group information (group class). In addition, the replicates for each group clustered together which indicates that the chemical response induced by each group was consistent and reproducible. PLS-DA revealed the separation of the tri-culture from the one-to-one cultures and mono-cultures (**Figure 4.7A**). The loadings plot identified the parent ions *m/z* 626 (outliers situated in the upper left quadrant in **Figure 4.7B**) which were elicited by the tri-cultures. For example, parent ion *m/z* 626.4187 (**Figure S4.4**) was situated in the upper left quadrant, contributing to the separation of the tri-cultures from the other experimental groups (**Figure 4.7B**). These findings agreed with those observed by PCA, which reinforce the previous observations.

In contrast with PCA, PLS-DA achieved the separation between the one-to-one culture of *Micrococcus* KRD142 and *P. aeruginosa* and the one-to-one culture of *Rhodococcus* KRD226 and *P. aeruginosa* (**Figure 4.7B**). These one-to-one cultures were also separated from *P. aeruginosa* mono-cultures and the tri-cultures (**Figure 4.7**). The loadings plot revealed the parent ions *m/z* 225, 260 and 286 that were elicited by these two experimental groups, the tri-culture and the *P. aeruginosa* mono-culture (outliers situated in the lower right quadrants in **Figure 4.7B**). These data suggests that specialised metabolites produced by *P. aeruginosa* mono-culture predominated under the one-to-one cultures. This indicates that under one-to-one culture, *P. aeruginosa* metabolites that are also produced under mono-culture, are able to inhibit the growth of the challenged strain.

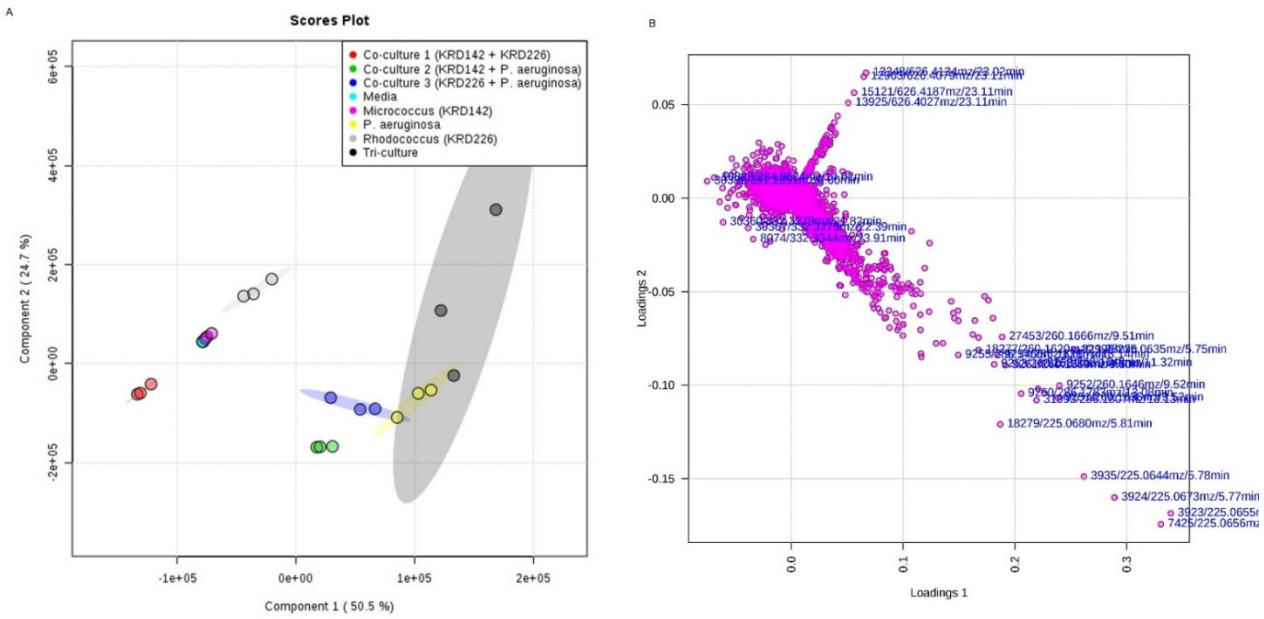

Figure 4.7. PLS-DA scores reveal the separation between mono-cultures, one-to-one cultures and tri-cultures of *Micrococcus* KRD142*, Rhodococcus* KRD226 and *P. aeruginosa* bacterial extracts and the loadings plot indicates the parent ions responsible for this separation. A) PLS-DA scores plot based on the two first PCs (PC1 and PC2). Each experimental group is colour-coded (red: *Micrococcus* KRD142 and *Rhodococcus* KRD226 one-to-one culture, green: *Micrococcus* KRD142 and *P. aeruginosa* one-to-one culture, blue: *Rhodococcus* KRD226 and *P. aeruginosa* one-to-one culture, turquoise: media control, pink: *Micrococcus* KRD142 mono-culture, grey: *Rhodococcus* KRD226 mono-culture, yellow: *P. aeruginosa* mono-culture and black: tri-culture). The ellipses show the 95% confidence limit. B) PLS-DA loadings plot. Each dot represents one parent ion from the dataset. Those parent ions situated with greater distance from the starting point drive the variance in the PLS-DA plot.

To identify the variables that discriminated the co-cultures, VIP scores were calculated. VIP scores were generated from the weighted sum of squares of the PLS loadings considering the amount of explained Y-variation in each dimension. VIP estimated the importance of the loadings in the PLS-DA model. Therefore, ranking the parent ions according to their contribution to the PLS-DA scores from most significant (P > 1) to insignificant (P < 1). VIP scores revealed that the parent ions *m/z* 626.4134, *m/z* 626.4079, *m/z* 626.4187 and *m/z* 626.4027 which were elicited by the tri-cultures, were considered within the 10 most significant (P = 16.636, 16.131, 13.993 and 12.657) parent ions (**Figure S4.5** and **Table S4.2**). VIP revealed the parent ion *m/z* 224.0834 which was not observed by PLS-DA (**Figure S4.5** and **Table S4.2**). This finding was interesting since *m/z* 224.0834 was detected in all one-to-one cultures and tri-cultures but not under mono-culture (**Figure S4.5**). This suggests that this parent ion was produced as a result of co-cultivation and, therefore, was not specific to one interaction.

To determine the chemical similarity produced between all experimental groups, a hierarchical cluster analysis was performed. The hierarchical cluster analysis was generated by using the algorithm Ward's linkage which combined all the experimental replicates for each group that began as a separate cluster until they belonged to one cluster. The results of this analysis are presented as a heatmap, which is a graphical representation of a matrix of distances where the experimental replicates are joined together in a hierarchical fashion according to their chemical similarity (**Figure 4.8**). The hierarchical cluster analysis revealed that the *Micrococcus* KRD142 and *P. aeruginosa* one-to-one culture, the *Rhodococcus* KRD226 and *P. aeruginosa* one-to-one culture, and the tri-culture, shared an interaction specific pattern (highlighted in boxes in **Figure 4.8**). These three groups shared the elicitation of 2197 parent ions that were not observed in the bacterial extracts of the mono-cultures. For example, the parent ions *m/z* 225, 260 and 286 as previously observed by the PCA and PLS-DA. This suggests that parent ions were elicited in all co-cultures as a chemical response to the interactions.

Interestingly, the hierarchical cluster analysis revealed the production of metabolites produced by the *Rhodococcus* KRD226 mono-culture, the *Micrococcus* KRD142 mono-culture and the one-to-one culture between these two strains despite that were not previously identified by PCA and PLS-DA (**Figure 4.8**). Furthermore, it was found that 8963 parent ions produced by mono-cultures were not detected in the co-cultures

and the tri-cultures (**Figure 4.8**). For example, the parent ion *m/z* 1027.6751 was detected in the *P. aeruginosa* mono-culture and suppressed in the tri-culture and one-to-one cultures (**Figure 4.9**). These data suggest that bacterial interactions impact the strains' secondary metabolism in both ways; by metabolite elicitation and metabolite suppression.

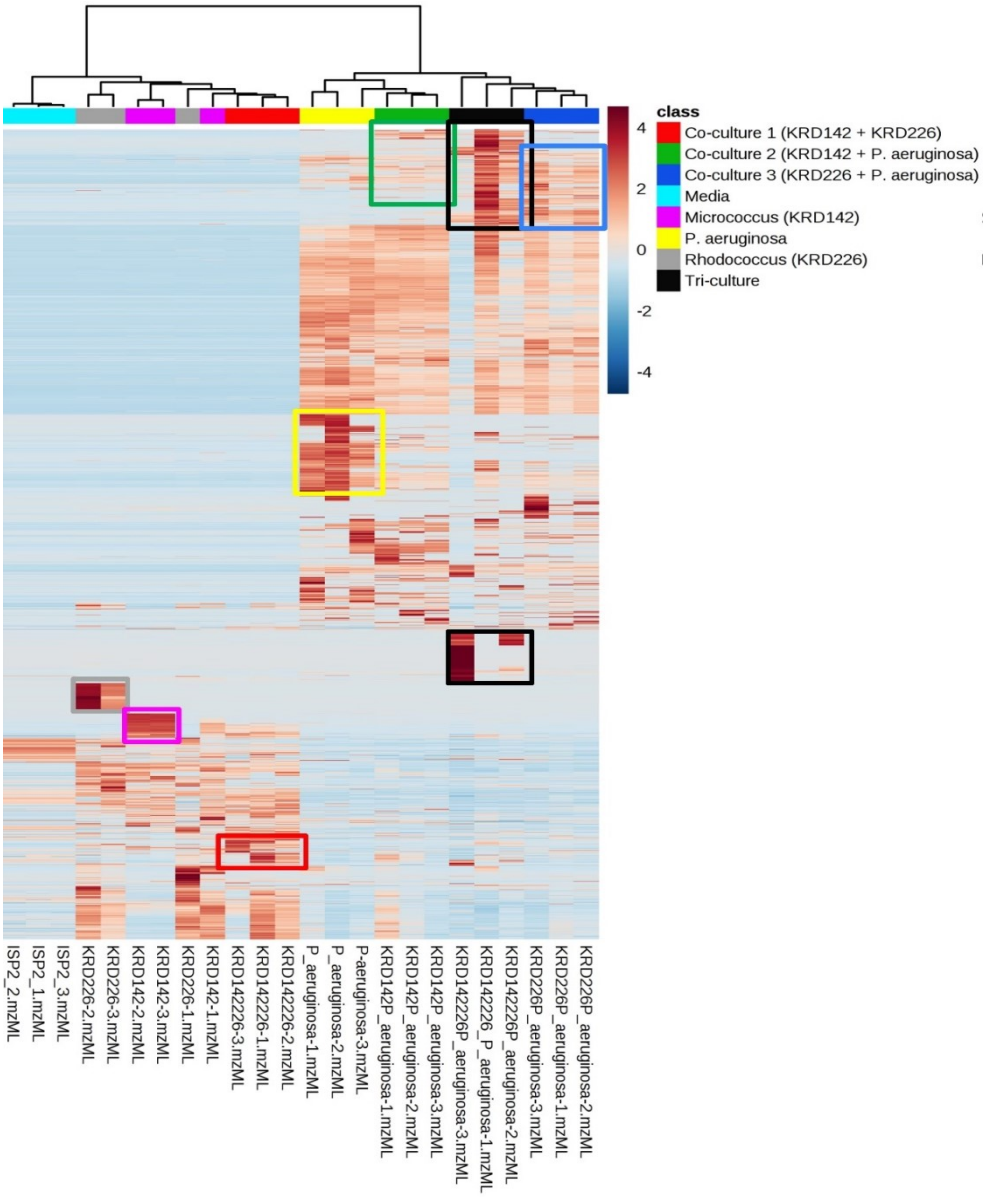

Figure 4.8. Hierarchical cluster analysis reveals the classification of experimental groups under two clades according to metabolite production similarity (right: *P. aeruginosa* mon-culture, *Micrococcus* KRD142 and *P. aeruginosa* one-to-one culture, *Rhodococcus* KRD226 and *P. aeruginosa* one-to-one culture, and tri-culture and left: media control, *Micrococcus* KRD142 and *Rhodococcus* KRD226 mono-culture and *Micrococcus* KRD142 and *Rhodococcus* KRD226 one-to-one culture). Each coloured cell on the map corresponds to a parent ion intensity value ranging from blue (decreased level) to red (increased level), x-axis represents each group's experimental replicate in the bottom row and experimental groups in the top row, y-axis represents the parent ions. The coloured boxes, highlight parent ions elicited in each experimental group.

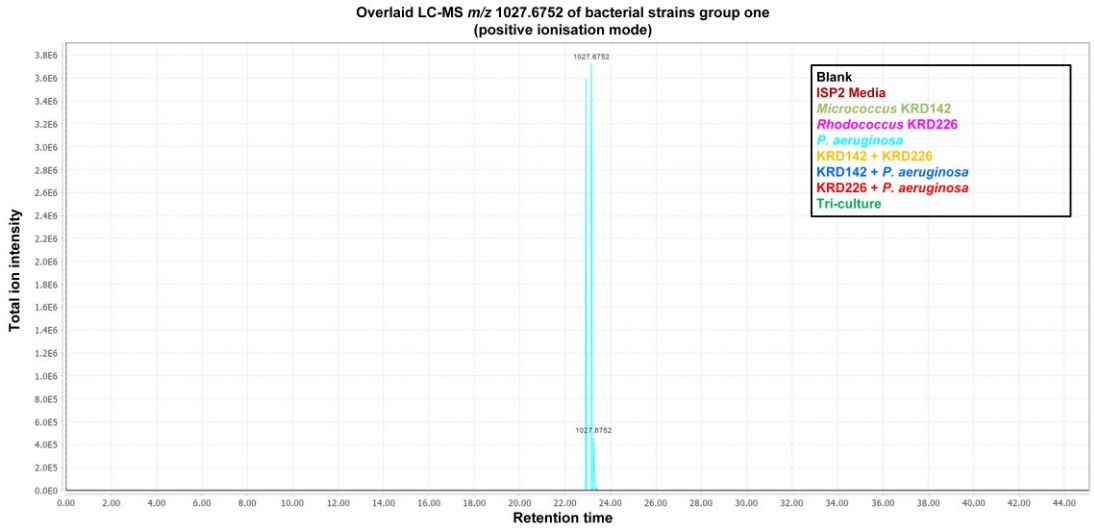

Figure 4.9. *P. aeruginosa* bacterial extract specific parent ion (*m/z* 1027.6752) detected in LC-MS positive ionisation mode. This ion was suppressed under the one-to-one cultures and tri-culture. The chromatogram indicates the parent ion intensity (y axis) and the retention time (x axis). This (*m/z* 1027.6752) is detected in the extracts of the *P. aeruginosa* mono-culture (colour-coded in turquoise).

To confirm the discrimination of the tri-culture from the mono-cultures, the volcano analysis (combination of fold change and t-test) was performed. This analysis evaluated if these parent ions were statistically significant ($p < 0.05$) between the mono-cultures and tri-cultures (**Figure 4.10**). The volcano plot was constructed by plotting the fold change (x axis) between the two conditions against the negative log (-10) of the p value (y axis). Parent ions with low p values appear towards the top of the plot and are the most significant. The volcano plot showed that a total of 4179 parent ions were statistically significant ($p < 0.05$) for discriminating the tri-culture from the mono-cultures (dots found further away from point 0 in the X axis, and higher up in the Y axis, **Figure 4.10**). Therefore, these results reinforce the previous findings observed by PCA and PLS-DA.

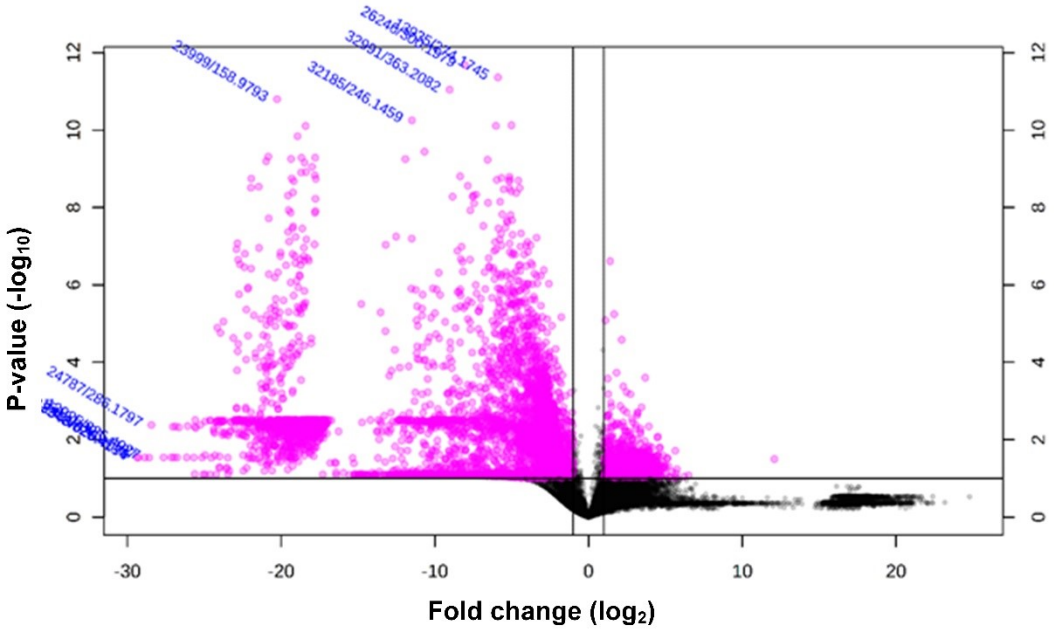

Figure 4.10. Volcano plot of mono-cultures (right) and tri-cultures (left). Each dot represents one parent ion. Statistically significant ($p < 0.05$) parent ions are coloured pink and non-significant parent ions are coloured black. The vertical axis (Y) indicates the p-value (in $-\log_{10}$ scale) with the thick line representing a p-value of 0.05. The horizontal axis (X) indicates the fold change between the experimental groups (in $\log_2$ scale). The further up in the Y-axis and further away from 0 in X-axis a parent ion is located, the more statistically significant ($p < 0.05$).

4.2.3 LC-MS analysis of group two (*Rhodococcus* KRD226, *Micromonospora* KRD244 and *Streptomyces* KRD257) reveals interaction specific parent ions

To determine the total number of parent ions that were interaction specific, all parent ions detected in each group were identified from all bacterial extracts. The total number was 23765, from which 520 parent ions originated from the media control, 396 parent ions were *Rhodococcus* KRD226 mono-culture specific, 732 were *Micromonospora* KRD244 mono-culture specific and 1642 were *Streptomyces* KRD257 mono-culture specific (**Table 4.2**). A total of 1321 ions were detected in the tri-culture extracts, 1211 in the *Rhodococcus* KRD226 and *Micromonospora* KRD244 one-to-one cultures, 1822 ions were detected in the bacterial extracts of the *Micromonospora* KRD244 and *Streptomyces* KRD257 one-to-one cultures, and 1769 were detected in the bacterial extracts of the *Rhodococcus* KRD226 and *Streptomyces* KRD257 one-to-one cultures (**Table 4.2**). There were then 14352

parent ions, 6393 of these were detected in more than one interaction and 7959 were shared between mono-cultures and co-cultures. These data indicate that 54% of all parent ions detected in this group (excluding parent ions detected in the media controls) were elicited by bacterial interactions (**Table 4.2**).

Table 4.2. Number of parent ions detected in positive ionisation for bacterial strains group two (*Rhodococcus* KRD226, *Micromonospora* KRD244 and *Streptomyces* KRD257). The columns indicate the replicate specific parent ions: ions detected only in one replicate, commonly detected: parent ions detected in two replicates of the same experimental group, and present in the three replicates: parent ions detected in the three replicates of the same experimental group. The last row (shared between two or more experimental groups), indicates the total number of parent ions that were detected in two or more experimental groups.

Bacterial extract	Replicate specific parent ions			Parent ions commonly detected in two experimental replicates			Present in the three replicates	Total
	1	2	3	1 and 2	1 and 3	2 and 3		
Rhodococcus KRD226 mono-culture	19	26	6	44	36	49	216	396
Micromonospora KRD244 mono-culture	8	39	44	6	10	59	566	732
Streptomyces KRD257	33	141	73	321	189	287	598	1642
One-to-one culture of *Rhodococcus* KRD226 and *Micromonospora* KRD244	48	23	100	69	41	56	874	1211
One-to-one culture of *Rhodococcus* KRD226 and *Streptomyces* KRD257	77	86	99	368	106	541	492	1769
One-to-one culture of *Micromonospora* KRD244 and *Streptomyces* KRD257	91	126	173	265	189	142	836	1822
Tri-culture	167	16	23	74	154	349	538	1321
Shared between two or more interactions								6393
Shared between mono-cultures and interactions								7959

To assess the chemical similarity between experimental groups prior to multivariate data analysis, a PCA of the unprocessed raw LC-MS data was performed (each score of the PCA plot represented one bacterial extract). The PCA discriminated all one-to-one cultures and the tri-culture from the mono-cultures (**Figure 4.11**). Furthermore, all experimental groups were separated from the media control and solvent blanks (**Figure 4.11** and **Table S4.3**). The tri-culture (eigenvalues PC1: -57.6898, -120.56, -122.067 and PC2: 29.43518, 28.91764, 27.19034), the *Micromonospora* KRD244 and *Streptomyces* KRD257 one-to-one culture (eigenvalues PC1: -79.5677, -50.5311, -119.257 and PC2: 14.94865, -4.5062, 28.72063) and the *Rhodococcus* KRD226 and *Streptomyces* KRD257 one-to-one culture (eigenvalues PC1: -54.0091, -100.787, -119.551 and PC2: -0.88586, 11.68399 and 8.582731) contributed to the largest variance of the PCA pot (**Figure 4.11** and **Table S4.3**)**.** The tri-culture and the one-to-one cultures with the *Streptomyces* KRD257 were situated closer to the *Streptomyces* KRD257 mono-culture than to the other mono-cultures (**Table S4.3**). This suggests the possible elicitation of interaction specific parent ions that were related to those produced by the *Streptomyces* strain. Similarly, metabolites produced under the *Rhodococcus* KRD226 and *Micromonospora* KRD244 one-to-one cultures were more related to the mono-cultures of the *Micromonospora* strain. This indicates these strains as possible producers of metabolites under one-to-one culture (**Table S4.3**).

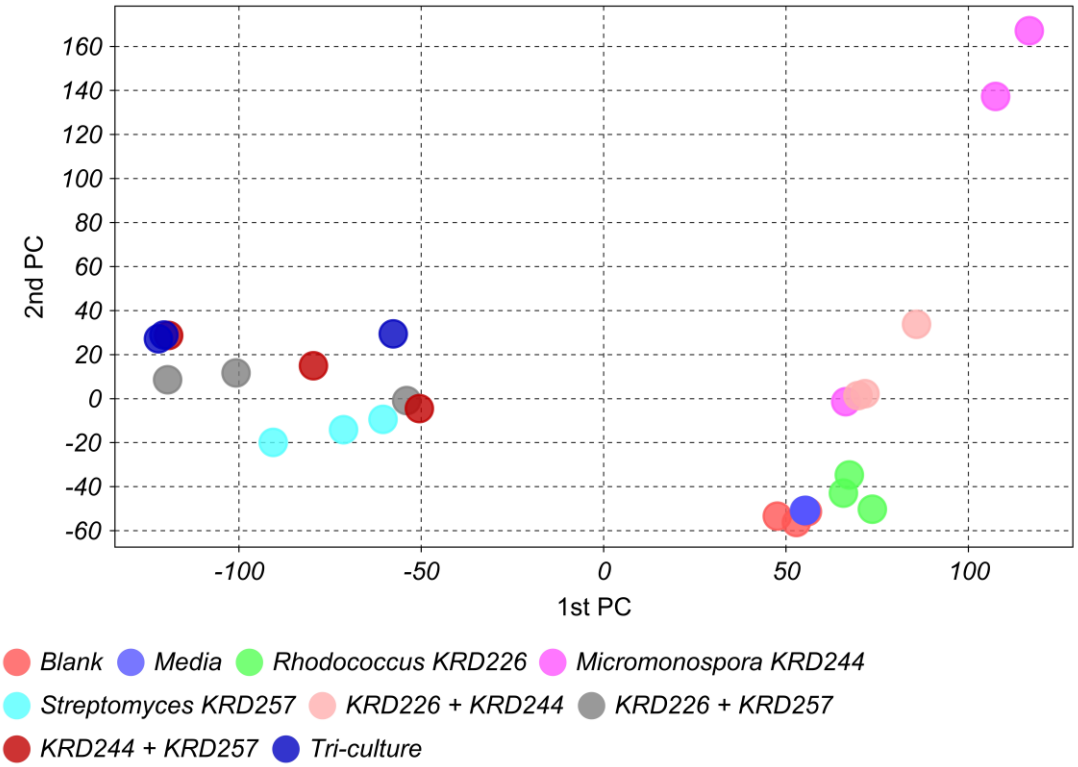

Figure 4.11. PCA scores reveal the separation between mono-cultures, one-to-one cultures and tri-cultures of *Rhodococcus* KRD226, *Micromonospora* KRD244 and *Streptomyces* KRD257 bacterial extracts. PCA scores are based on the first and second PCs (x-axis and y-axis). Each dot of the plot belongs to one bacterial extract. Each experimental group is colour-coded.

In order to detect LC-MS peaks that were interaction specific, chromatograms for all experimental groups were overlaid. Overlaid LC-MS chromatograms revealed the detection of *m/z* 1128.6597 which was detected under tri-culture and one-to-one cultures of the *Micromonospora* KRD244 and the *Streptomyces* KRD257, and the *Rhodococcus* KRD226 and *Micromonospora* KRD244 (**Figure 4.12**). These results suggest that this parent ion was produced by the *Micromonospora* strain under tri-culture and one-to-one culture.

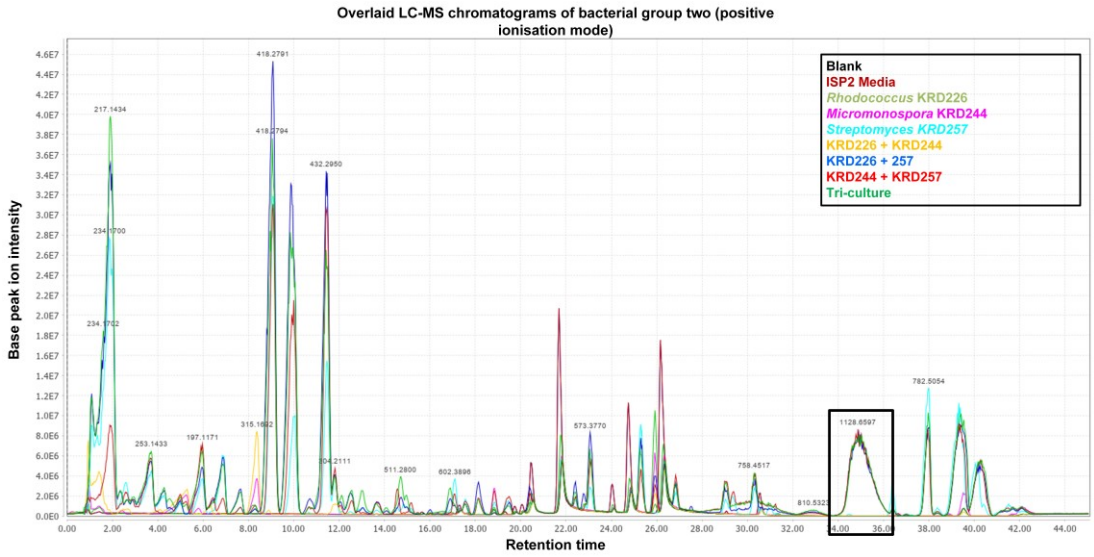

Figure 4.12. Positive ionisation mode LC-MS overlaid chromatograms of bacterial extracts from *Rhodococcus* KRD226, *Micromonospora* KRD244 and *Streptomyces* KRD257 mono-cultures, one-to-one cultures and tri-cultures. The chromatogram indicates the parent ion intensity (y axis) and the retention time (x axis). High intensity ions are labelled with the respective *m/z*. Each experimental group is colour coded. The black box highlights the peak that was detected under one-to-one cultures and tri-cultures but not by the mono-cultures.

4.2.4 Comparative metabolomics analysis of bacterial group two confirms metabolite production elicited by co-cultures

To confirm the group discrimination observed by the previous PCA and to detect parent ions responsible for this classification, processed LC-MS data (ion intensity values) was normalised (**Figure S4.6**) and subjected to multivariate data analysis.

To discriminate experimental groups that were producers of co-culture elicited parent ions, an unsupervised PCA was performed. The PCA plot was generated using Pareto scaling and the first five PCs. The PCA showed that the first two PCs explained 64.3% of the variance in the data set and these were enough to capture most of the information without losing important data (**Figure 4.13A**). The scree plot showed a large variation in slopes at the first PC and a smaller change at the second PC. These data indicate that the two first PCs captured enough variance (**Figure 4.14**). The PCA revealed that the extract replicates for each group clustered together which indicated consistent and reproducible results. The tri-cultures, two groups of one-to-one cultures (*Rhodococcus* KRD226 and *Streptomyces* KRD257, and *Micromonospora*

KRD244 and *Streptomyces* KRD257) clustered very close to each other (**Figure 4.13A**). PCA revealed that these groups (tri-culture and the two one-to-one cultures) clustered close to the *Streptomyces* KRD257 mono-culture (**Figure 4.13A**). These data suggests that interaction-elicited parent ions were produced by this strain. In addition, the mono-cultures of the *Rhodococcus* KRD226 and *Micromonospora* KRD244 and the one-to-one culture of these two strains clustered close to each other (**Figure 4.13A**). It was hypothesised that one-to-one cultures and tri-cultures produced parent ions that were elicited by bacterial competition but they were related to those produced by the mono-cultures.

Since many parent ions (8479) were detected in all the tri-cultures, one-to-one cultures and mono-cultures, a discrimination between all experimental groups was not observed. However, PCA revealed a separation between two subgroups of bacterial extracts. The first subgroup was the *Streptomyces* KRD257 mono-culture, tri-culture and one-to-one cultures of the *Rhodococcus* KRD226 and *Streptomyces* KRD257, and the *Micromonospora* KRD244 and *Streptomyces* KRD257 (**Figure 4.13A**). The second subgroup was the *Rhodococcus* KRD226 and *Micromonospora* KRD244 mono-cultures and the one-to-one culture between these two strains. The PCA loadings plot identified parent ions that contributed to this variance and the separation of these two groups (**Figure 4.13B**). The loading plots showed that these parent ions were observed as outliers in the middle right quadrants of the loadings plot for subgroup one (*m/z* 418.2785, 418.2804, 418.2813, 416.2635, 432.294, 432.2971, 432.2910, 796.5185, 796.5260, 796.5110) and the upper left quadrants for subgroup two (*m/z* 315.1694, 315.1726, 315.1730, 315.1671, 332.1957 and 332.1982) (**Figure 4.13B**). However, PCA results were not conclusive since a clear separation was not observed between the experimental groups of each sub-group. This complicated the identification of parent ions that were produced by the co-cultures.

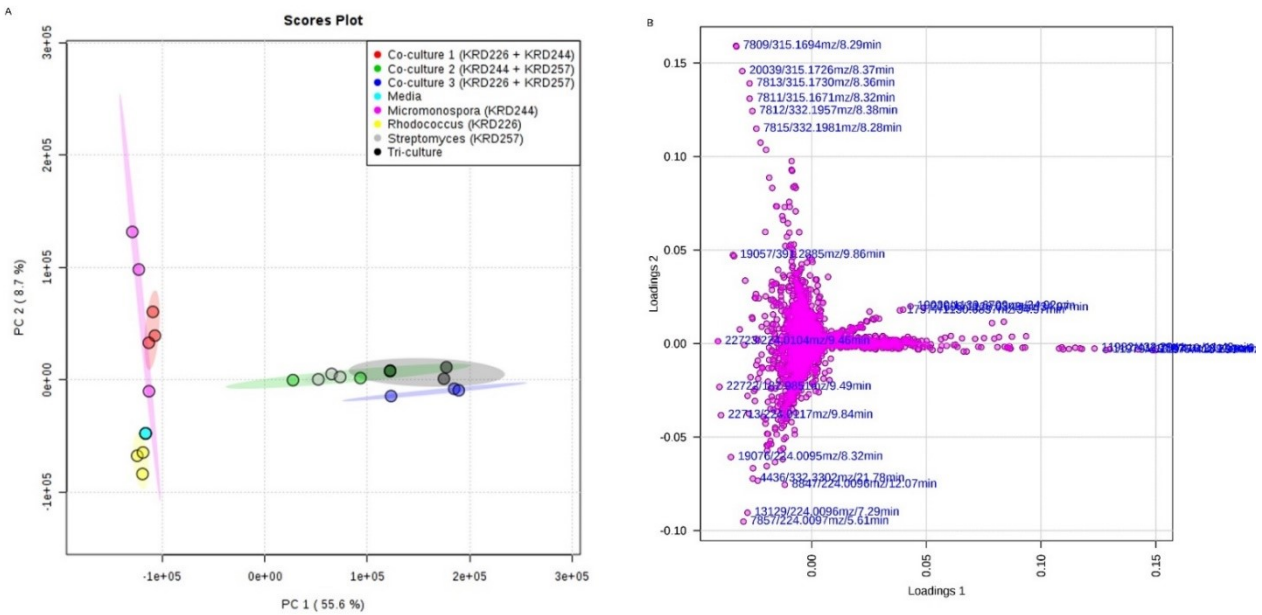

Figure 4.13. PCA scores reveal the separation between mono-cultures, one-to-one cultures and tri-cultures of *Rhodococcus* KRD226 and *Micromonospora* KRD244 and *Streptomyces* KRD257 bacterial extracts and the loadings plot indicate the parent ions responsible for this separation. A) PCA scores plot based on the two first PCs (PC1 and PC2). Each experimental group is colour-coded (red: *Rhodococcus* KRD226 and *Micromonospora* KRD244 one-to-one culture, green: *Micromonospora* KRD244 and *Streptomyces* KRD257 one-to-one culture, blue: *Rhodococcus* KRD226 and *Streptomyces* KRD257 one-to-one culture, turquoise: media control, pink: *Micromonospora* KRD244 mono-culture, yellow: *Rhodococcus* KRD226 mono-culture, grey: *Streptomyces* KRD257 mono-culture and black: tri-culture). The ellipses show the 95% confidence limit. B) PCA loadings plot. Each dot represents one parent ion from the dataset. Those parent ions situated with greater distance from the starting point of the loadings plot drive the variance in the PCA plot.

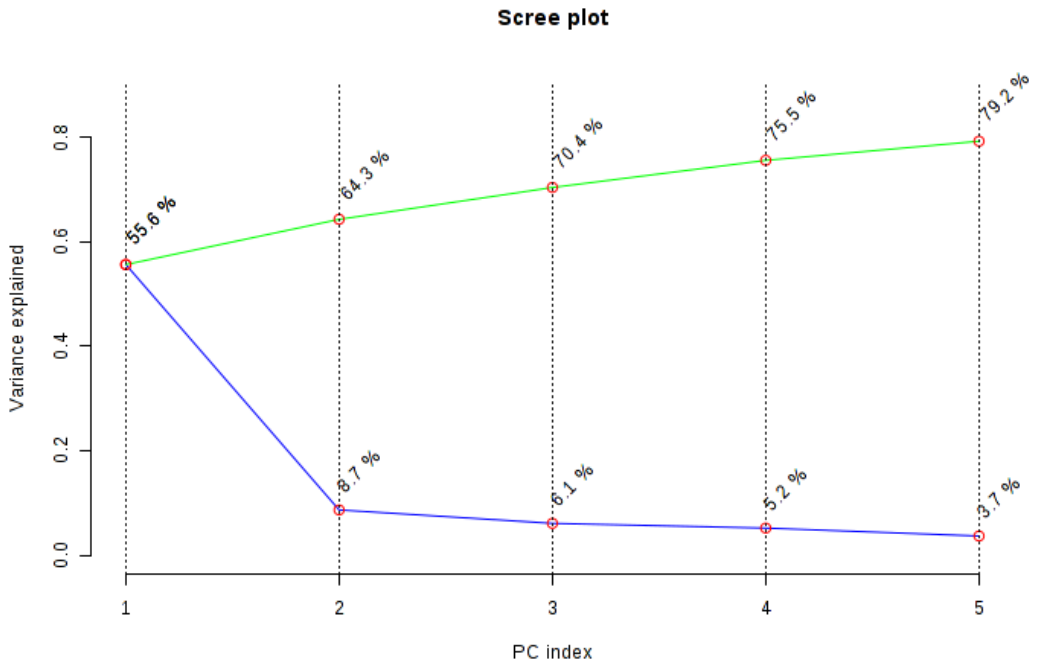

Figure 4.14. Scree plot shows the PCA variance explained by the first five PCs. The green line on top shows the accumulated variance explained; the blue line underneath shows the variance explained by individual PCs.

In order to achieve the maximum separation between experimental groups (mono-cultures, one-tone cultures and tri-cultures), data was further subjected to PLS-DA analysis. The R2 value was 0.61 and the Q2 value was 0.6, which were high enough to confirm the validity of the PLS-DA model (**Figure 4.15A**). The PLS-DA indicated that 60.1% of the variance of the dataset was explained by the first two PCs where the one-to-one cultures and the tri-culture contributed to the largest variance of PC1 (77%). PLS-DA revealed that all experimental groups except the *Micromonospora* KRD244 mono-culture, classified in separate quadrants from the media control. The bacterial extracts of the three mono-cultures were situated in different quadrants of the PLS-DA model (**Figure 4.15A**). This indicates chemical diversity between the three strains. Furthermore, the bacterial extracts of the one-to-one cultures between the *Micromonospora* KRD244 and the *Streptomyces* KRD257, and the *Rhodococcus* KRD226 and the *Streptomyces* KRD257 were situated closer to each other than to the other experimental groups (**Figure 4.15A**). The PLS-DA loadings plot showed the parent ions that contributed to the separation of these two one-to-one cultures from the other groups and between each other (lowest right outliers in **Figure 4.15B**), which

were not previously distinguishable by PCA. For example, the outliers that were situated in the quadrant of the *Micromonospora* KRD244 and the *Streptomyces* KRD257 one-to-one culture (*m/z* 416.2635, 432.2941, 416.2606, 416.2663, 432.2910 and 432.2971) were detected in this experimental group (**Figure 4.15A,B** and **Figure S4.8**). Furthermore, outliers *m/z* 418.2754, 418.2804 and 418.2813 (situated in the quadrant of the one-to-one culture of the *Rhodococcus* KRD226 and the *Streptomyces* KRD257 in **Figure 4.15B**) were specific to the one-to-one culture of the *Rhodococcus* KRD226 and *Streptomyces* KRD257 (**Figure S4.9**). The LC-MS overlaid chromatograms confirmed the detection of these parent ions under these experimental groups (**Figure S4.8** and **Figure S4.9**). These data indicate the production of group specific parent ions.

In contrast with the PCA, the tri-cultures were separated from all the other groups (**Figure 4.15A**). The PLS-DA loadings plot showed that parent ions *m/z* 796.5110, 796.5259 and 796.5185 were responsible for the discrimination of this group (**Figure 4.15B**). One parent ion (*m/z* 452.2791) that was detected under the one-to-one culture of the *Rhodococcus* KRD226 and *Micromonospora* KRD244 was identified through PLS-DA as specific to this interaction (lower left quadrant in **Figure 4.15B**). The LC-MS chromatograms revealed that these parent ions were specific to these groups (**Figure S4.9** and **Figure S4.10**). These findings reinforced the hypothesis that metabolites were produced as a result of bacterial interactions.

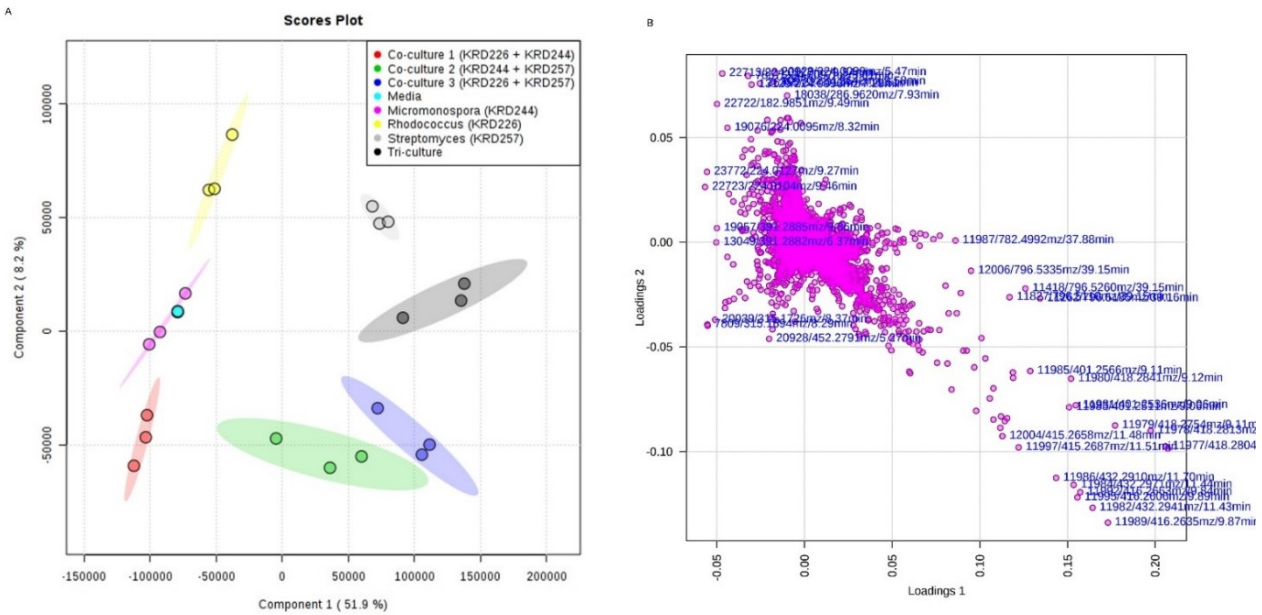

Figure 4.15. PLS-DA scores reveal the separation between mono-cultures, one-to-one cultures and tri-cultures of *Rhodococcus* KRD226, *Micromonospora* KRD244 and *Streptomyces* KRD257 bacterial extracts and the loadings plot indicate the parent ions responsible for this separation. A) PLS-DA scores plot based on the two first PCs (PC1 and PC2). Each experimental group is colour-coded (red: *Rhodococcus* KRD226 and *Micromonospora* KRD244 one-to-one culture, green: *Micromonospora* KRD244 and *Streptomyces* KRD257 one-to-one culture, blue: *Rhodococcus* KRD226 and *Streptomyces* KRD257 one-to-one culture, turquoise: media control, pink: *Micromonospora* KRD244 mono-culture, yellow: *Rhodococcus* KRD226 mono-culture, grey: *Streptomyces* KRD257 mono-culture and black: tri-culture). The ellipses show the 95% confidence limit. B) PCA loadings plot. Each dot represents one parent ion from the dataset. Those parent ions situated with greater distance from the starting point of the loadings plot drive the variance in the PCA plot.

To detect parent ions that were not detectable by the loadings plot, VIP scores were calculated. The first 50 parent ions that contributed the most (by descendent order) to the variance (P > 1) in bacterial strains group two are shown in **Figure 4.16** and **Table S4.4**. VIP revealed that the parent ions that were previously identified as tri-culture outliers by PLS-DA (*m/z* 796.5185, 796.5260 and 796.5110) contributed to the largest variance of the PLS-DA (P = 21.956, 20.513 and 19.194, respectively) (**Figure 4.16** and **Table S4.4**). The parent ions *m/z* 416.2635 (P = 16.93), 432.2941 (P = 16.717), 432.2971 (P = 15.599), 416.2663 (P = 15.292), 416.2606 (P = 15.279) and 432.2910 (P= 14.556) were detected under the one-to-one culture of the *Micromonospora* KRD244 and the *Streptomyces* KRD257 while *m/z* 418.2804 (P = 15.922), 418.2813 (P = 15.211), 418.2754 (P = 13.777) and 401.2536 (P = 12.056) were elicited by the *Rhodococcus* KRD244 and *Streptomyces* KRD257 one-to-one culture (**Figure 4.16** and **Table S4.4**). The parent ions *m/z* 415.2687 and 415.2658 were specific to these two one-to-one cultures (**Figure 4.16**) but were not detected under mono-culture or tri-culture. VIP classified the parent ion (*m/z* 452.2791) detected in the *Rhodococcus* KRD226 and *Micromonospora* KRD244 one-to-one culture within the 50 parent ions that contributed to the largest variance (P = 7.489). These findings suggest that in this case, all co-cultures elicited the production of metabolites that were not produced in mono-culture.

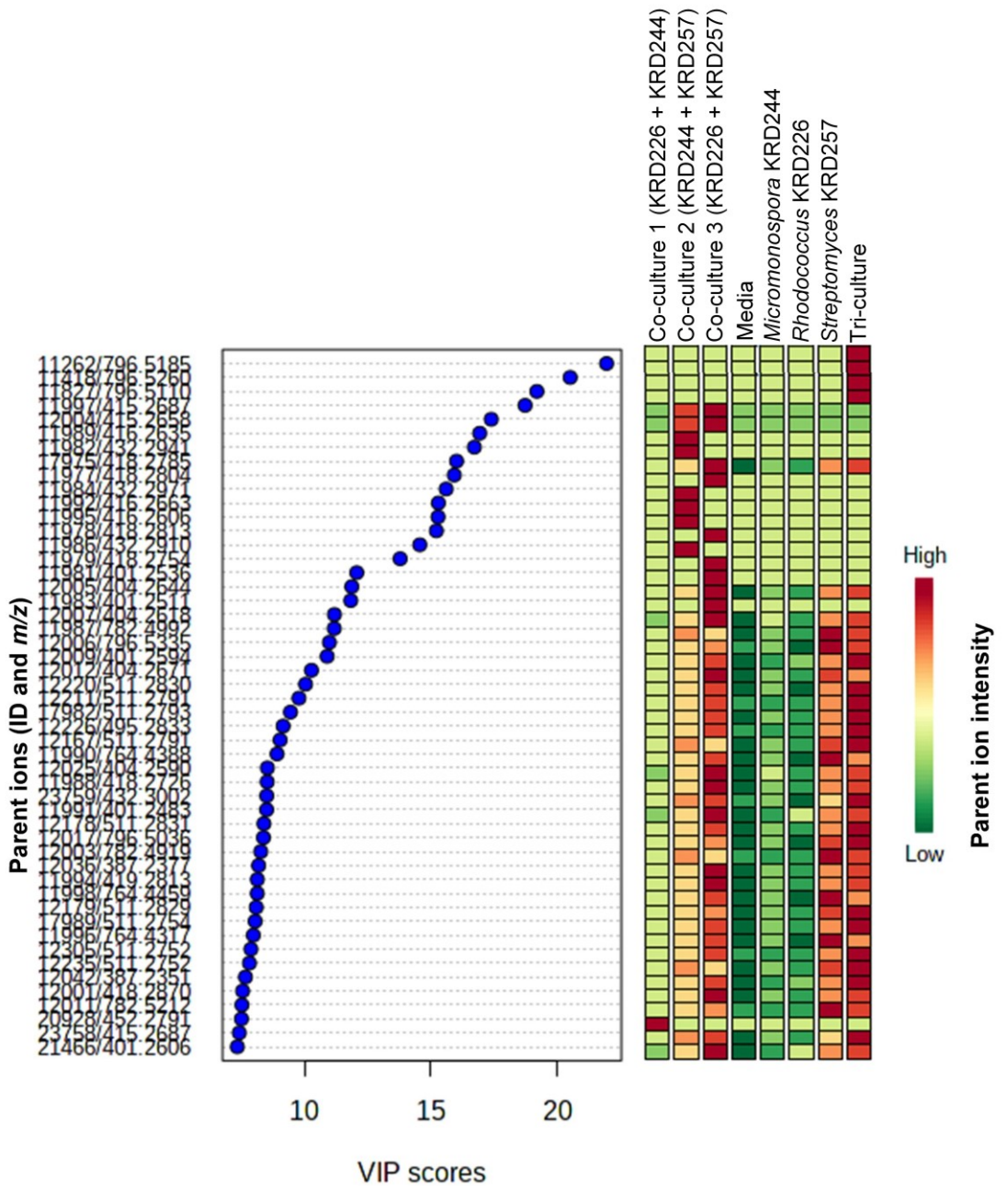

Figure 4.16. VIP scores plot reveals 50 parent ions identified by PLS-DA as tri-culture and co-culture specific. Blue dots indicate the VIP scores ranged between five and 25, scores that are P > 1 are considered significant. The coloured boxes on the right indicate the relative abundance of the corresponding parent ion in each experimental group. The VIP scores are detailed in supplementary **Table S4.4.**

4.3 Discussion

This chapter aimed at understanding if the strain phenotypic alterations from eight prioritised bacterial interactions (six one-to-one-cultures and two tri-cultures) were a result of specialised metabolite elicitation. Bacterial extracts were analysed by LC-MS and data was processed and compared using multivariate data analysis. This analysis focused on four strains isolated from marine sediments and *P. aeruginosa* that are producers of biologically active secondary metabolites against *S. aureus* and *E. faecalis*. The findings revealed that tri-cultures and one-to-one cultures elicited specialised metabolites. This was observed by the PCA and PLS-DA of the two bacterial groups (*P. aeruginosa*, *Micrococcus* KRD142 and *Rhodococcus* KRD226 and *Rhodococcus* KRD226, *Micromonospora* KRD244 and *Streptomyces* KRD257) which showed parent ions as outliers indicating interaction specific metabolites. The production of interaction specific metabolites reinforced the competitive behaviours between the strains and as previously observed suggested that these led to phenotypic alterations (Gonzalez *et al.*, 2011; Schoenian *et al.*, 2011; Yang *et al.*, 2011; Khalil *et al.*, 2019; Thissera *et al.*, 2020). The antagonism and the increased number of specialised metabolites by the ecologically relevant bacterial interactions between the *Rhodococcus* KRD226, the *Micromonospora* KRD244 and the *Streptomyces* KRD257 supported the hypothesis that the elicited metabolites were responsible for the morphological alterations such as aerial hyphae and growth inhibition. In line with these results, a previous report showed that the co-culture of *Streptomyces* sp. CMB-StM0423 and *Aspergillus* sp. CMB-AsM0423 resulted in a zone of clearance between the two strains (Khalil *et al.*, 2019). The MS analysis revealed that *Aspergillus* sp. produced cyclo-(l-Phe-trans-4-hydroxy-l-Pro) with antibacterial activity against *Streptomyces* strain and the *Streptomyces* sp. produced heronapyrrole B with antifungal activity against *Aspergillus* sp. (Khalil *et al.*, 2019). Therefore, this demonstrated that the inhibition was a result of the production of these two metabolites.

Interestingly, the phenotypic analysis of the co-culture between *Micrococcus* KRD142 and *Rhodococcus* KRD226 in chapter three did not show phenotypic effects while the LC-MS based comparative metabolomics analysis did not reveal induction of specialised metabolites. An hypothesis for this is that the strains were able to coexist since in the natural environment positive interactions may enhance the sharing of resources between strains (Galet *et al.*, 2015). However, this could simply be the result of two strains that have no negative physiological effects against each other.

Another relevant finding was the increased number of metabolites detected by the tri-cultures when compared to the one-to-one cultures and the mono-cultures. One explanation is that increasing the number of strains in a co-culture may increase the competition between strains (Fischer *et al.*, 2017). The tri-culture of *Saccharomyces cerevisiae*, *Acetobacter malorum* and *Lactobacillus plantarum* produced more acetoin than the co-culture of *Saccharomyces cerevisiae* and *Acetobacter malorum* (Fischer *et al.*, 2017). This suggests that more complex microbial communities can produce more specialised metabolites as a result of an increased number of bacterial interactions. However, the increased number of metabolites under co-culture can also result from metabolic cross-feeding where metabolites from one strain are used as nutrients by another strain (Smith *et al.,* 2019). For instance, under *E. coli* and *Salmonella enterica* co-culture, *E. coli* repeatedly secreted galactose to feed *S. enterica* enhancing the growth of *S. enterica* (Harcombe *et al.,* 2018). In contrast, syntrophic relationships can enable access to substrates that strains could not metabolise alone. For example, a strain that consumes hydrogen can enhance the fermentation of other products to become favourable (Morris *et al.,* 2013) and benefit all the strains. Additionally, an important limitation of the untargeted metabolomics approach followed here, is that PCA and PLS-DA multivariate data analysis do not consider that co-cultures are composed by more than one strain (Bertrand *et al.*, 2014). For that reason, in this case, comparative metabolomics might not always detect co-culture elicited metabolites (Bertrand *et al.*, 2014).

Previous reports postulated that bacteria living in marine environments developed these chemical defences as survival mechanism that reduce the presence of competitive microorganisms (Teasdale *et al.*, 2009; Núñez-Montero and Barrientos, 2018). In addition, this strategy enables them to adapt to the extreme conditions of these environments such as salinity, depth, lack of light, high pressure and low/high temperatures (Fenical, 1993). This competitive behaviour is more likely to occur in such complex habitats when nutrients are limited (Núñez-Montero and Barrientos, 2018). Therefore, considering that in the natural environment microorganisms are in constant interaction with one another (Serrano *et al.*, 2017), the ability of these five strains to produce metabolites with inhibitory activities under co-culture is likely a result of these competitive strategies. Similarly, previous studies showed that bacterial extracts isolated from marine sediments showed antibacterial activities against human pathogens such as *S. aureus* and *C. albicans* (Quintero *et al.*, 2018). For instance, a study discovered a novel metabolite, dentigerumycin E from the

ecologically relevant co-culture between the marine isolates *Streptomyces* sp. JB5 and *Bacillus* sp. GN1 (Shin *et al.*, 2018). Despite that the genomic analysis of the *Streptomyces sp.* JB5 previously identified the BGC that encoded dentigerumycin E, the production of this metabolite was first elicited under co-culture (Shin *et al.*, 2018). This reinforced that *Streptomyces sp.* JB5 produced dentigerumycin E as a defence mechanism. Therefore, these data suggest that the combination of metabolomics to compare between experimental conditions with genomics can advance the knowledge in how are metabolites produced and the factors that induce their production.

In conclusion, this chapter added insights in the understanding of chemical exchange between bacterial strains, where specialised metabolites were produced as a defence mechanism. This demonstrates the importance of the co-culture method for the discovery of novel natural products. In addition, it was demonstrated that MS-based metabolomics is a valuable approach for the prioritisation of strains and bacterial chemistry. LC/MS-based comparative metabolomics enabled the rapid detection of previously discovered metabolites, therefore, avoiding a time-consuming and expensive scale-up chromatography fractionation. However, future work in metabolite dereplication is necessary to establish novel metabolites. In future, it will be interesting to perform studies with more than three strains to understand more complex bacterial interactions and to increase microbial chemical diversity.

CHAPTER 5: BACTERIAL NTERACTIONS ARE IMPACTED BY GROWTH CONDITIONS

The study of bacterial interactions under laboratory conditions encounters challenges and limitations. This complicates the understanding of these interactions. One limitation is the timeframe that each strain requires to achieve exponential growth phase (Freilich *et al.*, 2011). This is important since specialised metabolites are produced through all growth stages (Čihák *et al.*, 2017; Arora *et al.*, 2020) and strains grow and develop at different rates (Khan *et al.*, 2018). In addition, this is relevant since secondary metabolites that are produced at later growth stages are not detected in short-incubation time experiments (Roullier *et al.*, 2016). To address this, time course studies investigate the incubation time at which strains achieve the maximal specialised metabolite production (Jacob *et al.*, 2017; Lim *et al.*, 2018). In addition, time optimisation for co-culture experiments also aim at unravelling interaction patterns triggered by chemical exchange (Patin *et al.*, 2018). This is important as it highlights the complexity of microbial interactions (Geurts *et al.*, 2017). For instance, the time series study (48, 72, 96, 120, 144, and 168 hours) of *S. coelicolor* under liquid culture revealed an increased production of prodiginines and other antibiotics such as phaeochromycin G at 96 hours (Lim *et al.*, 2018). It was found that *S. coelicolor* initiated its metabolite production at 96 hours achieving maximal production between 120 and 144 hours followed by a decrease (Lim *et al.*, 2018). Another comparative metabolomics time-course experiment (two, four, seven and nine days) of *Fusarium* and *Aspergillus* strains revealed that the number of produced metabolites increased over time, achieving the maximal production on day nine (Bertrand *et al.*, 2014). Furthermore, it also revealed the production time-frame of several parent ions. For example, *m/z* 481.032 was detected from the fourth to the nineth day while *m/z* 581.131 was only produced at day nine (Bertrand *et al.*, 2014). Similarly, *Shewanella xiamenensis* 318 produced capsimycin after 12 hours of growth while xiamenmycin A was produced at a later stage of the *S. xiamenensis* 318 lifespan (Zhu *et al.*, 2019). Therefore, these data suggest that investigating the impact of growth phases and time in bacterial co-cultures is key in understanding metabolite shifts and the elicitation of metabolites that are not produced under short incubation time (Geurts *et al.*, 2017; Patin *et al.*, 2018).

However, time course co-culture experiments present several limitations that need to be considered. First of all, all strains involved in the co-culture need to grow at least

at the start of their life cycle. Since these assays combine two or more strains, controlling their growth under liquid co-culture with OD_{600} readings is not viable. In addition, the competitive fitness of each strain can change during the experiment as their growth ratios variate over time. In chapters three and four the interaction between *Rhodococcus* KRD226 and *Micromonospora* KRD244 was prioritised as a result of an increased antibacterial activity against *S. aureus* compared to mono-cultures. However, less than five parent ions elicited by this co-culture were detected by LC-MS. Since both strains required different incubation times to achieve exponential growth this can limit the number of produced metabolites. Therefore, considering the potential bioactivity from this interaction, this chapter aimed at assessing the impact of growth phases and incubation time on the specialised metabolite production of this co-culture.

5.1 Aims and objective

The main objective of this chapter was to explore the secondary metabolite potential of a bioactive co-culture (*Rhodococcus* KRD226 and *Micromonospora* KRD244) by changing growth parameters (incubation time and growth phase) to understand how this impacts the secondary metabolism and chemical exchange.

Aim 1: to identify the chemical response of bacterial competition during two growth-phases (lag-phase and transitional-phase).

Aim 2: to investigate the influence of incubation time on competition and specialised metabolite production of the *Rhodococcus* KRD226 and *Micromonospora* KRD244 strains.

5.2 Results

To assess the impact of exponential-phase, lag-phase and incubation time on the secondary metabolism of the *Rhodococcus* KRD226 and *Micromonospora* KRD244 co-culture and mono-cultures, growth phase and time-series experiments were performed. These assays were carried out on ISP2 broth to keep consistent with previous experiments. The growth of each strain was monitored under mono-culture by taking OD_{600} readings every two hours for the *Rhodococcus* KRD226 and every 24 hours for the *Micromonospora* KRD244 from which growth curves were plotted.

5.2.1 Impact of growth phase on the strains' secondary metabolism

To evaluate the impact of exponential-phase on secondary metabolism the liquid mono-cultures of the two strains were mixed together when both strains were growing in transitional-phase (**Figure 5.1**). The growth curves showed that while *Rhodococcus* KRD226 entered exponential-phase after approximately 12 hours, *Micromonospora* KRD244 needed approximately 120 hours. Therefore, the strains were mixed together at 24 hours of *Rhodococcus* KRD226 growth and 168 hours of *Micromonospora* KRD244 growth (**Figure 5.1C and D**). The transitional-phase co-culture was then incubated for further seven days prior to LC-MS and multivariate data analysis. To assess the impact of lag-phase in secondary metabolism, both strains were inoculated together from time point zero (lag-phase co-culture) and incubated for seven days.

In order to determine if the strains were alive after growing under co-culture, a viability test was performed. The viability plates showed that *Rhodococcus* KRD226 was able to be cultured on solid media from the lag-phase and transitional-phase co-cultures (data not shown). However, the viability test was insufficient to determine if the *Micromonospora* KRD244 was alive as this assay was limited by the growth rate of the strains. As observed in **Figure 5.1**, *Rhodococcus* KRD266 grows faster than *Micromonospora* KRD244. Therefore, it is probable that *Micromonospora* KRD244 was masked by the fast growth of *Rhodococcus* KRD226 on the viability plates. Although other selective media were considered for these experiments, they were performed under ISP2 to keep consistency with previous co-culture experiments and to compare LC-MS results with previous metabolomics data.

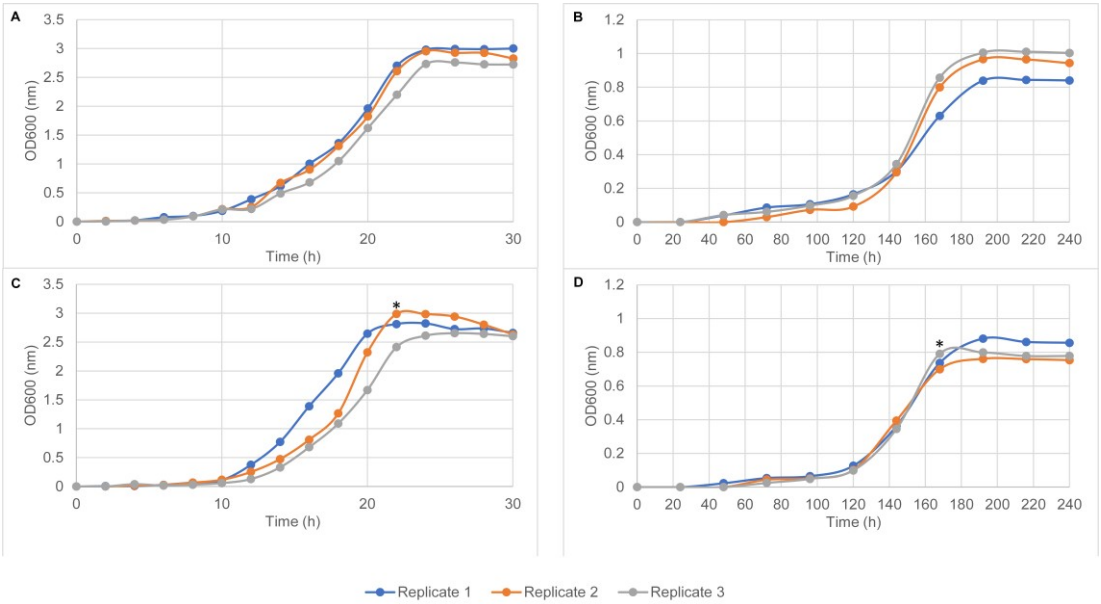

Figure 5.1. Growth curves representing the OD_{600} measurements for the *Rhodococcus* KRD226 and *Micromonospora* KRD244 mono-cultures. The x-axis indicates the time in hours and the y-axis the OD_{600}. Asterisk (*) indicates the time point at which each mono-culture was mixed with the other strain's mono-culture. A-B) *Rhodococcus* KRD226 and *Micromonospora* KRD244 mono-culture control, C-D) *Rhodococcus* KRD226 mono-culture and *Micromonospora* KRD244 mono-culture used for the transitional-phase co-culture.

To determine the influence of the exponential-phase and lag-phase co-culture in the production of bioactive metabolites, antimicrobial activity assays were performed. The antibacterial screening results revealed that co-cultures were bioactive against *S. aureus* (**Figure 5.2**). Antimicrobial activity was significantly larger (14 mm) in the transitional-phase co-culture than in the lag-phase co-culture (1-2 mm) (**Figure 5.2**). To assess if the elicitation of these bioactive metabolites was a result of direct physical contact or a response to mono-culture metabolites, cultures using pre-conditioned media were performed. These assays showed that *Rhodococcus* KRD226 and *Micromonospora* KRD244 were not affected by each other's pre-conditioned media (**Figure 5.3**). Furthermore, antibacterial activity was not detected. These results suggest that the bioactive metabolites were elicited by the transitional-phase co-culture only when the strains were physically growing together.

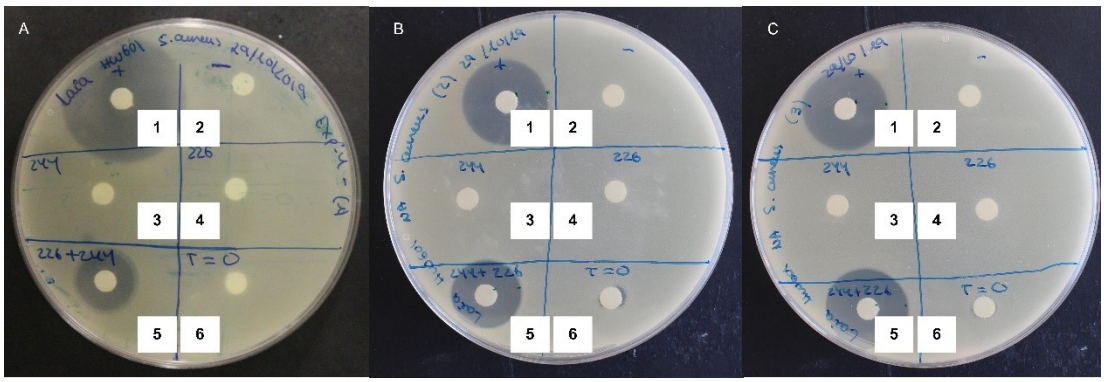

Figure 5.2. Bioactivity assays reveal antibacterial activity from the transitional-phase co-culture (5) against *S. aureus*. A-B) Experimental replicate one to replicate three. 1-6) Positive control (chloramphenicol), negative control (media extract), *Micromonospora* KRD244 mono-culture extract, *Rhodococcus* KRD226 mono-culture extract, transitional-phase co-culture extract and lag-phase co-culture extract.

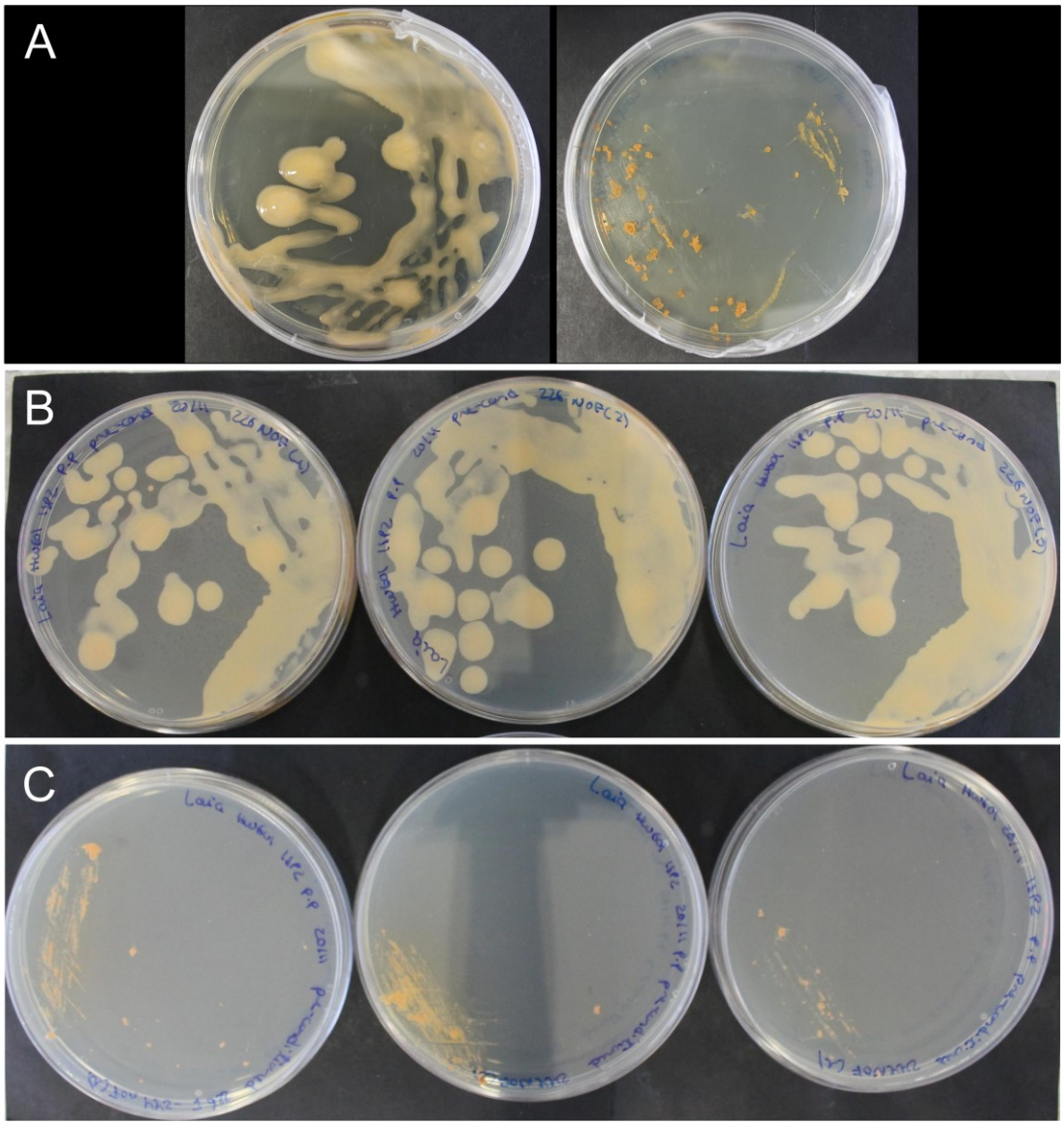

Figure 5.3. Pre-conditioned media assays reveal that the *Rhodococcus* KRD226 and *Micromonospora* KRD244 were able to grow in each other's pre-conditioned media. A-C) *Rhodococcus* KRD226 (left) and *Micromonospora* KRD244 (right) mono-culture control, *Rhodococcus* KRD226 growing on *Micromonospora* KRD244 pre-conditioned media and *Micromonospora* KRD244 growing on *Rhodococcus* KRD226 pre-conditioned media.

5.2.1.1 LC-MS analysis reveals that different growth phases impact the production of metabolites under co-culture

To determine the total number of parent ions detected for each experimental group, specific parent ions that belonged to each group were identified from all bacterial

extracts. The total number of detected parent ions was 17932 from which 1765 originated from the media control, 347 from the *Rhodococcus* KRD226 mono-culture, 839 from the *Micromonospora* KRD244 mono-culture, 10377 were transitional-phase co-culture specific and 1765 were lag-phase co-culture specific (**Table 5.1**). There were then 2839 parent ions that were shared between experimental groups (**Table 5.1**). These results indicate that 64% of parent ions were elicited by the transitional-phase co-cultures and over 80% between the transitional-phase and lag-phase co-cultures (**Table 5.1**).

Table 5.1. Number of parent ions detected in negative ionisation mode for experiment one. The columns indicate the replicate specific parent ions: ions detected only in one replicate, commonly detected: parent ions detected in two replicates of the same experimental group, and present in the three replicates: parent ions detected in the three replicates of the same experimental group. The last row (shared between two or more experimental groups), indicates the total number of parent ions that were detected in two or more experimental groups.

Bacterial extract	Replicate specific parent ions			Parent ions commonly detected in two experimental replicates			Present in the three replicates	Total
	1	2	3	1 and 2	1 and 3	2 and 3		
Rhodococcus KRD226 mono-culture	10	4	5	18	9	16	285	347
Micromonospora KRD244 mono-culture	21	33	29	86	34	67	569	839
Transitional-phase co-culture	498	463	255	367	241	557	7996	10377
Lag-phase co-culture	98	149	46	132	329	192	819	1765
Shared between two or more experimental groups								2839

To assess if the transitional-phase co-culture impacted the specialised metabolism of the strains, a PCA of the unprocessed LC-MS data was performed. The PCA revealed that the two groups of co-cultures were discriminated from the mono-cultures (**Figure 5.4**). Furthermore, the PC1 eigenvalues of the transitional-phase co-culture confirmed that this group contributed to the largest variance of PC1 (-218.645, -219.115 and -225.104) and that the lag-phase co-cultures contributed to the largest variance of PC2 (73.1563, 81.38069 and 76.6127) (**Table S5.1**). These data suggest the elicitation of specialised metabolites by the co-cultures.

In order to detect peaks that were detected under co-culture, the LC-MS chromatograms were overlaid and compared. The chromatograms revealed that over 10 parent ions were transitional-phase co-culture specific (*m/z* 393.2634, 638.3030, 640.2754, 650.2775, 652,2723, 652.2834, 654.2988, 696.3064, 763.3401, 777.3613 and 904.4092) (**Figure 5.5**). These data suggest that this co-culture elicited a metabolite that was responsible for the previously observed bioactivity. Furthermore, despite the separation by PCA for the lag-phase co-culture, specific peaks for this co-culture were not observed (**Figure 5.5**).

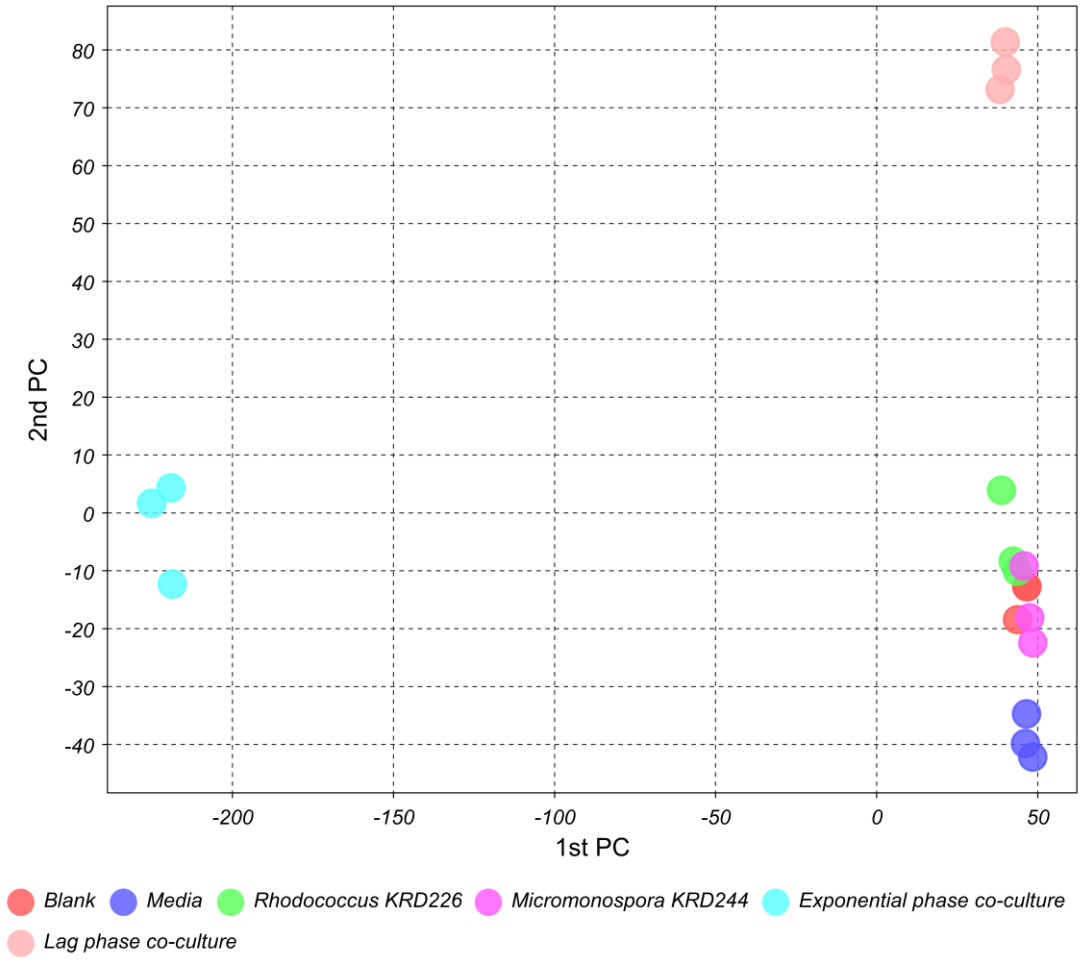

Figure 5.4. PCA scores reveal the separation of the *Rhodococcus* KRD226 and *Micromonospora* KRD244 transitional-phase co-culture and lag-phase co-culture from the mono-cultures. Score plots are based on the two first PCs (PC1 and PC2). Experimental groups are colour-coded.

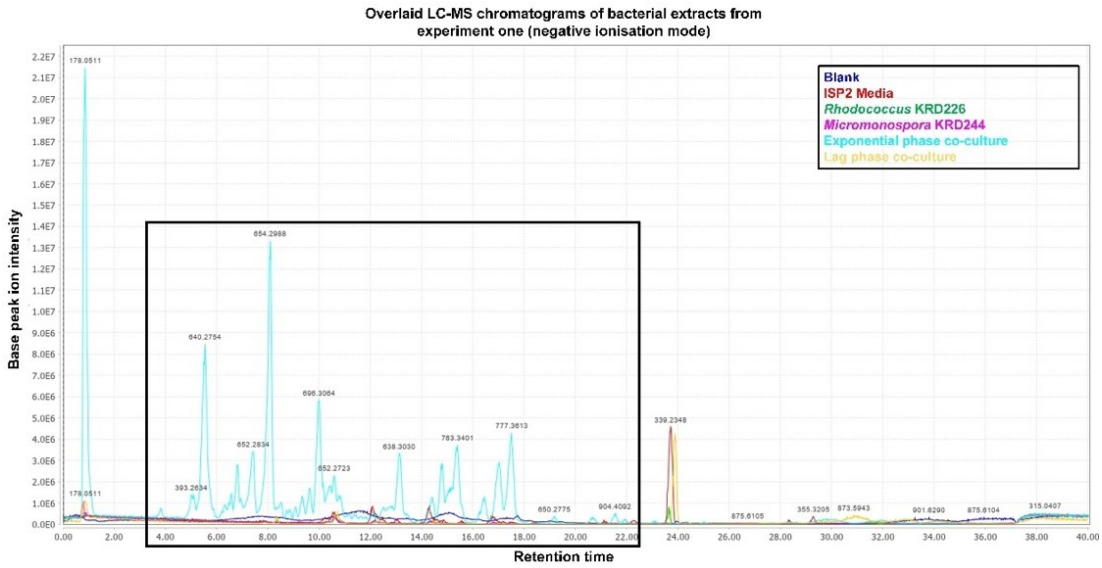

Figure 5.5. Parent ions *m/z* 393.2634, 638.3030, 640.2754, 650.2775, 652,2723, 652.2834, 654.2988, 696.3064, 763.3401, 777.3613 and 904.4092 elicited as a result of the *Rhodococcus* KRD226 and *Micromonospora* KRD244 transitional-phase co-culture detected in the LC-MS negative ionisation mode data. The chromatogram indicates the ion intensity (y axis) and the retention time (x axis). High intensity ions are labelled with the respective *m/z.* Each experimental group is colour-coded. The black box highlights the peaks (*m/z* 393.2634, 638.3030, 640.2754, 650.2775, 652,2723, 652.2834, 654.2988, 696.3064, 763.3401, 777.3613 and 904.4092) that were transitional-phase co-culture specific.

5.2.1.2 Comparative metabolomics analysis reveals a chemical response to transitional-phase co-cultures

In order to reveal metabolite shifts under two growth phases (lag-phase and exponential phase) between mono-cultures and co-cultures, LC-MS data was normalised (intensity values were mean-centred and divided by the square root of the standard deviation of each variable) (**Figure S5.1**). This reduced the effect of larger intensity ions. Then, data was subjected to multivariate data analysis.

PCA was applied to determine the clustering trends between the transitional-phase co-culture, the lag-phase co-culture and mono-cultures, and to visualise potential outliers. The PCA plot was generated using Pareto scaling and the first five components. The PCA showed that the first two PCs explained 85.7% of the variance in the data set and these were enough to capture most of the information without

losing important data (**Figure 5.6**). This was observed by the scree plot which showed the cumulative and individual variance explained by each PC (**Figure 5.7**). The scree plot revealed a large variation in slopes at the first PC and a smaller change at the second PC followed by a straight line (**Figure 5.7**). This indicates that the two first PCs captured enough variance to visualise the data in a low-dimensional linear subspace (**Figure 5.7**). The PCA indicated the extracts that best explained the variance (situated farthest away from zero) in the dataset (spectra of each bacterial extract). The PCA revealed the separation of both co-cultures from the mono-cultures and indicated their contribution to the largest variance (**Figure 5.6A**). In addition, the *Rhodococcus* KRD226 and *Micromonospora* KRD244 mono-cultures clustered together with the media control (**Figure 5.6A**). This suggests a limited production of metabolites by these two strains.

To identify which parent ions contributed to the classification of the co-cultures, the loadings plot was generated from the scores plot. This indicated the parent ions corresponding to each bacterial extract outlier found in the PCA plot. The loadings plot revealed that the parent ions that contributed the most to the PCA variance (PC1, 79%) were detected under the transitional-phase co-culture (outliers observed in the middle-left quadrants of the loadings plot, **Figure 5.6B**). These were *m/z* 298.0925, 654.2992, 640.2757, 763.3401 and 777.3613 (**Figure 5.6B**). For example, the parent ion *m/z* 654.2992 was situated under the PCA quadrants of the transitional-phase co-culture and was classified as an outlier in the loadings plot (**Figure 5.6B**). The loadings plot revealed that the parent ions that were detected under the lag-phase co-culture contributed to the variance of PC2 (6.7%). These were *m/z* 873.5951, 873.6123, 873.5777, 901.6624, 823.6275 and 847.5795 (right lower quadrant in the PCA loadings plot, **Figure 5.6B**). The production of transitional-phase co-culture specific metabolites was confirmed by the LC-MS chromatogram as previously observed. However, the LC-MS chromatograms showed that the lag-phase parent ions were background noise. These results suggest that during transitional-phase co-culture, specialised metabolites were elicited as a chemical response to the interaction.

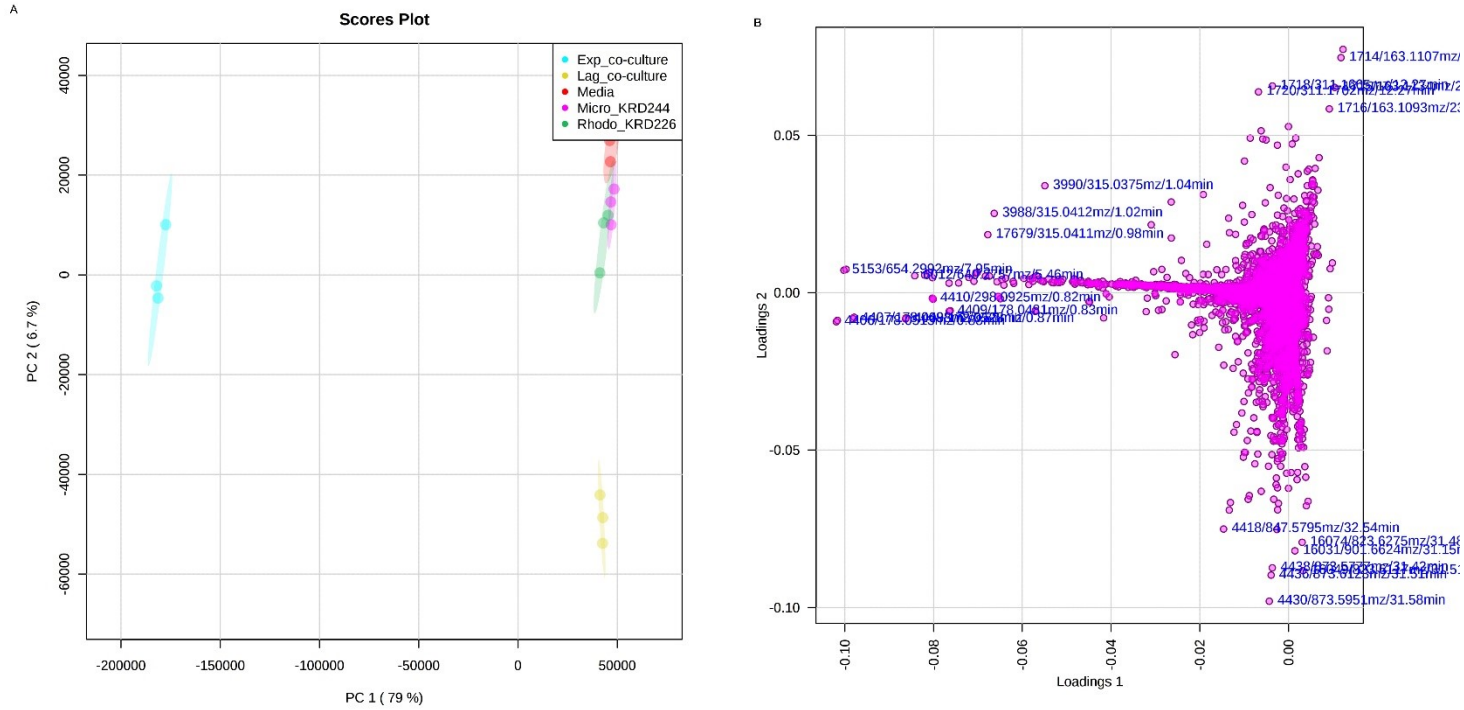

Figure 5.6. PCA scores reveal the separation of the transitional-phase and lag-phase co-cultures from the mono-cultures and the loadings plot indicates the parent ions responsible for the PCA scores separation. A) PCA scores plot based on the two first PCs (PC1 and PC2). Each experimental group is colour-coded (turquoise: transitional-phase co-culture, yellow: lag-phase co-culture, red: media, pink: *Micromonospora* KRD244 mono-culture and green: *Rhodococcus* KRD226 mono-culture). The ellipse shows the 95% confidence limit. B) PCA loadings plot. Each dot represents one parent ion from the dataset. Those parent ions situated with greater distance from the starting point of the loadings plot drive the variance in the PCA model. Some of these are labelled.

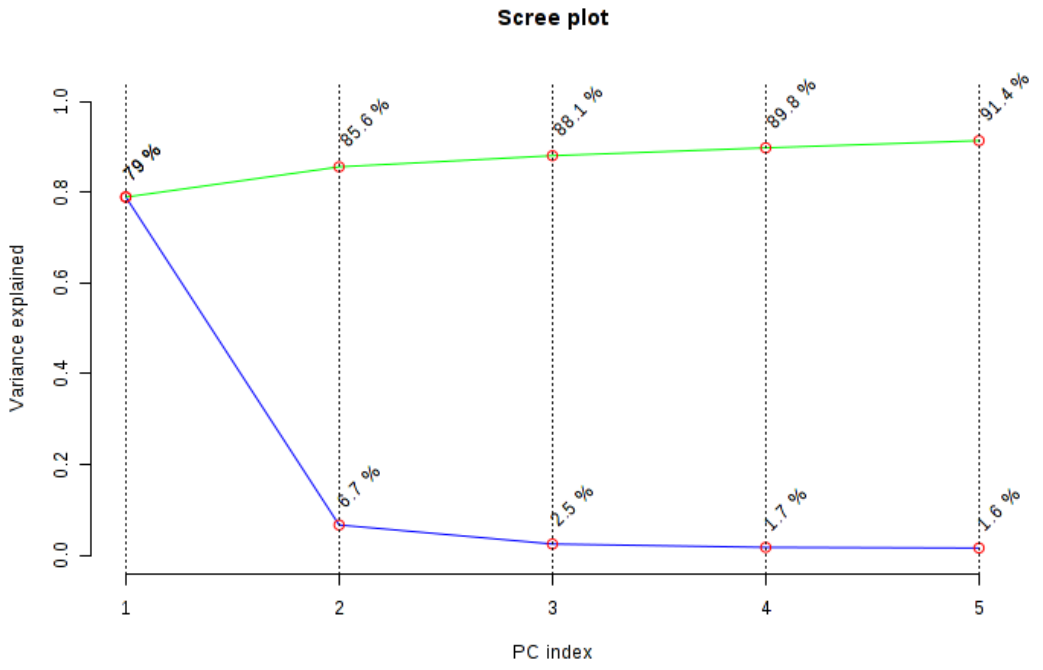

Figure 5.7. Scree plot shows the PCA variance explained by the first five PCs. The green line on top shows the accumulated variance explained; the blue line underneath shows the variance explained by individual PCs.

In order to improve the separation between experimental groups and to validate the results, data was further subjected to a PLS-DA. The PLS-DA cross validation showed that the R2 (predicted variation of the model) value was 0.99 and the Q2 (calculation of quality of the fit) value was 0.92. This indicated that the PLS-DA model was statistically well-supported (R2 and Q2 are close to one). In addition, Q2 was used to select the optimal number of PCs for PLS-DA classification (PC1 and PC2). PLS-DA revealed that 85.5% of the variance in the dataset was explained by the first two PCs (**Figure 5.8A**). Consistently with the PCA, the PLS-DA separated the two groups of co-cultures from each other and from the mono-cultures (**Figure 5.8**). The parent ions contributing to the largest variance of the PLS-DA model (PC1) were detected in the transitional phase co-cultures (shown as outliers in the left quadrant of the PLS-DA loadings plot, **Figure 5.8B**). These were *m/z* 654.2992, 640.2757, 763.3401 and 777.3613 **Figure 5.8B**). These data confirmed the production of specialised metabolites elicited by the transitional phase co-cultures and that this experimental group was responsible for driving the variance in the PCA and PLS-DA models.

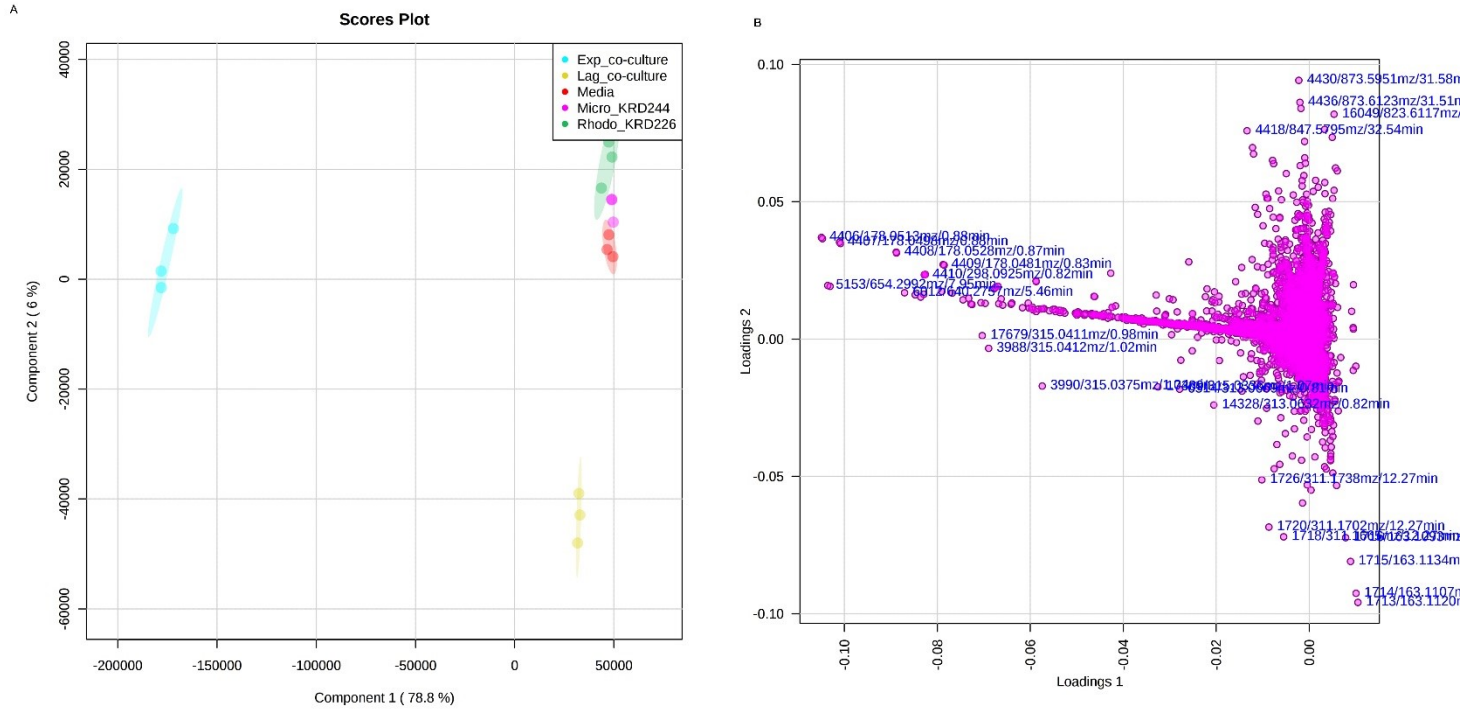

Figure 5.8. PLS-DA scores reveals the separation of the transitional-phase and lag-phase co-cultures from the mono-cultures and the loadings plot indicates the parent ions responsible for the PLS-DA scores separation. A) PLS-DA scores plot based on the two first PCs (PC1 and PC2). Each experimental group is colour-coded (turquoise: transitional phase co-culture, yellow: lag-phase co-culture, red: media control, pink: *Micromonospora* KRD244 mono-culture and green: *Rhodococcus* KRD226 mono-culture). The ellipse shows the 95% confidence limit. B) PLS-DA loadings plot. Each dot represents one parent ion from the dataset. Those parent ions situated with greater distance from the starting point of the loadings plot drive the variance in the PLS-DA model. Some of these are labelled.

To identify more parent ions that contributed to the discrimination of the transitional-phase co-culture, the VIP scores for each component of the PLS-DA model was calculated. VIP scores were generated from the weighted sum of squares of the PLS loadings considering the amount of explained Y-variation in each dimension. VIP revealed that from the 50 first parent ions that contributed the most to the variance (P > 1) of the PLS-DA model, 21 (*m/z* 654.2992, 654.2880, 178.0498, 640.2757, 654.3104, 654.2768, 298.0925, 640.2866, 640.2648, 696.3067, 652.2840, 652.2728, 696.2944, 640.2975, 696.3189, 654.2994, 654.2882, 777.3613, 652.2952, 315.0411 and 652.2617) were transitional-phase specific and four (178.0513, 315.0412, 178.0528 and 315.0375) were detected in both, the transitional-phase and the lag-phase co-cultures (**Figure 5.9** and **Table S5.2**). For example, *m/z* 654.2992 represented the largest score of a transitional-phase co-culture specific parent ion and was previously detected as an outlier by the PCA and PLS-DA for this group. These data suggest that mixing the strains during transitional-phase growth achieved competition between them which impacted their ability to produce secondary metabolites as a defence mechanism.

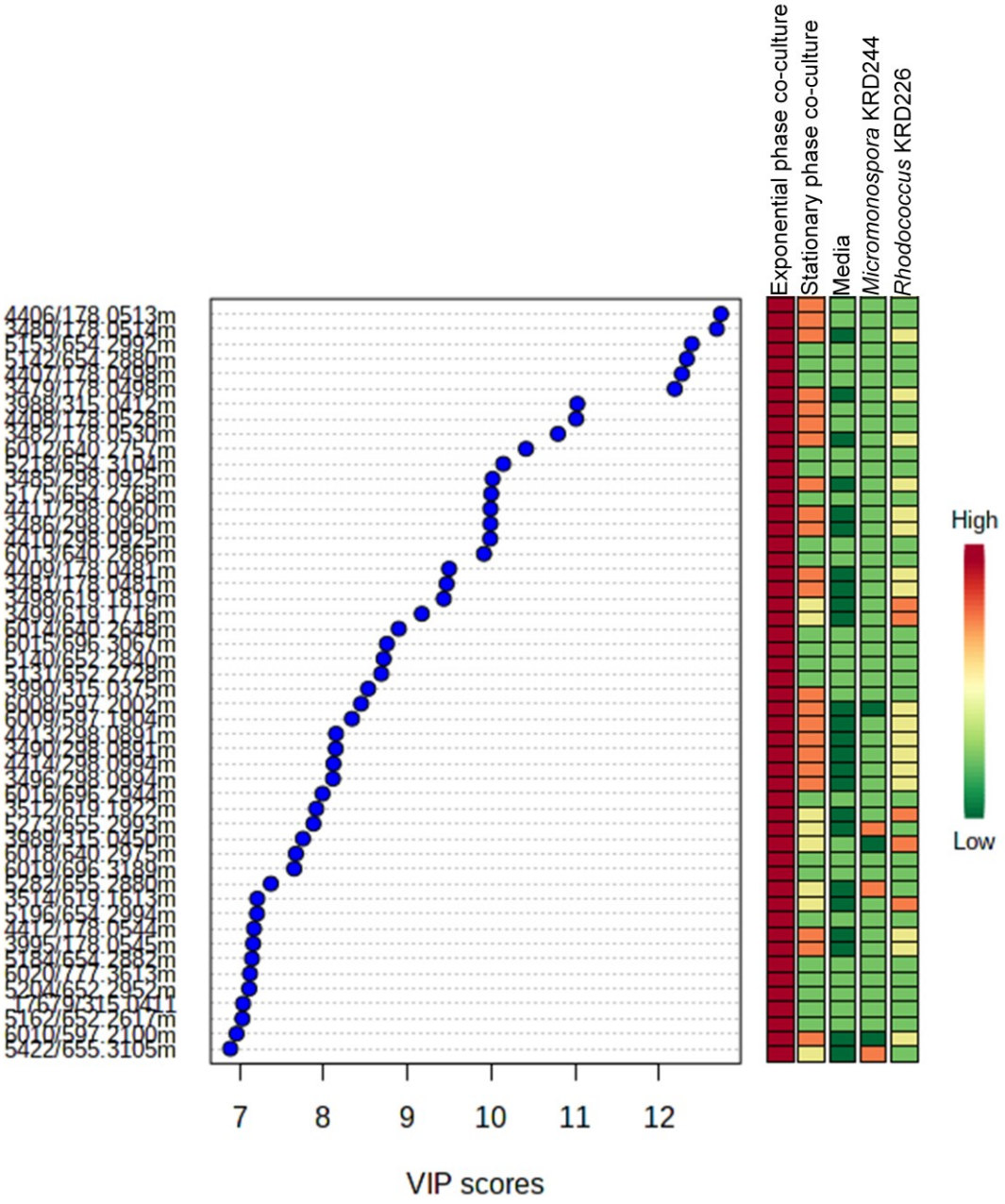

Figure 5.9. VIP scores plot reveals 21 transitional-phase co-culture specific parent ions. Blue dots indicate the VIP scores ranged between seven and 13, scores that are P > 1 are considered significant. The coloured boxes on the right indicate the ion intensity. VIP scores are detailed in the supplementary **Table S5.2**.

PCA, PLS-DA and VIP demonstrated the increased production of specialised metabolites by the transitional-phase co-culture when compared to the mono-cultures and the lag-phase co-culture. In order to confirm these results, the volcano analysis was performed. This analysis assessed if these parent ions were statistically significant ($p < 0.05$) between the mono-cultures and transitional-phase co-cultures

(**Figure 5.10.** and between the transitional-phase co-culture and the lag-phase co-culture (**Figure 5.11**). The volcano plot revealed that a total of 11741 parent ions were considered statistically significant ($p < 0.05$) in the comparison between mono-cultures and the transitional-phase co-culture and 11391 between the two groups of co-cultures (**Figure 5.10.** and **Figure 5.11**). For example, *m/z* 610.2800, 621.3257, 638.3035, 654.2880, 654.2992, 656.2336, 696.2944, 696.3067, 696.3189, 739.2753, 791.3844 and 793.3282 (pink dots in **Figure 5.10.** and **Figure 5.11**). This confirmed that these parent ions were elicited by co-cultivation and are responsible for most of the variance observed by PCA and PLS-DA. These results demonstrated that the transitional phase co-culture increased the number of specialised metabolites (10377 parent ions compared to 1186 between the two mono-cultures and 1765 from the lag-phase co-culture) and that over 80% of these were statistically significant.

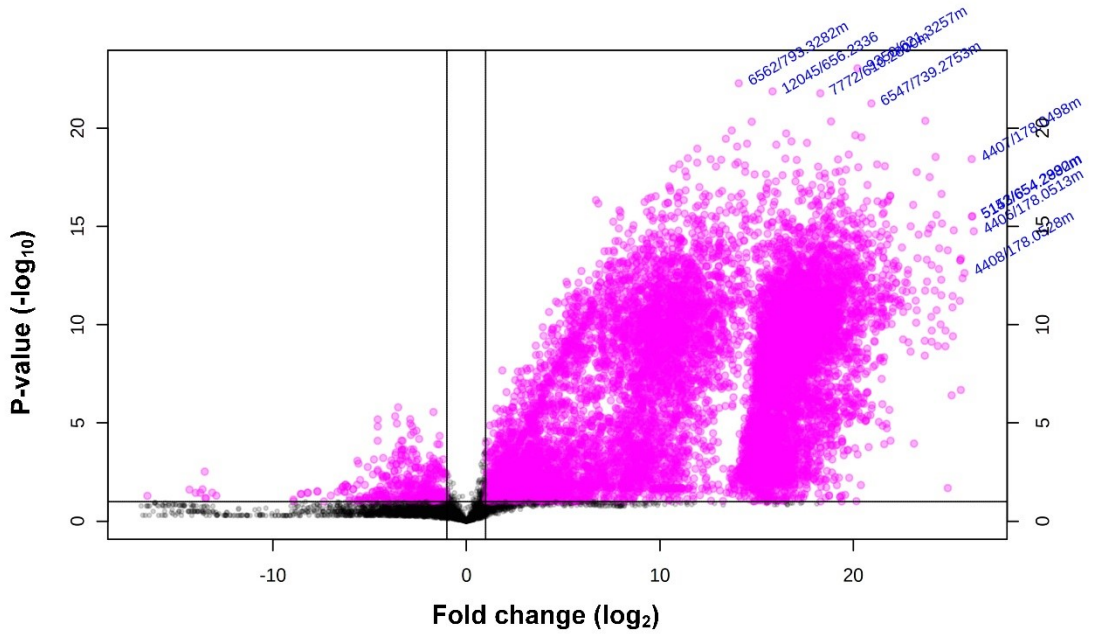

Figure 5.10. Volcano plot of mono-cultures (left) and transitional-phase co-culture (right). Each dot represents one parent ion. Statistically significant ($p < 0.05$) parent ions are coloured pink and non-significant parent ions are coloured black. The vertical axis (Y) indicates the p-value (in $-\log_{10}$ scale) with the thick line representing a p-value of 0.05. The horizontal axis (X) indicates the fold change between the experimental groups (in $\log_2$ scale). The further up in the Y-axis and further away from 0 in X-axis a parent ion is located, the more statistically significant ($p < 0.05$) such as the labelled parent ions (*m/z* 793.3282, 656.2336, 739.2753, 654.2992, 610.2800, 621.3257, 654.2880).

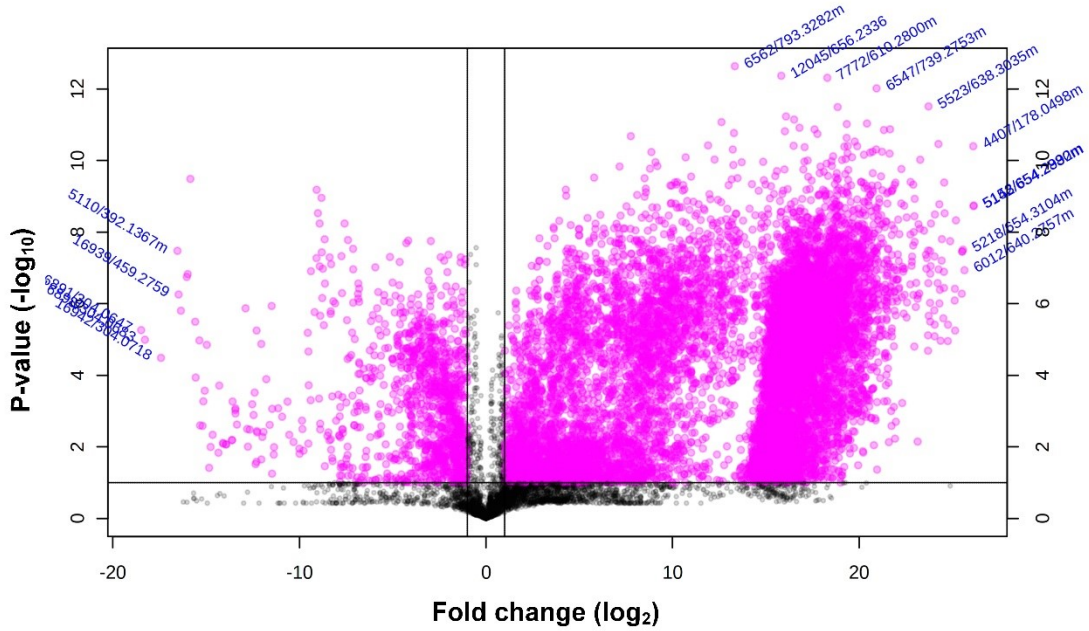

Figure 5.11. Volcano plot of lag-phase co-culture (left) and transitional-phase co-culture (right). Each dot represents one parent ion. Statistically significant ($p < 0.05$) parent ions are coloured pink and non-significant parent ions are coloured black. The vertical axis (Y) indicates the p-value (in $-\log_{10}$ scale) with the thick line representing a p-value of 0.05. The horizontal axis (X) indicates the fold change between the experimental groups (in $\log_2$ scale). The further up in the Y-axis and further away from 0 in X-axis a parent ion is located, the more statistically significant ($p < 0.05$) such as the labelled parent ions (transitional-phase co-culture: *m/z* 793.3282, 656.2336, 739.2753, 654.2992, 610.2800, 621.3257, 654.2880, 638.3035, 696.2944, 791.3844, 696.3067, 696.3189 and lag-phase co-culture: 391.1367, 459.2759, 304.0647, 304.0718).

5.2.2 Impact of growth phase and time on the strains' secondary metabolism

To evaluate the impact of time on the strains' secondary metabolism, the liquid mono-cultures of the two strains were mixed together during transitional growth phase and incubated for seven, 14, 21 and 28 days respectively, as observed in **Figure 5.12**. As previously observed, the growth curves showed that while *Rhodococcus* KRD226 entered exponential-phase after approximately 12 hours, *Micromonospora* KRD244 needed approximately 120 hours. Therefore, the strains were mixed together at 24 hours of *Rhodococcus* KRD226 growth and 168 hours of *Micromonospora* KRD244 growth (**Figure 5.12C-J**).

To determine if the strains were alive after growing under co-culture, a viability test was performed. The viability plates revealed that *Rhodococcus* KRD226 was able to be cultured on solid media from the co-cultures. However, as previously discussed, the viability test was insufficient to determine if the *Micromonospora* KRD244 was alive after growing under co-culture as this assay was limited by the growth rate of the strains. Despite this, the viability plates revealed that the two strains were not culturable from the 21 days-old transitional-phase co-culture (**Figure 5.13A**). Furthermore, to evaluate the impact of incubation time on the production of bioactive metabolites, antimicrobial activity assays were performed. The most relevant findings were found at 14, 21 and 28 days (**Figure 5.14B, C** and **D**). Antibacterial activity was observed at day 14 and 21 but not at day seven and 28 (**Figure 5.14**) which might explain the lack of growth of the two strains at day 21 on the viability test. The antibacterial screening results revealed that the *Micromonospora* KRD244 was bioactive against *S. aureus* at 21 and 28 days under mono-culture (**Figure 5.14C** and **D**).

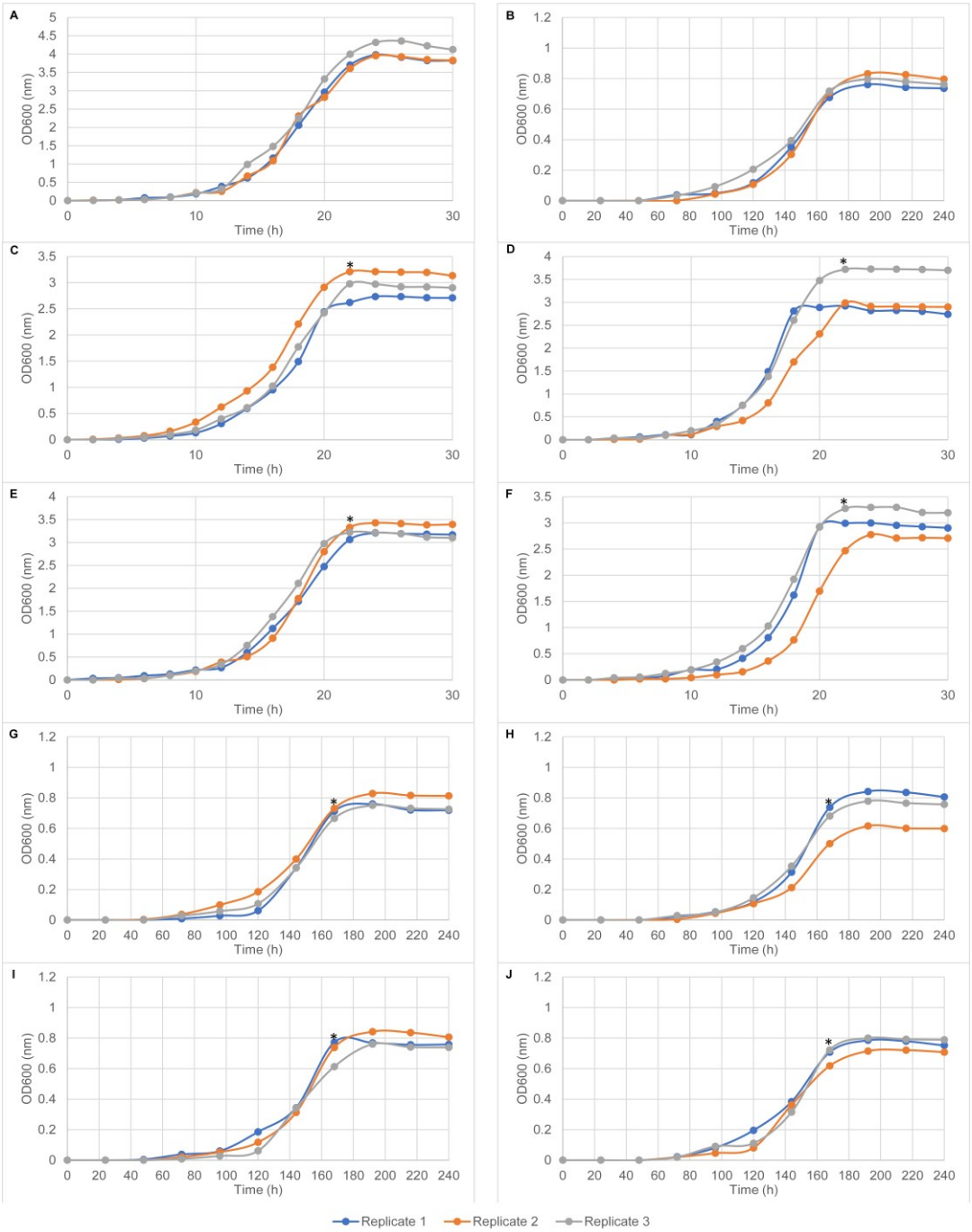

Figure 5.12. Growth curves representing the OD_{600} measurements for the *Rhodococcus* KRD226 and *Micromonospora* KRD244 mono-cultures. The x-axis indicates the time in hours and the y-axis the OD_{600}. Asterisk (*) indicates the time point at which each mono-culture was mixed with the other strain's mono-culture. A-B) *Rhodococcus* KRD226 and *Micromonospora* KRD244 mono-culture control, C-F) *Rhodococcus* KRD226 culture used for the seven (C), 14 (D), 21 (E) and 28 (F) day old transitional-phase co-culture, G-J) *Micromonospora* KRD244 culture used for the seven (G), 14 (H), 21 (I) and 28 (J) day old transitional-phase co-culture.

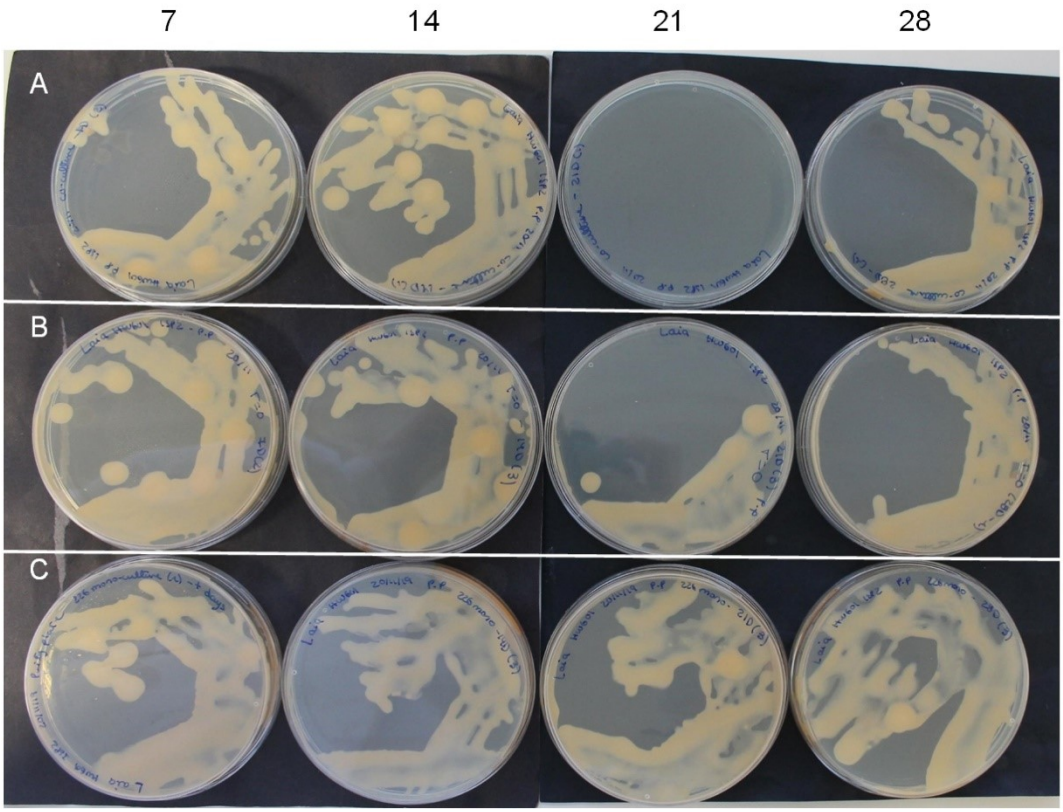

Figure 5.13. Viability plates from mono-cultures and co-cultures reveal lack of growth at day 21. Each column (7 to 28) indicates each time point (in days) when cultures were extracted. A-C) Transitional phase co-culture, lag-phase co-culture and *Rhodococcus* KRD226 mono-culture control.

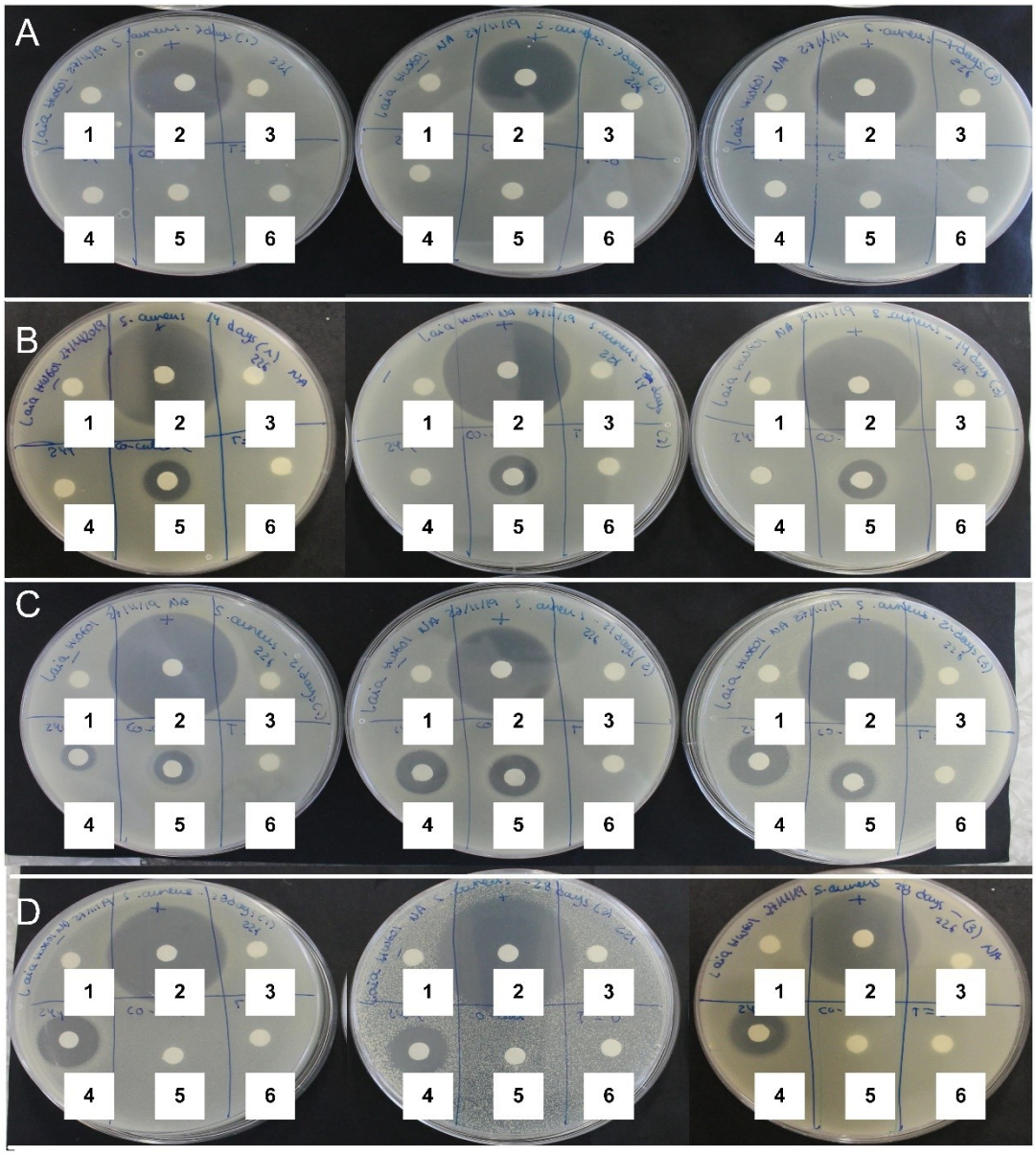

Figure 5.14. Bioactivity assays reveal antibacterial activity from the transitional-phase co-culture (5) and the *Micromonospora* KRD244 mono-culture (4) against *S. aureus*. A-D) Extracts from seven days-old cultures, 14 days, 21 days and 28 days.1-6). Negative control (media extract), positive control (chloramphenicol), *Micromonospora* KRD244 mono-culture extract, *Rhodococcus* KRD226 mono-culture extract, transitional phase co-culture extract and lag-phase extract.

To assess if the elicitation of bioactive metabolites was a result of direct physical contact between the *Rhodococcus* KRD226 and *Micromonospora* KRD244, cultures using pre-conditioned media were performed. These assays revealed that the strains were not affected by each other's pre-conditioned media. Furthermore, antibacterial

activity was not detected except for the 21 and 28-day old *Micromonospora* KRD244 pre-conditioned media and non-pre-conditioned media cultures (**Figure S5.2**). This was expected since it was previously observed that this strain produced metabolites under the 21 and 28-day old mono-cultures. These data suggest that physical contact between the two strains was responsible for the antibacterial activity observed from the liquid co-cultures. Another possibility is that specialised metabolites are produced at higher concentration under co-cultures where the two strains are in physical contact.

5.2.2.1 LC-MS analysis reveals the time-frame of maximal number of metabolites

To determine the total number of parent ions detected for each experimental group, specific parent ions that belonged to each group were identified from all bacterial extracts. The total number of detected parent ions was 26378 from which 6118 originated from the media control, 1465 from the *Rhodococcus* KRD226 mono-culture where; 214 from the seven-day old mono-cultures, 321 by the 14-day old mono-cultures, 414 by the 21-day old mono-cultures and 416 by the 28-day old mono-cultures (**Table 5.2**). Furthermore, 2356 ions were detected from the *Micromonospora* KRD244 mono-culture where; 196 were elicited by the seven-day old mono-cultures, 269 by the 14-day old mono-cultures, 648 by the 21-day old mono-cultures and 1243 by the 28-day old mono-cultures (**Table 5.2**). Then 5180 were transitional-phase co-culture specific where; 307 seven-day old co-culture, 979 14-day old co-culture, 3536 21-day old co-culture and 358 were 28-day old co-culture specific (**Table 5.2**). A total of 2109 parent ions were lag-phase co-culture specific where; 88 were detected in the seven-day old co-culture, 87 in the 14-day old co-culture, 254 in the 21-day old co-culture and 1680 in the 28-day old co-culture (**Table 5.2**). There were then other 9150 parent ions that were shared between experimental groups. These results revealed that 36% of these parent ions (excluding media parent ions) were elicited by co-cultivation and the number of detected metabolites increased over time achieving the maximal production between day 14 and 21 (**Table 5.2**).

Table 5.2. Number of parent ions detected in negative ionisation mode for experiment two. The columns indicate the replicate specific parent ions: ions detected only in one replicate, commonly detected: parent ions detected in two replicates of the same experimental group, and present in the three replicates: parent ions detected in the three replicates of the same experimental group. The last row (shared between two or more experimental groups), indicates the total number of parent ions that were detected in two or more experimental groups.

Bacterial extract	Replicate specific parent ions			Parent ions commonly detected in two experimental replicates			Present in the three replicates	Total
	1	2	3	1 and 2	1 and 3	2 and 3		
Micromonospora KRD244-7 days	32	3	13	24	11	15	98	196
Micromonospora KRD244-14 days	3	3	6	8	21	12	216	269
Micromonospora KRD244-21 days	33	7	15	67	46	87	396	648
Micromonospora KRD244-28 days	21	69	106	209	99	65	674	1243
Rhodococcus KRD226-7 days	4	14	15	11	18	7	145	214
Rhodococcus KRD226-14 days	6	3	9	1	3	3	296	321
Rhodococcus KRD226-21 days	9	10	13	26	24	26	306	414
Rhodococcus KRD226-28 days	10	13	4	9	12	5	463	516
Transitional phase co-culture-7 days	29	46	41	23	12	32	124	307
Transitional phase co-culture-14 days	29	20	43	103	201	114	469	979
Transitional phase co-culture-21 days	13	6	31	66	59	72	3289	3536
Transitional phase co-culture-28 days	3	0	1	29	28	36	261	358
Lag phase co-culture-7 days	12	7	0	5	3	0	61	88
Lag phase co-culture-14 days	21	2	4	0	0	7	53	87
Lag phase co-culture-21 days	7	3	3	0	4	6	231	254
Lag phase co-culture-28 days	57	59	165	236	99	123	941	1680
Shared between two or more experimental groups								9150

To determine if the production of specialised metabolites was constant over time in all experimental groups, and if this was different between the co-cultures and the mono-cultures, a PCA of the unprocessed raw LC-MS data was performed. The PCA discriminated four groups; the 14 and 21-day old transitional-phase co-cultures and the 21 and 28-day old *Micromonospora* KRD244 mono-cultures (data not shown), which coincided with the bioactive extracts. However, due to the large number of bacterial extracts, discrimination between other groups by PCA was not achieved. Therefore, a PCA was performed for each individual time point. The PCA revealed that the transitional-phase co-culture was discriminated at all time points as it was separated from the mono-cultures (**Figure 5.15**). In fact, after seven, 14 and 21 days of incubation, the transitional-phase co-cultures contributed to the most variance of the PCA as observed in **Figure 5.15A**, **B**, **C** and **Table S5.3.** The PC1 eigenvalues were -64.676341, -74.1074256 and -100.095911 (seven-day old extracts), -151.56086, -147.293943 and -155.415914 (14-day old extracts), -4.91565926, -2.97946848 and -3.00681853 (21-day old extracts) (**Table S5.3**). The PC2 eigenvalues were: -67.4880428, -73.7093774 and -83.0844092 (seven-day old extracts), -27.5078653, -16.9072121 and -7.62747782 (14-day old extracts) and 121.386007, 125.151139 and 124.458697 (21-day old extracts) (**Table S5.3**). In addition, the contribution to the variance of the PCA model by the 28-day old transitional-phase co-culture extracts decreased as eigenvalues were closer to zero (**Figure 5.15D** and **Table S5.3**). Furthermore, this correlated with the previously observed antibacterial activity against *S. aureus*. These data suggest a shift on secondary metabolism from producing bioactive metabolites between days seven and 21 to decreasing this production at a later stage.

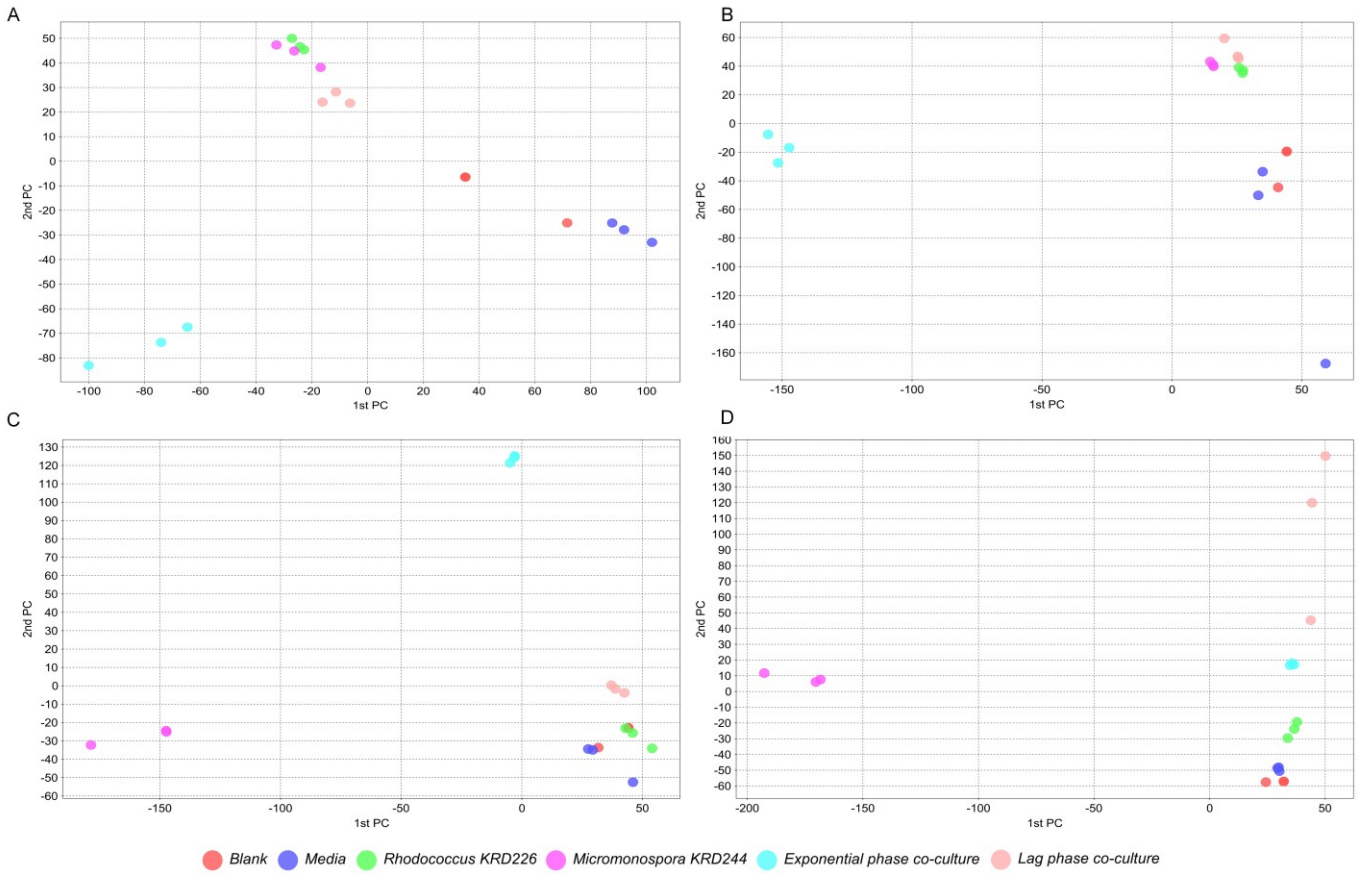

Figure 5.15. PCA scores reveal the separation of the transitional-phase and lag-phase co-cultures at the four time points (seven, 14, 21 and 28 days). Score plots are based on the two first PCs (PC1 and PC2). A-D) seven days, 14 days, 21 days and 28 days. Experimental groups are colour-coded.

The PCA for the four transitional-phase co-cultures separated the four groups from each other (**Figure 5.16** and **Table S5.4**). PCA revealed that the 14 and 21-day old co-cultures contributed to the largest variance (PC1 for the 14 days: -48.9095286, -55.624958 and -57.7503138, for the 21 days: -90.3700908, -89.2445473 and -86.8117912 and PC2 for the 14 days: -98.0500974, -92.4619959 and -83.907097 and for 21 days: 70.5660472, 75.3549106 and 77.2219593). These two groups were separated to the left quadrants of the PCA while the seven and 28-day old transitional-phase co-cultures were situated in the right quadrants (**Figure 5.16** and **Table S5.4**). These data suggest a negative correlation between the 14 and 21-day old co-cultures and the seven and 28-day old co-cultures.

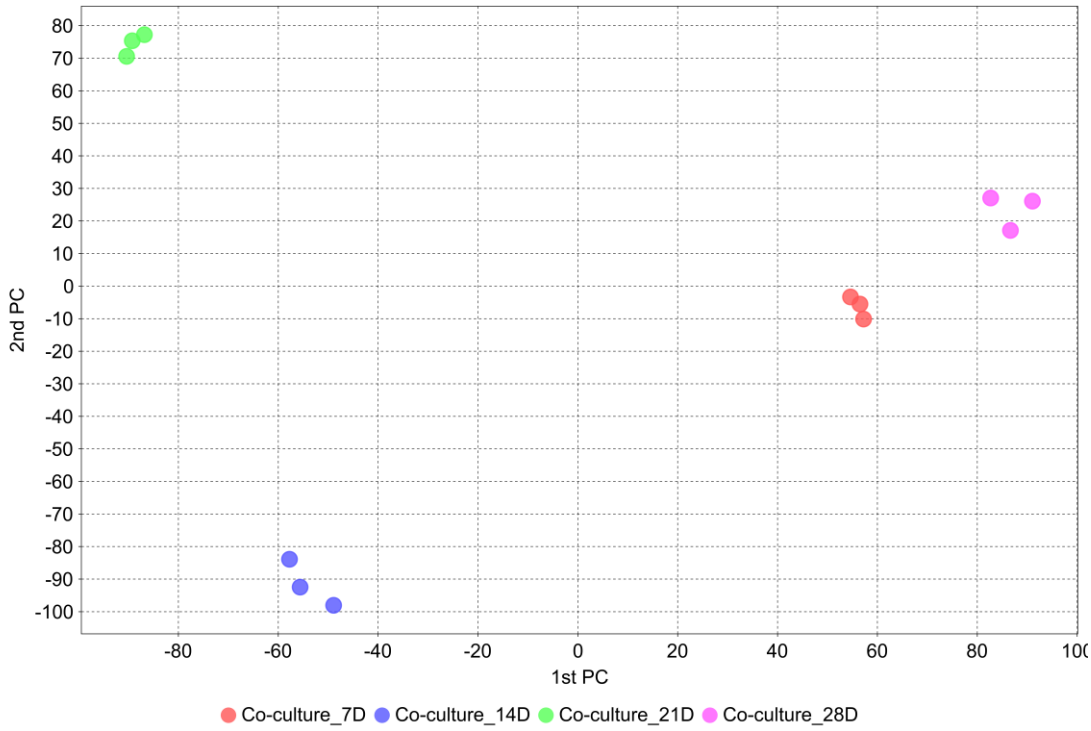

Figure 5.16. PCA scores reveal the separation between the four transitional-phase co-cultures (seven (7D), 14 (14D), 21 (21D) and 28 (28D) days) indicating the production of specific metabolites for each group. Score plots are based on the two first PCs (PC1 and PC2). Experimental groups are colour-coded.

In order to detect metabolite variations in the chemical profile of the 14 and 21-day old transitional phase co-cultures that were not detected in the other groups, the LC-MS chromatograms were overlaid (**Figure 5.17**). The chromatograms revealed the parent ions *m/z* 654.2879, 712.2982, 728.293 that were detected in both the 14 and 21-day old transitional phase co-cultures, the parent ions *m/z* 313.1558, 672.3046

and 770.3032 that were specific to the 14-day old transitional-phase co-culture and the parent ions *m/z* 293.2120, 295.2286, 546.2690 and 714.2793 that were detected in the 21-day old transitional-phase co-culture. These data suggests that metabolite production is not constant over time.

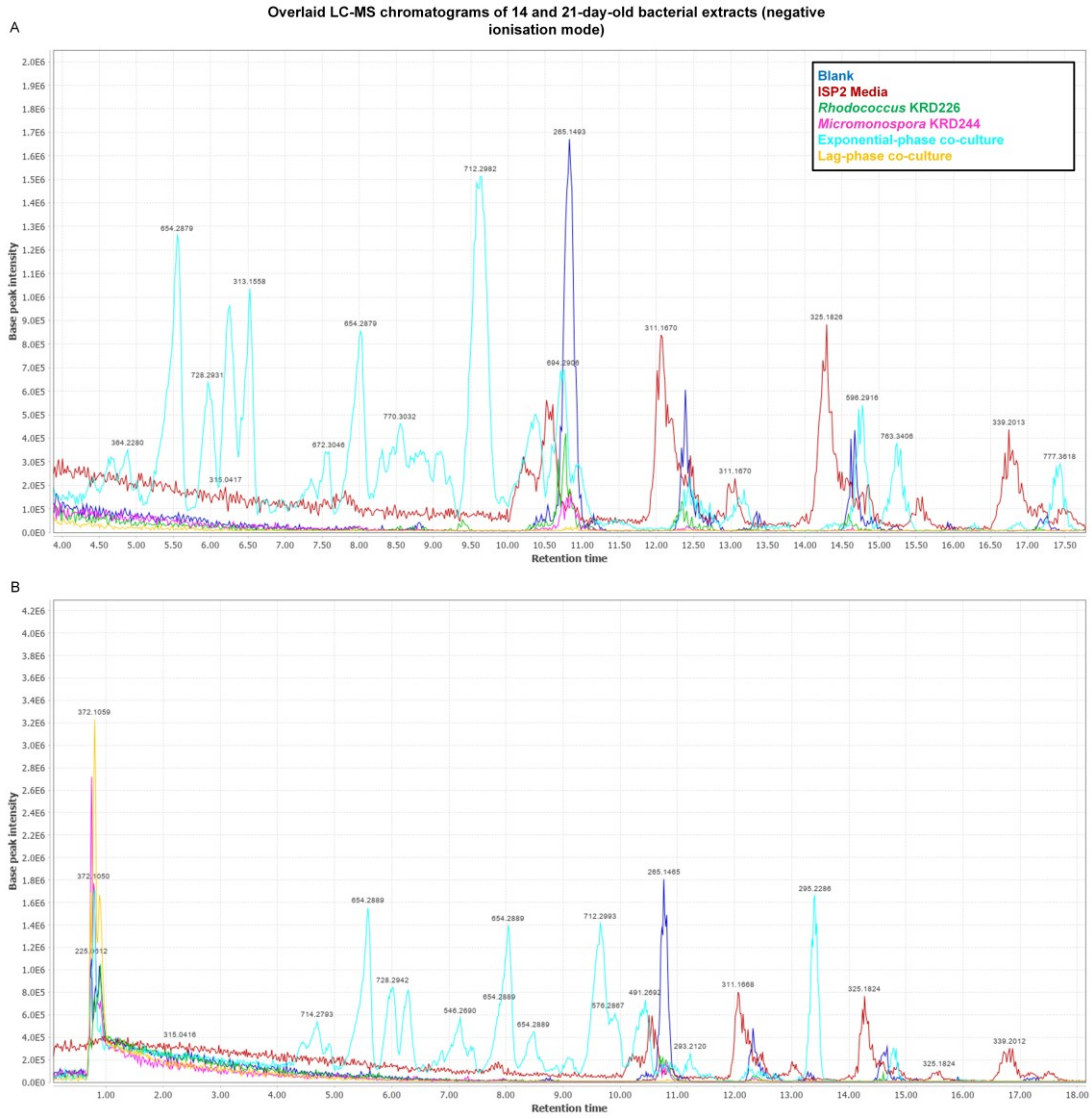

Figure 5.17. Parent ions *m/z* 293.2120, 295.2286, 313.1558, 546.2690, 654.2879, 672.3046, 712.2982, 714.2793, 728.293 and 770.3032 elicited as a result of the 14 and 21-days old transitional-phase co-culture detected in the LC-MS negative ionisation mode data. The chromatogram indicates the ion intensity (y axis) and the retention time (x axis). High intensity ions are labelled with the respective *m/z*. Each experimental group is colour-coded.

5.2.2.2 Comparative metabolomics analysis reveals that specialised metabolite production variates over time

To reveal metabolite shifts under two growth phases (lag and exponential) across time (seven, 14, 21 and 28 days), LC-MS data (ion intensity values) was normalised (**Figure S5.3**) and subjected to multivariate data analysis.

To identify experimental groups that produced specific metabolites, a PCA was performed. The PCA scores plot was generated using Pareto scaling and the first five PCs. PCA showed that 31.6% of the variance in the data set was explained by the first two PCs (**Figure 5.18A**) while 51.6% was explained by the first five PCs (**Figure 5.19**). This indicated that the variance between parent ions detected in all bacterial extracts was low and not high enough to represent a valid model (<60%) (Hair *et al.*, 2017). However, this could be the result of parent ions detected over the four time points such as *m/z* 163 (**Figure 5.18B**). Despite this, PCA revealed the spatial separation of the 14 and 21-day old transitional phase co-cultures from all the other groups and between each other (**Figure 5.18A**). The PCA loadings plot indicated the parent ions that contributed to this discrimination (outliers situated at the upper right quadrants in **Figure 5.18B**). These were *m/z* 654.3112, 712.3121 which were detected under the 21-day old transitional-phase co-culture, *m/z* 654.3195 which was detected under the 14-day old transitional-phase co-culture and *m/z* 654.2775, 654.2887, 654.2999, 683.2366, 712.2993, 728.2942 detected under both groups (**Figure 5.18B**). This confirmed that in this case, the chemical response under co-cultivation over time is not constant.

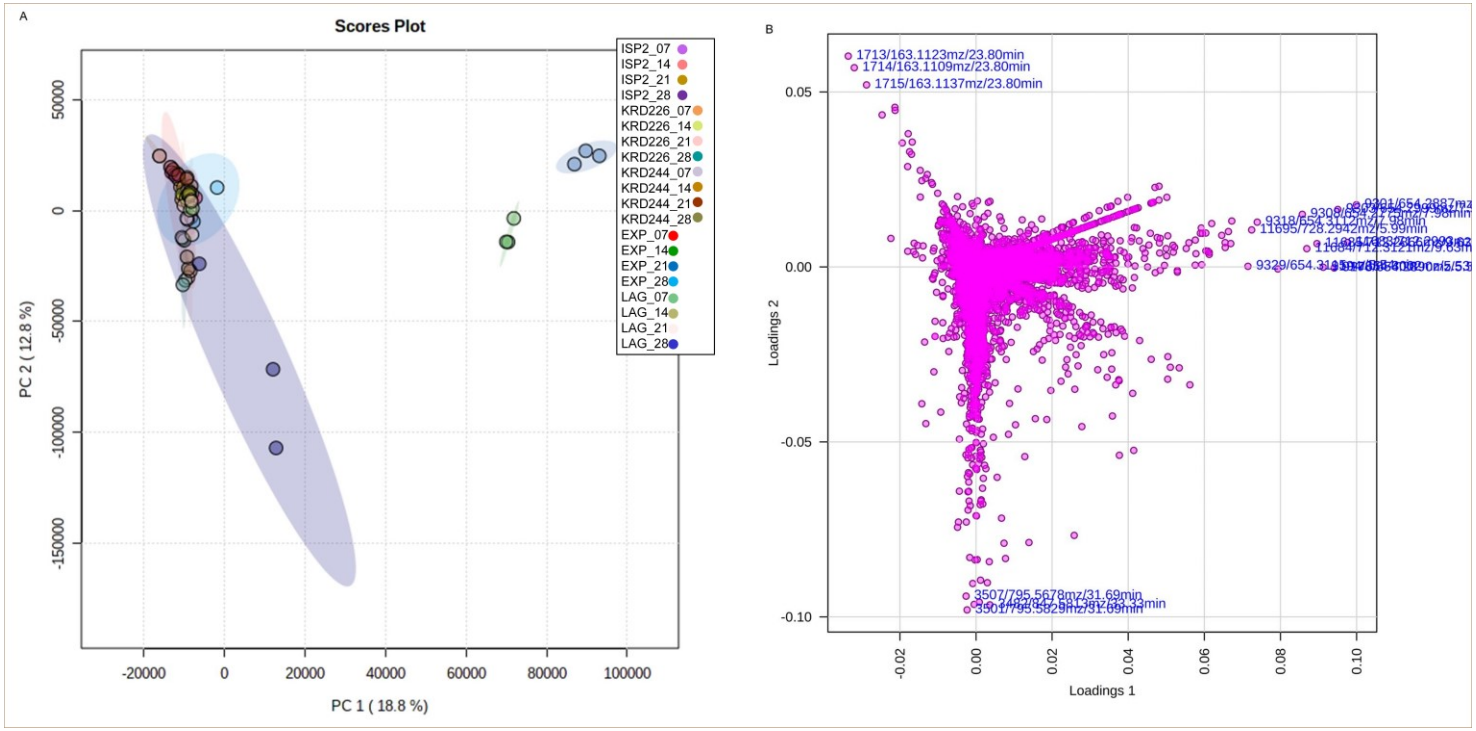

Figure 5.18. PCA scores reveals the separation of the 14 and 21 days-old transitional-phase co-cultures from all the other experimental groups and the loadings plot indicate the parent ions responsible for the separation. A) PCA scores plot based on the two first PCs (PC1 and PC2). Each experimental group is colour-coded. The ellipse shows the 95% confidence limit. B) PCA loadings plot. Each dot represents one parent ion from the dataset. Those parent ions situated with greater distance from the starting point of the loadings plot drive the variance in the PCA model. Some of these are labelled.

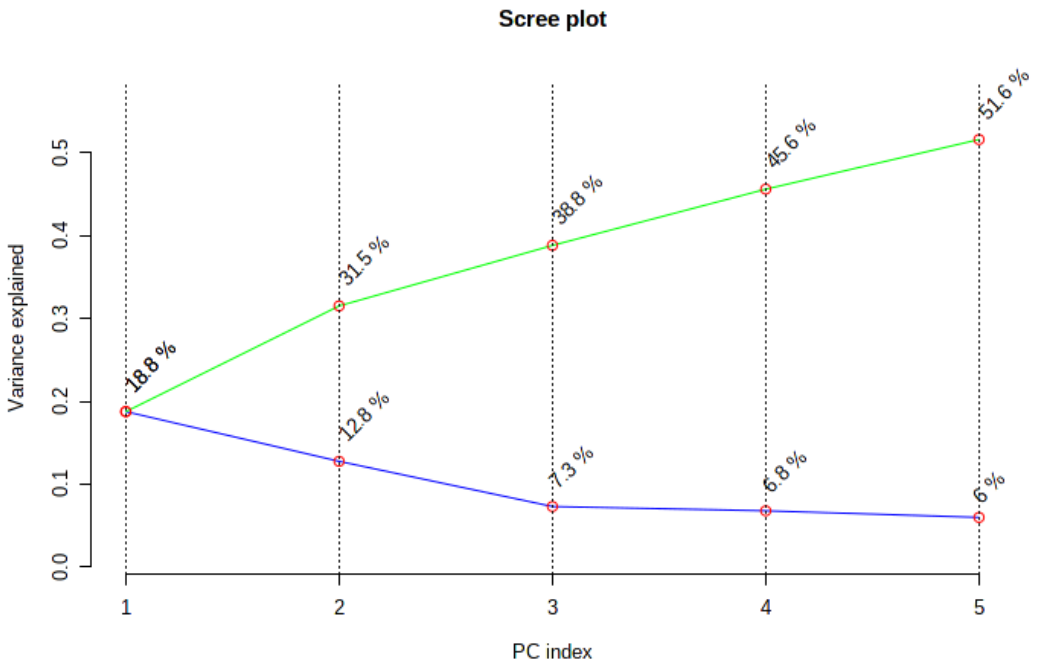

Figure 5.19. Scree plot shows the PCA variance of the time-course experiment explained by the first five PCs. The green line on top shows the accumulated variance explained; the blue line underneath shows the variance explained by individual PCs.

To facilitate the analysis and detection of specific parent ions for the 14 and 21-day old transitional-phase co-cultures, data was subjected to a further multivariate analysis for these two time-points. The PCA for the 14-day old culture extracts showed that 64.5% of the variance in the data set was explained by the first three PCs (**Figure 5.20A**). These were enough to capture most of the information without losing important data as observed by the large variation in slopes at the first PC and the smaller variation at the second and third PCs (**Figure 5.7**). PCA revealed that after 14 days of growth, the transitional-phase co-culture was separated from all the other groups (left quadrants of the PCA plot, **Figure 5.20A**). The PCA loadings plot was generated from the scores plot and revealed that the parent ions *m/z* 654.3195, 654.2999, 654.2890 and 712.2993 were responsible for the separation of the transitional-phase co-culture (upper left quadrant of the PCA loadings plot **Figure 5.20B**). As previously observed in the chromatograms and the PCA from all bacterial extracts, *m/z* 654.2999, 654.2890 and 712.2993 were also detected in the 21-day old transitional-phase co-culture. These data suggest the metabolite elicitation by this co-culture while production is limited under the other groups. In addition, these findings

reinforce that the metabolites *m/z* 654.2999, 654.2890 and 712.2993 were co-culture (transitional-phase) and time specific (14 and 21 days).

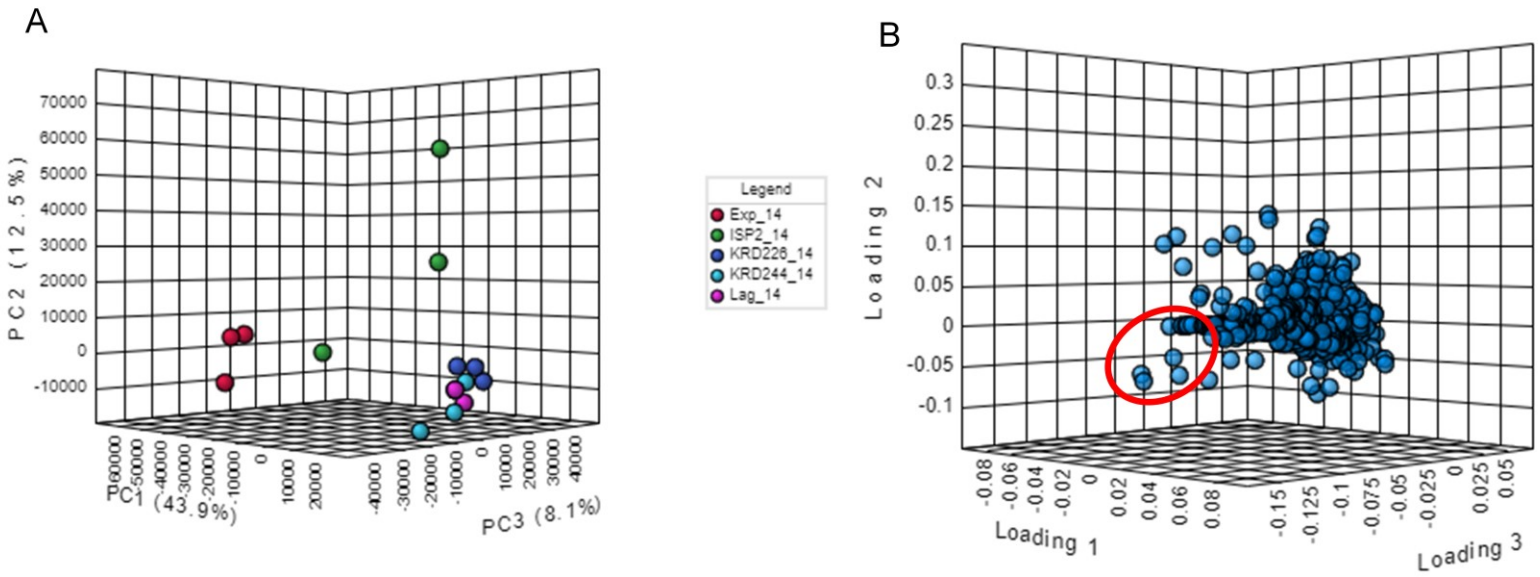

Figure 5.20. PCA scores reveals the separation of the 14-days old transitional-phase co-cultures from the mono-cultures and the loadings plot indicates the parent ions responsible for this separation. A) PCA scores plot based on the three first PCs (PC1, PC2 and PC3). Each experimental group is colour-coded (red: transitional-phase co-culture, green: media control (ISP2), blue: *Rhodococcus* KRD226 mono-culture, turquoise: *Micromonospora* KRD244 mono-culture and pink: lag-phase co-culture). B) PCA loadings plot. Each dot represents one parent ion from the dataset. Those parent ions situated with greater distance from the starting point of the loadings plot drive the variance in the PCA model. The red circle indicates the parent ions responsible for the discrimination of the transitional-phase co-culture.

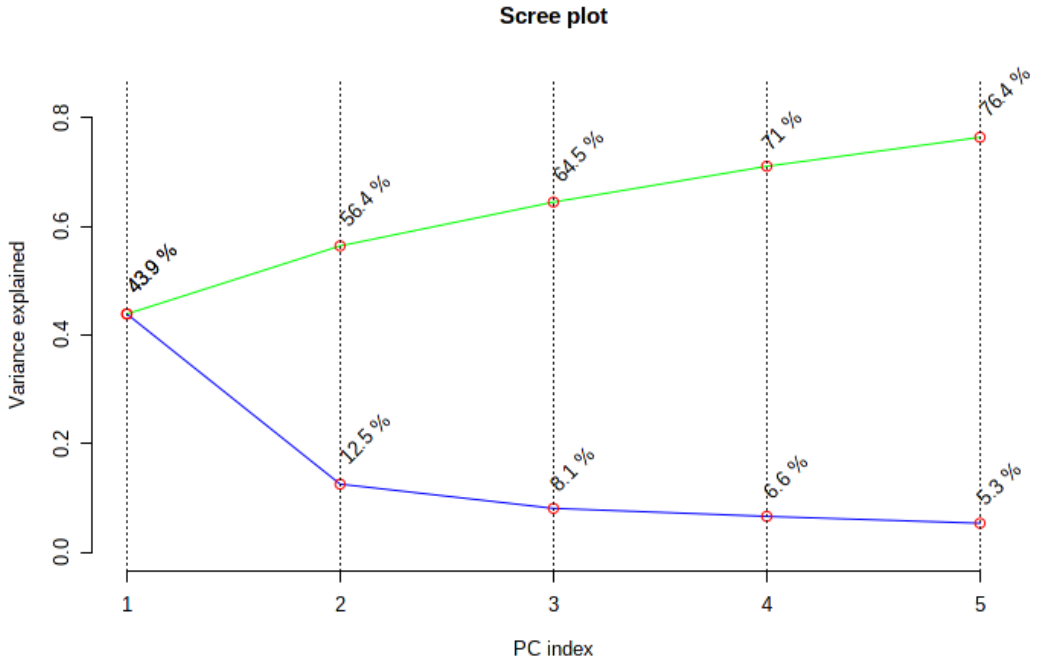

Figure 5.21. Scree plot shows the PCA variance between 14-day old bacterial extracts explained by the first five PCs. The green line on top shows the accumulated variance explained; the blue line underneath shows the variance explained by individual PCs.

To determine the parent ions that discriminated the 14-day old transitional-phase co-culture, LC-MS data was further subjected to a PLS-DA. The PLS-DA was generated by rotating the PCA components. The PLS-DA analysis reinforced the findings observed by the PCA since the same parent ions (*m/z* 654.3195, 654.2999, 654.2890 and 712.2993) were detected as those that contributed to the model variance (data not shown). The PLS-DA indicated a good predictive model since Q2 and R2 values were 0.77 and 0.99 respectively. Furthermore, to detect more parent ions that contributed to the variance since separation of the loadings plot difficulted their identification, the VIP scores for each component of the PLS-DA model was calculated. The 50 first parent ions identified by PLS-DA that contributed the most to the variance (P > 1), are shown in **Figure 5.22** and **Table S5.5.** VIP revealed that from 50 ions, 35 were elicited by the transitional-phase co-culture and were considered as the most significant (**Figure 5.22**). These were *m/z* 712.3121, 712.2866, 654.2890, 654.2887, 654.3002, 654.2999, 654.2775, 654.2778, 728.2940,

754.3148, 654.3115, 728.2942, 754.3009, 737.2722, 313.1563, 737.2856, 728.2808, 728.3072, 712.3248, 712.2738, 364.2286, 713.3075, 728.2810, 728.3074, 713.2947, 313.1600, 313.1526, 754.3287, 364.2333, 714.2791, 694.2915, 696.3079, 737.2588, 390.2433 and 364.2239 (**Figure 5.22** and **Table S5.5**). The parent ions *m/z* 694.2915, 696.3079, 713.2947, 713.3075, 714.2791, 737.2588, 737.2722 and 737.2856 were not previously distinguished by the PCA or PLS-DA plots (**Figure 5.22** and **Table S5.5**). The LC-MS chromatograms revealed that *m/z* 694.2915 and 696.3079 were detected under the 14-day old transitional-phase co-cultures (**Figure S5.5**). Furthermore, *m/z* 713.2947, 713.3075, 714.2791, 737.2588, 737.2722 and 737.2856 were detected under the 14-day old transitional co-culture and also at later growth stages (21-day old transitional-phase co-culture), coinciding with the two time points that produced antibacterial activity. VIP revealed the 14-days transitional-phase co-culture elicited parents ions *m/z* 364.2239, 364.2286 and 364.2333 (**Figure 5.22** and **Table S5.5**) which were also detected at later growth stages under the 28-day old *Micromonospora* KRD244 mono-culture. This suggests that the parent ions *m/z* 694.2915, 696.3079, 713.2947, 713.3075, 714.2791, 737.2588, 737.2722 and 737.2856 were specific to the transitional-phase co-culture at a specific time and that bioactivity observed by the 14- and the 21-day old transitional-phase co-cultures was produced by the same metabolites. Additionally, these data indicate that the parent ions *m/z* 364.2239, 364.2286 and 364.2333 were produced at earlier growth stages of the *Micromonospora* KRD244 strain as a chemical response to co-cultivation.

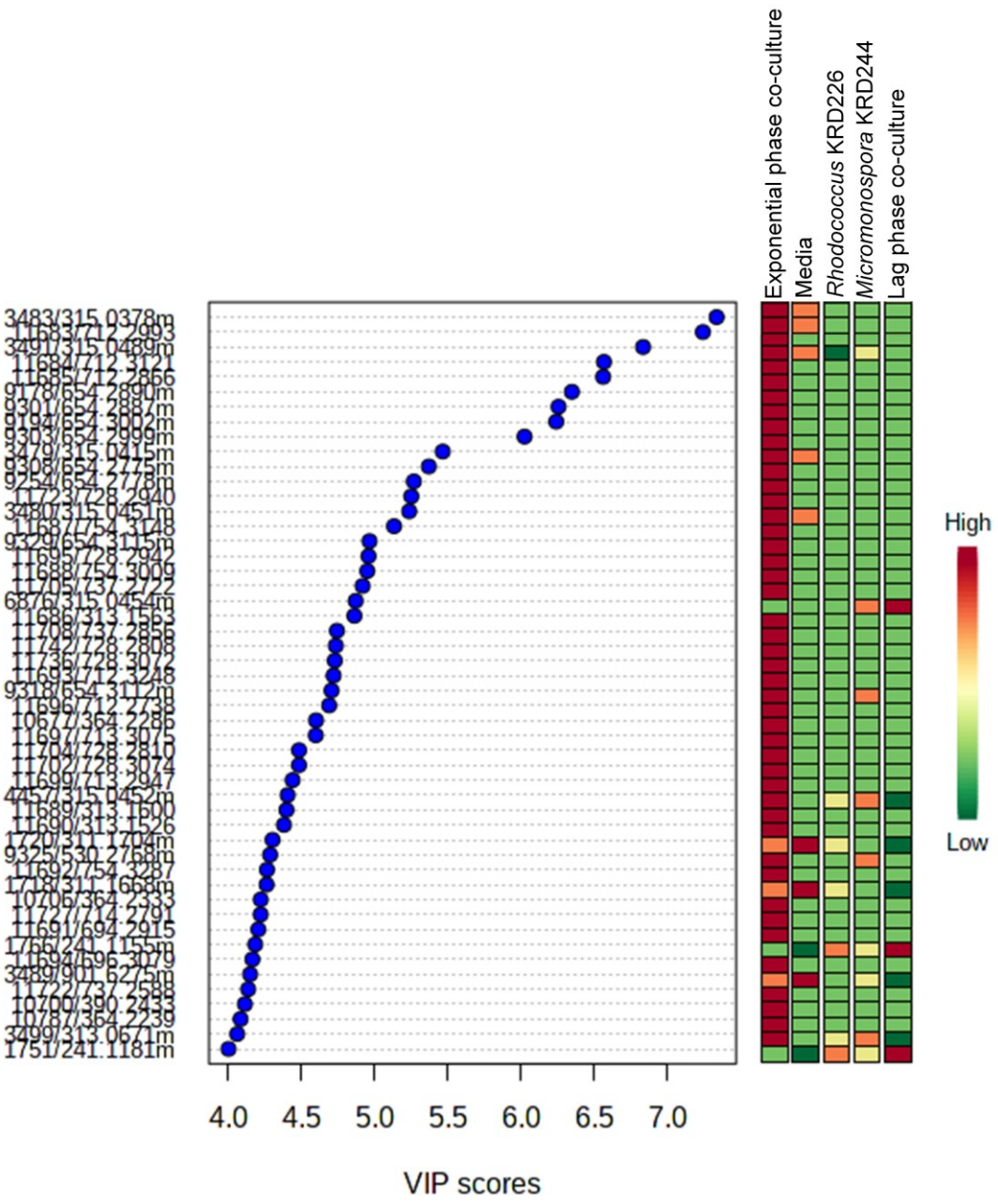

Figure 5.22. VIP scores plot reveals 35 parent ions elicited by the 14-day old transitional-phase co-culture. Blue dots indicate the VIP scores ranged between four and eight, scores that are P > 1 are considered significant. The coloured boxes on the right indicate the ion intensity. VIP scores are detailed in supplementary **Table S5.5.**

The PCA for the 21-day old cultures showed that 64.4% of the variance was explained by the first three PCs (**Figure 5.23A** and **Figure 5.24**). Consistently with the 14-day old transitional-phase co-culture findings, the 21-day old transitional-phase co-culture was responsible for most of the variance observed in the PCA model (**Figure 5.23A**).

The PCA loadings plot revealed that the parent ions responsible for this discrimination were *m/z* 654.2887, 654.2999, 654.2890, 712.2993, 654.2775, 654.3002 (outliers situated in the left quadrants of the PCA loadings plot, **Figure 5.23B**). This reinforces that the maximum metabolite production was achieved between the 14 and 21 days of growth.

The parent ions identified as co-culture outliers by PLS-DA coincided perfectly with those detected by PCA (data not shown). In addition, the PLS-DA cross-validation supported the predictability of the model since Q2 and R2 values were 0.85 and 0.99. The PLS-DA VIP analysis confirmed that the two parent ions *m/z* 295.2288 and 546.2693 previously observed in the LC-MS chromatograms were detected under the 21-day old transitional-phase co-cultures (**Figure 5.25**). Furthermore, VIP identified the parent ions with *m/z* of 277, 530, 576 and 655 (**Figure 5.25**) which were not previously observed and were detected under the transitional-phase co-culture as revealed by the LC-MS chromatograms (**Figure S5.6**). These were considered within the 50 most significant (1 < P) parent ions contributing to the variance of the model (**Figure 5.25** and **Table S5.6**).

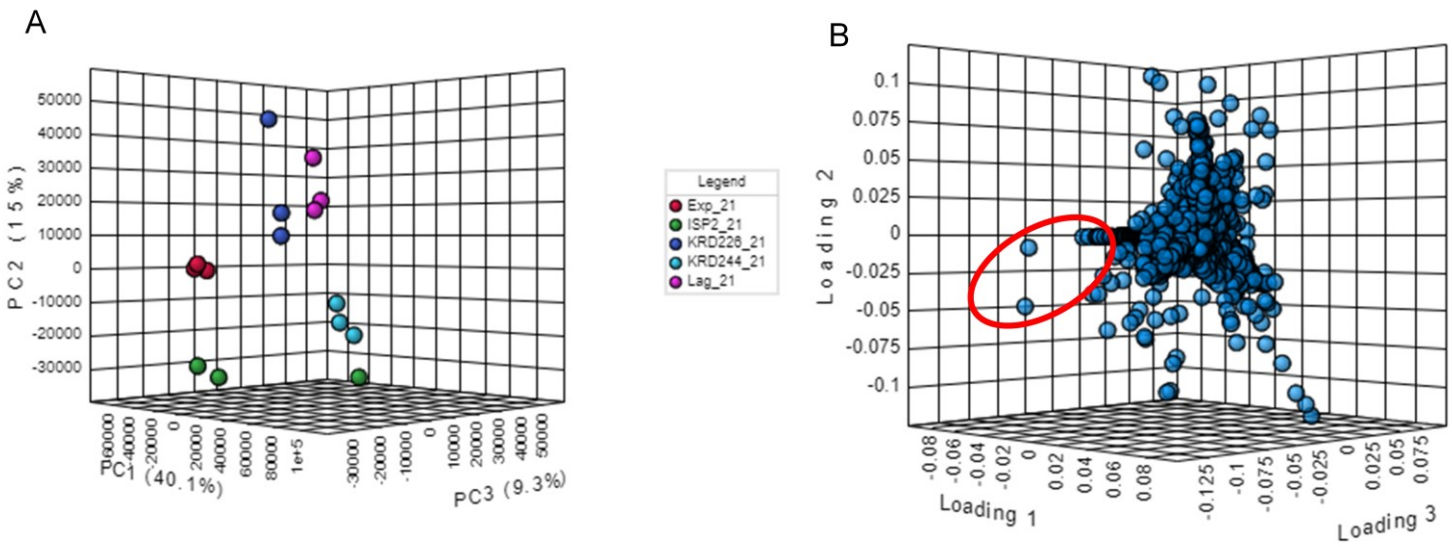

Figure 5.23. PCA scores reveals the separation of the 21-days old transitional-phase co-cultures from the mono-cultures and the loadings plot indicates the parent ions responsible for this separation. A) PCA scores plot based on the three first PCs (PC1, PC2 and PC3). Each experimental group is colour-coded (red: transitional-phase co-culture, green: media control (ISP2), blue: *Rhodococcus* KRD226 mono-culture, turquoise: *Micromonospora* KRD244 mono-culture and pink: lag-phase co-culture). B) PCA loadings plot. Each dot represents one parent ion from the dataset. Those parent ions situated with greater distance from the starting point of the loadings plot drive the variance in the PCA model. The red circle indicates the parent ions responsible for the discrimination of the transitional-phase co-culture.

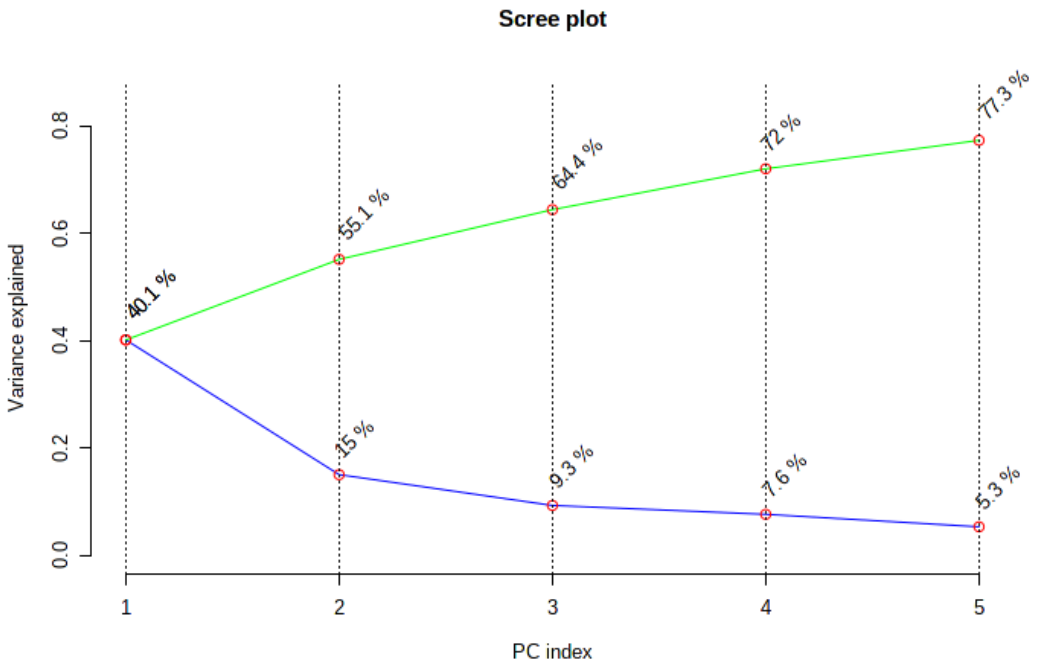

Figure 5.24. Scree plot shows the PCA variance between 21-day old bacterial extracts explained by the first five PCs. The green line on top shows the accumulated variance explained; the blue line underneath shows the variance explained by individual PCs.

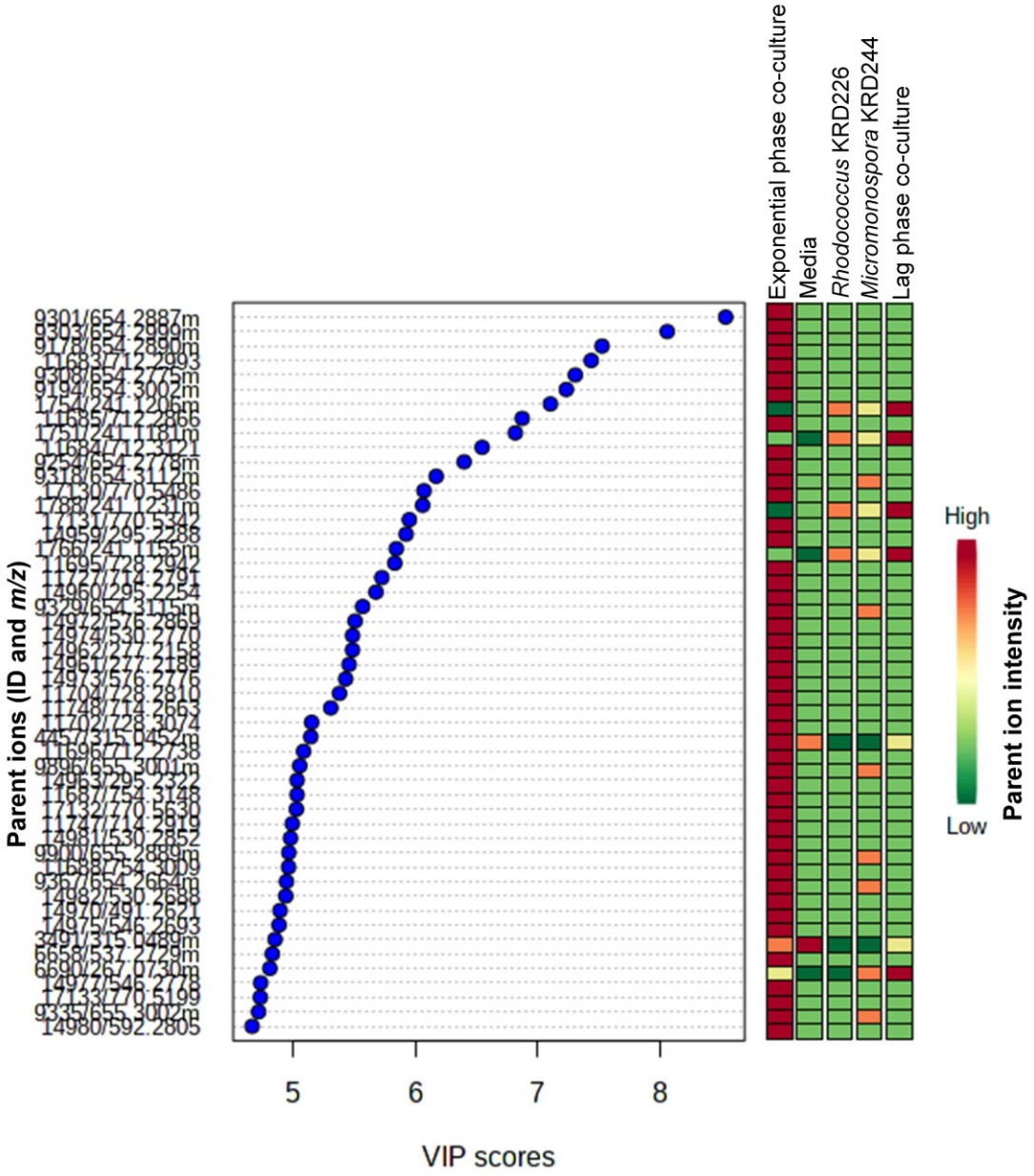

Figure 5.25. VIP scores plot reveals 37 parent ions elicited by the 21-day old transitional-phase co-culture. Blue dots indicate the VIP scores ranged between four and eight, scores that are P > 1 are considered significant. The coloured boxes on the right indicate the ion intensity. VIP scores are detailed in supplementary **Table S5.6**.

In order to reveal the impact of time in the production of transitional-phase co-culture-specific metabolites, the four transitional phase co-culture groups (seven, 14, 21 and 28 days) were compared by multivariate data analysis. The PCA showed that 62.3% of variance was explained by the first and second PCs of the PCA (**Figure 5.26A** and **Figure 5.27**). PCA revealed that the four groups of co-cultures separated from each

other. The seven and 28-day old co-cultures were situated closer to each other than to the 14- or 21-day old co-cultures (**Figure 5.26**). The PCA loadings plot confirmed the parent ions that were previously detected as group specific (**Figure 5.26B**). For example, *m/z* 277 and 295 for the 21-day old co-culture, *m/z* 313 for the 14-day old co-culture and *m/z* 654 and 712 ions were detected in both the 14- and 21-day old transitional-phase co-culture (outliers situated in the upper right quadrants and lower right quadrants in **Figure 5.26B**). The comparison between the four-time points transitional-phase co-cultures revealed the parent ions *m/z* 770.5486 and 770.5342 (**Figure S5.7**) which were detected under the 21- and 28-day old co-cultures (outliers situated in the upper right quadrants in **Figure 5.26B**). In addition, the PLS-DA did not reveal other outlier parent ions that were not identified by the PCA. However, the cross validation supported the variance observed in the PLS-DA since the R2 and Q2 values were 0.99 and 0.76, respectively. These data suggest that the parent ions detected in the 14-day old co-cultures are related with those detected in the 21-day old co-cultures. Furthermore, metabolites detected in the seven-day old co-cultures are related with those produced by the 28-day old co-cultures. In addition, these findings indicate metabolite shifts over time.

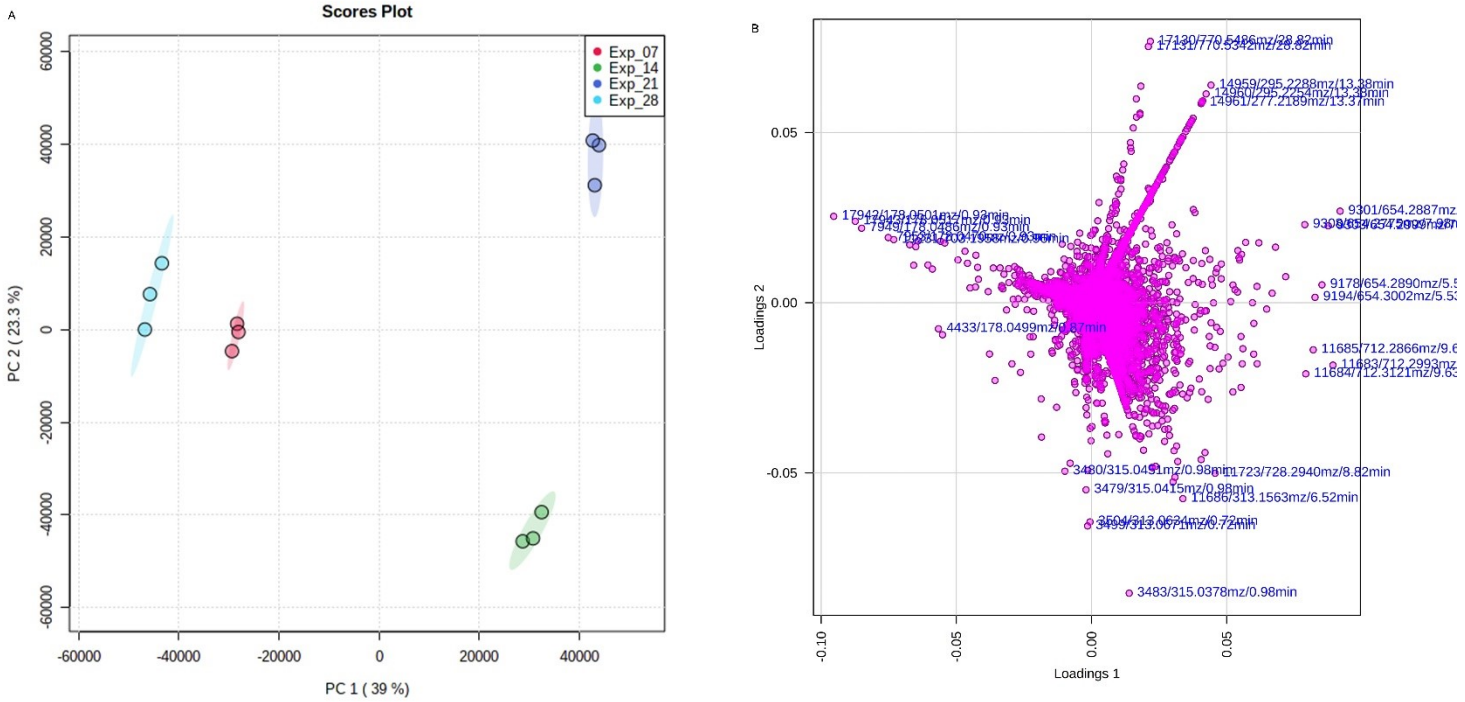

Figure 5.26. PCA scores reveals the separation between the four time points of the transitional-phase co-cultures and the loadings plot indicates the parent ions responsible for this separation. A) PCA scores plot based on the two first PCs (PC1 and PC2). Each experimental group is colour-coded (red: seven-day old transitional-phase co-culture, green: 14-day old transitional-phase co-culture, blue: 21-day old transitional-phase co-culture and turquoise: 28-day old transitional-phase co-culture). The ellipse shows the 95% confidence limit. B) PCA loadings plot. Each dot represents one parent ion from the dataset. Those parent ions situated with greater distance from the starting point of the loadings plot drive the variance in the PCA model. Some of these are labelled.

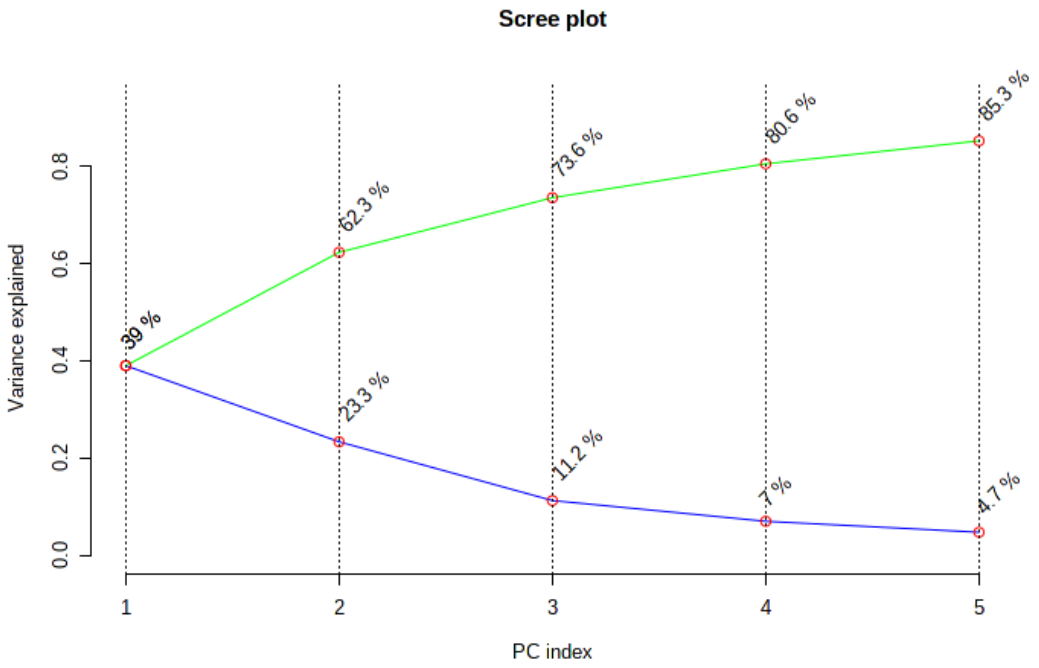

Figure 5.27. Scree plot shows the PCA variance between the four (seven, 14, 21 and 28) transitional-phase co-cultures explained by the first five PCs. The green line on top shows the accumulated variance explained; the blue line underneath shows the variance explained by individual PCs.

In order to have an overview of the chemical diversity produced between all experimental groups, a hierarchical cluster analysis was performed. The hierarchical cluster analysis heatmap confirmed that the 14 and 21-day old transitional-phase co-cultures were more related to each other than with the seven and 28-day old co-cultures (**Figure 5.28**). These four co-cultures were separated by the hierarchical cluster analysis in two clades (clade one; day seven and 28 and clade two; day 14 and 21, **Figure 5.28**). As previously observed, the 14 and 21-day old co-cultures produced more metabolites than the seven and 28-day old co-cultures (979 and 3536 compared to 307 and 358). The heatmap indicated that parent ions that were detected in the seven-day old co-culture were not detected after seven days (14-day old co-culture) (**Figure 5.28**). Similarly, parent ions detected at the 14-day old bacterial extracts were not detected in the 21-day old co-culture (**Figure 5.28**). Most of those detected in the 21-day old co-culture were not detected in the 28-day old co-cultures (**Figure 5.28**). This suggests that as a result of bacterial competition, the strains continue to produce metabolites that are not elicited at earlier growth stages as a

response to chemical signals. In addition, these data suggest that competition increased as the number of metabolites increased achieving maximum metabolite production between day 14 and 21.

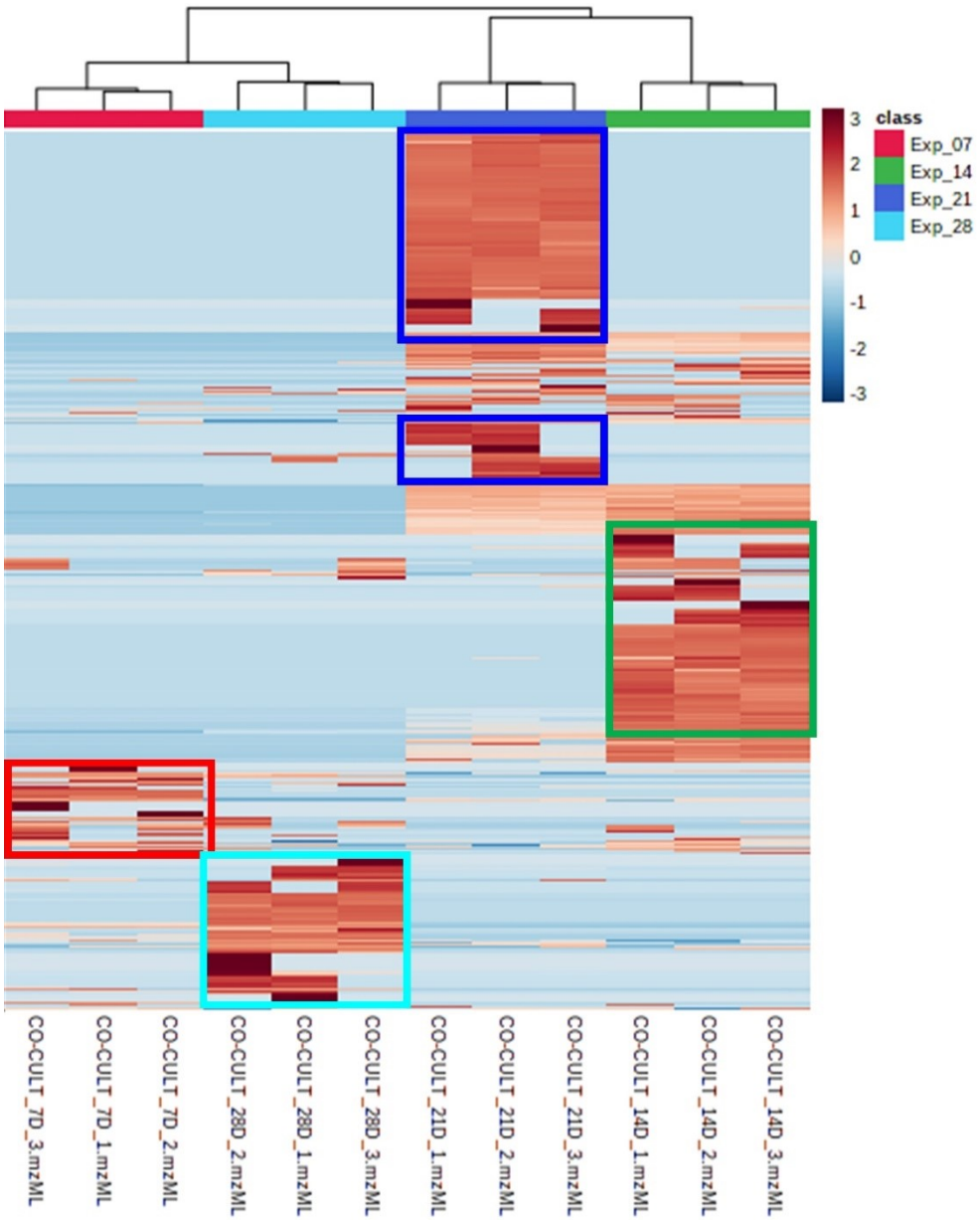

Figure 5.28. Experimental groups classified under two clades by the hierarchical cluster analysis according to metabolite production similarity (right: 14 and 21-day old transitional-phase co-culture and left: seven and 28-day old transitional-phase co-culture). Each coloured cell on the map corresponds to a parent ion intensity value ranging from blue (decreased level) to red (increased level), x-axis represents each group's experimental replicate in the bottom row and experimental groups in the top row, y-axis represents the parent ions. The coloured boxes, highlight parent ions elicited in each condition: red: seven-day old co-culture, green: 14-day old co-culture, blue: 21-day old co-culture, turquoise: 28-day old co-culture.

5.3 Discussion

In order to explore the chemical response of the *Rhodococcus* KRD226 and *Micromonospora* KRD244 strains across time and under different growth stages, the interaction between these two marine isolates and the mono-cultures were analysed by time-series experiments and under two growth phases. The results demonstrated that the outcome of bacterial interactions in the laboratory is influenced by the strains growth phase and the incubation period. In concordance with previous reports, the findings revealed that strains that reached transitional-phase did not longer require to outcompete the other strain (in lag-phase) due to an advanced growth (Burmeister *et al.*, 2019). This growth-related advantage suggested a decrease of the strains' competition fitness and of the production of inhibitory secondary metabolites (Ram *et al.*, 2019). On the other hand, the transitional-phase co-culture resulted in the elicitation of bioactive metabolites. It was hypothesised that this could be the result of competition between strains since they may share similar metabolic resources (Patin *et al.*, 2017; Tyc *et al.*, 2017; Shin *et al.*, 2018). However, further imaging mass spectrometry analysis combined with microscopy are necessary to better understand the interaction between these two strains and to obtain further conclusions.

The time-course experiment (seven, 14, 21 and 28 days) of the transitional-phase co-culture showed that metabolite production is not constant over time and this was a response to competition (Bertrand *et al.*, 2014; Azzollini *et al.*, 2018). It was observed that as time increased, co-culture elicited metabolites that were produced at earlier stages were suppressed at later time points while others were elicited towards the end of the incubation time. We hypothesise that at the start of the co-culture growth, metabolites were produced to counteract the effects of the competitor strain. Then, this production resulted in the enhanced elicitation of other secondary metabolites (response to chemical signs), increasing the survival of the producer strain (Pishchany *et al.*, 2018; Cabral *et al.*, 2018). Considering that the production of specialised metabolites require a high energy investment (Yan *et al.*, 2018), growing with a competitor supposed a stressful situation likely leading to metabolite elicitation (Chen *et al.*, 2015). Comparative metabolomics revealed an increased number of parent ions detected by the 14- and 21-day old transitional phase co-cultures which coincided with the two time points that produced bioactivity against *S. aureus*. This increase was followed by a decrease at day 28. This suggested that metabolites were induced over time to outcompete the competitor strain (Bertrand *et al.*, 2014; Azzollini

et al., 2018) and when competition was not required, metabolite production was switched off. Another possibility is that the producer strain started to enter death phase ceasing the production of metabolites. Interestingly, the multivariate data analysis results suggested that under these growth conditions the *Rhodococcus* KRD226 mono-culture is not susceptible to metabolite variation over time. A substantial shift of metabolite production was also not observed in the *Micromonospora* KRD244. In contrast, previous reports show that Actinobacterial strains such as *Salinispora,* are susceptible to chemical changes over incubation time (Patin *et al.*, 2018). One explanation is that these changes were not detected by the LC-MS. Additionally, the LC-MS used for this project does not capture changes in metabolite concentration. Therefore, if metabolites were produced at higher concentrations at different time points, this was not observed. However, given the complexity of bacterial interactions, it was hypothesised that these are more susceptible to metabolic variations (Zuñiga *et al.*, 2017). Therefore, the impact of time on the co-culture secondary metabolism demonstrated the complexity of bacterial interactions and the importance of growth parameters to aid the understanding of bacterial interplay and the production of specialised metabolites.

The competition between the *Rhodococcus* KRD226 and the *Micromonospora* KRD244 was reinforced by the pre-conditioned media analysis which suggested that when the two strains were growing in mono-culture, strain specific specialised metabolites did not affect the growth of each other. Contrary to these findings, previous studies reported that the medium of one strain affected the phenotype of the competitor strain and led to bioactivity against ESKAPE pathogens (Cabral *et al.*, 2018). However, while our findings indicate that specialised metabolites were produced as a result of direct physical contact between the strains, these reports focused on specialised metabolites that were elicited as a response to chemical signs from a mono-culture metabolite (Pishchany *et al.*, 2018; Cabral *et al.*, 2018). For example, *Amycolatopsis* sp. AA4 cultured in the pre-conditioned media of *S. coelicolor* M145 elicited antibiotic production as a response to a specialised metabolite produced by *S. coelicolor* M145 (Pishchany *et al.*, 2018). Similarly, the pre-conditioned media of *E. coli* killed *C. albicans* (Cabral *et al.*, 2018). It was found that a toxic soluble factor was produced by *E. coli* in mono-culture and was responsible for inhibiting *C. albicans* growth (Cabral *et al.*, 2018). Therefore, the findings reported here do not necessarily disagree. In addition, the fact that these metabolites were detected under co-culture, suggested that they are not produced under conventional

laboratory conditions (Adnani *et al.*, 2017). However, it is important to consider that even if the medium used for solid and liquid cultures was ISP2, strains adapt differently to the growth conditions which can directly affect the production of specialised metabolites (Pan *et al.*, 2019). For instance, while the liquid culture of *Streptomyces* sp. DT-A37 produced a new ring-opened lactam, the solid culture led to the discovery of an unknown holomycin and two new cyclopropaneacetic acid derivatives (Ding *et al.*, 2017). This suggested that this same interaction (*Rhodococcus* KRD226 and *Micromonospora* KRD244) was not only impacted by growth phase and incubation time but also by using solid and liquid cultures. In fact, more metabolites were elicited by liquid co-culture than solid co-culture.

Importantly, the findings agree with previous studies where it was reported that strains that meet in nature engage in a competitive environment (Beemelmanns *et al.*, 2017; Guo *et al.*, 2017; Benndorf *et al.*, 2018; Patin *et al.*, 2018) but this can be impacted by culture parameters (Crüsemann *et al.*, 2017). For example, the time-series study of the fungal strains *Eutypa lata* and *Botryosphaeria obtuse* co-culture revealed that interaction-elicited specialised metabolites decreased over time whereas others increased over time (Azzollini *et al.*, 2018). Another study showed that pyoverdine production by *P. aeruginosa* increased until nine hours of growth followed by a decrease (Ghoul *et al.*, 2016). Furthermore, these results are in line with previous reports that revealed the elicitation of specialised metabolites as a result of co-cultivation (Abdelwahab *et al.*, 2018; Moussa *et al.*, 2019). The co-culture of *Aspergillus fumigatus* MR2012 with two *Streptomyces leeuwenhoekii* strains (C34 and C58) led to the production of specialised metabolites under co-culture that were not produced under mono-culture (Wakefield *et al.*, 2017). The gene cluster encoding the bio synthesis of one of these metabolites (chaxapeptin) was previously identified in strain C34 but its production was not expressed under mono-culture (Wakefield *et al.*, 2017). Another study suggested that the co-cultivation of two *Penicillium* strains produced two metabolites (norlichexanthone and monocerin) to inhibit the growth of another strain (Chen *et al.*, 2015). Similarly, the co-cultivation of *Fusarium tricinctum* with *S. lividans* led to the production of the novel fusatricinones A–D and the new dihydrolateropyrone that were not detected under mono-culture (Moussa *et al.*, 2019). Therefore, in agreement with these reports we were able to reinforce the use of co-culture as a potential method for metabolite elicitation.

To conclude, this chapter showed the increased number of metabolites produced by the transitional-phase co-cultures over time. It was demonstrated that both the co-culture technique and changing growth conditions are potential methods to elicit metabolites that are not expressed under mono-culture. Using a wide range of experimental conditions can enhance chemical diversity and the number of metabolites detected by analytical tools (Romano *et al.*, 2018). In addition, the findings showed the complexity of bacterial interactions which can be higher in nature (Freilich *et al.*, 2011). Other environmental stressors that are found in their natural habitat (Ghoul and Mitri, 2017) such as nutrient depletion (Nicolitch *et al.*, 2019), changes in pH (Ratzke and Gore, 2018) and UV light (Reis-Mansur *et al.*, 2019) impact these interactions. For instance, competition for the acquisition of resources and space can increase as the number of bacterial species is higher (10^9 species) in the natural environment than in the laboratory (Traxler and Kolter, 2015; Coyte *et al.*, 2017). In future, one approach to grow bacterial strains in larger microbial communities and closer to environmental conditions is the microcosms. Microcosms are natural microbial communities grown in soil in the laboratory (Nicolitch *et al.*, 2019). In addition, future experiments should be performed to unravel and isolate the specialised metabolites that underpin the chemical responses of the *Micromonospora* and *Rhodococcus* interaction over time.

CHAPTER 6: IMAGING MASS SPECTROMETRY FOR THE ANALYSIS OF BACTERIAL INTERACTIONS

LC-MS and IMS are used in the discovery of specialised metabolites (Ellis *et al.*, 2019). However, the advantage of IMS over LC-MS is that it enables the spatial localisation of ionisable specialised metabolites on a surface (Watrous *et al.*, 2013; Parrot *et al.*, 2018). Therefore, the combination of IMS and comparative metabolomics of generated data (spatial metabolomics) aims to identify the exact location and distribution of each detected metabolite in a biological sample (Geier *et al.*, 2020). IMS requires minimal sample preparation compared to bioassay-guided methods where specialised metabolites are first extracted using organic solvents, and further purified using various separation methods (Zhang *et al.,* 2018). In microbial co-culture experiments, IMS is used to correlate interaction-elicited specialised metabolites to observed morphological colony alterations. This results from the fact that IMS enables the visualisation of metabolites that are localised at the evidenced phenotypic alteration zone (Araújo *et al.*, 2017; Geier *et al.*, 2020). In contrast with MS techniques, IMS offers the capability of untapping the potential roles of interaction-elicited metabolites under the specific co-culture (Spraker *et al.,* 2018). This reduces the number of specialised metabolites that are relevant under specific conditions (Spraker *et al.,* 2020). The biggest challenge presented by IMS analysis compared to other MS techniques relies on ejecting the ions of interest from the surface and ionisation (Spraker *et al.*, 2020). Several IMS instruments such as ToF-SIMS are operated under vacuum, which requires desiccated samples prior to analysis (Dunham *et al.*, 2017). Some samples cannot retain their structure under vacuum and need to be analysed with other techniques which results in a decreased spatial resolution (Spraker *et al.*, 2020). In addition, sample differences such as poor topography and salt concentration affect ionisation efficiency and the spatial distribution of metabolites (Dunham *et al.*, 2017). Therefore, it is often necessary to combine IMS with other analytical tools.

In IMS, the sample of interest is analysed with a microprobe that hits the surface and induces desorption of metabolites into the gas phase, where they are ionised (Dunham *et al.*, 2017; Buchberger *et al.*, 2018). Then, the MS detector collects a mass spectrum for each pixel of the selected area (Dunham *et al.*, 2017; Buchberger *et al.*, 2018). Once this area is analysed the beam moves onto a new selected region collecting mass spectra for each scanned pixel until the entire sample or areas of interest are analysed (Parrot *et al.*, 2018). A final average mass spectrum is created

from all the collected spectra and the spatial distribution of secondary metabolites are visualised as an image by false colour mapping (Watrous *et al.*, 2013; Parrot *et al.*, 2018). **Figure 6.1** shows an example of the spatial distribution of metabolites produced by a *C. albicans* colony (Watrous *et al.*, 2013). MALDI-ToF enabled the mapping of previously unreported metabolite distributions within the vegetative hyphae of *C. albicans* cultured on solid medium such as *m/z* 412 localised in the outer edge of the hyphae (**Figure 6.1**). This revealed that *m/z* 412 was involved in hyphae elongation (Watrous *et al.*, 2013). In addition, IMS analysis between *C.albicans* and *P. aeruginosa* revealed that rhamnolipids produced by *P. aeruginosa* inhibited hyphae formation in *C. albicans* as these were detected in the interaction interface (Watrous *et al.*, 2013). Recently, IMS was used to link metabolic phenotypes and bacterial interactions from the gill tissue of the deep-sea mussel *Bathymodiolus puteoserpensis* (Geier *et al.*, 2020). It was found that specialised metabolites such as PnE-Cer(34:2) are involved in the symbiosis between bacteria and *B. puteoserpensis* (Geier *et al.*, 2020). For example, PnE-Cer(34:2) was concentrated at the edge and the centre of the gill, which represented a potential niche for bacteria that degrades phosphonate (Geier *et al.*, 2020). Similarly, IMS was applied to antagonistic bacterial interactions where the strains elicited specialised metabolites to compete (Araújo *et al.,* 2017). These metabolites were identified at the zones of inhibition between strains (Araújo *et al.*, 2017). A previous spatial metabolomics study of *Burkholderia seminialis* interactions showed that the chemical defence of *B. seminalis* against cacao pathogens was the result of rhamnolipid production and other unidentified metabolites (Araújo *et al.*, 2017).

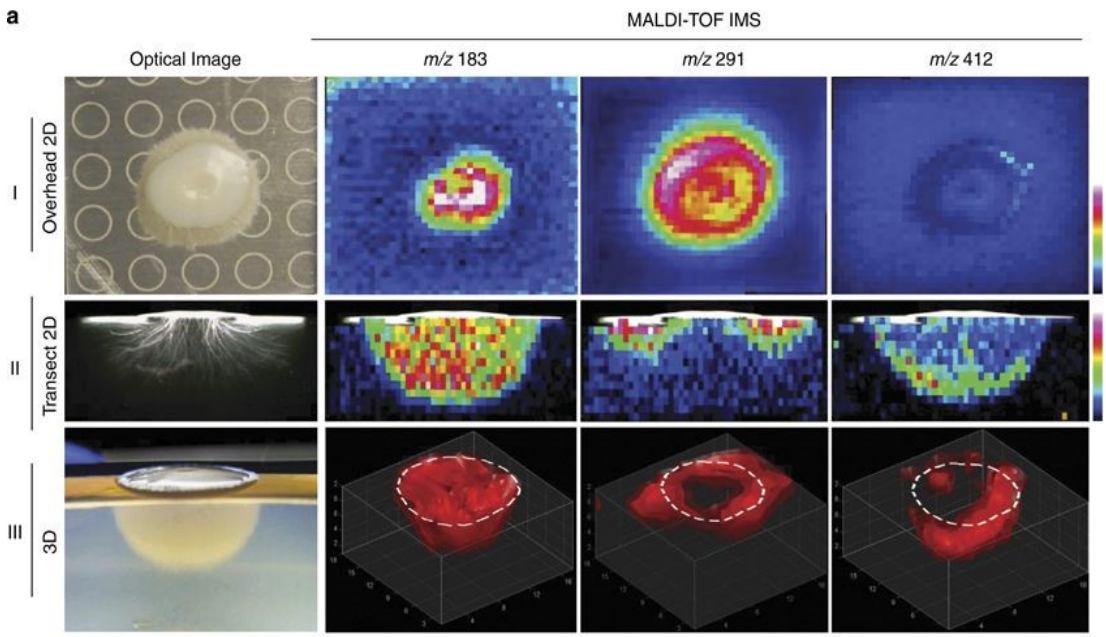

Figure 6.1. Comparison of 2D and 3D images of the metabolite spatial distribution produced by *C. albicans* colony analysed with MALDI-ToF (Watrous *et al.*, 2013). The gradient colour map represents ion signal intensity (blue indicates low intensity and red high intensity). I) 2D image taken from overhead the colony, II) 2D image of a colony transversal section and III) 3D image showing the whole *C. albicans* colony. Signal intensity at *m/z* 183 shows ion spatial distribution across the colony hyphae, signal intensity at *m/z* 291 is present at the colony edge and *m/z* 412 signal is detected at the hyphae edges (Watrous *et al.*, 2013).

6.1.1 ToF-SIMS and MALDI-ToF

ToF-SIMS and MALDI-ToF are two techniques that exist in the field of secondary ion IMS, which will be introduced here.

ToF-SIMS bombards the sample surface with an ion beam that induces the desorption/ionisation of secondary ions from the surface (Vickerman, 2009). The recent advances of novel primary ion beams in ToF-SIMS instrumentation resulted in the application of this instrument to biological extracts (Yoon and Lee, 2018). The main advantage of ToF-SIMS over MALDI-ToF is the capability of depth metabolite profiling and spatial distribution analysis of molecular ions. In addition, ToF-SIMS enabled the analysis directly from a solid surface without the necessity of disturbing the surface of the biological sample prior to analysis (Davies *et al.*, 2017; Dunham *et al.*, 2018; Yoon and Lee, 2018). Despite this, ToF-SIMS presents challenges for the analysis of biological samples as it requires flat and dry surfaces (Vickerman, 2009;

Ievlev *et al.*, 2017; Spraker *et al.*, 2020). The effects of a poor topography on ToF-SIMS analysis include the loss of ion signals and the acquisition of non-reliable data (Vickerman, 2009; Ievlev *et al.*, 2017). Additionally, the use of ion beams to sputter the sample surface results in significant fragmentation of metabolites, which can complicate the interpretation of mass spectra (Borodinov *et al.*, 2020). However, the combination of ToF-SIMS with other IMS techniques such as MALDI-ToF and other MS techniques such as tandem MS followed by the multivariate data analysis are applied to reduce these effects (Li *et al.*, 2018). For example, the combination of ToF-SIMS and MALDI-ToF resulted in the identification of 23 lipids and three oligosaccharides from *Pseudomonas putida* F1 biofilms, the discovery of specialised metabolites (*m/z* 120.1, 268.2, 417.2 and 523.5) involved in the interaction between *P. putida* F1 and *Shewanella oneidensis* that were not observed in mono-cultures and the effect of microbially influenced corrosion (Li *et al.*, 2018). Another study used ToF-SIMS to image the interior of *P. aeruginosa* biofilms attached in lung tissue and in glass slides (Davies *et al.*, 2017). ToF-SIMS enabled the detection of quorum sensing metabolites as well as unlabelled antimicrobials produced by *P. aeruginosa* biofilms while allowing the identification of their location within the bacterial biofilm (Davies *et al.*, 2017). In addition, the use of ion beams enables sub-micrometre spatial resolution (Ievlev *et al.*, 2018).

MALDI-ToF uses a laser absorbing matrix instead of an ion beam to produce ions from intact large metabolites with minimal fragmentation (Borodinov *et al.*, 2020). Therefore, the main advantage of MALDI-ToF is that it can yield high molecular weight metabolites (Spraker *et al.,* 2020) while enabling their preservation for identification (Borodinov *et al.,* 2020). Therefore, it is ideal for the analysis of many metabolites ranging from small to large metabolites (Borodinov *et al.*, 2020). The main disadvantage of laser ionisation is that limits the spatial resolution to 5-50μm. However, combined with ToF-SIMS enables both the detection and identification of intact metabolites with sub-cellular spatial resolution chemical imaging (Borodinov *et al.*, 2020). Hence, this technique is applied in microbiological studies such as the identification of bacterial species and the analysis of bacterial interactions (Watrous *et al.*, 2013; Araújo *et al.*, 2017; Ellis *et al.*, 2019; Geier *et al.*, 2020). For example, a previous study used MALDI IMS to characterise three *B. subtilis* strains and to examine cellular differentiation in biofilms (Si *et al.*, 2016). These results demonstrated the widely-accepted application of MALDI-ToF to compare spatial patterns of selected metabolites and to reveal the function of specialised metabolites

under specific interactions (Si *et al.*, 2016). Similarly, MALDI-ToF was used in a recent study to capture the metabolic exchange between the *Microcystis aeruginosa* and *Pseudomonas grimontii* interaction (Chen *et al.*, 2020). MALDI-ToF captured the distribution of metabolites (*m/z* 224, 256 and 1783) localised in the co-culture and revealed their possible role (Chen *et al.*, 2020). It was hypothesised that the parent ion *m*/*z* 224 (phenazine-1-carboxamide) was produced by *P. grimontii* to inhibit *M. aeruginosa* since it was detected at the inhibition zone (Chen *et al.*, 2020). *P. grimontii* resulted in the enhanced production of *m/z* 256 and 1783 by *M. aeruginosa.* However, these were detected where the two strains did not interact which indicated that they are related to QS of *M. aeruginosa* (Chen *et al.*, 2020). This demonstrated the capabilities of IMS to capture the chemical exchange in microbial interactions.

This chapter aimed at developing a sample preparation method for the analysis of bacterial co-cultures by ToF-SIMS without disturbing their surface. Furthermore, this thesis aimed to visualise the spatial distribution of specialised metabolites elicited by bacterial interactions that may be responsible for the production of phenotypic alterations.

6.2 Aims and objective

The objective of this chapter was to visualise the spatial distribution of specialised metabolites elicited by bacterial interactions.

Aim 1: to develop and to optimise a method for the analysis of bacterial cultures by ToF-SIMS analysis.

Aim 2: to validate the sample preparation method using *Streptomyces rimosus* ATCC10970.

Aim 3: to map the localisation of interaction-elicited metabolites between the *Rhodococcus* KRD231, *Microbacterium* KRD174 and *S. griseus*.

6.3 Results

6.3.1 Method development to analyse bacterial cultures on solid media by ToF-SIMS

In order to develop and optimise a method that would allow the analysis of bacterial interactions directly from solid media by ToF-SIMS, a total of four methods were compared. The methods were: oven-drying, freeze-drying, bacterial imprinting and nitrogen-drying. These methods were performed with *S. griseus* and *Rhodococcus* KRD231 since extracts from these strains were previously analysed with LC-MS. To analyse experimental samples by ToF-SIMS, sample dehydration and sample morphology were compared between the four methods (**Figure 6.2**). The oven-drying method revealed that to obtain complete colony dehydration the *Rhodococcus* KRD231 required five hours of drying while *S. griseus* and the media control required two. The colony height varied in all samples and the structural degradation observed at the edges (dry edges) rendered them unsuitable for ToF-SIMS (**Figure 6.2A**). The colony dehydration for the freeze-drying method (**Figure 6.2B**) required two hours for the three cases but also resulted in structural degradation and the colony height varied throughout the colonies. Freeze-dried samples were shrivelled from water removal and the surface was reduced leading to not enough bacterial surface for ToF-SIMS analysis (**Figure 6.2B**). These results suggest that all bacterial samples were shrivelled and dry to a degree where handling and flat surface analysis were not viable.

The bacterial imprinting (**Figure 6.2C**) revealed a flat surface contrary to oven-dried and freeze-dried methods. However, bacterial imprinting resulted in the loss of specialised metabolites that are diffused through the agar surface. The nitrogen-drying method (**Figure 6.2D**) presented a slight contraction at the edges of the solid media and the three experimental groups (*S. griseus, Rhodococcus* KRD231 and media control) acquired the same thickness. The thickness of the cultures was reduced by 1.5 – 2 mm, and there were no alterations in the strain morphology (**Figure 6.2D**). These data suggest that surface contraction occurs in a consistent manner in all experimental groups with minor phenotype changes in the middle of the culture where the bacterial colonies were placed. The nitrogen-drying method was therefore chosen for bacterial colony analysis using ToF-SIMS.

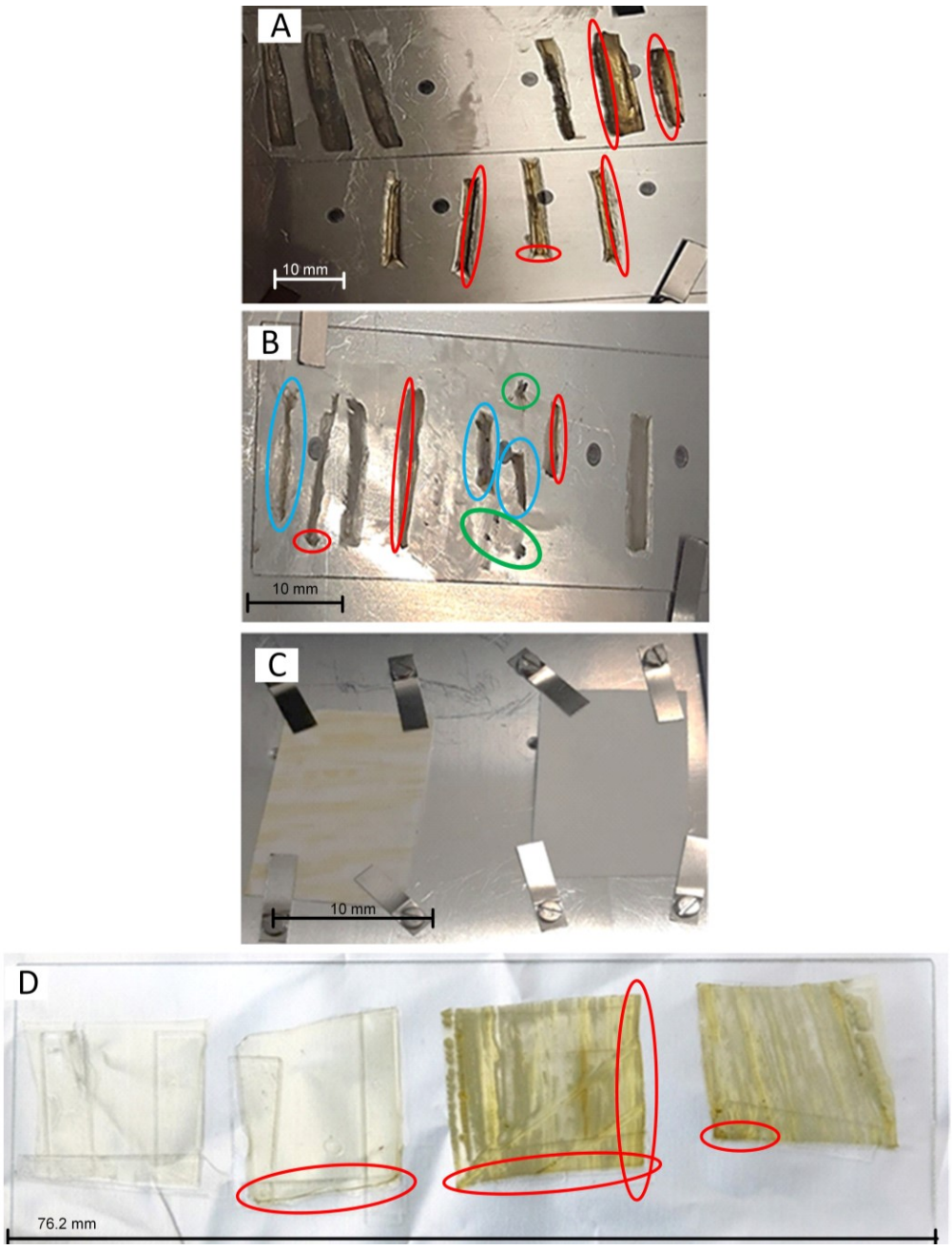

Figure 6.2. Comparison of bacterial sample methods for ToF-SIMS analysis. A) Oven-dried transversal sections. Top row: *S. griseus* (right) and *Rhodococcus* KRD231 (left), bottom row: media control. B) Freeze-dried transversal sections. From right to left: three control samples, three *S. griseus* samples and three *Rhodococcus* KRD231 samples. C) Bacterial imprinting. From right to left: *S. griseus* and *Rhodococcus* KRD231. D) Nitrogen-dried. From right to left: *S. griseus* and control. Circles indicate structural degradation (red: dry edge, blue: surface reduction from water removal and green: broken samples from dehydration).

6.3.2 Method validation for ToF-SIMS reveals matrix effect

In order to validate the sample preparation method for ToF-SIMS, the analysis of a bacterial interaction (*Microbacterium* KRD174*, Rhodococcus* KRD231 and *S. griseus*) was carried out as well as the analysis of *S. rimosus* ATCC10970 (oxytetracycline producer) to detect the production of the antibiotic oxytetracycline.

6.3.3 Analysis of bacterial competition between bacterial strains

ToF-SIMS enabled the spatial metabolite visualisation and comparison of a single colony, two colonies from two strains, and three colonies from three strains (*Rhodococcus* KRD231*, Microbacterium* KRD174 and *S. griseus*). ToF-SIMS analysis revealed the production of metabolites that were elicited by the interaction between the strains (**Figure 6.3**). **Figure 6.3** shows the spatial distribution of the interface between *Rhodococcus* KRD231 and *Microbacterium* KRD174. Selected parent ions elicited by the co-culture are observed in **Figure 6.3**. **Figure 6.3B** and **C** indicate the parent ions *m/z* 28.02 and *m/z* 39.02, respectively. These parent ions were only detected in the co-culture and their maximum ion intensity per pixel (maximal counts, MC) is indicated in bright yellow while lack of presence is indicated in black (zero counts). Additionally, the total counts (TC) for the entire image are also indicated. Results show that the MC of *m/z* 28.02 (**Figure 6.3B**) is detected at the interface between the two colonies and at the edge of the *Rhodococcus* KRD231. This suggests that this strain is likely responsible for the production of this ion during the interaction with *Microbacterium* KRD174. In addition, the MC of *m/z* 39.02 (**Figure 6.3C**) is detected at the interface between the strains. Therefore, is elicited by the co-culture but is not possible to determine which strain produces it. Furthermore, **Figure 6.3D** indicates the parent ion *m/z* 118.96 which is produced by the *Microbacterium* KRD174 as observed by the MC. These data suggest the production of co-culture specific metabolites. However, regardless of these interesting results, the ToF-SIMS analysis of the tri-culture was not reliable due to the introduction of air bubbles in the sample produced by the vacuum. This made data interpretation challenging. These findings indicate that further method development is necessary. Additionally, ToF-SIMS data is qualitative, and therefore, it was not possible to provide reliable and accurate absolutely quantitative results (conversion of ion intensities into ion concentrations).

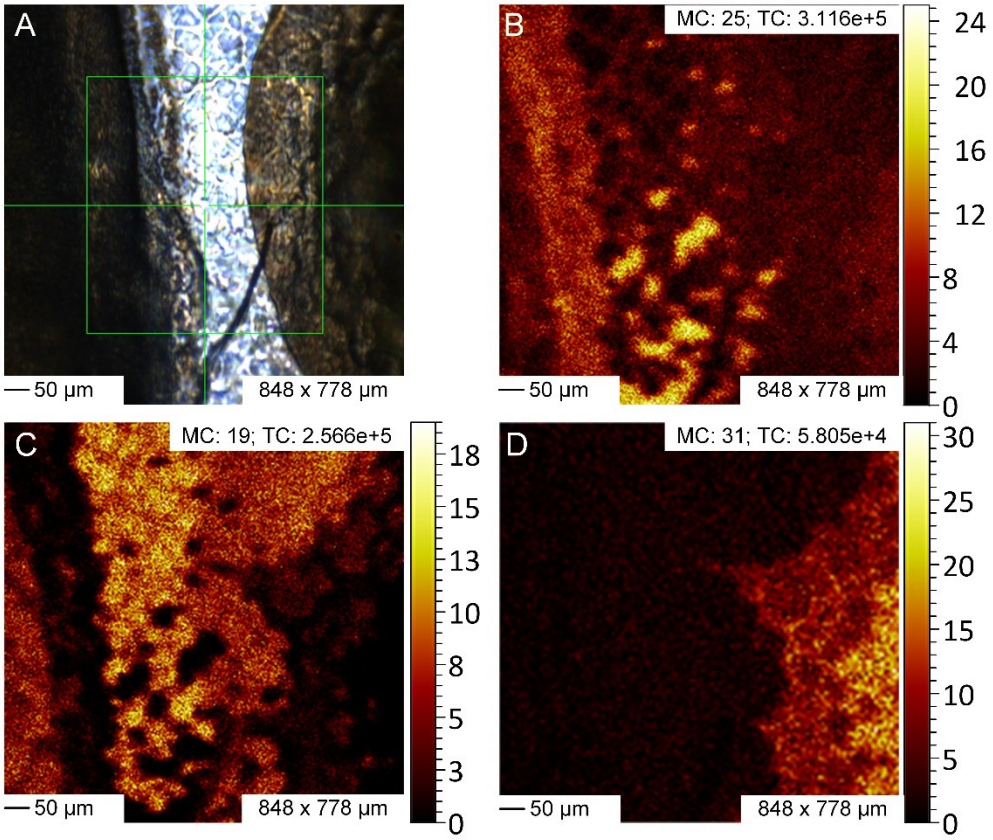

Figure 6.3. ToF-SIMS analysis of bacterial interactions on solid media between the *Rhodococcus* KRD231 and the *Microbacterium* KRD174. A) Microscopy picture of the analysed area. From right to left: *Microbacterium* KRD174, interface zone and *Rhodococcus* KRD231. B) Co-culture elicited parent ion *m/z* 28.02. C) Co-culture elicited parent ion *m/z* 39.02. D) Parent ion *m/z* 118.96 detected in the *Microbacterium* KRD174. The colour scale represents the maximal counts (MC) in one pixel and ranges from black (zero counts) to bright yellow (MC). TC indicates the total ion counts in the image.

6.3.4 Oxytetracycline detection from *Streptomyces rimosus*

To validate the nitrogen-dried method, *S. rimosus* ATCC10970 (oxytetracycline producer) was analysed from a liquid culture and solid culture using Emerson broth and Emerson agar for the production of oxytetracycline antibiotic. Oxytetracycline belongs to the tetracycline group of antibiotics and was the second tetracycline analogue to be discovered (Finlay *et al.,* 1950). Strain improvement for oxytetracycline was performed in *S. rimosus* ATCC10970 by random mutagenesis (Petkovic *et al.,* 2006).

ToF-SIMS analysis of solid media cultures of *S. rimosus* revealed that oxytetracycline was not detected (data not shown). In addition, when pure tetracycline was dissolved in the solid media, the tetracycline peak was also not observed. To ensure that oxytetracycline was in fact produced by *S. rimosus,* metabolite extracts from liquid cultures were analysed by LC-MS. The metabolite oxytetracycline was detected in the three experimental replicates of *S. rimosus* in positive (**Figure S6.1** and **Table S6.1**) and negative ionisation mode (**Figure S6.2** and **Table S6.1**). Despite that similar oxytetracycline fragmentation patterns were observed, oxytetracycline from *S. rimosus* cultures was not detected by ToF-SIMS (data not shown). These data suggest that the solid media results in a matrix effect that causes chemical variations. In turn, this complicates the interpretation of ToF-SIMS data.

6.4 Discussion

In order to visualise the spatial distribution of specialised metabolites elicited by bacterial interactions using ToF-SIMS, a sample preparation method was developed. SIMS analysis required samples that were vacuum compatible and free of topographical issues (Nuñez *et al.*, 2017). For this, sample degradation, sample topography and challenges regarding the introduction of the sample into the system were evaluated between four methods (oven-dried, freeze-dried, bacterial imprinting and nitrogen-dried). It was found that the oven-dried and freeze-dried methods resulted in poor topographical substrate since the height varied throughout the sample. In oven-dried method, the *S. griseus* and *Rhodococcus* KRD231 required different times to dry, leading to time inconsistency between bacterial samples. After dry, samples were very degraded and the edges were very crumbled posing worsened topography and complicating data interpretation. Additionally, topographical issues can lead to unwanted artefacts in SIMS chemical images and the spectra of the samples as well as the loss of secondary ion signals (Lee *et al.*, 2012). Therefore, due to the significant problems that oven dried and freeze-dried methods posed regarding deformation and introduction into the system, sample handling and flat surface analysis were not compatible with the ToF-SIMS requirements (Nuñez *et al.*, 2017). Contrary to oven-dried and freeze-dried, bacterial imprinting allowed a flat surface. However, due to the high-voltage that the instrument extractor poses, the fibres of these membranes were harmful for the ToF-SIMS instrument (not vacuum compatible). In addition, bacterial imprinting resulted in the loss of specialised metabolites that were diffused through the agar surface. From the four different methods that were assessed it was found that nitrogen-dried samples were the most suitable for ToF-SIMS analysis as previously observed (Dunham *et al.*, 2018). The sample surface posed small topographical issues that were non-avoidable, such as height difference within the *S. griseus* colony but these were minimal compared to the other methods.

To validate the nitrogen-drying method, bacterial interactions (*Rhodococcus* KRD231, *Microbacterium* KRD174 and *S. griseus*) were analysed in order to map the localisation of interaction-elicited metabolites. This analysis revealed metabolites that were elicited by the interaction between *Rhodococcus* KRD231 and *Microbacterium* KRD174. These were detected at the interface zone which suggested that they might be correlated with phenotypic alterations that were previously observed. ToF-SIMS provided excellent lateral resolution and sensitivity over a wide mass range,

nevertheless, the main limitation is that data is qualitative (Ievlev *et al.*, 2017) and quantitative results were not obtained. For this reason, if metabolites were produced in both mono-cultures and co-cultures, it can be challenging to differentiate them if they differ in concentration. Furthermore, *S. rimosus* ATCC10970 (oxytetracycline producer) samples were analysed in order to detect the metabolite oxytetracycline. Oxytetracycline was detected from *S. rimosus* cultures by LC-MS but not by ToF-SIMS. It was concluded that the matrix effect from the media components played a role in the detection of metabolites (Fletcher and Vickerman, 2013). Additionally, the sputtering process and the significant fragmentation of metabolites complicated data interpretation (Borodinov *et al.*, 2020). Furthermore, the air bubbles in the tri-culture that were produced by the vacuum indicated that further method optimisation is necessary for this type of biological samples.

Despite the growing interest in the study of bacterial chemical exchange by spatial metabolomics (Kellogg and Kang, 2020), to our knowledge ToF-SIMS is not applied for the study of bacterial interactions in solid medium. The lack of previous knowledge for the analysis of this type of biological samples complicated the method development and impacted the expected results. However, in line with previous studies, it was demonstrated that this analytical technique enables the visualisation of the spatial localisation of parent ions (Watrous *et al.*, 2010; Molina-Santiago *et al.*, 2019). Further studies should achieve the correlation of co-culture-elicited parent ions with the strain phenotypic alterations. Hence, this demonstrates the ability of IMS to gain insights in the understanding of chemical exchange (Watrous *et al.*, 2010; Boya *et al.*, 2017; Molina-Santiago *et al.*, 2019). Importantly, it highlights the ability of IMS to reveal potential roles of specialised metabolites under co-cultures (Watrous *et al.*, 2010; Boya *et al.*, 2017; Molina-Santiago *et al.*, 2019). For example, the spatial metabolomics analysis of surfactin produced by *B. subtilis* during the interaction between *B. subtilis* Δmatrix and *Pseudomonas chlororaphis* PCL1606 revealed that surfactin was localised in the interaction zone between the strains (Molina-Santiago *et al.*, 2019). Another IMS study demonstrated that *B. subtilis* inhibited the production of specialised metabolites and the aerial hyphae of *S. coelicolor* by the production of surfactin (Watrous *et al.*, 2010). Furthermore, *B. subtilis* wild type and PY79 strains produced a total of 23 and six co-culture specialised metabolites, respectively while *S. coelicolor*, produced a total of 13 interaction-specific metabolites (Watrous *et al.*, 2010). These results demonstrated the importance of the analysis of bacterial

interactions by spatial metabolomics to visualise chemical exchange and to map morphological alterations with interaction-elicited secondary metabolites.

Current challenges in the spatial metabolomics study of biological samples by ToF-SIMS are the potential loss of chemical data and the extensive molecular fragmentation (Lee, Bowen and Northen, 2010; Fletcher *et al.*, 2013; Cleland and Schroeter, 2018; Fu *et al.*, 2018). This complicates the identification of metabolites such as oxytetracycline even if they are ionised (Lee, Bowen and Northen, 2010; Fletcher *et al.*, 2013; Cleland and Schroeter, 2018; Fu *et al.*, 2018). For that reason, ToF-SIMS is a powerful technique to visualise the spatial localisation of metabolites when combined with LC-MS analysis. This provides reliable data and facilitates its interpretation (Fletcher *et al.*, 2013; Fu *et al.*, 2018). Future work should focus on developing a ToF-SIMS method for the analysis of bacterial colonies from solid media. Furthermore, it will be interesting to analyse the interaction between the *Rhodococcus* KRD226 and the *Micromonospora* KRD244 (chapter five) by 3D orbi-SIMS as it combines both techniques LC-MS/MS and ToF-SIMS. This instrument would provide the chromatogram overlay of both techniques enabling the potential identification of parent ions by MS/MS dereplication and the location mapping by ToF-SIMS. Metabolite dereplication by MS/MS and the spatial localisation of co-culture metabolites would facilitate the correlation between phenotypic alterations as a result of competition and interaction-elicited secondary metabolites.

CHAPTER 7: GENERAL DISCUSSION, CONCLUSIONS AND FUTURE DIRECTIONS

The rapid emergence of multidrug resistant bacterial strains poses a global threat to both human and animal health. For that reason, the search for new antimicrobials is constant but innovative approaches are necessary. Bacteria, in particular the *Actinobacteria* phylum, are a rich source of antibiotics as a result of their biosynthetic potential (Baltz, 2017). Over the years the study of bacterial interactions by co-cultivation became a powerful technique to elicit novel NPs that are not otherwise produced under mono-culture (Bertrand, *et al.*, 2014; Hoshino *et al.*, 2017; Shi *et al.*, 2017; Wakefield *et al.*, 2017; Anjum *et al.*, 2018). For instance, one of the latest discoveries by using this approach were the novel NPs chermebilaenes A and B which were elicited by the mixed fermentation of the marine isolates *Penicillium bilaiae* MA-267 and *Penicillium chermesinum* EN-480 (Meng *et al.*, 2020). This study assessed bacterial tri-cultures and one-to-one cultures, particularly between Actinobacterial strains isolated from marine sediments in order to elicit specialised metabolites. The assessment of these assays combined a phenotypic screening, pre-conditioned media, antibacterial assays and the comparative metabolomics of the bacterial extracts. This combination allowed the prioritisation of one interaction for further studies demonstrating its ability to rapidly detect interesting experimental groups. Additionally, this thesis aimed at developing a sample preparation method for ToF-SIMS to provide innovation in the way that interactions are analysed. Furthermore, this project aimed to understand the roles of specialised metabolites that produce morphological alterations of the strains under specific co-culture conditions.

The phenotypic screening revealed that strain inhibition predominated in the competitive interactions. These data indicated the possible chemical warfare between the strains as previously reported (Patin *et al.*, 2016; Geesink *et al.*, 2018). In fact, the LC/MS-based metabolomics revealed a chemical response of one-to-one cultures and tri-cultures where the elicitation of co-culture specific specialised metabolites was detected. This explained the strain phenotypic alterations and the increased bioactivity against *S. aureus and E. faecalis* (Ola *et al.*, 2013; Ebrahim *et al.*, 2016). In particular, one group of ecologically relevant interactions (*Rhodococcus* KRD226, *Micromonospora* KRD244 and *Streptomyces* KRD257) presented a diverse range of phenotypic alterations such as a white phenotype, inhibition and production of pigmented metabolites. Other interactions presented similar phenotypes and it was

hypothesised that this was the result of competition between strains. Some of these morphological patterns such as bald and white phenotypes can be explained by the fact that some specialised metabolites are capable of blocking aerial hyphae development and the production of spores by altering the expression of developmental genes (Yang *et al.*, 2009; Seyedsayamdost *et al.*, 2011; Schneider *et al.*, 2012; Traxler *et al.*, 2012). However, it is important to take into account that culture conditions such as rich-nutrient media lead to carbon catabolite repression (Romero-Rodríguez *et al.*, 2017). This negatively impacts morphological differentiation resulting in these phenotypes (Justice *et al.*, 2017; Liu *et al.*, 2017; Romero-Rodríguez *et al.*, 2017). In this case, ISP2 was used as culture medium which may have led to carbon catabolite repression. Carbon catabolite repression allowed the strains to use glucose as energy source enabling fast bacterial growth but repressing morphological differentiation and secondary metabolite production (Romero-Rodríguez *et al.*, 2018). Regardless of these limitations the *Rhodococcus* KRD226, *Micromonospora* KRD244 and *Streptomyces* KRD257 group produced metabolites that were not detected under mono-culture. Since these strains were isolated from the same sediment, it is likely that they compete for similar metabolic resources (Beemelmanns *et al.*, 2017; Khan *et al.*, 2018). In concordance with these findings, previous reports demonstrated that in fact, strain phenotypic alterations were a result of the production of metabolites under co-culture (Gonzalez *et al.*, 2011; Schoenian *et al.*, 2011; Khan *et al.*, 2018). For instance, the co-culture between *Halomonas* HL-48 and *Marinobacter* HL-58 (naturally occurring bacterial interaction) revealed phenotypic alterations in both strains (Khan *et al.*, 2018). These data suggested that these phenotypic alterations resulted from the response of *Halomans* HL-48 to chemical signals produced by *Marinobacter* HL-58 (Khan *et al.*, 2018). The detection of compounds that were not produced under co-culture was very interesting since it agrees with our hypothesis that suggests that bacterial interactions can lead to the elicitation of specialised metabolites.

As a result of inhibition between strains and an increased antibacterial activity against *S. aureus*, the interaction between *Rhodococcus* KRD226 and *Micromonospora* KRD244 was prioritised for LC-MS analysis. However, limited parent ions were elicited by this co-culture. Considering the antimicrobial activity produced by this interaction, this project explored the secondary metabolite potential of these strains. The impact of growth parameters (incubation time and growth phase) was assessed on the strains' secondary metabolism. This, reinforced previous findings that indicated

that while these strains may need to compete for resources, interactions between them are directly impacted by other growth conditions than the chosen medium (Kang *et al.*, 2013; Logue *et al.,* 2015; Adkar *et al.*, 2017). The time-course experiment demonstrated that metabolite production is not constant over time. This was expected since strains adapt to stressful conditions such as competitive environments leading to chemical changes (Patin *et al.,* 2018). Additionally, the growth-phase experiment revealed that metabolites were only elicited by the co-culture during transitional growth (Watrous *et al.*, 2013; Bertrand *et al.*, 2014; Azzollini *et al.*, 2018). Therefore, in agreement with previous work, this demonstrated that these two parameters influence strain phenotypes and can directly constrain the elicitation of metabolites (Freilich *et al.*, 2011; Ghoul and Mitri, 2017). However, it is important to consider that the increased number of metabolites under transitional-phase co-culture can also result from metabolic cross-feeding (Smith *et al.,* 2019). Furthermore, it should be assumed that interactions are more complex in the natural environment due to multiple factors such as nutrient limitation and nutrient composition (Liu *et al.*, 2017; Bertranda, 2019; Burmeister *et al.*, 2019). For instance, the *in situ* fertilization of three sites from tropical forest (Peruvian Andes-Amazon) showed that adding phosphorus promoted bacterial growth over fungal growth (Nottingham *et al.*, 2018). This suggested that under abundant phosphorus, bacteria outcompeted the fungi for nitrogen. Therefore, it was concluded that bacterial strains are susceptible to changing conditions which impact their ability to produce specialised metabolites. Innovation in the methods to analyse bacterial interactions such as combining multiple conditions can increase the understanding of chemical exchange and the roles of secondary metabolites. However, it is suggested that co-cultivation is based on serendipity (Nai and Meyer, 2018) and the poor reproducibility of this method needs to be considered (Martínez-Buitrago *et al.*, 2019).

To complement the analysis of chemical exchange between these interactions, it was necessary to understand how and why were these metabolites produced. For this, IMS techniques provide with the ability to map specialised metabolites in a co-culture with the producer strain (Chen *et al.*, 2020; Geier *et al.*, 2020). However, IMS instruments such as ToF-SIMS require samples that are free of topographical issues to minimise artefacts and to acquire good quality data. This is a current challenge in the spatial metabolomics study of biological samples (Cleland and Schroeter, 2018; Nuñez *et al.*, 2017). Therefore, this project aimed at the sample method development to analyse bacterial interactions directly from solid media. One method (nitrogen-dried

samples) presented a good surface for ToF-SIMS analysis and in fact, allowed the analysis of bacterial samples. In line with previous studies, ToF-SIMS enabled the visualisation of parent ions detected under co-culture (Watrous *et al.,* 2010; Molina-Santiago *et al.,* 2019). However, the matrix effect from the media components, the sputtering process and the significant fragmentation played a role in the detection of metabolites (Fletcher and Vickerman, 2013; Borodinov *et al.*, 2020). In addition, these challenges and the fact that ToF-SIMS data is qualitative, complicated the comparison to LC-MS data and the identification of previously detected interaction ions (Lee, Bowen and Northen, 2010; Fletcher *et al.,* 2013; Cleland and Schroeter, 2018; Fu *et al.,* 2018). Therefore, it was not possible to conclude that the metabolites observed at the interface zone by ToF-SIMS analysis were only produced under this condition. Additionally, these limitations complicated the identification of targeted metabolites such as tetracycline even when they were produced as previously demonstrated by the LC-MS data. Regardless of these limitations, with advanced knowledge of biological sample preparation, ToF-SIMS is capable of becoming a powerful technique to visualise the spatial localisation of metabolites.

7.1 Conclusions and future work

In conclusion, this work contributes to the understanding of chemical exchange during bacterial interactions, in particular in the interaction between two strains isolated from the same marine sediment. Additionally, this thesis demonstrated the need for a co-culture approach combined with other growth parameters to enhance chemical diversity. The findings showed that bacterial interactions can induce the production of metabolites but laboratory experiments are directly impacted by culture conditions and challenging limitations. Therefore, future directions should aim at developing standardised co-culture protocols to increase experimental reproducibility (Martínez-Buitrago *et al.*, 2019). In addition, an approach that could be followed in future to enhance metabolite production is the use of other selective media. Since the production of metabolites is impacted by environmental conditions and nutrient limitations (McCormick and Flärdh, 2012), low nutrient cultures could enhance strain development and production of metabolites. It would also be interesting to compare competitive patterns under different media conditions. Furthermore, to corroborate the LC-MS data, bacterial extracts from the two analysed bacterial groups should be further analysed by LC-MS/MS. This instrument increases sensitivity (noise reduction), provides more structural information and enables metabolite dereplication.

This data could then be analysed by GNPS to organise the metabolites into molecular networks enabling the identification of all metabolites that are produced by each group and those that are shared between conditions (Wang *et al.*, 2016). This could corroborate the previous hypotheses that suggested the strains that are likely producers of interaction-elicited metabolites under the analysed co-cultures. In addition, MS/MS and GNPS would enable the further prioritisation of bacterial extracts for large-scale fermentation, isolation and identification of bioactive metabolites. Following this prioritisation, crude extracts from large-scale fermentations should be partitioned using different solvents such as ethyl acetate, hexane and methanol to increase the metabolite profile variability. These fractions could be tested for bioactive metabolites which would facilitate compound purification and identification. This would test the observed hypothesis that suggested that the bioactive metabolites detected in these experiments were a result of bacterial interactions. Furthermore, future studies should focus on the whole genome analysis of the *Rhodococcus* KRD226 and *Micromonospora* KRD244 in order to reveal their biosynthetic potential and to correlate metabolomics data with genomics data. Although the strains were subjected to 16S rRNA amplification and sequencing, in future, whole genome analysis would enhance bacterial identification and gene prediction. Ideally, these two marine isolates could be sequenced with Illumina MiSeq and the genes correlated to specialised metabolite production could be identified and annotated using the antiSMASH platform. Then, GNPS would be used to identify metabolites and BiG-SCAPE and nplinker to link the BGCs to their products (Eldjárn *et al.,* 2020; Navarro-Muñoz *et al.,* 2020). Matching specialised metabolites to BGCs would further facilitate the discovery of their ecological function. Additionally, the identification of BGCs could facilitate the mapping of interaction specific metabolites to its producer. This can bring new insights in understanding bacterial interactions since LC-MS metabolomics alone is not capable of identifying the producer strain under co-culture. However, it enabled the discrimination of these interesting co-cultures as observed by the differences in their chemical profiles. In addition, integrating genomics and metabolomics data would enable more reliable results.

Further optimisation of the ToF-SIMS method should resolve the previously indicated challenges. This could provide with a method to analyse bacterial co-cultures directly from solid media. For example, developing ToF-SIMS holders to culture bacterial strains would be a great advantage as this would avoid cutting the sample in smaller pieces. In addition, this would include a much larger agar surface that could be of

interest. Furthermore, ToF-SIMS analysis was performed under vacuum requiring prior desiccation. Instrument optimisation including ionisation approaches performed under ambient conditions could enable the study of living microorganisms. Additionally, ToF-SIMS does not detect metabolites that are found in low concentration or that are difficult to ionise. Enhancing ionisation methods and organic matrices could improve the detection of metabolites. The optimisation of a ToF-SIMS method would potentially enable the correlation of competitive interactions with specialised metabolites. This could aim at resolving the hypothesis that indicated that these metabolites were responsible for phenotypic alterations. It will be interesting to analyse the interaction between the *Rhodococcus* KRD226 and the *Micromonospora* KRD244 by 3D orbi-SIMS and compare the results to the previous collected LC-MS data. Since this instrument provides the chromatogram overlay of both techniques (SIMS and MS/MS), it enables the mapping of metabolites with strain phenotypic alterations such as inhibition. Therefore, we would be able to confirm the previous hypotheses that suggested that these alterations were produced by interaction-elicited metabolites. Furthermore, MS/MS would enable metabolite dereplication facilitating the prioritisation of potentially unreported metabolites detected at the inhibition zones. Finally, to complement the study of this interaction, it would be interesting to subject the co-culture to liquid extraction surface analysis (LESA). LESA introduces small volumes of extraction solvent directly into the biological samples, pipettes the solvent out and introduces the sample into the MS (Spraker *et al.,* 2020). It is suggested that by doing this, LESA has the potential to detect ions that can be difficult to detect with the extraction of the entire culture (Spraker *et al.,* 2020). All together, these methods offer the advantage of adding insights in the understanding of bacterial interactions, the roles of metabolites under specific conditions and the elicitation of potentially novel NPs.

Bibliography

Abdel-Razek, A. S. *et al.* (2018) 'Penicisteroid C: New polyoxygenated steroid produced by co-culturing of *Streptomyces piomogenus* with *Aspergillus niger*', *Steroids*. 138, pp. 21–25.

Abdelwahab, M. F. *et al.* (2018) 'Induced secondary metabolites from the endophytic fungus *Aspergillus versicolor* through bacterial co-culture and OSMAC approaches', *Tetrahedron Letters*. 59(27), pp. 2647–2652.

Adkar, B. V. *et al.* (2017) 'Optimization of lag phase shapes the evolution of a bacterial enzyme', *Nature Ecology and Evolution*. 1(6), p. 149.

Adnani, N. *et al.* (2017) 'Co-culture of marine invertebrate-associated bacteria and interdisciplinary technologies enable biosynthesis and discovery of a new antibiotic, Keyicin', *ACS Chemical Biology*. 12(12), pp. 3093–3102.

Aharonowitz, Y., & Demain, A. L. (1978), 'Carbon catabolite regulation of cephalosporin production in *Streptomyces clavuligerus*'. *Antimicrobial agents and chemotherapy*. 14(2), pp. 159–164.

Ait Barka, E. *et al.* (2016) 'Taxonomy, physiology, and natural products of Actinobacteria', *Microbiology and Molecular Biology Reviews*. 80(1), pp. 1–43.

Altschul, S. F. *et al.* (1990) 'Basic local alignment search tool.', *Journal of molecular biology*. 215(3), pp. 403–10.

Amin, D. H. *et al.* (2020) 'Microbiological and molecular insights on rare Actinobacteria harboring bioactive prospective', *Bulletin of the National Research Centre*. 44(5), pp. 1–12.

Anjum, K. *et al.* (2018) 'Novel antifungal janthinopolyenemycins A and B from a co-culture of marine-associated *Janthinobacterium* spp. ZZ145 and ZZ148', *Tetrahedron Letters*. 59(38), pp. 3490–3494.

Araújo, F. D. S. *et al.* (2017) 'Desorption electrospray ionization mass spectrometry imaging reveals chemical defense of: *Burkholderia seminalis* against cacao pathogens', *RSC Advances*. 7(48), pp. 29953–29958.

Arbeit, R. D. *et al.* (2004) 'The safety and efficacy of daptomycin for the treatment of complicated skin and skin-structure infections', *Clinical Infectious Diseases*. 38(12), pp. 1673–1681.

Arora, D. *et al.* (2020) 'Expanding the chemical diversity through microorganisms co-culture: current status and outlook', *Biotechnology Advances*. 40, p. 107521.

Arpino, P., Baldwin, M. A. and McLafferty, F. W. (1974) 'Liquid chromatography-mass spectrometry. II—continuous monitoring', *Biological Mass Spectrometry*. 1(1), pp. 80–81.

Azzollini, A. *et al.* (2018) 'Dynamics of metabolite induction in fungal co-cultures by metabolomics at both volatile and non-volatile levels', *Frontiers in Microbiology*. 5(9), p. 72.

Baker, S. *et al.* (2018) 'Genomic insights into the emergence and spread of antimicrobial-resistant bacterial pathogens', *Science*. 360(6390), pp. 733–738.

Baltz, R. H. (2006) 'Marcel Faber Roundtable: Is our antibiotic pipeline unproductive because of starvation, constipation or lack of inspiration?', *Journal of Industrial Microbiology and Biotechnology*. 33(7), pp. 507–513.

Baltz, R. H. (2017) 'Gifted microbes for genome mining and natural product discovery', *Journal of Industrial Microbiology and Biotechnology*, 44(4–5), pp. 573–588.

Bauermeister, A. *et al.* (2019) 'Intra-clade metabolomic profiling of MAR4 *Streptomyces* from the Macaronesia Atlantic region reveals a source of anti-biofilm metabolites', *Environmental Microbiology*. 21(3), pp. 1099–1112.

Bayer-Santos, E. *et al.* (2019) 'The opportunistic pathogen *Stenotrophomonas maltophilia* utilizes a type IV secretion system for interbacterial killing', *PLoS Pathogens*. 15(9), p. e1007651.

Bayly, C. L. and Yadav, V. G. (2017) 'Towards precision engineering of canonical polyketide synthase domains: Recent advances and future prospects', *Molecules*. 22(2), p. 235.

Beemelmanns, C. *et al.* (2017) 'Macrotermycins A-D, glycosylated macrolactams from a termite-associated *Amycolatopsis* sp. M39', *Organic Letters*. 19(5), pp. 1000–1003.

Behie, S. W. *et al.* (2017) 'Molecules to ecosystems: Actinomycete natural products in situ', *Frontiers in Microbiology*. 7, pp. 2149.

Belknap, K. C. *et al.* (2020) 'Genome mining of biosynthetic and chemotherapeutic gene clusters in *Streptomyces* bacteria', *Scientific Reports*. 10(1), pp. 1–9.

Bello-López, J. M. *et al.* (2019) 'Horizontal gene transfer and its association with antibiotic resistance in the genus *Aeromonas* spp.', *Microorganisms*. 7(9), p. 363.

Benndorf, R. *et al.* (2018) 'Natural products from actinobacteria associated with fungus-growing termites', *Antibiotics*. 7(3), p. 83.

Bentley, S. D. *et al.* (2002) 'Complete genome sequence of the model actinomycete *Streptomyces coelicolor* A3(2)', *Nature*. 417(6885), pp. 141–147.

Bérdy, J. and View, A. P. (2005) 'Bioactive microbial metabolites', *The Journal of antibiotics*. 58(1), pp. 1–26.

van Bergeijk, D. A. *et al.* (2020) 'Ecology and genomics of Actinobacteria: new concepts for natural product discovery', *Nature Reviews Microbiology*. 18(10), pp. 546–558.

Bertrand, S., Bohni, N., *et al.* (2014) 'Metabolite induction via microorganism co-culture: A potential way to enhance chemical diversity for drug discovery', *Biotechnology Advances*. 32(6), pp. 1180–1204.

Bertrand, S., Azzollini, A., *et al.* (2014) 'Multi-well fungal co-culture for de novo metabolite-induction in time-series studies based on untargeted metabolomics', *Mol. BioSyst.* 10(9), pp. 2289–2298.

Bertranda, R. L. (2019) 'Lag phase is a dynamic, organized, adaptive, and evolvable period that prepares bacteria for cell division', *Journal of Bacteriology*. 201(7), p. e00697.

Betancur, L. A. *et al.* (2017) 'Marine Actinobacteria as a source of compounds for phytopathogen control: An integrative metabolic-profiling / bioactivity and taxonomical approach', *PLOS ONE*. 12(2), p. e0170148.

Bibb, J. M. (2005) 'Regulation of secondary metabolism in streptomycetes', *Current Opinion in Microbiology*. 8(2), pp. 208–215.

Blaženović, I. *et al.* (2018) 'Software tools and approaches for compound identification of LC-MS/MS data in metabolomics', *Metabolites*. 8(2), p. 31.

Blin, K. *et al.* (2019) 'AntiSMASH 5.0: Updates to the secondary metabolite genome mining pipeline', *Nucleic Acids Research*. 47(W1), pp. W81–W87.

Bode, H. B. *et al.* (2002) 'Big effects from small changes: Possible ways to explore

nature's chemical diversity', *ChemBioChem*. 3(7), pp. 619–627.

Borodinov, N. *et al.* (2020) 'Toward nanoscale molecular mass spectrometry imaging via physically constrained machine learning on co-registered multimodal data', *npj Computational Materials*. 6(1), pp. 1–8.

Boya, C. A. *et al.* (2017) 'Imaging mass spectrometry and MS/MS molecular networking reveals chemical interactions among cuticular bacteria and pathogenic fungi associated with fungus-growing ants', *Scientific Reports*. 7(1), p. 5604.

Boya, C. A. *et al.* (2019) 'Fungus-growing ant's microbial interaction of *Streptomyces* sp. and *Escovopsis* sp. through molecular networking and MALDI Imaging', *Natural Product Communications.* 14(1), pp. 63–66.

Brian, P., Riggle, P. J., Santos, R., A., Champness, W., C. (1996) 'Global negative regulation of *Streptomyces coelicolor* antibiotic synthesis mediated by an *absA*-encoded putative signal transduction system', *J Bacteriol*. 178(11), pp. 3221-3231.

Brickner, S. J. *et al.* (1996) 'Synthesis and antibacterial activity of U-100592 and U-100766, two oxazolidinone antibacterial agents for the potential treatment of multidrug-resistant gram-positive bacterial infections', *Journal of Medicinal Chemistry*. 39(3), pp. 673–679.

Brockmann, H. and Henkel, W. (1951) 'Pikromycin, ein bitter schmeckendes Antibioticum aus Actinomyceten (Antibiotica aus Actinomyceten, VI. Mitteil', *Chemische Berichte*. 84, p. 284-288.

Buchberger, A. R. *et al.* (2018) 'Mass Spectrometry Imaging: A review of emerging advancements and tuture insights', *Analytical Chemistry*. 90(1), pp. 240–265.

Burmeister, A. *et al.* (2019) 'A microfluidic co-cultivation platform to investigate microbial interactions at defined microenvironments', *Lab on a Chip*. 19(1), pp. 98–110.

Cabral, D. J. *et al.* (2018) 'Microbial competition between *Escherichia coli* and *Candida albicans* reveals a soluble fungicidal factor', *Microb Cell.* 5(5), pp. 249–255.

Camus, L. *et al.* (2020) 'Trophic cooperation promotes bacterial survival of *Staphylococcus aureus* and *P. aeruginosa*', *ISME Journal*. 14(12), pp. 3093–3105.

Caraballo-Rodríguez, A. M., Dorrestein, P. C. and Pupo, M. T. (2017) 'Molecular inter-kingdom interactions of endophytes isolated from *Lychnophora ericoides*', *Scientific*

Reports. 7(1), pp. 1–14.

Cavaliere, M. *et al.* (2017) 'Cooperation in microbial communities and their biotechnological applications', *Environmental Microbiology*. 19(8), pp. 2949–2963.

Challis, G. L. and Hopwood, D. A. (2003) 'Synergy and contingency as driving forces for the evolution of multiple secondary metabolite production by *Streptomyces species*', *Proceedings of the National Academy of Sciences of the United States of America*. 100(2), pp. 14555–14561.

Chambers, M. C. *et al.* (2012) 'A cross-platform toolkit for mass spectrometry and proteomics', *Nature Biotechnology*. 30(10), pp. 918–920.

Chang, P. T. *et al.* (2020) 'Thiopeptide defense by an ant's bacterial symbiont', *Journal of Natural Products*. 83(3), pp. 725–729.

Chater, K. F. *et al.* (1989) 'The developmental fate of *S. coelicolor* hyphae depends upon a gene product homologous with the motility σ factor of *B. subtilis*', *Cell*. 59(1), pp. 133–143.

Chater, K. F. and Chandra, G. (2006) 'The evolution of development in *Streptomyces* analysed by genome comparisons', *FEMS Microbiology Reviews*. 30(5), pp. 651–672.

Chen, H. *et al.* (2015) 'A new fusarielin analogue from *Penicillium* sp. isolated from the Mediterranean sponge *Ircinia oros*', *Tetrahedron Letters*. 56(39), pp. 5317–5320.

Chen, J. *et al.* (2019) 'Chemistry and biology of siderophores from marine microbes', *Marine Drugs*. 17(10), pp. 562.

Chen, Q. *et al.* (2020) 'Imaging mass spectrometry of interspecies metabolic exchange revealed the allelopathic interaction between *Microcystis aeruginosa* and its antagonist', *Chemosphere*. 259, p. 127430.

Chen, R., Wong, H. and Burns, B. (2019) 'New Approaches to detect biosynthetic gene clusters in the environment', *Medicines*. 6(1), p. 32.

Chng, C., Lum, A. M., Vroom, J. A., & Kao, C. M. (2008) 'A key developmental regulator controls the synthesis of the antibiotic erythromycin in *Saccharopolyspora erythraea*', *Proceedings of the National Academy of Sciences of the United States of America*. 105(32), pp. 11346–11351.

Chong, J., Yamamoto, M. and Xia, J. (2019) 'MetaboAnalystR 2.0: from raw spectra

to biological insights', *Metabolites*. 9(3), p. 57.

Čihák, M. *et al.* (2017) 'Secondary metabolites produced during the germination of *Streptomyces coelicolor*', *Frontiers in Microbiology*. 8, p. 2495.

Claessen, D. *et al.* (2003) 'A novel class of secreted hydrophobic proteins is involved in aerial hyphae formation in *Streptomyces coelicolor* by forming amyloid-like fibrils', *Genes and Development*. 17(14), pp. 1714–1726.

Claessen, D. *et al.* (2004) 'The formation of the rodlet layer of streptomycetes is the result of the interplay between rodlins and chaplins', *Molecular Microbiology*. 53(2), pp. 433–443.

Cleland, T. P. and Schroeter, E. R. (no date) 'A Comparison of common mass spectrometry approaches for paleoproteomics'. 17(3), pp. 936–945.

Comroe, J. H. (1978) 'Pay dirt - the story of Streptomycin. Part 1. From Waksman to Waksman', *American Review of Respiratory Disease*. 117(4), pp. 773–781.

Costello, M. J., Cheung, A. and De Hauwere, N. (2010) 'Surface area and the seabed area, volume, depth, slope, and topographic variation for the world's seas, oceans, and countries', *Environmental Science and Technology*. 44(23), pp. 8821–8828.

Covington, B. C. *et al.* (2018) 'Response of secondary metabolism of hypogean actinobacterial genera to chemical and biological stimuli', *Applied and Environmental Microbiology*. 84(19), p. e01125.

Covington, B. C., McLean, J. A. and Bachmann, B. O. (2017) 'Comparative mass spectrometry-based metabolomics strategies for the investigation of microbial secondary metabolites', *Natural Product Reports*. 15(12), p. 383.

Coyte, K. Z. *et al.* (2017) 'Microbial competition in porous environments can select against rapid biofilm growth', *Proceedings of the National Academy of Sciences of the United States of America*. 114(2), pp. 161–170.

Coyte, K. Z. and Rakoff-Nahoum, S. (2019) 'Understanding competition and cooperation within the mammalian gut microbiome', *Current Biology*. 29(11), pp. 538–544.

Crüsemann, M. *et al.* (2017) 'Prioritizing natural product diversity in a collection of 146 bacterial strains based on growth and extraction protocols', *Journal of Natural Products*. 80(3), pp. 588–597.

D'Souza, G. *et al.* (2018) 'Ecology and evolution of metabolic cross-feeding interactions in bacteria', *Natural Product Reports*. 5, pp. 455–488.

D H Bergey; William B Whitman; M Goodfellow; Peter Kämpfer; Hans-Jürgen Busse (2012) '*Actinobacteria* phylum' In Bergey's Manual of Systematics of Archaea and Bacteria. *New York : Springer.*

Dang, T. and Süssmuth, R. D. (2017) 'Bioactive peptide natural products as lead structures for medicinal use', *Accounts of Chemical Research*. 50(7), pp. 1566–1576.

Darwin, C. (1860) 'The origin of species, by means of natural selection, or the preservation of favored races in the struggle for life', *Br Foreign Med Chir Rev.* 25(50), pp. 367–404.

Davies, J. (1990) 'What are antibiotics? Archaic functions for modern activities', *Molecular Microbiology*. 4(8), pp. 1227–1232.

Davies, S. K. *et al.* (2017) 'Visualizing antimicrobials in bacterial biofilms: Three-dimensional biochemical imaging using TOF-SIMS', *mSphere*. 2(4), p. e00211.

Defilippi, S. *et al.* (2017) 'Fungal competitors affect production of antibacterial lipopeptides in *Bacillus subtilis* strain B9-5', 44(4), pp. 374–383.

Demain, A. L. (1989) 'Carbon source regulation of idiolite biosynthesis', in *Regulation of Secondary Metabolism in Actinomycetes (1st ed.).* CRC Press.

Demain, A. L. and Fang, A. (2000) 'The natural functions of secondary metabolites', *Advances in biochemical engineering/biotechnology*. 69, p. 1–39.

Demarque, D. P. *et al.* (2020) 'Mass spectrometry-based metabolomics approach in the isolation of bioactive natural products', *Scientific Reports*. 10(1), pp. 1–9.

Desgagné-Penix, I. (2020) 'Biosynthesis of alkaloids in Amaryllidaceae plants: a review', *Phytochemistry Reviews*. 20, pp. 409–431.

Dey, P. *et al.* (2020) 'Analysis of alkaloids (indole alkaloids, isoquinoline alkaloids, tropane alkaloids)', in *Recent Advances in Natural Products Analysis*. Elsevier.

Dhakal, D., Sohng, J. K. and Pandey, R. P. (2019) 'Engineering actinomycetes for biosynthesis of macrolactone polyketides', *Microbial Cell Factories*. 18(1), p. 137.

DiMasi, J. A., Grabowski, H. G. and Hansen, R. W. (2016) 'Innovation in the pharmaceutical industry: New estimates of R&D costs', *Journal of Health Economics*.

47, pp. 20–33.

Ding, C. hong *et al.* (2018) 'The improvement of bioactive secondary metabolites accumulation in *Rumex gmelini Turcz* through co-culture with endophytic fungi', *Brazilian Journal of Microbiology*. 49(2), pp. 362–369.

Ding, H. *et al.* (2017) 'Derivatives of Holomycin and Cyclopropaneacetic Acid from *Streptomyces* sp. DT-A37', *Chemistry & Biodiversity*. 14(9), p. e1700140.

Doroghazi, J. R. and Buckley, D. H. (2014) 'Intraspecies comparison of *Streptomyces* pratensis genomes reveals high levels of recombination and gene conservation between strains of disparate geographic origin', *BMC Genomics*. 14(1), p. 611.

Duncan, K. *et al.* (2014) 'Bioprospecting from marine sediments of New Brunswick, Canada: Exploring the relationship between total bacterial diversity and actinobacteria diversity', *Marine Drugs*. 12(2), pp. 899–925.

Dunham, S. J. B. *et al.* (2017) 'Mass spectrometry imaging of complex microbial communities', *Accounts of Chemical Research*. 50(1), pp. 96–104.

Dunham, S. J. B. *et al.* (2018) 'Quantitative SIMS Imaging of Agar-Based Microbial Communities', *Analytical Chemistry*. 90(9), pp. 5654–5663.

Earl, J. P. *et al.* (2018) 'Species-level bacterial community profiling of the healthy sinonasal microbiome using Pacific Biosciences sequencing of full-length 16S rRNA genes', *Microbiome*. 6(1), p. 190.

Ebrahim, W. *et al.* (2016) 'Metabolites from the fungal endophyte *Aspergillus austroafricanus* in axenic culture and in fungal–bacterial mixed cultures', *Journal of Natural Products*. 79(4), pp. 914–922.

Eguchi, R. *et al.* (2019) 'Classification of alkaloids according to the starting substances of their biosynthetic pathways using graph convolutional neural networks', *BMC Bioinformatics*. 20(1), p. 380.

El-Hawary, S. S. *et al.* (2018) 'New Pim-1 kinase inhibitor from the co-culture of two sponge-associated Actinomycetes', *Frontiers in Chemistry*. 6, p. 538.

Eldjárn, G. H. *et al.* (2021) 'Ranking microbial metabolomic and genomic links using correlation-based and feature-based scoring functions', *PLoS Comput Biol.* 17(5), p. e1008920.

Ellis, B. M. *et al.* (2019) ‘Spatiochemically profiling microbial interactions with membrane scaffolded desorption electrospray ionization-ion mobility-imaging mass spectrometry and unsupervised segmentation’, *Analytical Chemistry*. 91(21), pp. 13703–13711.

Engl, T. *et al.* (2018) ‘Evolutionary stability of antibiotic protection in a defensive symbiosis’, *Proceedings of the National Academy of Sciences of the United States of America*. 115(9), pp. 2020–2029.

Evans, K. C. *et al.* (2018) ‘Quorum-sensing control of antibiotic resistance stabilizes cooperation in *Chromobacterium violaceum*’, *ISME Journal*. 12(5), pp. 1263–1272.

Feling, R. H. *et al.* (2003) ‘Salinosporamide A: A highly cytotoxic proteasome inhibitor from a novel microbial source, a marine bacterium of the new genus *Salinospora*’, *Angewandte Chemie - International Edition*. 42(3), pp. 355–357.

Fenical, W. (1993) ‘Chemical Studies of Marine Bacteria: Developing a New Resource’, *Chemical Reviews*. 93(5), pp. 1673–1683.

Fiehn, O. (2001) ‘Combining genomics, metabolome analysis, and biochemical modelling to understand metabolic networks’, *Comparative and Functional Genomics*. 2, pp. 150–168.

Finlay, A. C., G. L. Hobby, S. Y. P’An, P. P. Regna, J. B. Routien, D. B. Seeley, G. M. Shull, *et al.* (1950) ‘Terramycin, a New Antibiotic’, *Science*. 111(2874), p. 85.

Firn, R. (2010) ‘Why do organisms make NPs?’ *in Nature’s Chemicals: The Natural Products that shaped our world, Nature’s Chemicals: The Natural Products that Shaped our World*. Oxford University Press, Oxford.

Fischer, C. *et al.* (2017) ‘Metabolite exchange between microbiome members produces compounds that influence drosophila behavior’, *eLife*. 6, p. 18855.

Flärdh, K., Findlay, K. C. and Chater, K. F. (1999) ‘Association of early sporulation genes with suggested developmental decision points in *Streptomyces coelicolor* A3(2)’, *Microbiology*. 145 (9), pp. 2229–2243.

Fleming, A. (1929) ‘On the antibacterial action of cultures of a penicillium, with special reference to their use in the isolation of *B. influenzae*’, *British journal of experimental pathology*, 10(1923), pp. 226–236.

Fletcher, J. S. *et al.* (2013) ‘Evaluating the challenges associated with time-of-fight

secondary ion mass spectrometry for metabolomics using pure and mixed metabolites', *Metabolomics*. 9(3), pp. 535–544.

Fletcher, J. S. and Vickerman, J. C. (2013) 'Secondary Ion Mass Spectrometry: characterizing complex samples in two and three Dimensions', *Analytical Chemistry*. 85(2), pp. 610–639.

Foster, K. R. and Bell, T. (2012) 'Competition, not cooperation, dominates interactions among culturable microbial species', *Current Biology*, 22(19), pp. 1845–1850.

Fox Ramos, A. E. *et al.* (2019) 'Natural products targeting strategies involving molecular networking: different manners, one goal', *Natural Product Reports*. 36(7), pp. 960–980.

Freilich, S. *et al.* (2011) 'Competitive and cooperative metabolic interactions in bacterial communities', *Nature Communications*. 2(1), p. 589.

Fu, T. *et al.* (2018) 'Tandem mass spectrometry imaging and *in situ* characterization of bioactive wood metabolites in amazonian tree species *Sextonia rubra*'. *Anal chem.* 90 (12), pp. 7535–7543

Fujii, T, Gramajo, H. C, Takano, E, Bibb, M. J. (1996) 'redD and actII-ORF4, pathway-specific regulatory genes for antibiotic production in *Streptomyces coelicolor* A3(2), are transcribed in vitro by an RNA polymerase holoenzyme containing sigma hrdD. *J Bacteriol.* 178(11), pp. 3402-3405.

Galet, J. *et al.* (2015) '*Pseudomonas fluorescens* pirates both ferrioxamine and ferricoelichelin siderophores from *Streptomyces ambofaciens*', *Applied and Environmental Microbiology*, 81(9), pp. 3132–3141.

Galindo-Prieto, B., Eriksson, L. and Trygg, J. (2014) 'Variable influence on projection (VIP) for orthogonal projections to latent structures (OPLS)', *Journal of Chemometrics*. 28(8), pp. 623–632.

Gao, B. and Gupta, R. S. (2012) 'Phylogenetic framework and molecular signatures for the main clades of the phylum Actinobacteria', *Microbiology and Molecular Biology Reviews*. 76(1), pp. 66–112.

Garbeva, P. *et al.* (2014) 'Volatile-mediated interactions between phylogenetically different soil bacteria', *Frontiers in Microbiology*. 5, p. 289.

Gardinassi, L. G. *et al.* (2017) 'Bioinformatics tools for the interpretation of

metabolomics data', *Current Pharmacology Reports*. 3, pp. 374–383.

Geesink, P. *et al.* (2018) 'Growth promotion and inhibition induced by interactions of groundwater bacteria', *FEMS microbiology ecology*. 9(11), pp. 1–8.

Gehrke, E. J. *et al.* (2019) 'Silencing cryptic specialized metabolism in *Streptomyces* by the nucleoid-associated protein Lsr2', *eLife*. 19(8), p. e47691.

Geier, B. *et al.* (2020) 'Spatial metabolomics of in situ host–microbe interactions at the micrometre scale', *Nature Microbiology*. 5(3), pp. 498–510.

Genilloud, O. (2017) 'Actinomycetes: still a source of novel antibiotics', *Natural Product Reports*. 38(3), pp. 1203–1232.

Genilloud, O. (2018) 'Mining actinomycetes for novel antibiotics in the omics era: Are we ready to exploit this new paradigm?', *Antibiotics*. 7(4), p. 85.

Geurts, B. P. *et al.* (2017) 'Combining ANOVA-PCA with POCHEMON to analyse micro-organism development in a polymicrobial environment', *Analytica Chimica Acta*. 963, pp. 1–16.

Ghoul, M. *et al.* (2016) 'Pyoverdin cheats fail to invade bacterial populations in exponential phase', *Journal of Evolutionary Biology*. 29(9), pp. 1728–1736.

Ghoul, M. and Mitri, S. (2017) 'The ecology and evolution of microbial competition', *Trends in Microbiology*. 24(10), pp. 833–845.

Goettler, W. *et al.* (2007) 'Morphology and ultrastructure of a bacteria cultivation organ: The antennal glands of female European beewolves, *Philanthus triangulum* (*Hymenoptera, Crabronidae*)', *Arthropod Structure and Development*. 36(6), pp. 1–9.

Gonzalez, D. J. *et al.* (2011) 'Microbial competition between *Bacillus subtilis* and *Staphylococcus aureus* monitored by imaging mass spectrometry', *Microbiology*. 157(9), pp. 2485–2492.

Goodfellow, M. and Williams, S. T. (2003) 'Ecology of Actinomycetes', *Annual Review of Microbiology*. 37, pp. 189–216.

Gorke, B., and Jorg, S. (2008), 'Carbon catabolite repression in bacteria: many ways to make the most out of nutrients', *Nature Reviews Microbiology*. 6(8), p. 613.

Govic, Y. *et al.* (2019) 'Non-ribosomal peptide synthetase gene clusters in the human pathogenic fungus *Scedosporium apiospermum*', *Frontiers in Microbiology*. 10, p.

2062.

Greule, A., Izoré, T., Iftime, D. *et al*. (2019), 'Kistamicin biosynthesis reveals the biosynthetic requirements for production of highly crosslinked glycopeptide antibiotics', *Nat Commun*. 10, p. 2613.

Griffith, R. S. (1981) 'Introduction to vancomycin', *Reviews of Infectious Diseases*. 3(200), p. 4.

Grim, C. M., Luu, G. T. and Sanchez, L. M. (2019) 'Staring into the void: demystifying microbial metabolomics', *FEMS Microbiology Letters*. 366(11), p. 135.

Gubbens, J., Janus, M., Florea, B. I., Overkleeft, H. S. and van Wezel G. P. (2016) 'Identification of glucose kinase-dependent and -independent pathways for carbon control of primary metabolism, development and antibiotic production in *Streptomyces coelicolor* by quantitative proteomics', *Mol Microbiol*. 86, pp. 1490–1507.

Guillonneau, R. *et al.* (2018) 'Multispecies biofilm development of marine bacteria implies complex relationships through competition and synergy and modification of matrix components', *Frontiers in Microbiology*. 9, p. 1960.

Guo, H. *et al.* (2017) 'Isolation, biosynthesis and chemical modifications of Rubterolones A-F: rare tropolone alkaloids from *Actinomadura* sp. 5-2', *Chemistry - A European Journal*. 23(39), pp. 9338–9345.

Hair, J. F. *et al.* (2017) *Multivariate Data Analysis: Seventh Edition*. *Prentice Hall*. Pearson education.

Hamed, R. B., J. Ruben, G. C., Luc, H., Christian, D., Michael A. M., and Christopher, J. S. (2013), 'TheeEnzymes of β-Lactam biosynthesis', *Natural Product Reports*. 30(1), pp. 21–107.

Harcombe, W. R., Jeremy, M. Chacón, E. M., Adamowicz, L. M., and Christopher, J. M. (2018) 'Evolution of bidirectional costly mutualism from byproduct consumption' *Proceedings of the National Academy of Sciences of the United States of America.* 115 (47), pp. 12000–12004.

Hay, M. *et al.* (2014) 'Clinical development success rates for investigational drugs', *Nature Biotechnology*. 32(1), pp. 40–51.

Helfrich, E. J. N. *et al.* (2019) 'Bacterial terpene biosynthesis: Challenges and opportunities for pathway engineering', *Beilstein Journal of Organic Chemistry*. 15, p.

2889–2906.

Henke, M. T. and Kelleher, N. L. (2016) ‘Modern mass spectrometry for synthetic biology and structure-based discovery of natural products’, *Natural Product Reports*. 33(8), pp. 942–50.

Hertweck, C. *et al.* (2007) ‘Type II polyketide synthases: Gaining a deeper insight into enzymatic teamwork’, *Natural Product Reports*. 24(1), pp. 162–190.

Van Der Heul, H. U. *et al.* (2018) ‘Regulation of antibiotic production in Actinobacteria: new perspectives from the post-genomic era’, *Natural Product Reports*. 35(6), pp. 575–604.

Hibbing, M. E. *et al.* (2010) ‘Bacterial competition: Surviving and thriving in the microbial jungle’, *Nature Reviews Microbiology*. 8, pp. 15–25.

Hiscox, J. *et al.* (2017) ‘Threesomes destabilise certain relationships: multispecies interactions between wood decay fungi in natural resources’, *FEMS microbiology ecology*. 93(3), pp. 1-11.

Ho, Y. N., Shu, L. J. and Yang, Y. L. (2017) ‘Imaging mass spectrometry for metabolites: technical progress, multimodal imaging, and biological interactions’, *Wiley Interdisciplinary Reviews: Systems Biology and Medicine*. 9(5), p. 1387.

Högberg, L. D., Heddini, A. and Cars, O. (2010) ‘The global need for effective antibiotics: Challenges and recent advances’, *Trends in Pharmacological Sciences*. 31(11), pp. 509–15.

Horinouchi, S., and Beppu, T. (2007) 'Hormonal control by A-factor of morphological development and secondary metabolism in *Streptomyces'*, *Proc Jpn Acad Ser B Phys Biol Sci*. 83(9-10), pp. 277-95.

Hoshino, S. *et al.* (2017) ‘Mycolic acid containing bacterium stimulates tandem cyclization of polyene macrolactam in a lake sediment derived rare Actinomycete’, *Organic Letters*. 19(18), pp. 4992–4995.

Hunt, A. C. *et al.* (2005) ‘The bldC developmental locus of *Streptomyces coelicolor* encodes a member of a family of small DNA-binding proteins related to the DNA-binding domains of the MerR family’, *Journal of Bacteriology*. 187(2), pp. 716–28.

Ievlev, A. V. *et al.* (2017) ‘Automated interpretation and extraction of topographic information from time of flight secondary ion mass spectrometry data’, *Scientific*

Reports. 7(1), pp. 1–7.

Ievlev, A. V. *et al.* (2018) 'Nanoscale electrochemical phenomena of polarization switching in ferroelectrics', *ACS Applied Materials and Interfaces*. 10(44), pp. 38217–38222.

Ishizuka, H., Horinouchi, S., Kieser, H. M., Hopwood, D. A., Beppu, T. (1992) 'A putative 2-component regulatory system involved in secondary metabolism in *Streptomyces* spp', *J Bacteriol.* 174, pp. 7585–7594.

Jacob, J. *et al.* (2017) 'Enhanced antibacterial metabolite production through the application of statistical methodologies by a Streptomyces nogalater NIIST A30 isolated from Western Ghats forest soil', *PLOS ONE*. 12(4), p. e0175919.

Jiménez, C. (2018) 'Marine Natural Products in medicinal chemistry', *ACS Medicinal Chemistry Letters*. 9(10), pp. 959–961.

Jomori, T. *et al.* (2020) '*Mycobacterium smegmatis* alters the production of secondary metabolites by marine-derived *Aspergillus niger*', *Journal of Natural Medicines*. 74(1), pp. 76–82.

Justice, N. B. *et al.* (2017) 'Environmental selection, dispersal, and organism interactions shape community assembly in high-throughput enrichment culturing', *Applied and Environmental Microbiology*. 83(20), pp. 01253–01317.

Kang, D. *et al.* (2013) 'Culture condition-dependent metabolite profiling of Aspergillus fumigatus with antifungal activity', *Fungal Biology*. 117(3), pp. 211–219.

Katz, L. and Baltz, R. H. (2016) 'Natural product discovery: past, present, and future', *Journal of Industrial Microbiology {&} Biotechnology*, 43(2), pp. 155–176.

Kawai, S., Mukai, T., Mori, S., Mikami, B., and Murata, K. (2005) 'Hypothesis: structures, evolution, and ancestor of glucose kinases in the hexokinase family', *J Biosci Bioeng.* 99, pp. 320–330.

Kealey, C., Creaven, C. A., Murphy, C. D., Brady, C. B. (2017) 'New approaches to antibiotic discovery', *Biotechnol Lett*. 39(6), pp. 805-817.

Kellogg, J. and Kang, S. (2020) 'Metabolomics, an essential tool in exploring and harnessing microbial chemical ecology', *Phytobiomes Journal*. 4(3), pp. 2471–2906.

Kersten, R. D. *et al.* (2013) 'Bioactivity-guided genome mining reveals the Lomaiviticin

biosynthetic gene cluster in *Salinispora tropica*', *ChemBioChem*. 14(8), pp. 955–62.

Ketola, T., Saarinen, K. and Lindström, L. (2017) 'Propagule pressure increase and phylogenetic diversity decrease community's susceptibility to invasion', *BMC Ecology*. 17(1), p. 15.

Khalil, Z. G. *et al.* (2019) 'Inter-Kingdom beach warfare: Microbial chemical communication activates natural chemical defences', *The ISME Journal*. 13(1), pp. 147–158.

Khan, N. *et al.* (2018) 'Phenotypic responses to interspecies competition and commensalism in a naturally-derived microbial co-culture', *Scientific Reports*. 8(1), pp. 1–9.

Kildgaard, S. *et al.* (2017) 'A dereplication and bioguided discovery approach to reveal new compounds from a marine-derived fungus *Stilbella fimetaria*', *Marine Drugs*. 15(8), p. 253.´

Kim, E. S., Hong, H. J., Choi, C. Y., & Cohen, S. N. (2001), 'Modulation of actinorhodin biosynthesis in *Streptomyces lividans* by glucose repression of *afsR2* gene transcription'. *Journal of bacteriology*. 183(7), pp. 2198–2203.

Kim, H. W. *et al.* (2019) 'Exploring novel secondary metabolites from natural products using pre-processed mass spectral data', *Scientific Reports*. 9(1), p. 17430.

Kinkel, L. L. *et al.* (2014) 'Sympatric inhibition and niche differentiation suggest alternative coevolutionary trajectories among Streptomycetes', *ISME Journal*, 8(2), pp. 249–256.

Koe, B. K., Sobin, B. A. and Celmer, W. D. (1956) 'PA 132, a new antibiotic. I. Isolation and chemical properties.', *Antibiotics annual*. 1957, pp. 672–675.

Kong, W. *et al.* (2018) 'Designing microbial consortia with defined social interactions', *Nature Chemical Biology*. 14, pp. 821–829.

Krause, K. M., Alisa W. S., Timothy R. K., and Lynn E. C. (2016) 'Aminoglycosides: An Overview', *Cold Spring Harbor Perspectives in Medicine*. 6(6), p. 027029.

Kroiss, J. *et al.* (2010) 'Symbiotic streptomycetes provide antibiotic combination prophylaxis for wasp offspring', *Nature Chemical Biology*. 6(4), pp. 261–263.

Kronheim, S., Daniel-Ivad, M., Duan, Z. *et al.* (2018), 'A chemical defence against

phage infection', *Nature.* 564, 283–286.

Kudo, F., and Tadashi E. (2016), 'Aminoglycoside antibiotics: new insights into the biosynthetic machinery of old drugs', *Chemical Record*. 16(1), pp. 4–18.

Kuhlisch, C. and Pohnert, G. (2015) 'Metabolomics in chemical ecology', *Natural Product Reports*. 32(7), pp. 937–955.

Kwakman, J. H., Postma, P. W., (1994) 'Glucose kinase has a regulatory role in carbon catabolite repression in *Streptomyces coelicolor*. *J Bacteriol*. 176(9), pp. 2694–2698.

Lane, D. J. (1991) '16S/23S rRNA Sequencing', *in bacterial systematics*. John Wiley and Sons, New York.

Lawlor, E. J., Baylis, H. A. and Chater, K. F. (1987) 'Pleiotropic morphological and antibiotic deficiencies result from mutations in a gene encoding a tRNA-like product in *Streptomyces coelicolor* A3(2).', *Genes & development*. 1(10), pp. 1305–10.

Lee, D., Bowen, B. and Northen, T. (2010) 'Mass spectrometry–based metabolomics, analysis of metabolite-protein interactions, and imaging', *BioTechniques*, 49(2), pp. 557–565.

Lee, J. L. S. *et al.* (2012) 'Topography and field effects in secondary ion mass spectrometry Part II: Insulating samples', *Surface and Interface Analysis*. 22(10), pp. 1718–1728.

Lee, N. *et al.* (2020) 'Iron competition triggers antibiotic biosynthesis in *Streptomyces coelicolor* during coculture with *Myxococcus xanthus*', *ISME Journal*. 14(5), pp. 1111–1124.

Lee, Y. C. *et al.* (2020) 'Prevalence of fosfomycin resistance and gene mutations in clinical isolates of methicillin-resistant *Staphylococcus aureus*', *Antimicrobial Resistance and Infection Control*. 9(1), p. 135.

Li, B. *et al.* (2018) 'A versatile strategy for characterization and imaging of drip flow microbial biofilms'. 90(11), pp. 6725–6734.

Li, B. and Webster, T. J. (2018) 'Bacteria antibiotic resistance: New challenges and opportunities for implant-associated orthopedic infections', *Journal of Orthopaedic Research*. 36(1), pp. 22–32.

Liang, L. *et al.* (2019) ‘Discovery of a new natural product and a deactivation of a quorum sensing system by culturing a “Producer” bacterium with a heat-killed “Inducer” culture’, *Frontiers in Microbiology*. 9, p. 3351.

Lichman, B. R. (2020) ‘The scaffold-forming steps of plant alkaloid biosynthesis’, *Natural Product Reports*. 38(1), pp. 103–129.

Lim, Y. *et al.* (2018) ‘Non-targeted metabolomics unravels a media-dependent prodiginines production pathway in *Streptomyces coelicolor* A3(2)’, *PLOS ONE*. 13(11), p. e0207541.

Liu, G., Chater, K. F., Chandra, G., Niu, G., and Tan, H. (2013) 'Molecular regulation of antibiotic biosynthesis in *Streptomyces'*, *Microbiol. Mol. Biol. Rev.* 77, pp. 112–143.

Liu, L., Cheng, Y., Lyu, M. *et al*. (2019) 'AveI, an AtrA homolog of *Streptomyces avermitilis*, controls avermectin and oligomycin production, melanogenesis, and morphological differentiation', *Appl Microbiol Biotechnol*. 103, pp. 8459–8472.

Liu, A. *et al.* (2017) ‘Growth-altering microbial interactions are responsive to chemical context’, *PLOS ONE*. 12(3), p. e0164919.

Logue, J. B., Findlay, S. E. G. and Comte, J. (2015) ‘Editorial: Microbial responses to environmental changes’, *Frontiers in Microbiology*. 6, p.1364.

López-Agudelo, V. A., Gómez-Ríos, D. and Ramirez-Malule, H. (2021) ‘Clavulanic acid production by *Streptomyces clavuligerus*: Insights from systems biology, strain engineering, and downstream processing’, *Antibiotics*. 10(1), p. 84.

Lories, B. *et al.* (2020) ‘Biofilm bacteria use stress responses to detect and respond to competitors’, *Current Biology*. 30, pp. 1231–1244.

Lu, F., Hou, Y., Zhang, H. *et al.* (2017) 'Regulatory genes and their roles for improvement of antibiotic biosynthesis in *Streptomyces*. *Biotech.* 3(7), p. 250.

Ludwig, W. *et al.* (2012) ‘Road map of the phylum Actinobacteria’, in *Bergey’s Manual of Systematic Bacteriology*. New York : Springer.

Luján, A. M., Gómez, P. and Buckling, A. (2015) ‘Siderophore cooperation of the bacterium *Pseudomonas fluorescens* in soil’, *Biology Letters*. 11(2), p. 20140934.

Ma, Y. J., Zheng, L. P. and Wang, J. W. (2019) ‘Inducing perylenequinone production from a bambusicolous fungus *Shiraia* sp. S9 through co-culture with a fruiting body-

associated bacterium *Pseudomonas fulva* SB1', *Microbial Cell Factories*. 18(1), p. 121.

Maglangit, F. *et al.* (2020) 'A co-culturing approach enables discovery and biosynthesis of a bioactive indole alkaloid metabolite', *Molecules*. 25(2), p. 256.

Manhart, M. and Shakhnovich, E. I. (2018) 'Growth tradeoffs produce complex microbial communities on a single limiting resource', *Nature Communications*. 9(1), pp. 1–9.

Manteca, Á. and Yagüe, P. (2018) '*Streptomyces* differentiation in liquid cultures as a trigger of secondary metabolism', *Antibiotics*. 7(2), p. 41.

Manyi-Loh, C. *et al.* (2018) 'Antibiotic use in agriculture and its consequential resistance in environmental sources: Potential public health implications', *Molecules*. 23(4), p. 795.

Marmann, A. *et al.* (2014) 'Co-cultivation - a powerful emerging tool for enhancing the chemical diversity of microorganisms', *Marine Drugs*. 12(2), pp. 1043–1065.

Maroniche, G. A. *et al.* (2017) 'Molecular identification of *Azospirillum* spp.: Limitations of 16S rRNA and qualities of rpoD as genetic markers', *Microbiological Research*. 195, pp. 1–10.

Martínez-Buitrago, P. A., Ramos, F. A. and Castellanos, L. (2019) 'Binary co-culture selection from marine-derived microorganisms for differential production of specialized metabolites', *Quimica Nova*. 42(7), pp. 713–719.

Martínez-Núñez, M. A. and López, V. E. L. y (2016) 'Nonribosomal peptides synthetases and their applications in industry', *Sustainable Chemical Processes*. 4(13), pp. 2–8.

Mayfield, M. M. and Stouffer, D. B. (2017) 'Higher-order interactions capture unexplained complexity in diverse communities', *Nature Ecology and Evolution*. 1(3), pp. 1–7.

McCormick, J. R. and Flärdh, K. (2012) 'Signals and regulators that govern *Streptomyces* development', *FEMS Microbiology Reviews*. 36(1), pp. 206–231.

McDowall, K. J., Thamchaipenet, A., Hunter IS. Phosphate control of oxytetracycline production by *Streptomyces rimosus* is at the level of transcription from promoters overlapped by tandem repeats similar to those of the DNA-binding sites of the OmpR

family. J Bacteriol. 1999 May;181(10):3025-32.

McDonald, L. A., Barbieri, L. R., Carter, G. T., Lenoy, E., Lotvin, J., Petersen, P. J., Siegel M. M., Singh, G. and Williamson, R. T. (2002) 'Structures of the muraymycins, novel peptidoglycan biosynthesis inhibitors', *J Am Chem Soc*. 124(35), pp. 10260–10261.

Mcguire, J. M. *et al.* (1952) 'Ilotycin, a new antibiotic', *Antibiotics & chemotherapy*. 2(6), pp. 281–3.

Mee, M. T. *et al.* (2014) 'Syntrophic exchange in synthetic microbial communities', *Proceedings of the National Academy of Sciences of the United States of America*. 111(20), pp. 2149–2156.

Van Der Meij, A. *et al.* (2017) 'Chemical ecology of antibiotic production by Actinobacteria', *FEMS Microbiology Reviews*. 41(3), pp. 392–416.

Meng, L.-H. *et al.* (2020) 'Chermebilaenes A and B, new bioactive meroterpenoids from co-cultures of marine-derived isolates of *Penicillium bilaiae* MA-267 and *Penicillium chermesinum* EN-480', *Marine Drugs*. 18(7), p. 339.

Merrick, M. J. (1976) 'A morphological and genetic mapping study of bald colony mutants of *Streptomyces coelicolor*', *Journal of General Microbiology*. 96(2), pp. 299–315.

Michelsen, C. F. *et al.* (2016) 'Evolution of metabolic divergence in *P. aeruginosa* during long-term infection facilitates a proto-cooperative interspecies interaction', *ISME Journal*. 10(6), pp. 1330–1336.

Miller, B. R. and Gulick, A. M. (2016) 'Structural biology of nonribosomal peptide synthetases', *Methods in Molecular Biology*. 1401, 3–29.

Milne, S. B. *et al.* (2013) 'Sum of the parts: Mass spectrometry-based metabolomics', *Biochemistry*, 52(22), pp. 3829–3840.

Mindlin, S. Z. and Petrova, M. A. (2017) 'On the origin and distribution of antibiotic resistance: permafrost bacteria studies', *Molecular Genetics, Microbiology and Virology*. 32, pp. 169–179.

Mogollón, N. G. S. *et al.* (2018) 'Comprehensive two-dimensional gas chromatography-mass spectrometry combined with multivariate data analysis for pattern recognition in Ecuadorian spirits', *Chemistry Central Journal*. 12(1). p. 102.

Mohimani, H. *et al.* (2018) ‘Dereplication of microbial metabolites through database search of mass spectra’, *Nature Communications*. 9(1), p. 4035.

Molina-Santiago, C. *et al.* (2019) ‘The extracellular matrix protects *Bacillus subtilis* colonies from *Pseudomonas* invasion and modulates plant co-colonization’, *Nature Communications*. 10(1), p. 1919.

Momeni, B., Xie, L. and Shou, W. (2017) ‘Lotka-Volterra pairwise modeling fails to capture diverse pairwise microbial interactions’, *eLife*. 6, p. 25051.

Montalbán-López, M. *et al.* (2020) ‘New developments in RiPP discovery, enzymology and engineering’, *Natural Product Reports*. 38(1), pp. 130–239.

Morris, B. E., Henneberger, R., Huber, H., and Moissl-Eichinger, C. (2013) 'Microbial syntrophy: interaction for the common good', *FEMS Microbiol*. 37, 384–406.

Moussa, M. *et al.* (2019) ‘Co-culture of the fungus *Fusarium tricinctum* with *Streptomyces lividans* induces production of cryptic naphthoquinone dimers’, *RSC Advances*. 9(3), pp. 1491–1500.

Moutinho, T. J. *et al.* (2017) ‘Novel co-culture plate enables growth dynamic-based assessment of contact-independent microbial interactions’, *PLoS ONE*. 12(8), p. e0182163.

Nah, H.-J. *et al.* (2017) ‘Cloning and heterologous expression of a large-sized natural product biosynthetic gene cluster in *Streptomyces* species’, *Frontiers in Microbiology*, 8, p. 394.

Nai, C. and Meyer, V. (2018) ‘From axenic to mixed cultures: technological advances accelerating a paradigm shift in microbiology’, *Trends in Microbiology*. 26(6), pp. 538–554.

Navarro-Muñoz, J. C. *et al.* (2020) ‘A computational framework to explore large-scale biosynthetic diversity’, *Nature Chemical Biology*. 16(1), pp. 60–68.

Nett, M., Ikeda, H. and Moore, B. S. (2009) ‘Genomic basis for natural product biosynthetic diversity in the actinomycetes’, *Natural Product Reports*. 26(11), pp. 1362–1384.

Newman, D. J. and Cragg, G. M. (2020) ‘Natural Products as Sources of New Drugs over the Nearly Four Decades from 01/1981 to 09/2019’, *Journal of Natural Products*. 83(3), pp. 770–803.

Nicolitch, O. *et al.* (2019) ‘A microcosm approach highlights the response of soil mineral weathering bacterial communities to an increase of K and Mg availability’, *Scientific Reports*. 9(1), pp. 1–13.

Niu, G., Chater, K. F., Tian, Y., Zhang, J., and Tan, H. (2016) 'Specialised metabolites regulating antibiotic biosynthesis in *Streptomyces* spp', *FEMS Microbiol*. 40, pp. 554–573.

Noble, R. L., Beer, C. T. and Cutts, J. H. (1959) ‘Further biological activities of vincaleukoblastine-an alkaloid isolated from *Vinca rosea* (L.)’, *Biochemical Pharmacology*. 20, 1023–1031.

Nottingham, A. T. *et al.* (2018) ‘Nutrient limitations to bacterial and fungal growth during cellulose decomposition in tropical forest soils’, *Biology and Fertility of Soils*. 54(2), pp. 219–228.

Nouioui, I., Lorena, C., Marina G. L., Jan P. M. K., Tanja W., Nikos C. K., Rüdiger P., Hans P. K., Michael G. and Markus G. (2018). 'Genome-based taxonomic classification of the phylum Actinobacteria.” *Frontiers in Microbiology*. 9.

Nudrat-Hazarika, Shabiha Thakur, D. (2020) ‘*Actinobacteria*’. *In Beneficial Microbes in Agro-Ecology, Bacteria and Fungi.* Academic press.

Núñez-Montero, K. and Barrientos, L. (2018) ‘Advances in antarctic research for antimicrobial discovery: A comprehensive narrative review of bacteria from antarctic environments as potential sources of novel antibiotic compounds against human pathogens and microorganisms of industrial importance’, *Antibiotics*. 7(4), p. 90.

Nuñez, J. *et al.* (2017) ‘NanoSIMS for biological applications: Current practices and analyses’, *Biointerphases*. 13(3), p. 03B301.

O’Neill, J. (2014) ‘Antimicrobial Resistance : Tackling a crisis for the health and wealth of nations’, *Review on Antimicrobial Resistance*, pp. 1–16.

Ogawa, Y. and Yonehara, H. (1969) ‘The structure of pentalenolactone (PA-132)Setsuo Takeuchi’, *Tetrahedron Letters*. 10(32), pp. 2737–2740.

Oh, D. C. *et al.* (2005) ‘Libertellenones A-D: Induction of cytotoxic diterpenoid biosynthesis by marine microbial competition’, *Bioorganic and Medicinal Chemistry*. 13(17), pp. 5267–5273.

Ola, A. R. B. *et al.* (2013) ‘Inducing secondary metabolite production by the

endophytic fungus *Fusarium tricinctum* through coculture with *Bacillus subtilis*', *Journal of Natural Products*. 76(11), pp. 2094–2099.

Pan, R. *et al.* (2019) 'Exploring structural diversity of microbe secondary metabolites using OSMAC strategy: A literature review', *Frontiers in Microbiology*. 10, p. 294.

Pandey, N, and M Cascella (2021) 'Beta Lactam Antibiotics' In StatPearls; Treasure Island, StatPearls Publishing.

Paquette, S. J. and Reuter, T. (2020) 'Properties of an antimicrobial molecule produced by an *Escherichia coli* champion', *Antibiotics*. 9(1), p. 6.

Parrot, D. *et al.* (2018) 'Imaging the unimaginable: Desorption electrospray ionisation - Imaging Mass Spectrometry (DESI-IMS) in Natural Product research', *Planta Medica*. 84(9-10), pp. 584–593.

Patin, N. V. *et al.* (2017) 'Effects of actinomycete secondary metabolites on sediment microbial communities', *Applied and Environmental Microbiology*. 83(4), pp. 02676-02716.

Patin, N. V. *et al.* (2018) 'The role of inter-species interactions in *Salinispora* specialized metabolism', *Microbiology.* 164(7), pp. 946–955.

Patin, N. V *et al.* (2016) 'Competitive strategies differentiate closely related species of marine actinobacteria', *The ISME Journal*. 10(2), pp. 478–490.

Perault, A. I. and Cottera, P. A. (2018) 'Three distinct contact-dependent growth inhibition systems mediate interbacterial competition by the cystic fibrosis pathogen burkholderia dolosa', *Journal of Bacteriology*. 200(22), p. e00428.

Pérez, J. *et al.* (2011) '*Myxococcus xanthus* induces actinorhodin overproduction and aerial mycelium formation by *Streptomyces coelicolor*', *Microbial Biotechnology*, 4(2), pp. 175–183.

Petersen, L.-E., Kellermann, M. Y. and Schupp, P. J. (2020) 'Secondary metabolites of marine microbes: from natural products chemistry to chemical ecology', *in YOUMARES 9 - The Oceans: Our Research, Our Future.* Springer International Publishing, pp. 159–180.

Peterson, E. and Kaur, P. (2018) 'Antibiotic resistance mechanisms in bacteria: Relationships between resistance determinants of antibiotic producers, environmental bacteria, and clinical pathogens', *Frontiers in Microbiology*. 9(1), p.

2828.

Petkovic, H., Cullum, J., Hranueli, D., Hunter, I. S., Peric-Concha, N., Pigac, J., Thamchaipenet, A., Vujaklija, D. and Long, P. F. (2006) 'Genetics of *Streptomyces rimosus*, the oxytetracycline producer', *Microbiol Mol Biol Rev*. 70, pp. 704–728.

Pishchany, G. *et al.* (no date) 'Amycomicin is a potent and specific antibiotic discovered with a targeted interaction screen'. *Proc Natl Acad Sci USA*. 115(40), pp. 10124–10129.

Pluskal, T. *et al.* (2010) 'MZmine 2: Modular framework for processing, visualizing, and analyzing mass spectrometry-based molecular profile data', *BMC Bioinformatics*. 11, p. 395.

Purves, K. *et al.* (2016) 'Using molecular networking for microbial secondary metabolite bioprospecting', *Metabolites*. 6(1), p. 2.

Pye, C. R. *et al.* (2017) 'Retrospective analysis of natural products provides insights for future discovery trends', *Proceedings of the National Academy of Sciences of the United States of America*. 114(22), pp. 5601–5606.

Qin, S. *et al.* (2009) 'Isolation, diversity, and antimicrobial activity of rare actinobacteria from medicinal plants of tropical rain forests in *Xishuangbanna China*', *Applied and Environmental Microbiology*. 75(19), pp. 6176–6186.

Quintero, M. *et al.* (2018) 'Bioprospecting from marine coastal sediments of Colombian Caribbean: screening and study of antimicrobial activity', *Journal of Applied Microbiology*. 125(3), pp. 753–765.

Ram, Y. *et al.* (2019) 'Predicting microbial growth in a mixed culture from growth curve data', *Proceedings of the National Academy of Sciences of the United States of America*. 116(29), pp. 14698–14707.

Rashid, N. A. *et al.* (2019) 'Performance of classification analysis: A comparative study between PLS-DA and integrating PCA+LDA', *Mathematics and Statistics*. 7(4), p. 24–28.

Ratzke, C. and Gore, J. (2018) 'Modifying and reacting to the environmental pH can drive bacterial interactions', *PLOS Biology*. 16(3), p. e2004248.

Reddy, G. K. *et al.* (2020) 'Exploring novel bacterial terpene synthases', *PLoS ONE*. 15(4), p. e0232220.

Reis-Mansur, M. C. P. P. *et al.* (2019) ‘Carotenoids from UV-resistant Antarctic *Microbacterium* sp. LEMMJ01’, *Scientific Reports*. 9(1), pp. 1–14.

Ren, D. *et al.* (2015) ‘High prevalence of biofilm synergy among bacterial soil isolates in cocultures indicates bacterial interspecific cooperation’, *ISME Journal*. 9(1), pp. 81–89.

Reverter, M. *et al.* (2018) ‘Metabolome variability for two Mediterranean sponge species of the genus *Haliclona*: specificity, time, and space’, *Metabolomics*. 14(9), pp. 1–12.

Risdian, C., Mozef, T. and Wink, J. (2019) ‘Biosynthesis of polyketides in *Streptomyces*’, *Microorganisms*. 7(5), p. 124.

Robinson, M. (2016) ‘A Dictionary of Biology (7th edition)’, *Reference Reviews.* 30(6), pp. 25–25.

Rodríguez-García, A., Barreiro, C., Santos-Beneit, F., Sola-Landa, A., and Martín, J.F. (2007) 'Genome-wide transcriptomic and proteomic analysis of the primary response to phosphate limitation in *Streptomyces coelicolor* M145 and in a ΔphoP mutant', *Proteomics*. 7, pp. 2410–2429.

Romano, S. *et al.* (2018) ‘Extending the “one strain many compounds” (OSMAC) principle to marine microorganisms’, *Marine Drugs*. 16(7), p. 244.

Romero-Rodríguez, A. *et al.* (2016) ‘Carbon catabolite regulation of secondary metabolite formation and morphological differentiation in *Streptomyces coelicolor*’, *Applied Biochemistry and Biotechnology*. 180(6), pp. 1152–1166.

Romero-Rodríguez, A. *et al*. (2016) 'Transcriptomic analysis of a classical model of carbon catabolite regulation in *Streptomyces coelicolor*', *BMC Microbiology.* 16, p. 77.

Romero-Rodríguez, A. *et al.* (2017) 'Carbon catabolite regulation in *Streptomyces*: New insights and lessons learned', *World Journal of Microbiology and Biotechnology*. 33, p. 162.

Romero-Rodríguez, A. *et al.* (2018) ‘Interplay between carbon, nitrogen and phosphate utilization in the control of secondary metabolite production in *Streptomyces*’, *International Journal of General and Molecular Microbiology*. 111(5), pp. 761–781.

Roullier, C. *et al.* (2016) ‘Time dependency of chemodiversity and biosynthetic

pathways: AnLC-MS metabolomic study of Marine-Sourced *Penicillium*', *Marine Drugs*. 14(5), p. 103.

Ruhe, Z. C., Low, D. A. and Hayes, C. S. (2013) 'Bacterial contact-dependent growth inhibition', *Trends in Microbiology*. 21(5), pp. 230–237.

Russel, J. *et al.* (2017) 'Antagonism correlates with metabolic similarity in diverse bacteria', *Proceedings of the National Academy of Sciences*. 114(40), pp. 10684–

10688.

Rzagalinski, I. and Volmer, D. A. (2017) 'Quantification of low molecular weight compounds by MALDI imaging mass spectrometry – A tutorial review', *Biochimica et Biophysica Acta - Proteins and Proteomics*. 1865(7), pp. 726–739.

Santos-Beneit, F., Rodriguez-Garcia, A., Sola-Landa, A., and Martin, J.F. (2009), 'Cross-talk between two global regulators in *Streptomyces:* PhoP and AfsR interact in the control of afsS, pstS and phoRP transcription'. *Mol Microbiol*. 72, pp. 53–68.

Sathe, S. and Kümmerli, R. (2020) 'Antagonistic interactions subdue inter-species green-beard cooperation in bacteria', *Journal of Evolutionary Biology*. 33(9), pp. 1245–1255.

Schäberle, T. F., Orland, A. and König, G. M. (2014) 'Enhanced production of undecylprodigiosin in *Streptomyces coelicolor* by co-cultivation with the corallopyronin A-producing myxobacterium, *Corallococcus coralloides*', *Biotechnology Letters*. 36(3), pp. 641–648.

Schatz, A., Bugle, E. and Waksman, S. A. (1944) 'Streptomycin, a substance exhibiting antibiotic activity against gram-positive and gram-negative nacteria ', *Experimental Biology and Medicine*. 55(1), pp. 66–69.

Schmidt-Dannert, C. (2015) 'Biosynthesis of terpenoid natural products in fungi', *Advances in Biochemical Engineering/Biotechnology*. 148, 19–61.

Schneider, J. *et al.* (2012) 'Streptomycin-induced expression in *Bacillus subtilis* of YtnP, a lactonase-homologous protein that inhibits development and streptomycin production in *Streptomyces griseus*', *Applied and Environmental Microbiology*. 78(2), pp. 599–603.

Schoenian, I. *et al.* (2011) 'Chemical basis of the synergism and antagonism in microbial communities in the nests of leaf-cutting ants', *Proceedings of the National*

Academy of Sciences. 108(5), pp. 1955–1960.

Schorn, M. A. *et al.* (2016) 'Sequencing rare marine actinomycete genomes reveals high density of unique natural product biosynthetic gene clusters', *Microbiology.* 162(12), pp. 2075–2086.

Schumacher, M. A. *et al.* (2017) 'The *Streptomyces* master regulator BldD binds c-di-GMP sequentially to create a functional BldD2-(c-di-GMP)4 complex', *Nucleic Acids Research*. 45(11), pp. 6923–6933.

Sekurova, O. N., Schneider, O. and Zotchev, S. B. (2019) 'Novel bioactive natural products from bacteria via bioprospecting, genome mining and metabolic engineering', *Microbial Biotechnology*. 12(5), pp. 828–844.

Senges, C. H. R. *et al.* (2018) 'The secreted metabolome of *Streptomyces chartreusis* and implications for bacterial chemistry', *Proceedings of the National Academy of Sciences of the United States of America*. 115(10), pp. 2490–2495.

Serpi, M., Valentina, F. and Fabrizio, P. (2016) 'Nucleoside derived antibiotics to fight microbial drug resistance: New utilities for an established class of drugs?' *Journal of Medicinal Chemistry*. 59(23), pp. 10343–10382.

Serrano, R. *et al.* (2017) 'Co-culturing of fungal strains against *Botrytis cinerea* as a model for the induction of chemical diversity and therapeutic agents', *Frontiers in Microbiology*. 8, p. 649.

Seyedsayamdost, M. R. *et al.* (2011) 'Structure and biosynthesis of amychelin, an unusual mixed-ligand siderophore from *Amycolatopsis* sp. AA4', *Journal of the American Chemical Society*. 133(30), pp. 11434–11437.

Shi, Y. *et al.* (2017) 'Synthetic multispecies microbial communities reveals shifts in secondary metabolism and facilitates cryptic natural product discovery', *Environmental Microbiology*. 19(9), pp. 3606–3618.

Shimizu, Y., Ogata, H. and Goto, S. (2017) 'Type III Polyketide Synthases: Functional Classification and Phylogenomics', *ChemBioChem*. 18(1), pp. 50–65.

Shin, D. *et al.* (2018) 'Coculture of marine *Streptomyces* sp. with *Bacillus* sp. produces a new piperazic acid-bearing cyclic peptide', *Frontiers in Chemistry*. 6(1), p. 498.

Shiraishi, T. and Kuzuyama, T. (2019) 'Recent advances in the biosynthesis of nucleoside antibiotics', *J Antibiot.* 72, pp. 913–923.

Shirling, E. B. and Gottlieb, D. (1966) 'Methods for characterizing *Streptomyces*', *International Journal*. 16(3), pp. 313–340.

Si, T. *et al.* (2016) 'Characterization of *Bacillus subtilis* colony biofilms via mass spectrometry and fluorescence imaging', *Journal of Proteome Research*. 15(6), pp.

1955–1962.

Sjövall, P. and Lausmaa, J. (2011) 'ToF-SIMS', In: Reitner J., Thiel V. (eds) *Encyclopedia of Geobiology. Encyclopedia of Earth Sciences Series.*

Smith, Jeff and Velicer, G. J. (2019) 'Facultative social exploitation among *Myxoccocus* bacteria due to non-responsive local competition', *bioRxiv*, p. 833517.

Smith, N. W., Paul, R. S., Altermann, E., Roy, N. C., and Warren, C. M. (2019) 'The classification and evolution of bacterial cross-feeding', *Frontiers in Ecology and Evolution*. 7, p. 153.

Socio, G. V. *et al.* (2019) 'Measurement and prediction of antimicrobial resistance in bloodstream infections by ESKAPE pathogens and Escherichia coli', *Journal of Global Antimicrobial Resistance*. 19, pp. 154–160.

Soldatou, S. *et al.* (2021) 'Comparative metabologenomics analysis of polar Actinomycetes', *Marine Drugs*. 19(2), p. 103.

Som, N. F. *et al.* (2017) 'The MtrAB two-component system controls antibiotic production in streptomyces coelicolor A3(2)', *Microbiology*. 163(10), pp. 1415–1419.

Sorokina, M. and Steinbeck, C. (2020) 'Review on natural products databases: Where to find data in 2020', *Journal of Cheminformatics*. 12(1), p. 20.

Sousa, J. *et al.* (2020) 'Bayesian multiple hypotheses testing in compositional analysis of untargeted metabolomic data', *Analytica Chimica Acta*. 1097(1), pp. 49-61.

Spraker, J. E. *et al.* (2018) 'Conserved responses in a war of small molecules between a plant-pathogenic bacterium and fungi', *mBio*. 9(3), p. e00820.

Spraker, J. E., Luu, G. T. and Sanchez, L. M. (2020) 'Imaging mass spectrometry for natural products discovery: A review of ionization methods', *Natural Product Reports*. 37(2), pp. 150–162.

Straight, P. D., Willey, J. M. and Kolter, R. (2006) 'Interactions between *Streptomyces coelicolor a*nd *Bacillus subtilis:* Role of surfactants in raising aerial structures', *Journal*

of Bacteriology, 188(13), pp. 4918–4925.

Stubbendieck, R. M. *et al.* (2019) 'Competition among nasal bacteria suggests a role for siderophore-mediated interactions in shaping the human nasal microbiota', *Applied and Environmental Microbiology*. 85(10), pp. 02406–02418.

Stubbendieck, R. M. and Straight, P. D. (2016) 'Multifaceted interfaces of bacterial competition', *Journal of Bacteriology*, 198(16), pp. 2145–2155.

Su, T. L. (1948) 'Micrococcin, an antibacterial substance formed by a strain of *Micrococcus*', *British journal of experimental pathology*. 29(5), pp. 473–481.

Subramani, R. and Sipkema, D. (2019) 'Marine rare actinomycetes: A promising source of structurally diverse and unique novel natural products', *Marine Drugs*. 17(5), p. 249.

Süssmuth, R. D. and Mainz, A. (2017) 'Nonribosomal Peptide Synthesis—Principles and Prospects', *Angewandte Chemie - International Edition*. 56(14), pp. 3770–3821.

Świątek, M., Tenconi, E., Rigali, S. and Van Wezel, P. G. (2012) 'Functional analysis of the N-acetylglucosamine metabolic genes of *Streptomyces coelicolor* and role in control of development and antibiotic production', *Journal of Bacteriology.* 194(5), pp. 1136–1144.

Takahashi, Y. and Nakashima, T. (2018) 'Actinomycetes, an inexhaustible source of naturally occurring antibiotics', *Antibiotics*. 7(2), p. 45.

Tahlan, K. and Susan E. J. (2013) 'Origins of the β-Lactam rings in Natural Products' *Journal of Antibiotics.* 66, pp. 401–410.

Teasdale, M. E. *et al.* (2009) 'Secondary metabolites produced by the marine bacterium *Halobacillus salinus* that Inhibit quorum sensing-controlled phenotypes in gram-negative bacteria', *Applied and Environmental Microbiology*. 75(3), pp. 567–72.

Tenconi, E. *et al.* (2018) 'Production of prodiginines is part of a programmed cell death process in *Streptomyces coelicolor*', *Frontiers in Microbiology*. 9(1), p. 1742.

Tenconi, E. *et al.* (2020) 'Prodiginines postpone the onset of sporulation in *Streptomyces coelicolor'*, *Antibiotics*. 9(12), p. 847.

Thissera, B. *et al.* (2020) 'Induction of cryptic antifungal pulicatin derivatives from *Pantoea agglomerans* by microbial co-culture', *Biomolecules*. 10(2), p. 268.

Tillotson, R. D. *et al.* (1998) 'A surface active protein involved in aerial hyphae formation in the filamentous fungus *Schizophillum commune* restores the capacity of a bald mutant of the filamentous bacterium *Streptomyces coelicolor* to erect aerial structures', *Molecular Microbiology*. 30(3), pp. 595–602.

Tomm, H. A., Ucciferri, L. and Ross, A. C. (2019) 'Advances in microbial culturing conditions to activate silent biosynthetic gene clusters for novel metabolite production', *Journal of Industrial Microbiology and Biotechnology*. 46(9-10), pp. 1381–1400.

Travin, D. Y., Bikmetov, D. and Severinov, K. (2020) 'Translation-Targeting RiPPs and Where to Find Them', *Frontiers in Genetics*. 11, p. 226.

Traxler, M. F. *et al.* (2012) 'Interspecies modulation of bacterial development through iron competition and siderophore piracy', *Molecular Microbiology*. 86(3), pp. 628–644.

Traxler, M. F. and Kolter, R. (2015) 'Natural products in soil microbe interactions and evolution', *Natural Product Reports*. 32(7), pp. 956–970.

Trivella, D. B. B. and de Felicio, R. (2018) 'The tripod for bacterial Natural Product discovery: genome mining, silent pathway induction, and mass spectrometry-based molecular networking', *mSystems*. A3(2), p. e00160.

Tschowri, N. *et al.* (2014) 'Tetrameric c-di-GMP mediates effective transcription factor dimerization to control *Streptomyces* development', *Cell.* 158(5), pp. 1136–1147.

Tshikantwa, T. S. *et al.* (2018) 'Current trends and potential applications of microbial interactions for human welfare', *Frontiers in Microbiology*. 9(1), p. 1156.

Tyc, O. *et al.* (2014) 'Impact of interspecific interactions on antimicrobial activity among soil bacteria', *Frontiers in Microbiology*. 5(1), p. 567.

Tyc, O., de Jager, V. C. L., *et al.* (2017) 'Exploring bacterial interspecific interactions for discovery of novel antimicrobial compounds', *Microbial Biotechnology*. 10(4), pp. 910–925.

Tyc, O., Song, C., *et al.* (2017) 'The Ecological Role of Volatile and Soluble Secondary Metabolites Produced by Soil Bacteria', *Trends in Microbiology*. 25(4), pp. 280–292.

Tyurin, A., Alferova, V. and Korshun, V. (2018) 'Chemical Elicitors of Antibiotic Biosynthesis in Actinomycetes', *Microorganisms*. 6(2), p. 52.

Udwary, D. W. *et al.* (2007) ‘Genome sequencing reveals complex secondary metabolome in the marine actinomycete *Salinispora tropica*’, *Proceedings of the National Academy of Sciences of the United States of America*. (25), pp. 10376–81.

Umezawa, H. (1958) 'Kanamycin: its discovery', *Annals of the New York Academy of Sciences*. 76(2), pp. 20-26.

Vaidyanathan, S. *et al.* (2008) ‘TOF-SIMS investigation of *Streptomyces coelicolor*, a mycelial bacterium’, *Applied Surface Science*. 225(4), pp. 922–925.

Ventura, M. *et al.* (2007) ‘Genomics of Actinobacteria: tracing the evolutionary history of an ancient phylum’, *Microbiology and Molecular Biology Reviews*. 71(3), pp. 495–548.

Venturelli, O. S. *et al.* (2018) ‘Deciphering microbial interactions in synthetic human gut microbiome communities’, *Molecular Systems Biology*. 14(6), p. e8157.

Vetsigian, K., Jajoo, R. and Kishony, R. (2011) ‘Structure and evolution of *Streptomyces* interaction networks in soil and in silico’, *PLoS Biology*, 9(10), p. 1001184.

Vickerman, J. C. (2009) ‘Molecular Surface Mass Spectrometry by SIMS’, in *Surface Analysis - The Principal Techniques: Second Edition*. Wiley.

Vignolle, G. A. *et al.* (2020) ‘Novel approach in whole genome mining and transcriptome analysis reveal conserved RiPPs in *Trichoderma* spp’, *BMC genomics.* 21(1), p. 258.

De Vijlder, T. *et al.* (2018) ‘A tutorial in small molecule identification via electrospray ionization-mass spectrometry: The practical art of structural elucidation’, *Mass Spectrometry Reviews*. 37(5), pp. 607–629.

Wakefield, J. *et al.* (2017) ‘Dual induction of new microbial secondary metabolites by fungal bacterial co-cultivation’, *Frontiers in Microbiology*. 8, p. 1284.

Waksman, S. and Lecehevalier, H. (1949) 'Neomycin, a new antibiotic active against streptomycin resistant bacteria, including tuberculosis organisms', *Science*. 109(2830), pp. 305–307.

Wang, J. *et al.* (2020) ‘Biosynthesis of aromatic polyketides in microorganisms using type II polyketide synthases’, *Microbial Cell Factories*. 19(1), p. 110.

Wang, M. *et al.* (2016) ‘Sharing and community curation of mass spectrometry data with Global Natural Products Social Molecular Networking’, *Nature Biotechnology*. 34(8), pp. 828–837.

Watrous, J. *et al.* (2010) ‘Capturing bacterial metabolic exchange using thin film desorption electrospray ionization-imaging mass spectrometry’, *Analytical Chemistry*. doi: 10.1021/ac9027388.

Watrous, J. D. *et al.* (2013) ‘Microbial metabolic exchange in 3D’, *ISME Journal*. 7(4), pp. 770–780.

Wei, J., He, L., and Niu, G. (2018) 'Regulation of antibiotic biosynthesis in actinomycetes: perspectives and challenges', *Synth. Syst. Biotechnol.* 3, oo. 229–235.

Weinstein M. J., Luedemann G. M., Oden E. M., Wagman G. H., Rosselet J. P., Marquez J. A. *et al.* (1963), 'Gentamicin, a new antibiotic complex from *Micromonospora*'. *Journal of Medicinal Chemistry.* 6 (4): 463–464.

Wellington, E. M. H. *et al.* (1992) ‘Taxonomic status of *Kitasatosporia*, and proposed unification with *Streptomyces* on the basis of phenotypic and 16S rRNA analysis and emendation of *Streptomyces* Waksman and Henrici 1943, 339(AL)’, *International Journal of Systematic Bacteriology*. 42(1), pp. 156-60.

Westhoff, S., Kloosterman, A., *et al.* (2020) ‘Competition sensing alters antibiotic production in *Streptomyces*’, *mbio.* 12 (1), p. e02729-02820.

Westhoff, S., Otto, S. B., *et al.* (2020) ‘Spatial structure increases the benefits of antibiotic production in *Streptomyces **’, *Evolution*. 74(1), pp. 179–187.

Westhoff, S., van Wezel, G. P. and Rozen, D. E. (2017) ‘Distance-dependent danger responses in bacteria’, *Current Opinion in Microbiology*. 36(1), pp. 95–101.

Whiffen, A. J., Bohonos, N. and Emerson, R. L. (1946) ‘The Production of an Antifungal Antibiotic by *Streptomyces griseus.*’, *Journal of bacteriology*. 52(5), pp.

610–611.

Whitman, W. B., Coleman, D. C. and Wiebe, W. J. (1998) ‘Prokaryotes: The unseen majority’, *Proceedings of the National Academy of Sciences of the United States of America*. 95(12), pp. 6578–6583.

Wolfender, J. L. *et al.* (2019) 'Accelerating metabolite identification in Natural Product research: Toward an ideal combination of liquid chromatography-high resolution tandem mass spectrometry and NMR profiling, in silico databases, and chemometrics', *Analytical Chemistry*. 91(1), pp. 704–742.

Worley, B. and Powers, R. (2013) 'Multivariate Analysis in Metabolomics', *Current Metabolomics*. 1(1), pp. 97–107.

Wray, L. J., and Fisher, S. (1993) 'The *Streptomyces coelicolor* glnR gene encodes a protein similar to other bacterial response regulators, *Gene.* 130(1), pp. 145–150.

Wright, E. S. and Vetsigian, K. H. (2016) 'Inhibitory interactions promote frequent bistability among competing bacteria', *Nature Communications*. 7, p. 11274.

Wright, G. D. (2019) 'Unlocking the potential of natural products in drug discovery', *Microbial Biotechnology*. 12(1), pp. 55–57.

Xia, J. *et al.* (2015) 'MetaboAnalyst 3.0-making metabolomics more meaningful', *Nucleic Acids Research*. 43(1), pp. 251–257.

Yan, Q. *et al.* (2018) 'Secondary metabolism and interspecific competition affect accumulation of spontaneous mutants in the GacS-GacA regulatory system in Pseudomonas protegens', *mBio*. 9(1), p. e01845.

Yang, J. Y. *et al.* (2012) 'Primer on Agar-Based Microbial Imaging Mass Spectrometry', *Journal of Bacteriology*. 194(22), pp. 6023–6028.

Yang, Y. L. *et al.* (2009) 'Translating metabolic exchange with imaging mass spectrometry', *Nature Chemical Biology*, 5(12), pp. 885–887.

Yang, Y. L. *et al.* (2011) 'Connecting chemotypes and phenotypes of cultured marine microbial assemblages by imaging mass spectrometry', *Angewandte Chemie - International Edition*. 50(26), pp. 5839–5842.

Yao, L. *et al.* (2016) 'Discovery of novel xylosides in co-culture of basidiomycetes *Trametes versicolor* and *Ganoderma applanatum* by integrated metabolomics and bioinformatics', *Scientific Reports*. 6(1), pp. 1–13.

Yoon, S. and Lee, T. G. (2018) 'Biological tissue sample preparation for time-of-flight secondary ion mass spectrometry (ToF–SIMS) imaging', *Nano Convergence*. 5(1), p. 24.

Yu, D. *et al.* (2012) ‘Type III polyketide synthases in natural product biosynthesis’, *IUBMB Life*. 64(4), pp. 285-95.

Yu, M. *et al.* (2019) ‘New Metabolites From the Co-culture of Marine-Derived Actinomycete *Streptomyces rochei* MB037 and Fungus *Rhinocladiella similis* 35’, *Frontiers in Microbiology*. 10, p. 915.

Zelezniak, A. *et al.* (2015) ‘Metabolic dependencies drive species co-occurrence in diverse microbial communities’, *Proceedings of the National Academy of Sciences of the United States of America*. 112(20), pp. 6449–6454.

Zhalnina, K. *et al.* (2018) ‘Need for laboratory ecosystems to unravel the structures and functions of soil microbial communities mediated by chemistry’, *mBio*. 9(4), p. e01175.

Zhang, X. Andres, S. and Elliot, M. A. (2021) 'Interplay between Nucleoid-Associated Proteins and Transcription Factors in Controlling Specialized Metabolism in *Streptomyces'. ASM journals.* 12(4).

Zhang, Z. *et al.* (2020) ‘Towards a General Understanding of Bacterial Interactions’, *Trends in Microbiology*. 28(10), pp. 783-785.

Zhang, Q. W., Lin, L. G. and Ye, W. C. (2018) ‘Techniques for extraction and isolation of natural products: A comprehensive review’, *Chinese Medicine,* 13, p. 20.

Zhang, S. *et al.* (2018) ‘Interkingdom microbial consortia mechanisms to guide biotechnological applications’, *Microbial Biotechnology*. 11(5), pp. 833–847.

Zhang, Z., Wang, Y. and Ruan, J. (1997) ‘A proposal to revive the genus *Kitasatospora* (Omura, Takahashi, Iwai, and Tanaka 1982)’, *International Journal of Systematic Bacteriology*. 47(4), pp. 1048-54.

Zhao, K. *et al.* (2019) ‘Coexistence of microbial species in structured communities by forming a hawk-dove game like interactive relationship’, *Frontiers in Microbiology*. 10, p. 807.

Zhao, L., Zhang, Q. and Zhang, D. (2016) ‘Evolution alters ecological mechanisms of coexistence in experimental microcosms’, *Functional Ecology*. 30(8), pp. 1440–1446.

Zhu, X. M. *et al.* (2019) ‘Dynamical modelling of secondary metabolism and metabolic switches in *Streptomyces xiamenensis* 318’, *Royal Society Open Science*. 6(4), p. 190418.

Ziemert, N. *et al.* (2012) 'The natural product domain seeker NaPDoS: A phylogeny based bioinformatic tool to classify secondary metabolite gene diversity', *PLoS ONE*. 7(3), p. e34064.

Zotchev, S. B. (2014) 'Genomics-based insights into the evolution of secondary metabolite biosynthesis in actinomycete bacteria', *In: Pontarotti P. (eds) Evolutionary Biology: Genome Evolution, Speciation, Coevolution and Origin of Life*. pp. 35–45.

Zuñiga, C., Zaramela, L. and Zengler, K. (2017) 'Elucidation of complexity and prediction of interactions in microbial communities', *Microbial Biotechnology*. 10(6), pp. 1500–1522.

Supplementary information

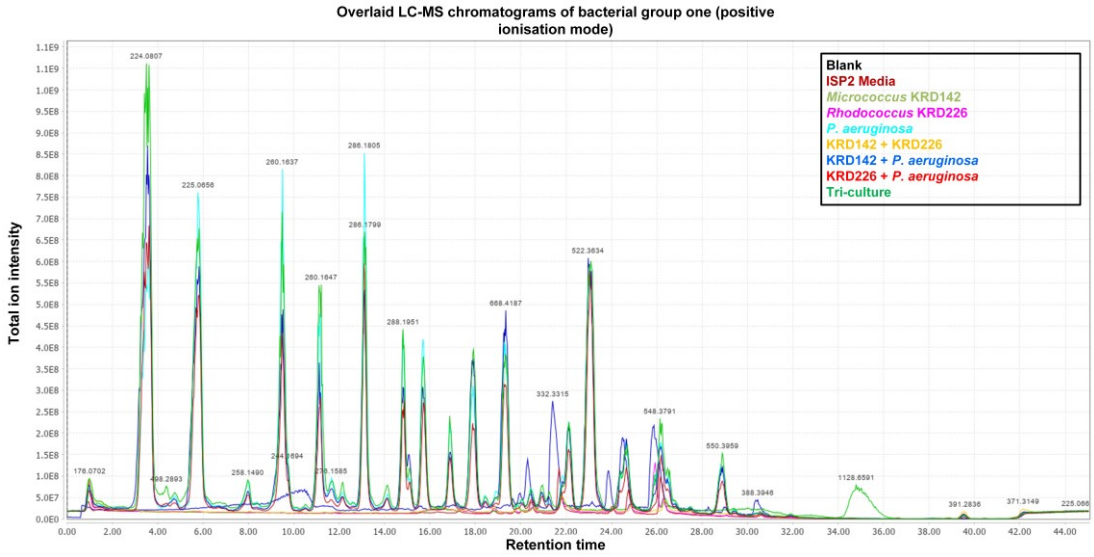

Figure S4.1. Positive ionisation mode LC-MS overlaid chromatograms of bacterial extracts from *Micrococcus* KRD142*, Rhodococcus* KRD226 and *P. aeruginosa* mono-cultures, one-to-one cultures and tri-cultures. The chromatogram indicates the parent ion intensity (y axis) and the retention time (x axis). High intensity ions are labelled with the respective *m/z*. The different experimental groups are colour-coded.

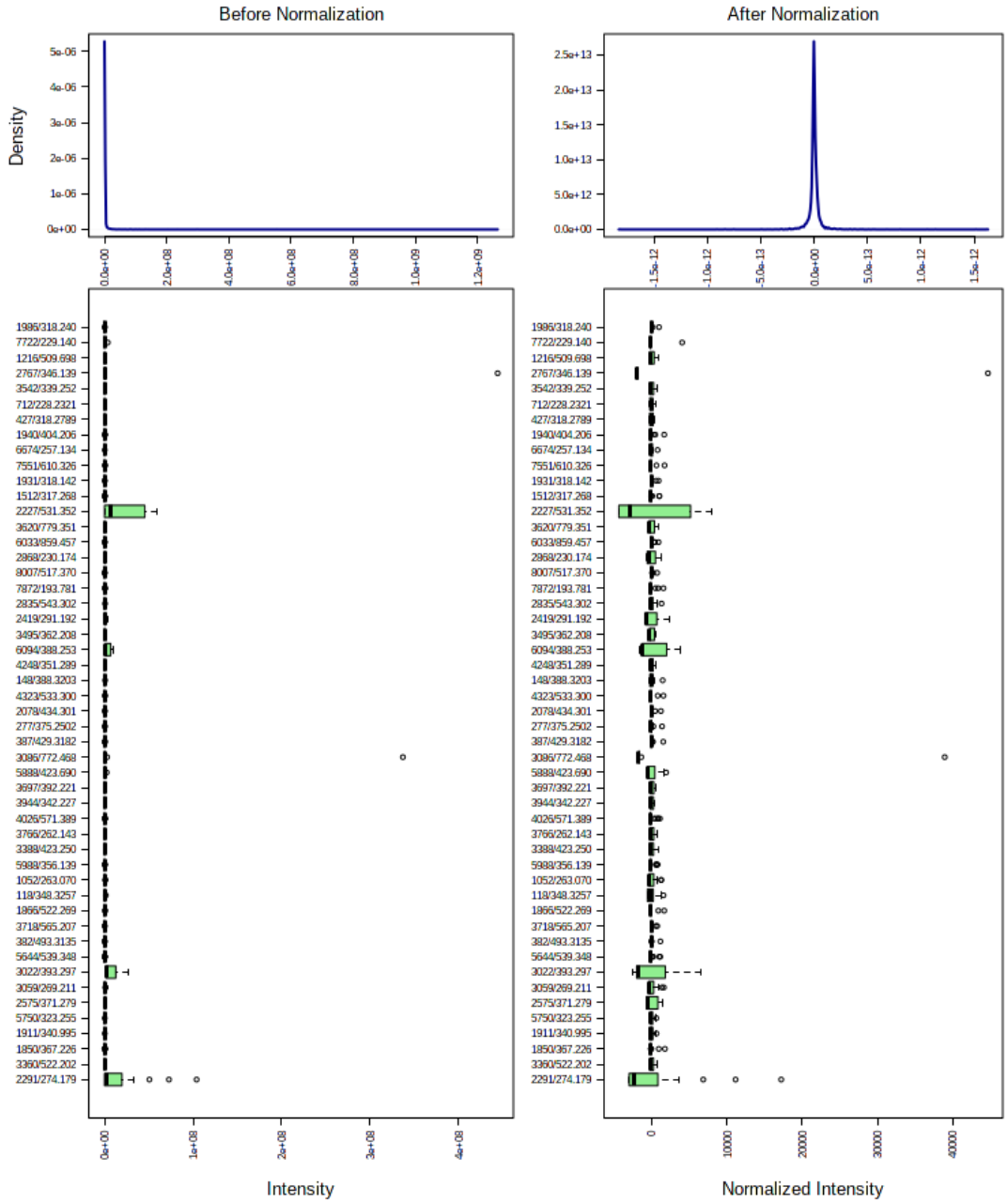

Figure S4.2. Box plots and kernel density plots before and after normalization by Pareto scaling for bacterial strains group one (*Micrococcus* KRD142, *Rhodococcus* KRD226 and *P. aeruginosa*). The boxplots show at most 50 parent ions.

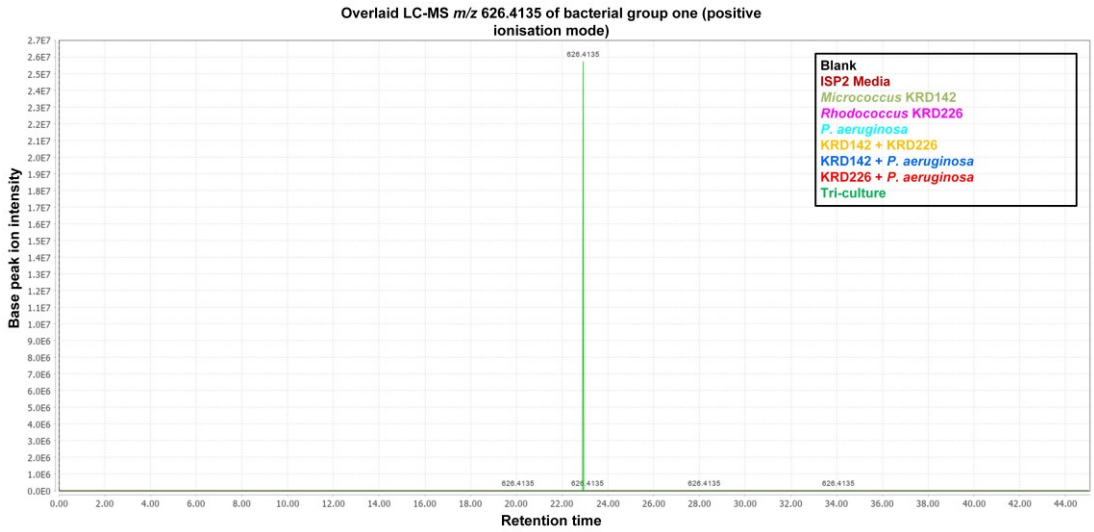

Figure S4.3. Parent ion *m/z* 626.4135 elicited as a result of the *Micrococcus* KRD142, *Rhodococcus* KRD226 and *P. aeruginosa* tri-culture interaction detected in the LC-MS positive ionisation mode data. The chromatogram indicates the parent ion intensity (y axis) and the retention time (x axis). This peak is detected in the extracts of the tri-culture (colour-coded in green).

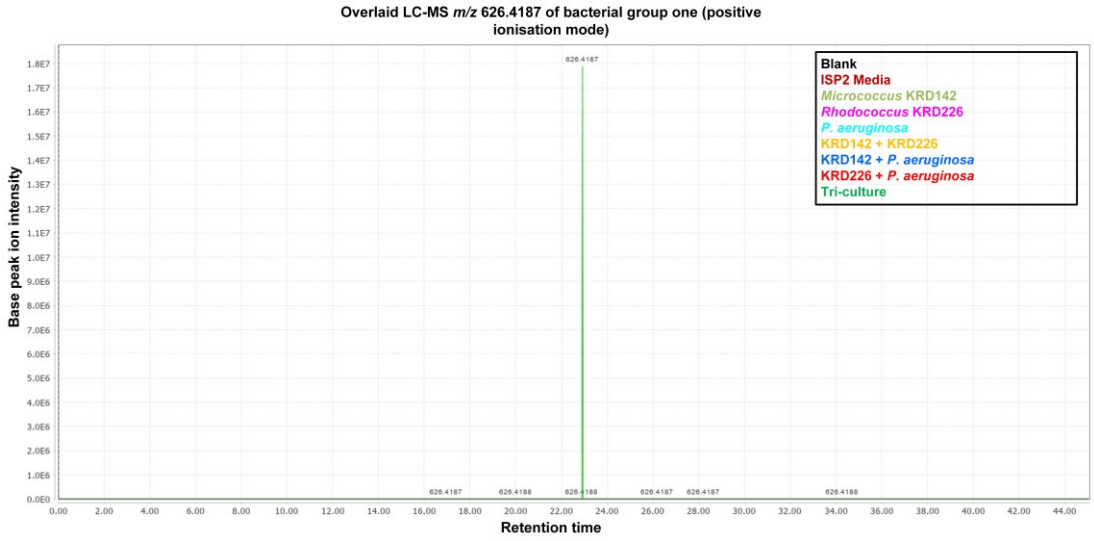

Figure S4.4. Parent ion *m/z* 626.4187 elicited as a result of the *Micrococcus* KRD142, *Rhodococcus* KRD226 and *P. aeruginosa* tri-culture interaction detected in the LC-MS positive ionisation mode data. The chromatogram indicates the parent ion intensity (y axis) and the retention time (x axis). This peak is detected in the extracts of the tri-culture (colour-coded in green).

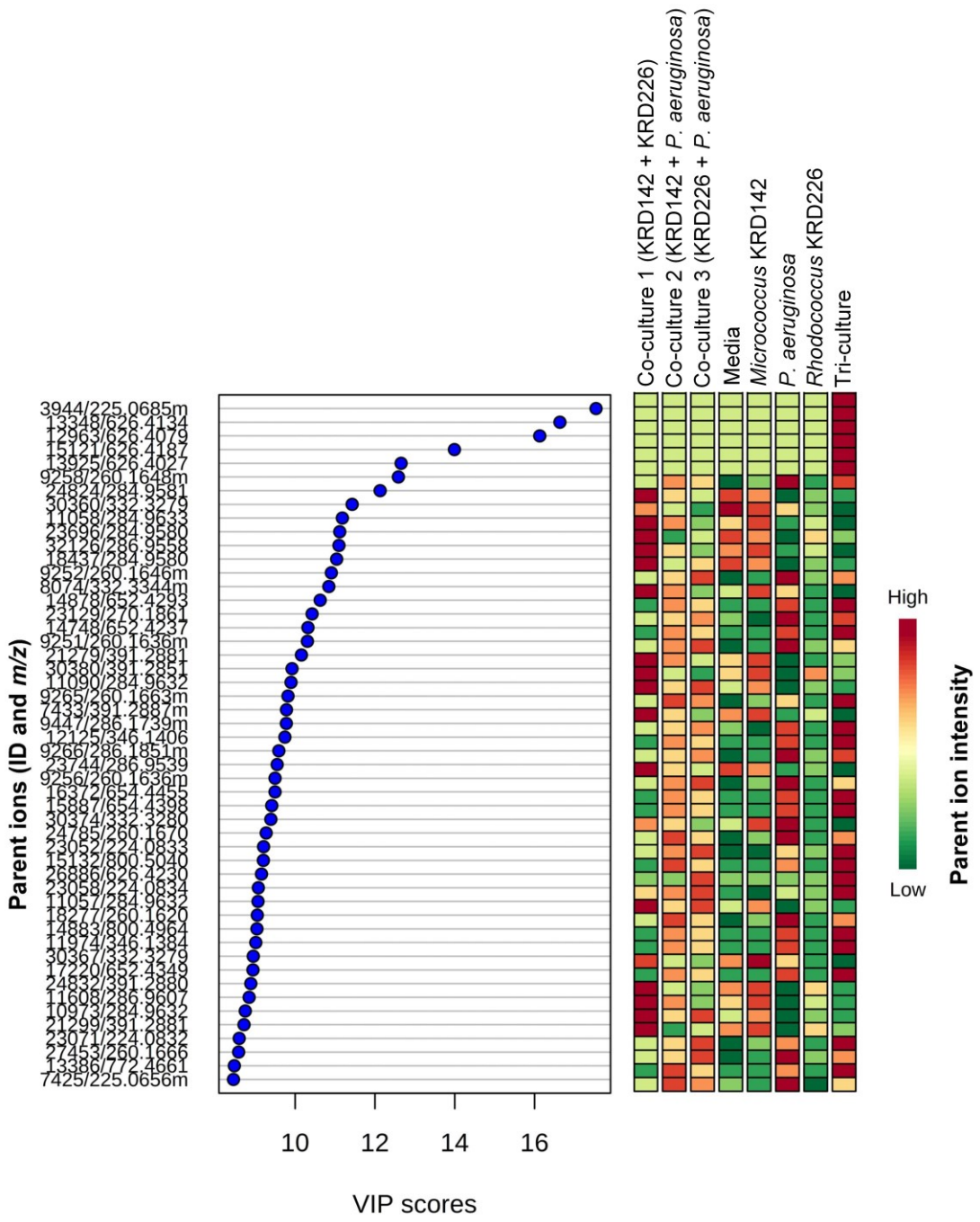

Figure S4.5. VIP scores plot reveals elicited parent ions by the *Micrococcus* KRD142, *Rhodococcus* KRD226 and *P. aeruginosa* tri-culture and one-to-one cultures. The coloured boxes on the right indicate the parent ion intensity. Blue dots indicate the VIP scores ranged between eight and 18, scores that are P > 1 are considered significant. VIP scores are detailed in the supplementary **Table S4.2**.

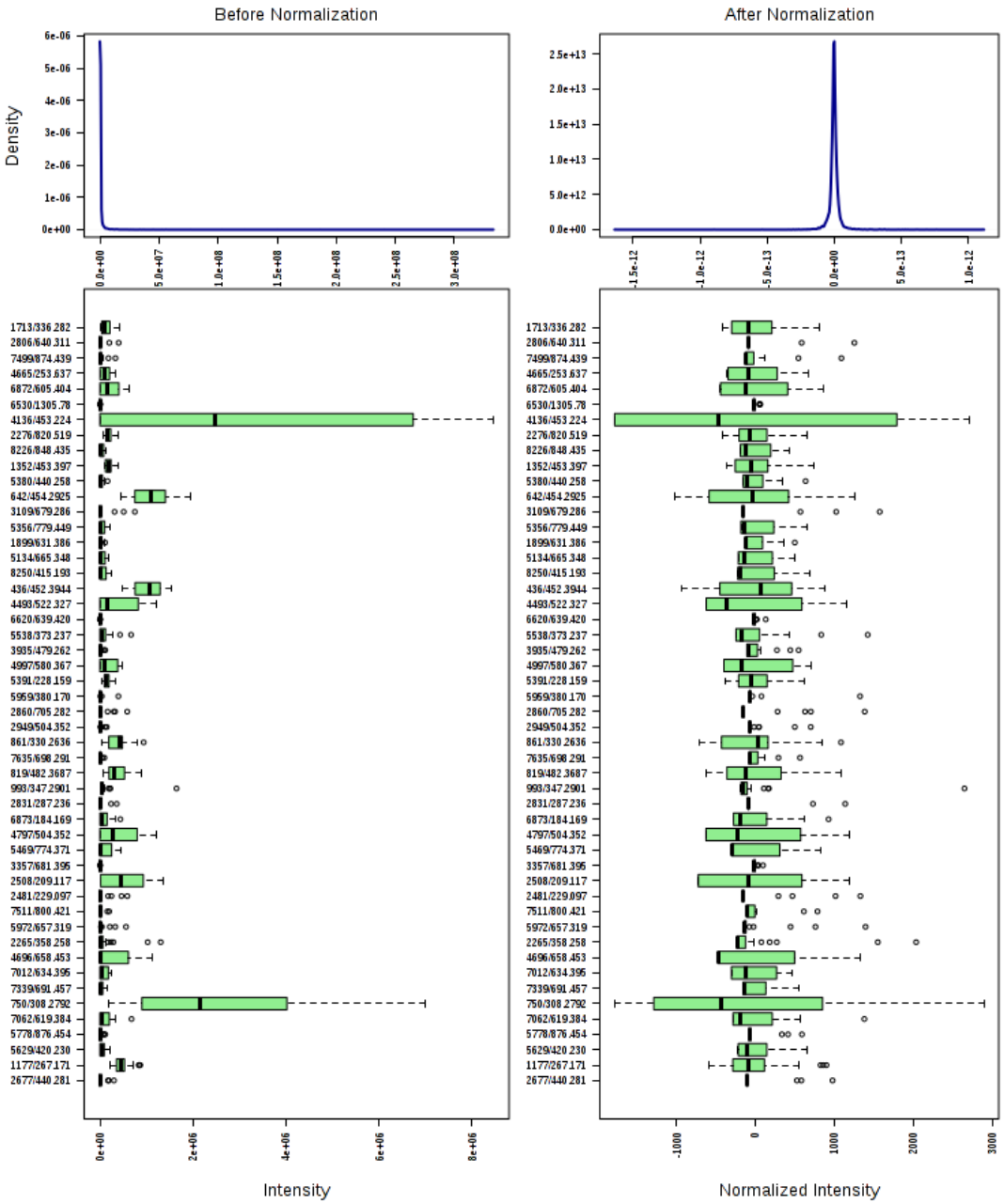

Figure S4.6. Box plots and kernel density plots before and after normalization by Pareto scaling for bacterial strains group two (*Rhodococcus* KRD226, *Micromonospora* KRD244 and *Streptomyces* KRD257). The boxplots show at most 50 parent ions.

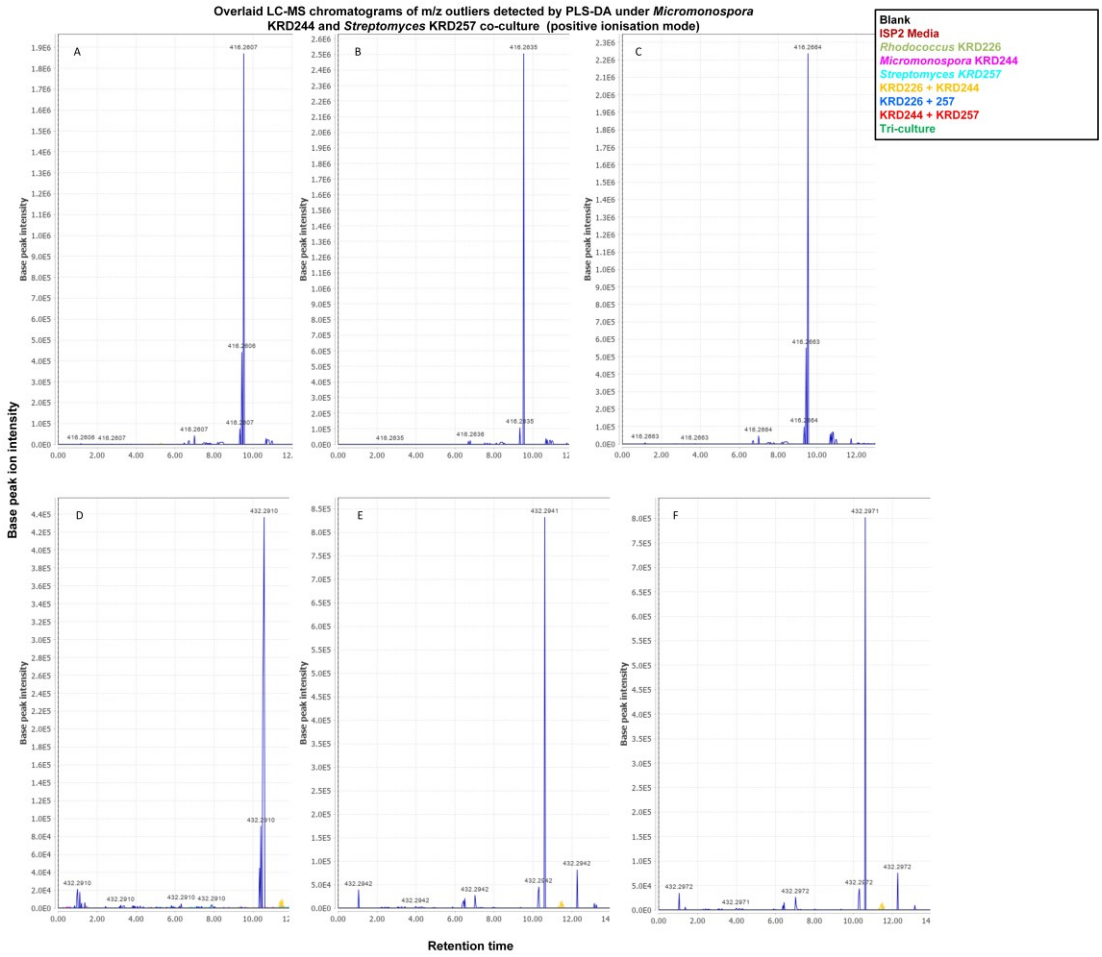

Figure S4.7. Parent ions *m/z* 416.2607, 416.2635, 416.2664, 432.2910, 432.2941 and 432.2971 elicited as a result of the *Rhodococcus* KRD226 and *Streptomyces* KRD257 one-to-one co-culture interaction detected in the LC-MS positive ionisation mode data. The chromatogram indicates the parent ion intensity (y axis) and the retention time (x axis). Experimental groups are colour-coded. A-F) *m/z* 416.2607, 416.2635, 416.2664, 432.2910, 432.2941 and 432.2971.

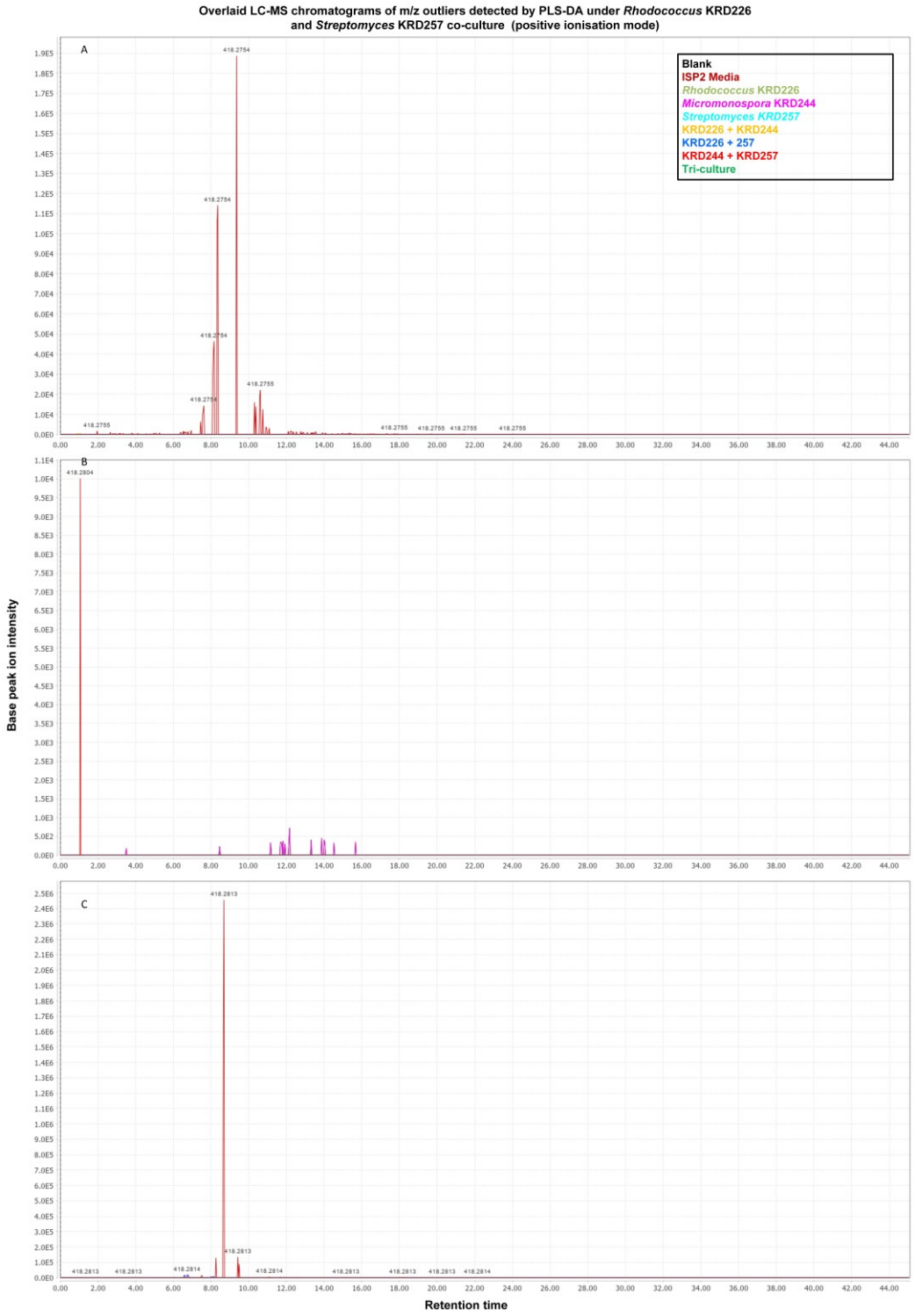

Figure S4.8. Parent ions *m/z* 418.2754, 418.2804 and 418.2813 elicited as a result of the *Micromonospora* KRD244 and *Streptomyces* KRD257 one-to-one co-culture interaction detected in the LC-MS positive ionisation mode data. The chromatogram indicates the parent ion intensity (y axis) and the retention time (x axis). Experimental groups are colour-coded. A-C) *m/z* 418.2754, 418.2804 and 418.2813.

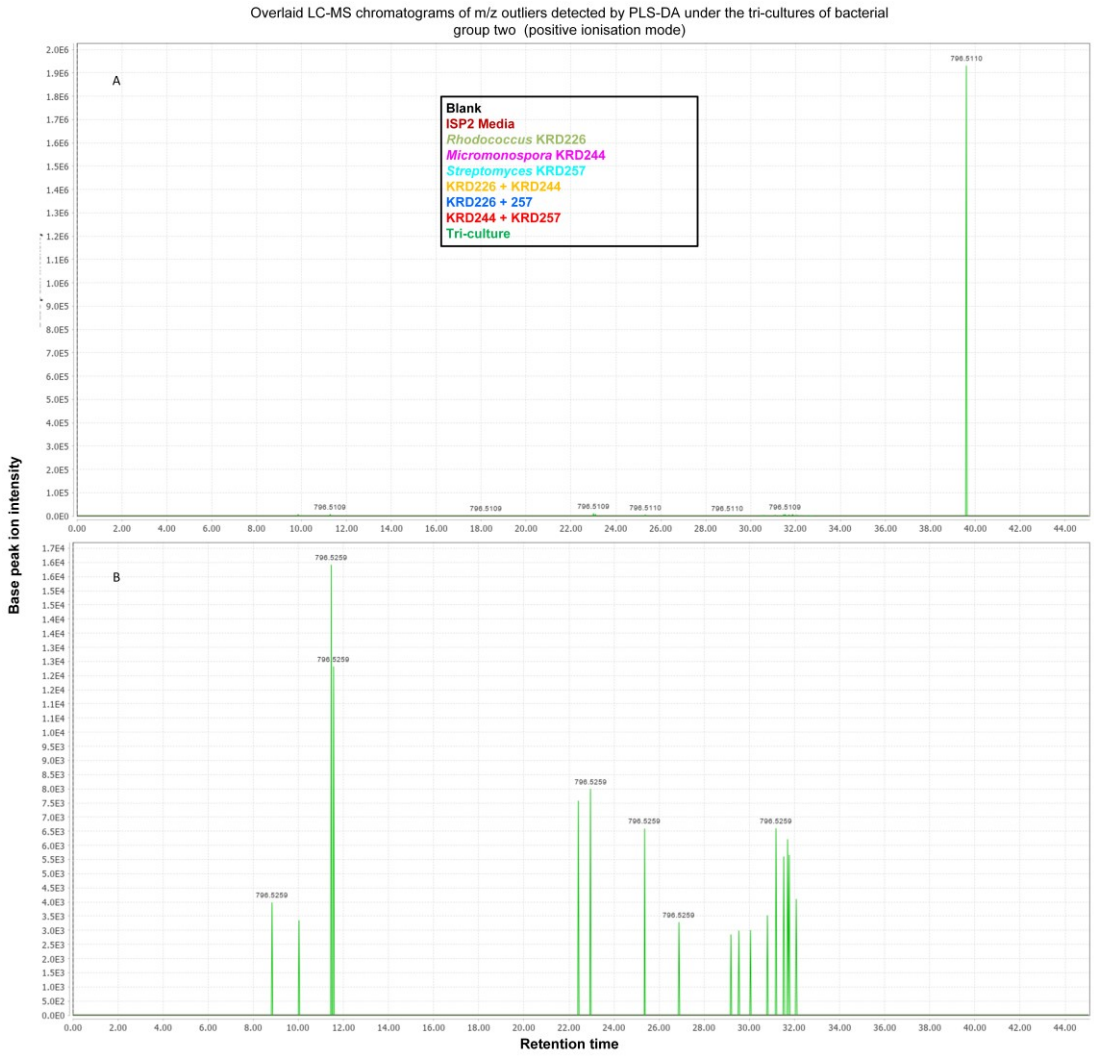

Figure S4.9. Parent ions *m/z* 796.5110 and 796.5259 elicited as a result of the *Rhodococcus* KRD226, *Micromonospora* KRD244 and *Streptomyces* KRD257 tri-culture interaction detected in the LC-MS positive ionisation mode data. The chromatogram indicates the parent ion intensity (y axis) and the retention time (x axis). Experimental groups are colour-coded. A) *m/z* 796.5110 and B) *m/z* 796.5259.

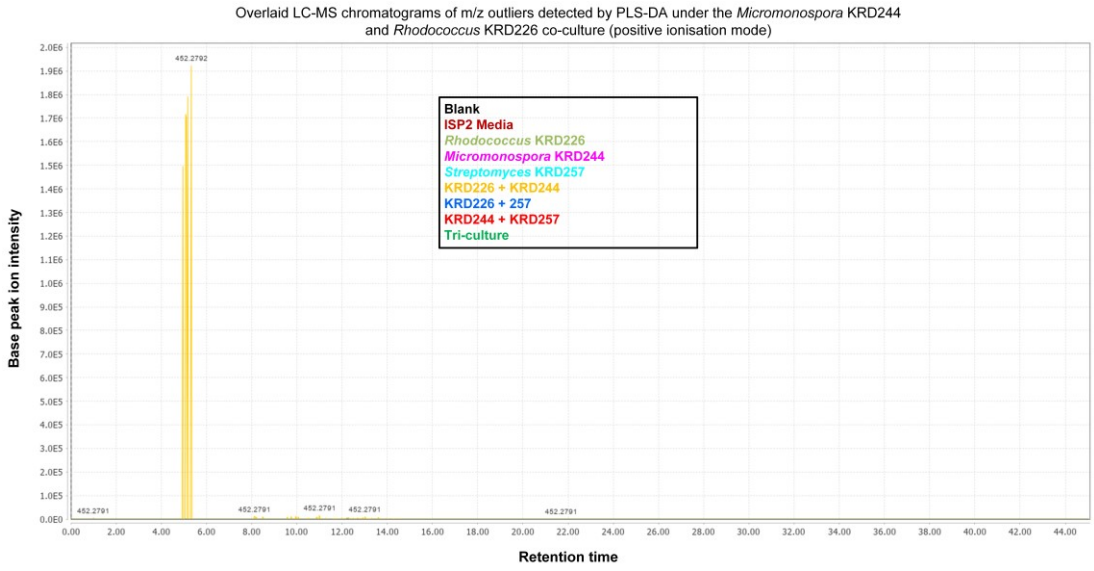

Figure S4.10. Parent ion *m/z* 452.2792 elicited as a result of the *Rhodococcus* KRD226 and *Micromonospora* KRD244 one-to-one interaction culture detected in the LC-MS positive ionisation mode data. The chromatogram indicates the parent ion intensity (y axis) and the retention time (x axis). Experimental groups are colour-coded.

Table S4.1. Eigenvalues of principal components one and two (1st PC and 2nd PC) from PCA for extracts of bacterial strains group one that contributed to the PCA variance (*Micrococcus* KRD142, *Rhodococcus* KRD226 and *P. aeruginosa*).

Bacterial extract (in triplicate)	1st PC	2nd PC
*P. aeruginosa*_1	-169.751522	-41.4877786
*P. aeruginosa*_2	-200.574023	-44.7004258
*P. aeruginosa*_3	-164.011788	-34.9596196
Co-culture 1_1 (*Micrococcus* KRD142 and *Rhodococcus* KRD226)	107.452303	-22.4267997
Co-culture 1_2 (*Micrococcus* KRD142 and *Rhodococcus* KRD226)	106.193611	-20.7921197
Co-culture 1_3 (*Micrococcus* KRD142 and *Rhodococcus* KRD226)	100.570648	-14.010673
Co-culture 2_1 (*Micrococcus* KRD142 and *P. aeruginosa)*	-118.172398	-28.7127518
Co-culture 2_2 (*Micrococcus* KRD142 and *P. aeruginosa)*	-116.4717	-21.0213761
Co-culture 2_3 (*Micrococcus* KRD142 and *P. aeruginosa)*	-125.550965	-19.9445235
Co-culture 3_1 (*Rhodococcus* KRD226 and *P. aeruginosa)*	-79.5018441	3.35676652
Co-culture 3_2 (*Rhodococcus* KRD226 and *P. aeruginosa*)	-120.844779	1.98236743
Co-culture 3_3 (*Rhodococcus* KRD226 and *P. aeruginosa*)	-160.87685	2.05811138
Tri-culture	-175.618642	24.8277222
Tri-culture	-71.8180446	59.5405149
Tri-culture	2.42437554	300.467533

Table S4.2. PLS-DA VIP scores of the first 50 most significant (P > 1) parent ions detected in the bacterial extracts of bacterial strains group one (*Micrococcus* KRD142, *Rhodococcus* KRD226 and *P. aeruginosa*) identified by PLS-DA.

PLS-DA VIP scores			
Parent ion (ID/mz/retention time)	Comp. 1	Comp. 2	Comp. 3
3944/225.0685mz/5.79min	17.541	11.987	11.781
13348/626.4134mz/23.02min	16.636	10.847	14.924
12963/626.4079mz/23.11min	16.131	10.517	14.471
15121/626.4187mz/23.11min	13.993	9.1233	12.549
13925/626.4027mz/23.11min	12.657	8.2519	11.359
9258/260.1648mz/11.32min	12.588	13.224	11.787
24824/284.9581mz/11.67min	12.131	7.8187	7.1482
30360/332.3279mz/21.82min	11.43	7.2875	6.7156
11058/284.9633mz/18.08min	11.184	7.3352	6.6702
23696/284.9580mz/9.83min	11.119	7.1196	6.6712
32126/286.9558mz/16.23min	11.099	7.0626	6.3152
18437/284.9580mz/15.29min	11.041	7.1461	6.7252
9252/260.1646mz/9.52min	10.908	14.302	12.72
8074/332.3344mz/23.91min	10.845	7.2805	6.4839
14878/652.4293mz/26.18min	10.629	6.9899	7.7783
23129/270.1861mz/15.72min	10.426	9.719	8.9263
14748/652.4237mz/26.18min	10.322	6.7885	7.5384
9251/260.1636mz/9.52min	10.308	14.185	12.677
21279/391.2881mz/17.28min	10.158	6.733	6.7527
30380/391.2851mz/6.60min	9.9224	6.3843	5.698
11090/284.9632mz/22.04min	9.8978	6.8672	6.5654
9265/260.1663mz/11.29min	9.8215	10.787	9.7742
7433/391.2887mz/16.37min	9.7836	6.2705	5.6751
9447/286.1739mz/13.00min	9.7797	6.2869	5.8777
12125/346.1406mz/5.75min	9.7439	6.3106	9.999
9266/286.1851mz/13.16min	9.5922	6.2931	7.3201
23744/286.9539mz/10.80min	9.5505	6.2842	5.9473
9256/260.1636mz/11.29min	9.4973	13.186	11.85
16372/654.4455mz/28.86min	9.4972	6.266	6.5405
15887/654.4398mz/28.84min	9.4146	6.211	6.4909
30374/332.3280mz/24.72min	9.392	6.4599	5.8196
24785/260.1670mz/11.20min	9.2742	8.4824	7.7255
23052/224.0833mz/9.33min	9.2096	5.897	5.5441
15132/800.5040mz/24.68min	9.2041	6.0446	6.8666
26886/626.4230mz/23.13min	9.1575	5.9701	8.2195
23058/224.0834mz/7.78min	9.0786	5.777	5.6538
11057/284.9632mz/22.00min	9.0701	6.1976	6.066
18277/260.1620mz/11.28min	9.0522	9.8484	9.7259
14883/800.4964mz/24.68min	9.0433	5.9398	6.7264

11974/346.1384mz/5.75min	9.0147	5.8366	9.2475
30367/332.3279mz/22.39min	8.9518	5.8026	5.3647
17220/652.4349mz/26.19min	8.9438	5.8815	6.5671
24832/391.2880mz/4.94min	8.8901	5.6703	5.0708
11608/286.9607mz/18.43min	8.8477	5.7635	5.163
10973/284.9632mz/21.92min	8.751	5.9389	5.6639
21299/391.2881mz/7.49min	8.7195	5.541	5.0147
23071/224.0832mz/11.49min	8.5988	5.5737	5.124
27453/260.1666mz/9.51min	8.5846	11.288	10.152
13386/772.4661mz/19.34min	8.4766	5.4929	8.6516
7425/225.0656mz/5.77min	8.4554	20.804	18.686

Table S4.3. Eigenvalues of principal components one and two (1st PC and 2nd PC) from PCA for extracts of bacterial strains group two that contributed to the PCA variance (*Rhodococcus* KRD226, *Micromonospora* KRD244 and *Streptomyces* KRD257).

PCA score plot (eigenvalues)		
Bacterial extract (in triplicate)	1st PC	2nd PC
Co-culture 1_1 (*Rhodococcus* KRD226 and *Micromonospora* KRD244)	71.64574	2.259822
Co-culture 1_2 (*Rhodococcus* KRD226 and *Micromonospora* KRD244)	69.70811	1.368121
Co-culture 1_3 (*Rhodococcus* KRD226 and *Micromonospora* KRD244)	85.77996	33.78489
Co-culture 2_1 (*Micromonospora* KRD244 *and Streptomyces* KRD257*)*	-79.5677	14.94865
Co-culture 2_2 (*Micromonospora* KRD244 *and Streptomyces* KRD257*)*	-50.5311	-4.5062
Co-culture 2_3 (*Micromonospora* KRD244 *and Streptomyces* KRD257)	-119.257	28.72063
Co-culture 3_1 (*Rhodococcus* KRD226 *and Streptomyces* KRD257*)*	-54.0091	-0.88586
Co-culture 3_2 (*Rhodococcus* KRD226 a*nd Streptomyces* KRD257*)*	-100.787	11.68399
Co-culture 3_3 (*Rhodococcus* KRD226 *and Streptomyces* KRD257*)*	-119.551	8.582731
Tri-culture	-57.6898	29.43518
Tri-culture	-120.56	28.91764
Tri-culture	-122.067	27.19034

Table S4.4. PLS-DA VIP scores of the first 50 most significant (P > 1) parent ions detected in the bacterial extracts of bacterial strains group two (*Rhodococcus* KRD226, *Micromonospora* KRD244 and *Streptomyces* KRD257) identified by PLS-DA.

PLS-DA VIP scores			
Parent ion (ID/mz/retention time)	Comp. 1	Comp. 2	Comp. 3
11262/796.5185mz/39.16min	21.956	14.717	14.229
11418/796.5260mz/39.15min	20.513	13.752	13.296
11827/796.5110mz/39.15min	19.194	12.863	12.436
11997/415.2687mz/11.51min	18.728	20.433	19.822

12004/415.2658mz/11.48min	17.386	18.972	18.405
11989/416.2635mz/9.87min	16.93	15.931	15.406
11982/432.2941mz/11.43min	16.717	15.792	15.279
17975/418.2785mz/9.09min	16.012	17.453	16.972
11977/418.2804mz/9.09min	15.922	19.77	19.448
11984/432.2971mz/11.44min	15.599	14.734	14.256
11992/416.2663mz/9.84min	15.292	14.378	13.906
11995/416.2606mz/9.89min	15.279	14.39	13.916
11978/418.2813mz/9.09min	15.211	18.884	18.575
11986/432.2910mz/11.70min	14.556	13.758	13.313
11979/418.2754mz/9.11min	13.777	17.113	16.837
11981/401.2536mz/9.06min	12.056	14.974	14.73
12005/404.2644mz/6.81min	11.861	7.9006	7.6354
11983/401.2511mz/9.06min	11.82	14.685	14.447
12007/404.2618mz/6.86min	11.172	7.4676	7.2179
11987/782.4992mz/37.88min	11.165	8.0314	7.8342
12006/796.5335mz/39.15min	10.973	8.4697	8.2078
12009/401.2594mz/9.10min	10.884	8.1183	7.8447
12012/404.2671mz/6.84min	10.263	6.8126	6.5832
12220/511.2830mz/14.87min	10.03	6.4592	6.2431
12211/511.2791mz/14.91min	9.7674	6.3407	6.126
17982/511.2793mz/12.03min	9.4314	6.1771	5.9686
12226/495.2833mz/16.81min	9.1409	5.886	5.6874
12167/511.2791mz/13.10min	9.0213	5.7922	5.6069
11990/764.4388mz/25.31min	8.8986	6.4071	6.2605
12025/404.2590mz/7.16min	8.5172	5.7101	5.5197
11988/418.2726mz/9.09min	8.5077	10.067	9.7987
23759/432.3002mz/11.36min	8.4911	8.8148	8.5574
11991/401.2483mz/9.08min	8.4868	10.087	9.834
12178/511.2831mz/11.86min	8.3783	5.5267	5.3442
12017/796.5036mz/39.07min	8.3615	7.0162	6.7922
12003/782.4919mz/37.66min	8.2562	6.0429	5.8905
12036/387.2377mz/6.91min	8.1701	5.4781	5.2965
11994/419.2813mz/9.08min	8.1172	8.4922	8.2489
11998/764.4459mz/25.31min	8.1146	5.7848	5.654
12179/511.2829mz/13.10min	8.074	5.2042	5.0312
17989/511.2754mz/12.00min	8.0328	5.2878	5.1097
11996/764.4317mz/25.32min	7.9609	5.7968	5.6619
12305/511.2752mz/14.86min	7.8643	5.1444	4.9706
12235/511.2752mz/13.08min	7.805	5.0118	4.8509
12042/387.2351mz/6.94min	7.6484	5.1382	4.9684
12001/418.2870mz/9.11min	7.5369	7.2901	7.0778
12011/782.5212mz/37.67min	7.5076	5.1851	5.0675
20928/452.2791mz/5.27min	7.489	5.3558	5.5207
23758/415.2687mz/11.37min	7.4046	9.3224	9.0726
21466/401.2606mz/9.10min	7.326	6.8772	6.7238

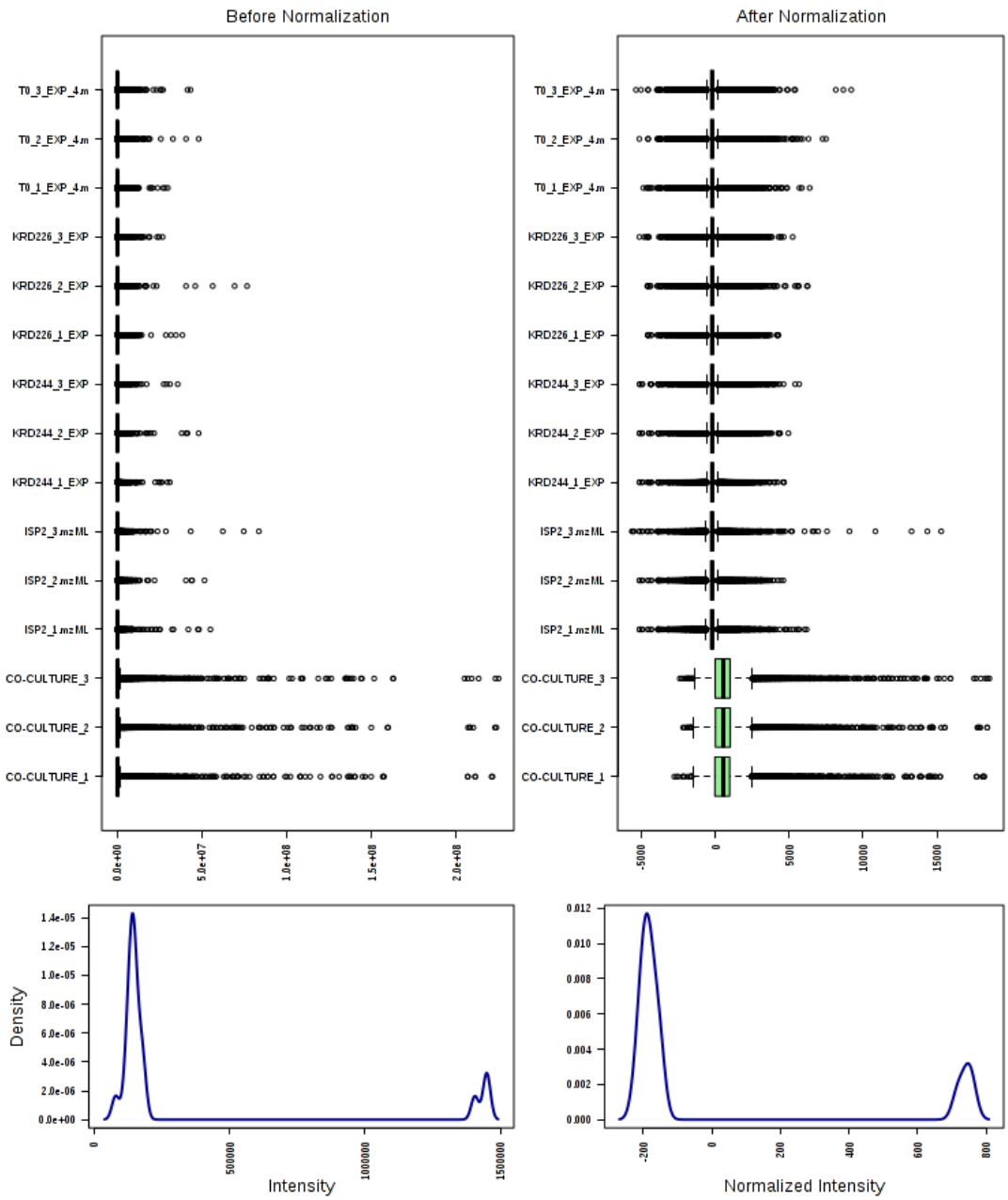

Figure S5.1. Box plots and kernel density plots before and after normalization by Pareto scaling for bacterial interactions in liquid media (experiment one). The boxplots show at most 50 parent ions.

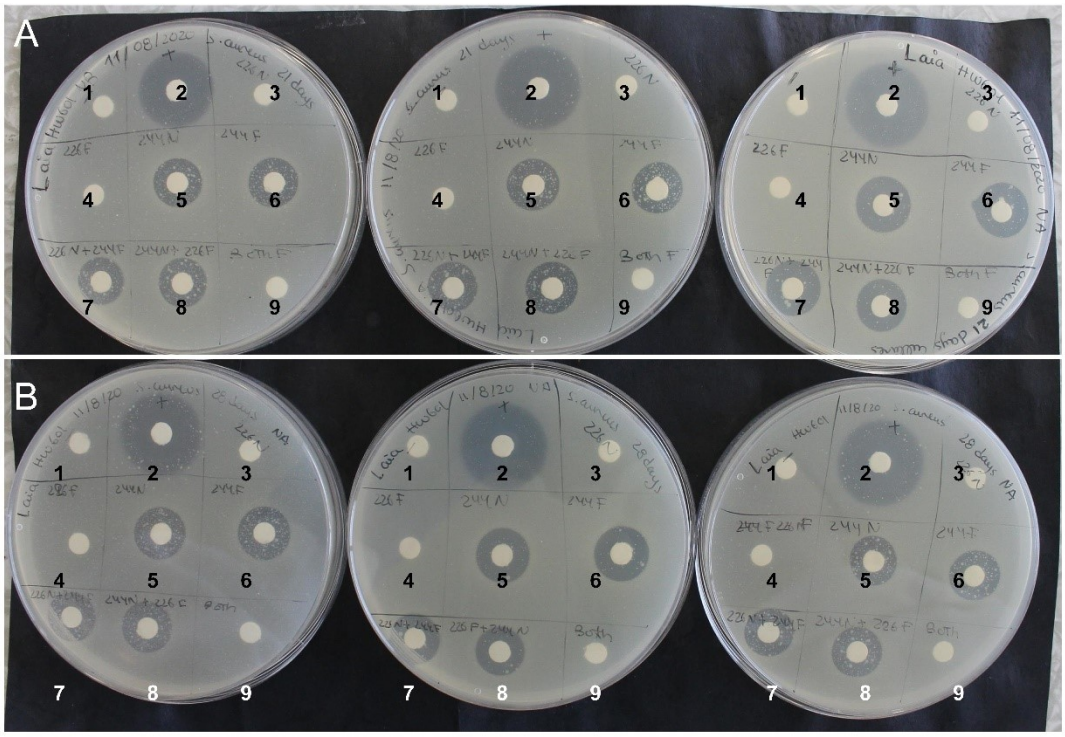

Figure S5.2. Antibacterial activity assays against *S. aureus* from pre-conditioned media extracts of experiment three (in triplicate). A-B) Extracts from 21 days-old cultures and extracts from 28-day old cultures. 1-9) Negative control (media extract), positive control (chloramphenicol), *Rhodococcus* KRD226 mono-culture extract, *Rhodococcus* KRD226 pre-conditioned media mono-culture extract, *Micromonospora* KRD244 mono-culture extract, *Micromonospora* KRD244 pre-conditioned media mono-culture extract, extract of *Rhodococcus* KRD226 inoculated into the *Micromonospora* KRD244 pre-conditioned media, extract of *Micromonospora* KRD244 inoculated into the *Rhodococcus* KRD226 pre-conditioned media, co-culture control.

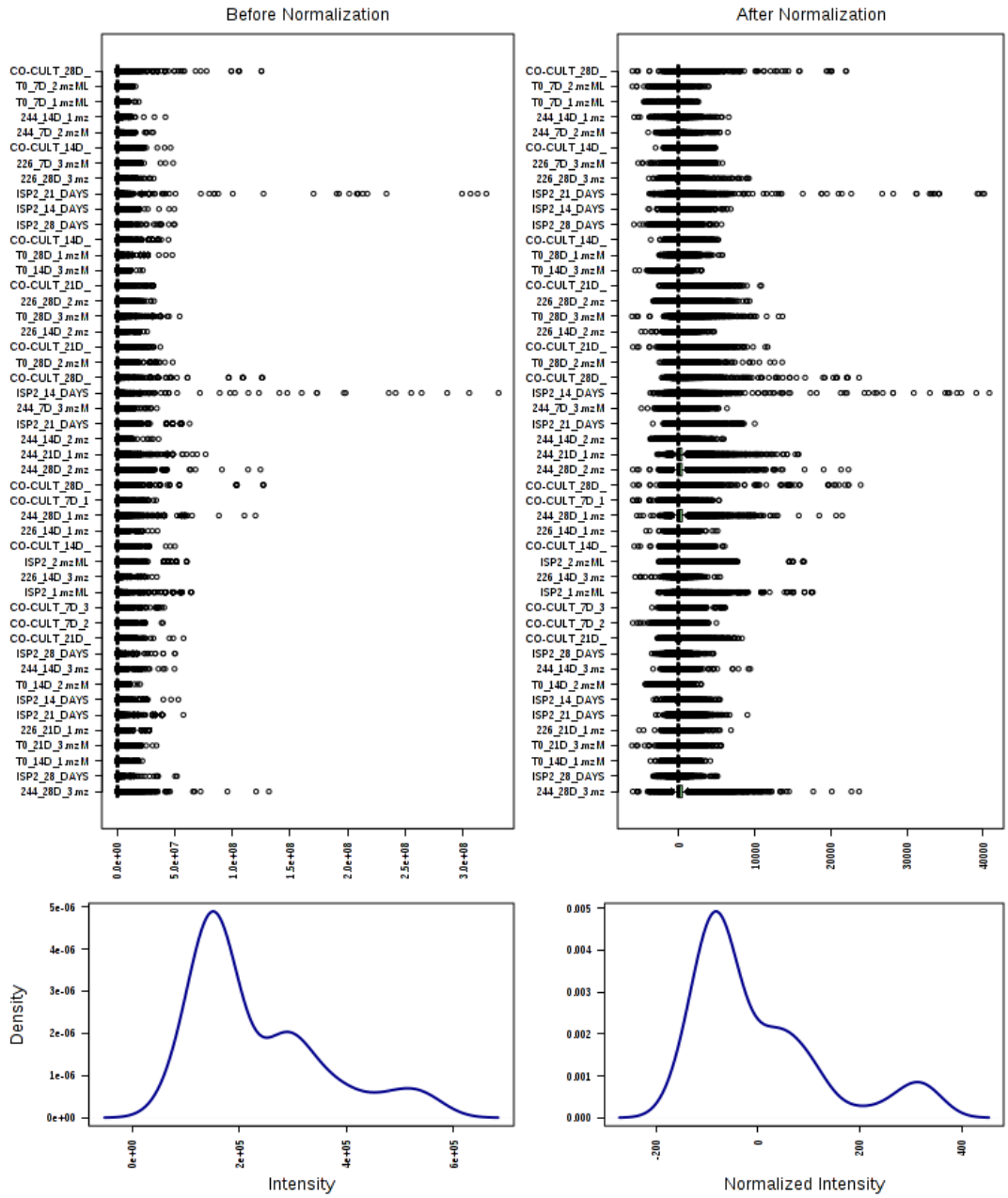

Figure S5.3. Box plots and kernel density plots before and after normalization by Pareto scaling for bacterial interactions in liquid media (experiment three). The boxplots show at most 50 parent ions.

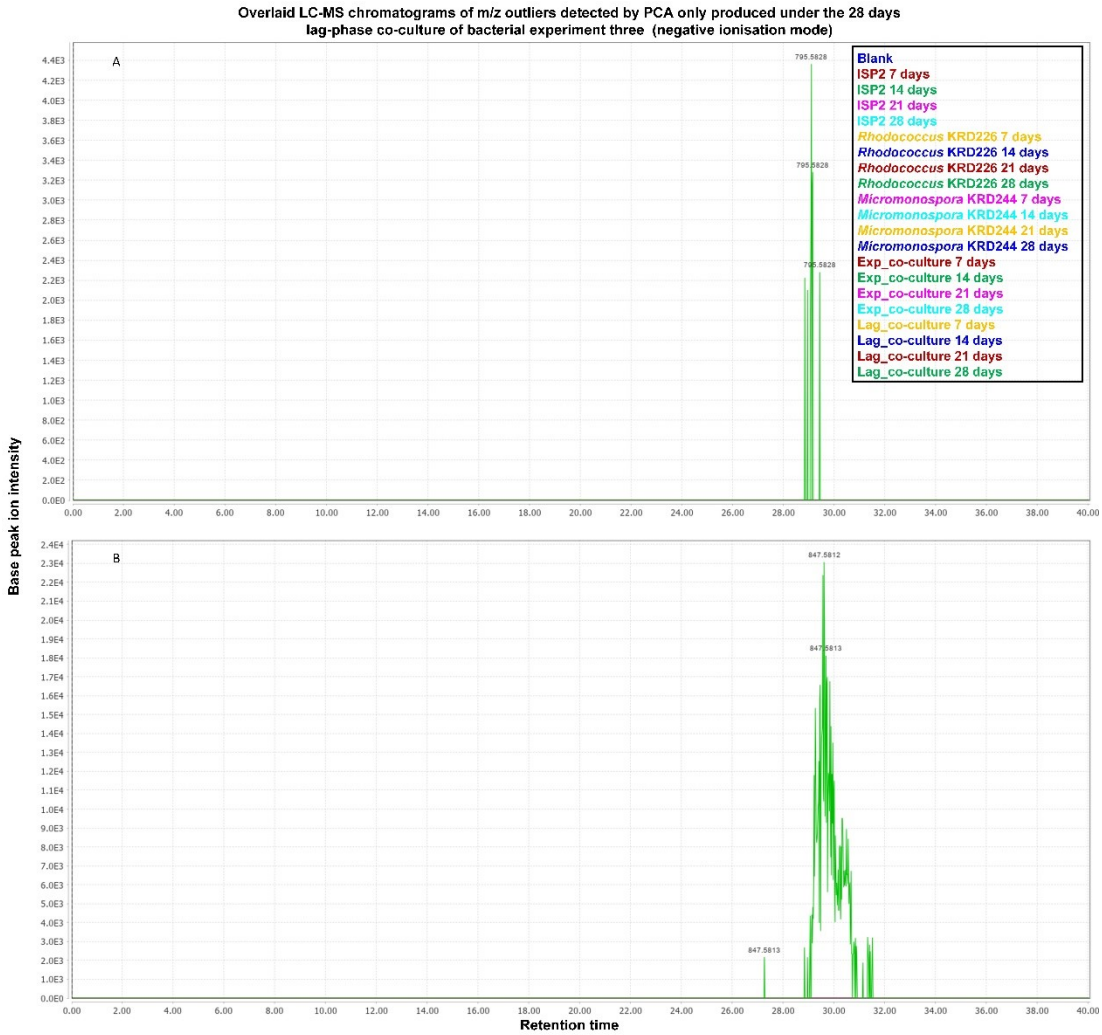

Figure S5.4. Parent ions *m/z* 795.5828 and *m/z* 847.5812 elicited as a result of the *Micromonospora* KRD244 and *Rhodococcus* KRD226 28-days old lag-phase co-culture interaction detected in the LC-MS negative ionisation mode data. The chromatogram indicates the parent ion intensity (y axis) and the retention time (x axis). Experimental groups are colour-coded. A) *m/z* 795.5828 and B) *m/z* 847.5812.

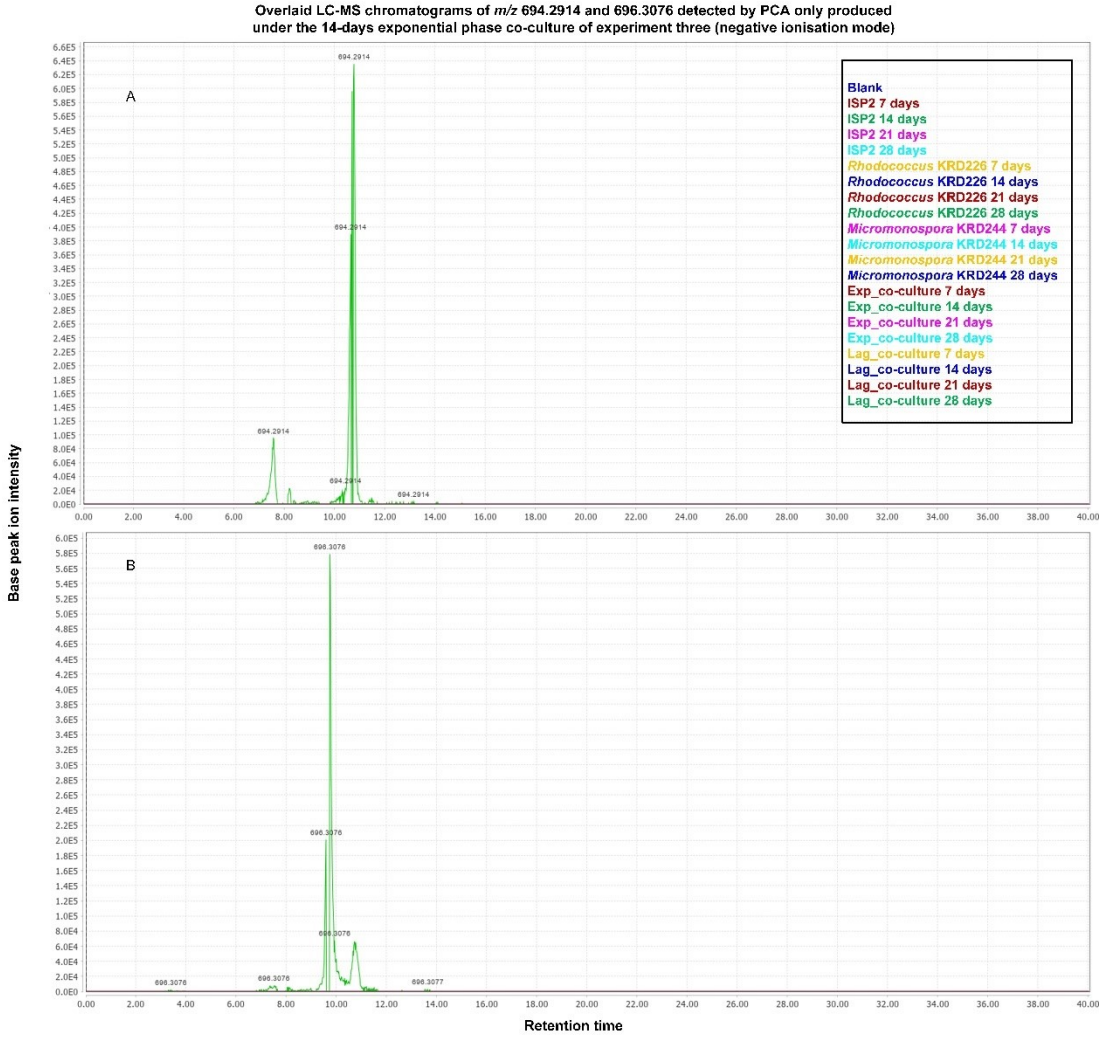

Figure S5.5. Parent ions *m/z* 694.2914 and *m/z* 696.3076 elicited as a result of the *Micromonospora* KRD244 and *Rhodococcus* KRD226 14-day old transitional-phase co-culture interaction detected in the LC-MS negative ionisation mode data. The chromatogram indicates the parent ion intensity (y axis) and the retention time (x axis). Experimental groups are colour-coded. A) *m/z* 694.2914 B) *m/z* 696.3076.

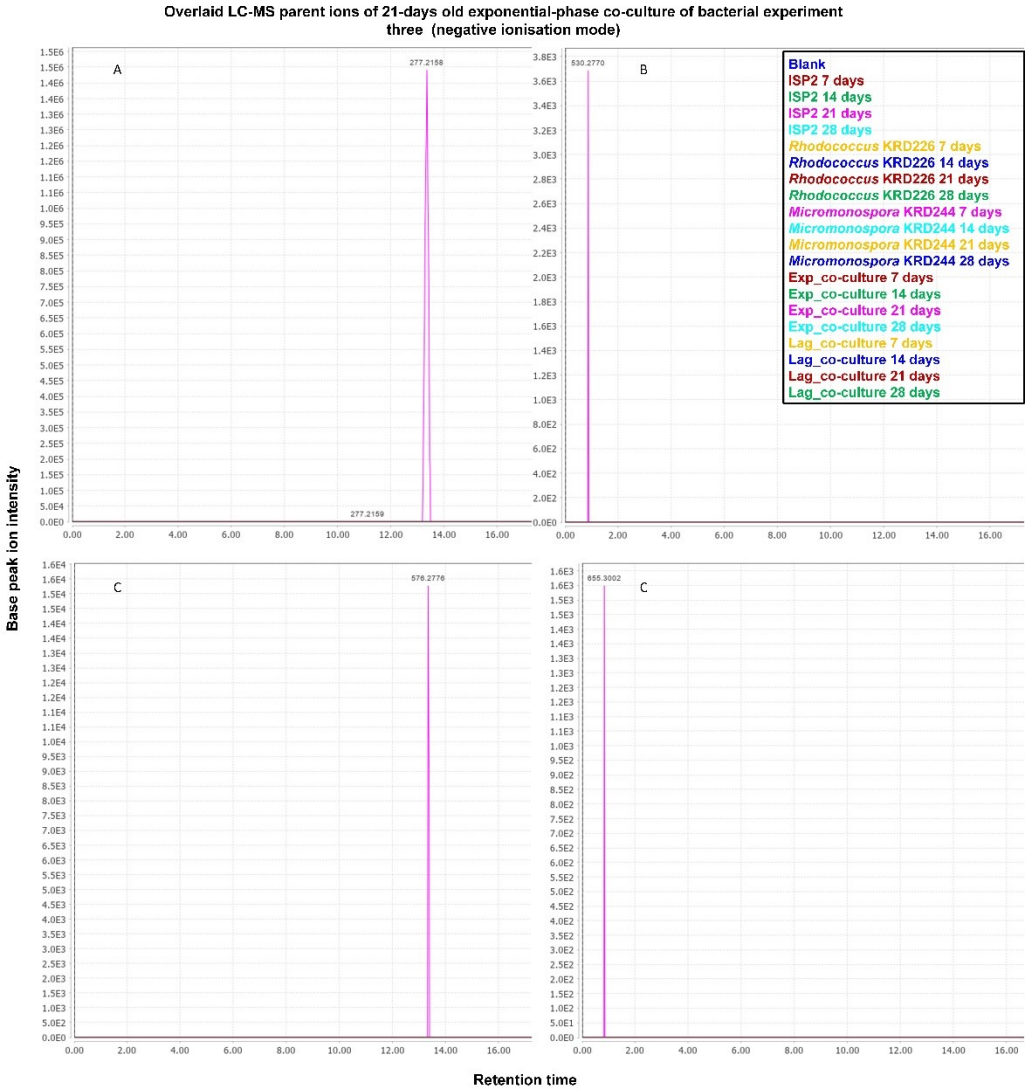

Figure S5.6. Parent ions *m/z* 277.2158, 530.2770, 576.2776 and 655.3002 elicited as a result of the *Micromonospora* KRD244 and *Rhodococcus* KRD226 21-day old transitional-phase co-culture interaction detected in the LC-MS negative ionisation mode data. The chromatogram indicates the parent ion intensity (y axis) and the retention time (x axis). Experimental groups are colour-coded. A-D) *m/z* 277.2158, 530.2770, 576.2776 and 655.3002.

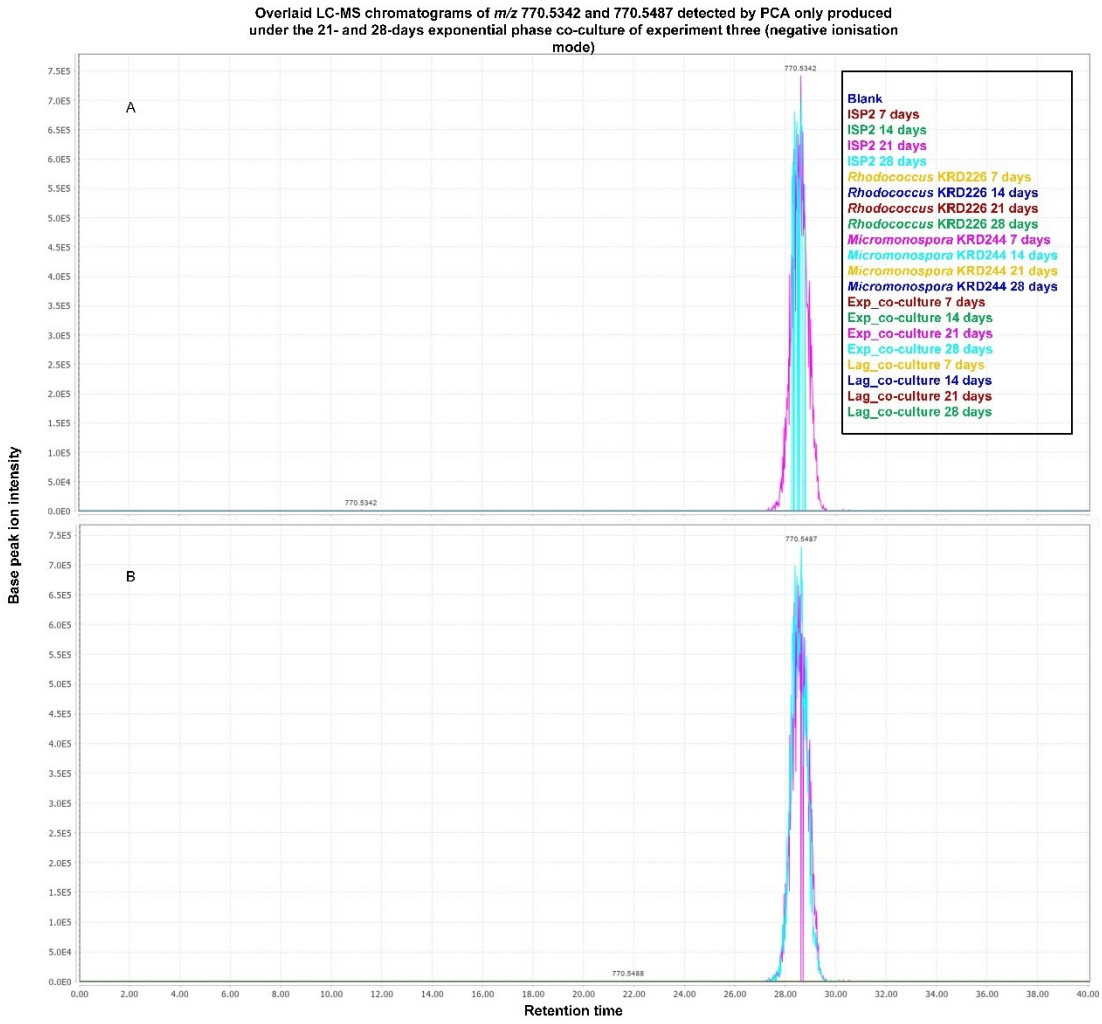

Figure S5.7. Parent ions *m/z* 770.5342 and 770.5487 elicited as a result of the *Micromonospora* KRD244 and *Rhodococcus* KRD226 21 and 28-day old transitional-phase co-culture interaction detected in the LC-MS negative ionisation mode data. The chromatogram indicates the parent ion intensity (y axis) and the retention time (x axis). Experimental groups are colour-coded. A) *m/z* 770.5342 and B) *m/z* 770.5487.

Table S5.1 Eigenvalues of principal components one and two (1st PC and 2nd PC) from PCA for extracts of experiment one contributing to the PCA variance.

PCA score plot (eigenvalues)		
Bacterial extract (in triplicate)	1st PC	2nd PC
Transitional phase co-culture_1	-218.645	-12.3025
Transitional phase co-culture_2	-225.104	1.647619
Transitional phase co-culture_3	-219.115	4.337649
Lag-phase co-culture_1	38.27098	73.15635
Lag-phase co-culture_2	39.9029	81.38069
Lag-phase co-culture_3	40.22655	76.6127

Table S5.2. PLS-DA VIP scores of the first 50 most significant (P > 1) parent ions detected in the bacterial extracts of experiment one identified by PLS-DA.

PLS-DA VIP scores			
Parent ion (ID/mz/retention time)	Comp. 1	Comp. 2	Comp. 3
4406/178.0513mz/0.88min	12.734	10.223	9.6632
3480/178.0514mz/0.88min	12.685	10.135	9.5828
5153/654.2992mz/7.95min	12.387	9.9438	9.4003
5142/654.2880mz/7.95min	12.328	9.8961	9.3566
4407/178.0498mz/0.88min	12.269	9.8495	9.3115
3479/178.0498mz/0.88min	12.184	9.7492	9.2189
3988/315.0412mz/1.02min	11.022	9.0172	8.5233
4408/178.0528mz/0.87min	11.009	8.7296	8.2456
3482/178.0530mz/0.87min	10.793	8.6109	8.1419
6012/640.2757mz/5.46min	10.412	8.3595	7.9005
5218/654.3104mz/7.95min	10.141	8.1418	7.6956
3485/298.0925mz/0.82min	10.013	7.9996	7.5551
5175/654.2768mz/7.95min	9.9973	8.0245	7.5883
4411/298.0960mz/0.84min	9.9891	7.9757	7.5325
3486/298.0960mz/0.84min	9.9887	7.9755	7.5323
4410/298.0925mz/0.82min	9.9851	8.0156	7.5788
6013/640.2866mz/5.41min	9.9108	7.9578	7.5199
4409/178.0481mz/0.83min	9.4958	7.6087	7.1958
3481/178.0481mz/0.83min	9.4666	7.5868	7.1746
3498/619.1819mz/0.84min	9.4322	7.5881	7.1669
3499/619.1716mz/0.84min	9.1713	7.3797	6.9702
6014/640.2648mz/5.47min	8.896	7.1419	6.7511
6015/696.3067mz/9.84min	8.7551	7.0315	6.6429
5140/652.2840mz/7.33min	8.7161	6.9953	6.6166
5131/652.2728mz/7.33min	8.6877	6.9722	6.5955

3990/315.0375mz/1.04min	8.532	6.8391	6.4725
6008/597.2002mz/0.85min	8.4479	6.7799	6.4131
6009/597.1904mz/0.86min	8.339	6.6923	6.3309
4413/298.0891mz/0.82min	8.1495	6.515	6.1529
3490/298.0891mz/0.82min	8.1458	6.5124	6.1505
4414/298.0994mz/0.83min	8.1185	6.4786	6.1186
3496/298.0994mz/0.83min	8.1123	6.4736	6.1139
6016/696.2944mz/9.78min	7.9885	6.4136	6.0621
3512/619.1922mz/0.85min	7.914	6.3653	6.0119
5273/655.2993mz/7.99min	7.8808	6.329	5.9834
3989/315.0450mz/0.94min	7.7549	6.5079	6.1507
6018/640.2975mz/5.33min	7.6713	6.1594	5.8199
6019/696.3189mz/9.84min	7.6513	6.1455	5.8053
5282/655.2880mz/7.99min	7.3732	5.9213	5.5989
3514/619.1613mz/0.84min	7.2111	5.8042	5.4822
5196/654.2994mz/5.54min	7.2084	5.787	5.4702
4412/178.0544mz/0.87min	7.1715	5.7101	5.3984
3995/178.0545mz/0.87min	7.1618	5.7045	5.3929
5184/654.2882mz/5.54min	7.1477	5.7378	5.4248
6020/777.3613mz/17.38min	7.1246	5.7206	5.4067
5204/652.2952mz/7.37min	7.1149	5.7105	5.4003
17679/315.0411mz/0.98min	7.0422	5.631	5.597
5162/652.2617mz/7.27min	7.034	5.6446	5.3411
6010/597.2100mz/0.85min	6.9651	5.5905	5.2878
5422/655.3105mz/7.96min	6.8905	5.5338	5.2309

Table S5.3. Eigenvalues of principal components one and two (1st PC and 2nd PC) from PCA for all extracts of experiment three that contributed to the PCA.

PCA score plot (eigenvalues)		
Bacterial extract (in triplicate)	1st PC	2nd PC
Transitional_phase_co-culture_7_days_1	-64.676341	-67.4880428
Transitional_phase_co-culture_7_days_2	-74.1074256	-73.7093774
Transitional_phase_co-culture_7_days_3	-100.095911	-83.0844092
Transitional_phase_co-culture_14_days_1	-151.56086	-27.5078653
Transitional_phase_co-culture_14_days_2	-147.293943	-16.9072121
Transitional_phase_co-culture_14_days_3	-155.415914	-7.62747782
Transitional_phase_co-culture_21_days_1	-4.91565926	121.386007
Transitional_phase_co-culture_21_days_2	-2.97946848	125.151139
Transitional_phase_co-culture_21_days_3	-3.00681853	124.458697
Lag_phase_co-culture_28_days_1	43.7612956	45.2889131
Lag_phase_co-culture_28_days_2	44.3462327	119.931425
Lag_phase_co-culture_28_days_3	50.0959001	149.689969

Table S5.4. Eigenvalues of principal components one and two (1st PC and 2nd PC) from PCA for all transitional-phase co-culture extracts of experiment three.

PCA score plot (eigenvalues)		
Bacterial extract (in triplicate)	1st PC	2nd PC
Transitional_phase_co-culture_7_days_1	54.6075336	-3.33194999
Transitional_phase_co-culture_7_days_2	56.504985	-5.52482127
Transitional_phase_co-culture_7_days_3	57.2269292	-10.1208058
Transitional_phase_co-culture_14_days_1	-48.9095286	-98.0500974
Transitional_phase_co-culture_14_days_2	-55.624958	-92.4619959
Transitional_phase_co-culture_14_days_3	-57.7503138	-83.907097
Transitional_phase_co-culture_21_days_1	-90.3700908	70.5660472
Transitional_phase_co-culture_21_days_2	-89.2445473	75.3549106
Transitional_phase_co-culture_21_days_3	-86.8117912	77.2219593
Transitional_phase_co-culture_28_days_1	82.6817183	27.0587742
Transitional_phase_co-culture_28_days_2	91.046292	26.0926905
Transitional_phase_co-culture_28_days_3	86.6437716	17.1023857

Table S5.5. PLS-DA VIP scores of the first 50 most significant (P > 1) parent ions detected in the 14-day old bacterial extracts of experiment three identified by PLS-DA.

PLS-DA VIP scores			
Parent ion (ID/mz/retention time)	Comp. 1	Comp. 2	Comp. 3
3483/315.0378mz/0.98min	7.3342	6.3019	6.6219
11683/712.2993mz/9.63min	7.2406	6.4345	6.2411
3491/315.0489mz/0.90min	6.8324	5.9652	6.0609
11684/712.3121mz/9.63min	6.5652	5.8374	5.661
11685/712.2866mz/9.63min	6.5596	5.8306	5.6542
9178/654.2890mz/5.53min	6.3462	5.641	5.4707
9301/654.2887mz/7.97min	6.2548	5.5631	5.3938
9194/654.3002mz/5.53min	6.2392	5.5475	5.3795
9303/654.2999mz/7.97min	6.0226	5.356	5.193
3479/315.0415mz/0.98min	5.4644	4.8712	5.5626
9308/654.2775mz/7.98min	5.3694	4.7716	4.6279
9254/654.2778mz/5.53min	5.2672	4.6805	4.5397
11723/728.2940mz/8.82min	5.2498	4.6675	4.5264
3480/315.0451mz/0.98min	5.2355	4.6604	5.3107
11687/754.3148mz/6.26min	5.1319	4.5628	4.425
9329/654.3115mz/5.54min	4.9646	4.4156	4.2814
11695/728.2942mz/5.99min	4.9577	4.4065	4.2738
11688/754.3009mz/6.26min	4.9491	4.4009	4.2679
11705/737.2722mz/10.37min	4.9173	4.3719	4.2396
6876/315.0454mz/0.85min	4.87	5.6943	5.6464
11686/313.1563mz/6.52min	4.8613	4.3208	4.1905
11708/737.2856mz/10.36min	4.742	4.2169	4.089
11742/728.2808mz/8.82min	4.7344	4.2079	4.081
11736/728.3072mz/8.82min	4.7275	4.2042	4.0767
11693/712.3248mz/9.63min	4.7191	4.1981	4.0703
9318/654.3112mz/7.98min	4.705	4.1866	4.0595
11696/712.2738mz/9.63min	4.6891	4.166	4.041
10677/364.2286mz/4.86min	4.5993	4.0874	3.9642
11697/713.3075mz/9.63min	4.5974	4.0879	3.964
11704/728.2810mz/5.99min	4.4832	3.9834	3.8639
11702/728.3074mz/6.00min	4.4829	3.9852	3.8649
11699/713.2947mz/9.63min	4.4393	3.9453	3.8266
4457/315.0452mz/0.90min	4.4052	4.302	4.6329
11689/313.1600mz/6.52min	4.3974	3.91	3.7917
11690/313.1526mz/6.52min	4.3804	3.8915	3.7748
1720/311.1704mz/12.32min	4.3023	6.9298	6.744
9325/530.2768mz/2.19min	4.2859	3.8389	3.7251
11692/754.3287mz/6.26min	4.2643	3.7925	3.6776
1718/311.1668mz/12.32min	4.2616	6.9012	6.6988

10706/364.2333mz/4.86min	4.2215	3.7532	3.6395
11727/714.2791mz/4.67min	4.2211	3.7521	3.6389
11691/694.2915mz/10.75min	4.2049	3.7395	3.6261
1766/241.1155mz/0.89min	4.1842	4.6457	4.5017
11694/696.3079mz/9.70min	4.1648	3.7029	3.5907
3489/901.6275mz/32.64min	4.1494	4.9609	5.0491
11722/737.2588mz/10.37min	4.1362	3.676	3.5653
10700/390.2433mz/4.85min	4.1132	3.6551	3.545
10787/364.2239mz/4.85min	4.084	3.6279	3.5191
3499/313.0671mz/0.72min	4.0608	3.7751	3.7535
1751/241.1181mz/0.89min	4.0019	5.1641	5.0235

Table S5.6. PLS-DA VIP scores of the first 50 most significant (P > 1) parent ions detected in the 21-day old bacterial extracts of experiment three identified by PLS-DA.

PLS-DA VIP scores			
Parent ion (ID/mz/retention time)	Comp. 1	Comp. 2	Comp. 3
9301/654.2887mz/7.97min	8.5318	7.5892	7.4877
9303/654.2999mz/7.97min	8.0552	7.164	7.0683
9178/654.2890mz/5.53min	7.5231	6.6919	6.6025
11683/712.2993mz/9.63min	7.4348	6.6124	6.5241
9308/654.2775mz/7.98min	7.3056	6.499	6.4121
9194/654.3002mz/5.53min	7.2317	6.4321	6.3462
1754/241.1206mz/0.89min	7.1022	6.915	6.8236
11685/712.2866mz/9.63min	6.8722	6.1123	6.0306
1751/241.1181mz/0.89min	6.8161	6.8907	6.8074
11684/712.3121mz/9.63min	6.545	5.8199	5.7423
9254/654.2778mz/5.53min	6.3982	5.6919	5.6158
9318/654.3112mz/7.98min	6.1706	5.5045	5.4305
17130/770.5486mz/28.82min	6.0712	5.4634	5.3907
1788/241.1231mz/0.89min	6.0598	5.6621	5.5858
17131/770.5342mz/28.82min	5.9517	5.3556	5.2843
14959/295.2288mz/13.38min	5.9246	5.271	5.2005
1766/241.1155mz/0.89min	5.8453	5.8763	5.8099
11695/728.2942mz/5.99min	5.8326	5.187	5.1178
11727/714.2791mz/4.67min	5.7273	5.0941	5.026
14960/295.2254mz/13.38min	5.6792	5.0533	4.9856
9329/654.3115mz/5.54min	5.5708	4.9649	4.8983
14972/576.2869mz/9.83min	5.509	4.8995	4.8341
14974/530.2770mz/9.80min	5.4879	4.8806	4.8154
14962/277.2158mz/13.37min	5.4876	4.8821	4.8168
14961/277.2189mz/13.37min	5.46	4.8568	4.7918
14973/576.2776mz/9.83min	5.4318	4.8315	4.7669

11704/728.2810mz/5.99min	5.3817	4.7865	4.7225
11748/714.2663mz/4.67min	5.3102	4.7235	4.6603
11702/728.3074mz/6.00min	5.1543	4.5835	4.5224
4457/315.0452mz/0.90min	5.147	4.4653	4.4265
11696/712.2738mz/9.63min	5.0886	4.5269	4.4664
9896/655.3001mz/8.00min	5.0575	4.5087	4.4481
14963/295.2322mz/13.38min	5.0359	4.4795	4.4196
11687/754.3148mz/6.26min	5.0355	4.4777	4.418
17132/770.5630mz/28.56min	5.03	4.5267	4.4665
11747/714.2919mz/4.67min	4.9966	4.4433	4.384
14981/530.2852mz/9.80min	4.982	4.4302	4.3711
9900/655.2889mz/8.00min	4.9682	4.4291	4.3696
11688/754.3009mz/6.26min	4.966	4.4164	4.3575
9367/654.2664mz/7.99min	4.949	4.4136	4.3543
14982/530.2688mz/9.80min	4.9434	4.3968	4.3381
14970/491.2621mz/10.42min	4.8967	4.3561	4.2978
14975/546.2693mz/7.17min	4.8887	4.3484	4.2903
3491/315.0489mz/0.90min	4.8559	4.6606	4.6499
6658/537.2729mz/10.51min	4.8336	4.2994	4.2419
6690/267.0730mz/0.77min	4.8139	5.817	5.7668
14977/546.2778mz/7.17min	4.7385	4.2142	4.158
17133/770.5199mz/28.56min	4.7357	4.2612	4.2045
9335/655.3002mz/5.54min	4.7215	4.2041	4.1478
14980/592.2805mz/7.16min	4.6689	4.1533	4.0977

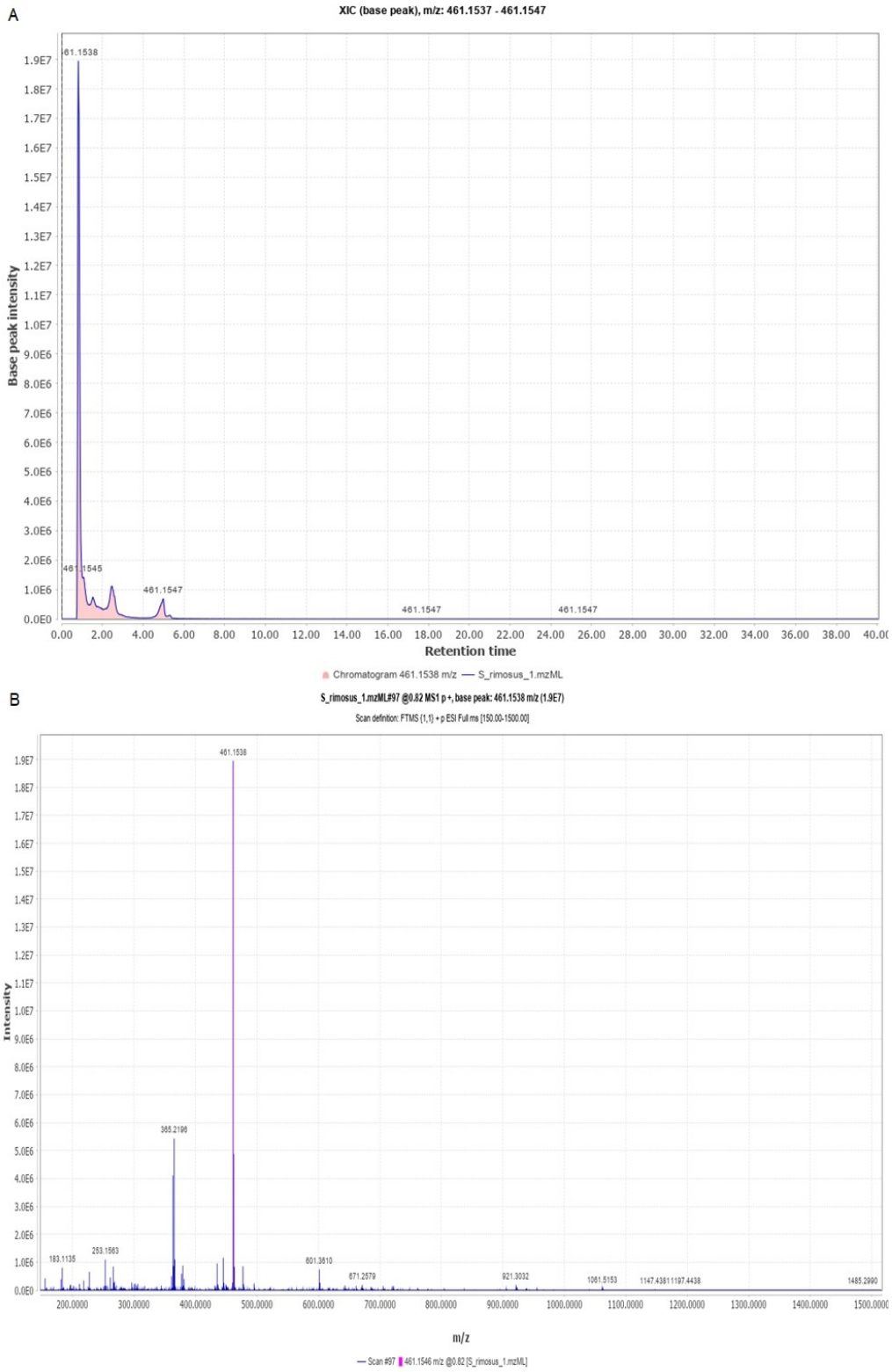

Figure S6.1. Oxytetracycline detected from the *S. rimosus* extracts by LC-MS positive mode. A) *S. rimosus* bacterial extract chromatogram B) mass spectrum of chromatogram base peak oxytetracycline 461.1538 *m/z* (highlighted in red).

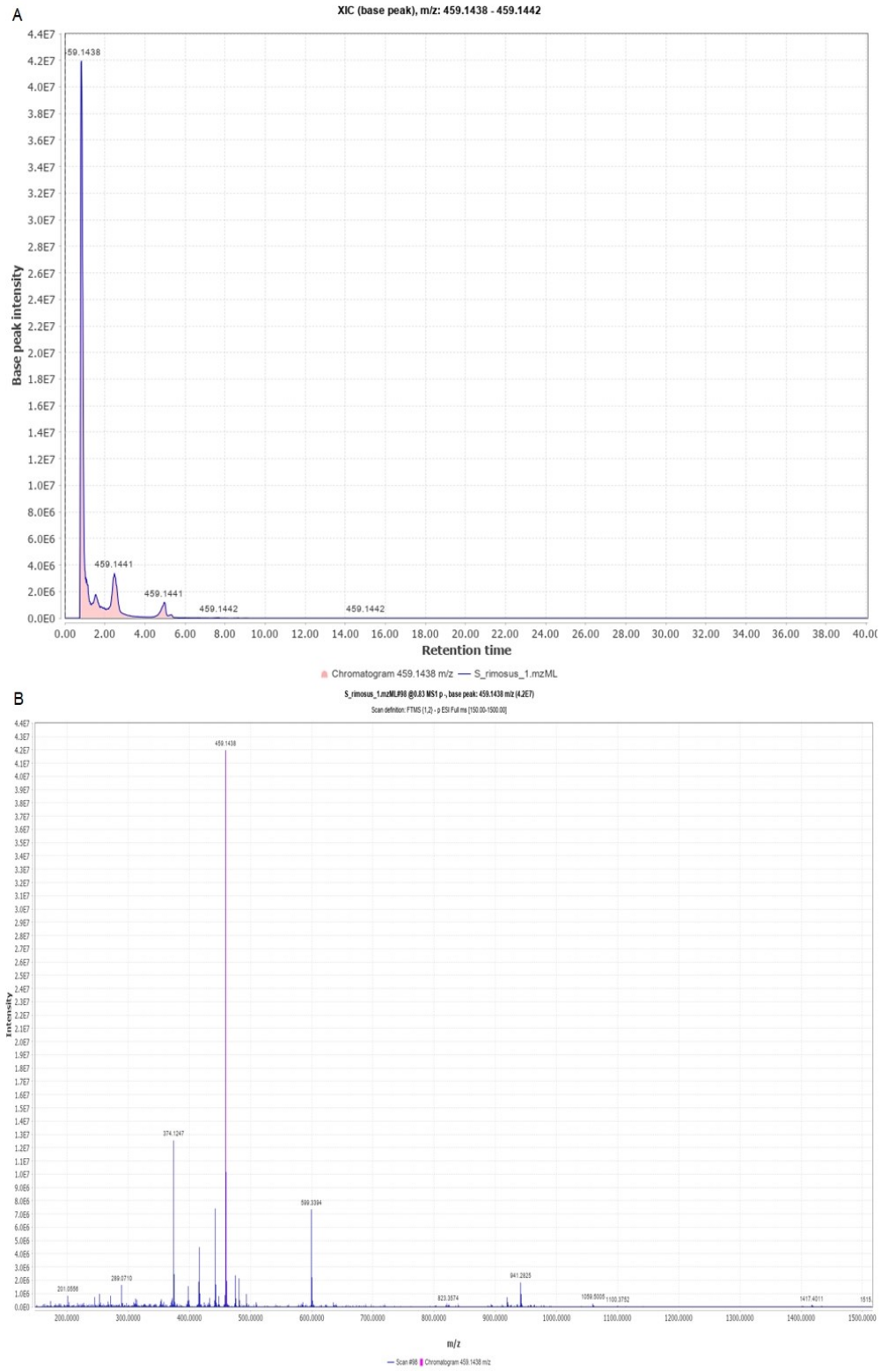

Figure S6.2. Oxytetracycline detected from the *S. rimosus* extracts by LC-MS negative mode. A) *S. rimosus* bacterial extract chromatogram B) mass spectrum of chromatogram base peak oxytetracycline 459.1438 *m/z* (highlighted in red).

Table S6.1. Oxytetracycline antibiotic detected in the *S. rimosus* bacterial extracts by LC-MS negative and positive mode.

Ionisation mode	*m/z*			Rt (min)			MW	Molecular formula	Metabolite ID
	Replicate 1	Replicate 2	Replicate 3	Replicate 1	Replicate 2	Replicate 3			
Negative	459.1438	459.1437	459.1436	0.832404	0.815144	0.814929	460.14819	C22H24N2O9	Oxytetracycline
Positive	461.1538	461.1538	461.1535	0.824139	0.840087	0.840054			

MEDIA RECIPES

ISP2 (per Litre of dH2O)

4 g Yeast extract powder

10 g Malt extract powder

4 g Dextrose

20 g Agar (if solid media)

18 g Instant Ocean

NA (per Litre of dH2O)

5 g Peptone

3 g Beef extract

15 g Agar (if solid media)

SNA (per Litre of dH2O)

5 g Peptone

3 g Beef extract

7.5 g Agar (if solid media)

Emerson agar (per Litre of dH2O)

4 g Beef extract

1 g Yeast extract1

4 g Peptone

10 g Dextrose

2.5 g NaCl